Dose-response-time data analysis

Karl Robert Andersson

Thesis
Submitted to the University of Warwick
for the degree of
Doctor of Philosophy in Engineering

Biomedical and Biological Systems
School of Engineering
University of Warwick
Coventry, United Kingdom, 2017

Table of Contents

List of Figures **iv**

List of Tables **vi**

Abbreviations and symbols **vii**

Acknowledgments **xii**

Declaration **xiv**

I Introduction **1**

Introduction **2**

1 Background and literature review **6**

1.1 PK-PD modelling 6

1.2 Dose-response-time data analysis 8

1.2.1 Instantaneous response models 9

1.2.2 Turnover models 13

1.2.3 Kinetic-Pharmacodynamic models 14

1.3 Summary and perspectives 16

2 Methods and models **21**

2.1 Model selection 22

2.1.1 Biophase function 22

2.1.2 Pharmacodynamic model 24

2.1.3 Mixed-effects modelling 29

2.2 Parameter identifiability 36

2.2.1 Identifiability methods . . . 37
2.3 Parameter estimation . . . 41
2.3.1 Linear models . . . 42
2.3.2 Nonlinear models . . . 46
2.3.3 Nonlinear mixed-effects models . . . 56
2.3.4 Profile likelihood . . . 61
2.3.5 Software . . . 62
2.4 Sensitivity analysis . . . 62
2.4.1 Methods . . . 63
2.5 Model evaluation . . . 63
2.5.1 Quantitative analysis . . . 64
2.5.2 Qualitative analysis . . . 68
2.6 Summary . . . 70

II Analysis and results 72

3 Background 73
3.1 Nicotinic acid-induced antilipolysis . . . 73
3.2 Pharmacokinetics of NiAc . . . 75
3.3 Data . . . 79
3.3.1 Outline of experimental procedures . . . 79

4 DRT I - Free fatty acid dynamics 84
4.1 Model development . . . 84
4.2 The biophase function . . . 85
4.2.1 Selection process of biophase models . . . 85
4.2.2 The final biophase model . . . 87
4.3 The pharmacodynamic model . . . 88
4.3.1 Structural identifiability . . . 91
4.3.2 Modelling between-subject variability . . . 92
4.4 Parameter estimation . . . 92
4.4.1 Initial parameter estimates . . . 92
4.5 Results and validation . . . 94
4.5.1 Model predictions . . . 100
4.5.2 Shrinkage analysis . . . 101
4.5.3 Sensitivity analysis . . . 101
4.5.4 Goodness-of-fit plots . . . 103
4.6 Discussion . . . 103
4.6.1 DRT modelling . . . 103
4.6.2 Strategy when selecting the biophase model . . . 104
4.6.3 DRT model . . . 105

4.6.4 Control theory . . . 106
4.6.5 Inter-individual and intra-individual variability . . . 107

5 DRT II - Free fatty acid and insulin dynamics 108
5.1 Model development . . . 109
5.1.1 Disease modelling and inter-study variability . . . 109
5.1.2 Notation conventions . . . 110
5.2 The biophase function . . . 110
5.3 The pharmacodynamics of insulin . . . 110
5.4 The pharmacodynamics of FFA . . . 115
5.4.1 Structural identifiability . . . 118
5.5 Parameter estimation . . . 119
5.6 Results and validation . . . 122
5.6.1 Biophase dynamics . . . 122
5.6.2 Insulin model . . . 122
5.6.3 FFA model . . . 129
5.6.4 Shrinkage analysis . . . 133
5.6.5 Predicted FFA lowering . . . 134
5.6.6 Comparison to exposure-driven analysis . . . 135
5.6.7 Goodness-of-fit plots . . . 135
5.6.8 Sensitivity analysis . . . 135
5.7 Discussion . . . 139
5.7.1 Model evolution . . . 139
5.7.2 Model characteristics . . . 139
5.7.3 Model evaluation . . . 140

6 Conclusions 143
6.1 Future work . . . 147

Appendices 166

A Mathematica code - Identifiability analysis of DRT I model 167

B Mathematica code - Parameter estimation of DRT I model 169

C Mathematica code - Identifiability analysis of DRT II insulin model 173

D Exposure-driven pharmacodynamic modelling - DRT II study 175

List of Figures

1.1 Examples of pharmacokinetic models 8
1.2 Conceptual figure of DRT analysis 10
1.3 Biophase models presented by Smolen 11
1.4 Biophase-driven turnover model 14

2.1 Biophase library 23
2.2 Example—response-time data 27
2.3 Example - response-time data 33
2.4 Example—response-concentration course 45
2.5 Example—$E_{\max}$ model fitted with Newton's method 55
2.6 Model validation—Visual Predictive Check plots 68
2.7 Model validation—Individual predictions 69
2.8 Model validation—Qualitative evaluations 70

3.1 Mechanisms of NiAc and insulin-induced antilipolysis in adipose tissue 74
3.2 NiAc pharmacokinetics for lean Sprague-Dawley and obese Zuecker rats . . . 75

4.1 Biophase library 85
4.2 Example of FFA-time course data 89
4.3 Schematic structure of FFA model 90
4.4 Visual predictive check plots for the FFA model and data 97
4.5 Individually fitted FFA response-time courses 98
4.6 Population predicted biophase drug amount 99
4.7 Long-term model predicted effect of NiAc on FFA 100
4.8 Local senitivity analysis—FFA model 102
4.9 Goodness-of-fit plots—FFA model—lean and obese rats 104

5.1 NiAc-FFA dependencies in the current and previous studies 109
5.2 The selected biophase functions 111
5.3 Example of insulin-time course data 112
5.4 Mechanisms of insulin dynamics 114
5.5 Example of FFA-time course data 116
5.6 Mechanisms of FFA dynamics 117
5.7 VPC for insulin and FFA model and data—lean Sprague-Dawley rats 123
5.8 Individual fits for insulin and FFA model—lean Sprague-Dawley rats 124
5.9 Fitted biophase amount for insulin and FFA model—lean Sprague-Dawley rats 125
5.10 VPC for insulin and FFA model and data—obese Zucker rats 126
5.11 Individual fits for insulin and FFA model—obese Zucker rats 127
5.12 Fitted biophase amount for insulin and FFA model—obese Zucker rats 128
5.13 Model simulation of acute and chronic action of NiAc exposure 133
5.14 Model predicted reduction in FFA exposure 134
5.15 Goodness-of-fit plots—insulin and FFA model—lean Sprague-Dawley rats . . 136
5.16 Goodness-of-fit plots—insulin and FFA model—obese Zucker rats 137
5.17 Local senitivity analysis—FFA model 138

D.1 Visual predictive checks for lean Sprague-Dawley rats 178
D.2 Visual predictive checks for obese Zucker rats 179
D.3 Model predicted reduction in FFA exposure 185
D.4 Predicted steady-state concentration-response behaviour 185

List of Tables

I List of published articles 4

1.1 Published DRT studies 20

2.1 Parameter estimate uncertainty—linear model example 46
2.2 Parameter estimate uncertainty—nonlinear model example 56

3.1 Study I data characteristics 79
3.2 Study II data characteristics 80

4.1 Evolution of biophase model structure 86
4.2 DRT I summary of model 93
4.3 Estimated system rate constants with corresponding half-lives 95
4.4 DRT I model parameter estimates and between-subject variability 96
4.5 Comparison between DRT and exposure-driven pharmacodynamics analysis . 100
4.6 Model residual additive errors 101
4.7 η-shrinkage of the EBE's 101

5.1 DRT II summary of model 121
5.2 Turnover half-lives 129
5.3 DRT II model parameter estimates and between-subject variability 132
5.4 Insulin and FFA model residual additive errors 133
5.5 η-shrinkage of the EBE's 134
5.6 Comparison between DRT and exposure-driven pharmacodynamic analysis . 135

D.1 Turnover half-lives 180
D.2 Parameter estimates and uncertainties 184

Abbreviations and symbols

Name	Definition or explanation
$\boldsymbol{\beta}$	model parameters
$\hat{\boldsymbol{\beta}}$	parameter estimates
β_0	intercept parameter
β_1	slope parameter
γ	Hill exponent
δ	lumped diffusion parameter
$\boldsymbol{\eta}_i$	random effects of individual i
λ	first-order elimination rate from the biophase compartment
$\boldsymbol{\Omega}$	covariance matrix
$\boldsymbol{\phi}_i$	parameters of individual i
σ	residual error
$\boldsymbol{\theta}$	system parameters
θ_μ	fixed effect
$\hat{\boldsymbol{\theta}}_{\mathrm{ML}}$	maximum likelihood estimate
$\boldsymbol{\Theta}$	feasible parameter space
$A_{\mathrm{a}}(t)$	drug amount in the absorption compartment at time t
$A_{\mathrm{b}}(t)$	drug amount in the biophase at time t
$A_{\mathrm{c}}(t)$	drug amount in the systemic fluid compartment at time t
$A_{\mathrm{d}}(t)$	drug amount in the tissue depot compartment at time t
$A_{\mathrm{g}}(t)$	drug amount in the gut at time t
$A_{\mathrm{sc}}(t)$	drug amount in the subcutaneous compartment at time t
$A(t)$	drug amount in the§ plasma compartment at time t

AC	adenylate cyclase
ACTH	adrenocorticotropin
AIC	Akaike information criterion
ATGL	adenosine triglyceride lipase
ATP	adenosine triphosphate
B_k	approximated Hessian at kth iteration
BFGS	Broyden-Fletcher-Goldfarb-Shanno (algorithm)
$C(t)$	drug concentration in the plasma at time t
C_{50}	steady-state concentration that produces 50% of the effect
$C_{\mathrm{e}}(t)$	drug concentration in the effect compartment at time t
$C_{\mathrm{p}}(t)$	drug concentration in the plasma compartment at time t
$C_{\mathrm{t}}(t)$	drug concentration in the tissue compartment at time t
cAMP	cyclic adenosine monophosphate
CDF	cumulative distribution function
Cl	clearance
Cl_{cr}	clearance of creatine
Cl_{d}	inter-compartmental distribution
Cl_{de}	clearance of desirudin
CV	coefficient of variation
D	drug dose
D_{IV}	bolus drug dose
$D_{\mathrm{KL}}(\boldsymbol{\theta})$	Kullback-Leibler divergence
D_{SC}	subcutaneous drug dose
DAISY	Differential Algebra for Identifiability of SYstems
DFP	Davidon-Fletcher-Powell (algorithm)
DRT	dose-response-time
$\boldsymbol{e}$	observed residuals
$\boldsymbol{e}_{ij}$	residual variability at time t_j for individual i
$E(t)$	drug effect at time t
E_0	baseline effect
$E_{\max}$	efficacy
EAR	Exact arithmetic rank
EBE	Empirical Bayes Estimates
ED_{50}	potency
EDK_{50}	infusion rate that gives half-measured response
EM	Expectation-Maximisation
EPO	erythropoietin
F	bioavailability or biophase availability
$F(t)$	FFA concentration at time t
FFA	free fatty acids
FOCE	first-order conditional estimation (without interactions)

FOCEI	first-order conditional estimation with interactions
GN	Gauss-Newton
$H(A_\mathrm{b})$	drug-mechanism function
Hb	haemoglobin
HSL	hormone sensitive lipase
$\mathcal{I}(\boldsymbol{\theta})$	expected Fisher information
$\mathcal{I}(\hat{\boldsymbol{\theta}}_\mathrm{ML})$	observed Fisher information
$I(t)$	insulin concentration at time t
$I_\mathrm{KL}(\boldsymbol{\theta})$	Kullback-Leibler information
I_max	efficacy (maximal inhibitory effect)
IC_{50}	potency (plasma concentration were 50% of the effect is attained)
ID_{50}	potency (biophase drug amount were 50% of the effect is attained)
$\mathrm{Inf}(t)$	function dependent on infusion protocol
$IR(t)$	virtual infusion rate at time t
IV	intravenous
IPRED	individual predictions
IWRES	individual weighted residuals
k	first-order elimination rate
k_{10}	first-order elimination rate from the plasma compartment
k_{12}	first-order distribution rate from the plasma to the tissue compartment
k_{21}	first-order distribution rate from the tissue to the plasma compartment
k_a	first-order absorption rate
k_ag	absorption rate from the gut compartment
k_asc	absorption rate from the subcutaneous compartment
k_e	first-order elimination rate
k_eo	first-order elimination rate from the plasma to the biophase
k_in	turnover rate
k_off	rate constant for dissociation
k_on	rate constant for association
k_out	fractional turnover rate
$k_\mathrm{out,max}$	maximal fractional turnover rate
k_tol	fractional turnover rate of moderator
K_d	dissociation constant
K_i	integral gain parameter
K_m1	Michaelis constant, first pathway
K_m2	Michaelis constant, second pathway
K_mg	Michaelis constant, gut
K_M	Michaelis constant
K_max	maximal toxic effect
K-PD	kinetic-pharmacodynamic
KL	Kullback-Leibler

KM	Levenberg-Marquardt
$l(\boldsymbol{\theta}; \boldsymbol{y})$	log-likelihood function
$l(\boldsymbol{\theta}, \boldsymbol{\Omega}, \boldsymbol{R}; \boldsymbol{y})$	population log-likelihood function
$[L]$	free ligand concentration
$[LR]$	ligand-receptor complex concentration
$L(\boldsymbol{\theta}; \boldsymbol{y})$	likelihood function
$L(\boldsymbol{\theta}, \boldsymbol{\Omega}, \boldsymbol{R}; \boldsymbol{y})$	population likelihood function
$\mathcal{L}_f$	extended *Lie derivative* differential operator
$\mathcal{L}_f^{(k)}$	k:th repeated Lie derivative
M_0	moderator baseline
$M_i(t)$	moderator response at time t
MCEM	Monte Carlo Expectation-Maximisation
ML	maximum likelihood
MM	Michaelis-Menten
MSE	mean squared error
n	number of observations
N	number of individuals in the population
NiAc	nicotinic acid
NLME	nonlinear mixed-effects models
ODE	ordinary differential equation
p	amplification factor
$\boldsymbol{p}_k$	search direction
$\boldsymbol{p}_k^{\mathrm{N}}$	Newton step
$\boldsymbol{p}_k^{\mathrm{GN}}$	Gauss-Newton step
$\boldsymbol{p}_k^{\mathrm{GN}}$	Levenberg-Marquardt step
P-P	probability-probability
PBPK	physiologically-based PK
PD	pharmacodynamic
PDE3B	phosphodiesterase 3B
PDF	probability density function
PK	pharmacokinetic
PKA	protein kinase A
PL	Profile Likelihood
PO	*per os* (Latin for by mouth, i.e., oral drug administration).
Q-Q	quantile-quantile
QRPEM	Quasi-Random Parametric Expectation-Maximisation
$[R]$	free receptor concentration
$\boldsymbol{R}$	residual matrix
$R(t)$	pharmacodynamic response
R_0	baseline response
$\widehat{R}_i(t)$	predicted response at time t for individual i

RSD	relative standard deviation
RSE	relative standard error
$S_{\max}$	efficacy (maximal stimulatory effect)
$S_n(\boldsymbol{\beta}$	sum of squares
SA	sensitivity analysis
SAEM	Stochastic Approximation Expectation-Maximisation
SC	subcutaneous
SD_{50}	potency (biophase drug amount were 50% of the effect is attained)
SDE	stochastic differential equation
STS	standard two-stage (method)
SVD	singular value decomposition
SYNT	endogenous NiAc synthesis
T_{Tx}	duration of toxic effect
TG	triglyceride
$\boldsymbol{u}_i(t)$	input functions
V	volume of distribution of the drug
$V_{\max}$	maximal elimination rate
$V_{\max 1}$	maximal elimination rate, first pathway
$V_{\max 2}$	maximal elimination rate, second pathway
$V_{\max g}$	maximal absorption rate, from the gut
V_{p}	volume of distribution, plasma compartment
V_{t}	volume of distribution, tissue compartment
VPC	visual predictive check
$\boldsymbol{x}_0$	initial conditions
$\dot{\boldsymbol{x}}_i(t)$	state variables for the ith individual at time t
$\boldsymbol{X}$	design matrix
$\boldsymbol{y}$	dependent variables
y_{ij}	observations of the system at times t_j for individual i
$\boldsymbol{Z}_i$	covariates of individual i

Acknowledgments

This work would not have been possible without the support and encouragement I have received during my time as a PhD student. I would first and foremost like to express my sincerest gratitude to my principal thesis advisors. Thank you, Johan Gabrielsson, for being an excellent mentor. Besides your experience and vast knowledge in quantitative pharmacology, you possess a contagious curiosity of exploring what is unknown to you - a perfect trait when working in an interdisciplinary field. Thanks to Mats Jirstrand for always being accessible and sharing your expertise in all aspects of model identification. Your enthusiasm and compassion contribute to an inspiring and pleasurable working environment. The both of you have taught me a great deal about how to conduct scientific research. Many thanks to my advisors at the University of Warwick, Michael Chappell and Neil Evans. Thank you for providing valuable discussions on model development in general, and identifiability analysis in particular. Also, big thanks for all of your corrections of my somewhat flawed British grammar. I would like to express my appreciation to Michael for coordinating the IMPACT project.

Many colleagues have aided me in my research. Joachim Almquist at Fraunhofer-Chalmers Centre is greatly acknowledged for valuable discussions concerning parameter estimation and parameter uncertainty, and for guidance on the in-house developed Mathematica framework for nonlinear mixed-effects estimation. Thanks to Christine Ahlström and Tobias Kroon at AstraZeneca for generating the data that I have analysed. Thank you, Nick Oakes, for providing feedback on my pharmacodynamic models and for sharing your insights on metabolic diseases. I would like to thank my roommates and colleagues David Janzén and Linnea Bergenholm who endured spending every waking hour with me in Britain. I would also like to send my warmest well-wishes to the entire A407 Biomedical Superhero group.

I would not have pursued a research career if it had not been for the support and inspiration from Marija Cvijovic at the Chalmers University of Technology. Thanks for

believing in me and my capability.

Me and Tony Johansson have studied together since upper secondary school. Besides being the closest of friends, you have patiently answered my mathematical queries and laughed inexplicably at my horrible, stupid humour. Thank you, and good luck on your future academic career. I would like to thank my dearest friends, Filip and Anton, and the infamous "You was smoochin' with my brother!" chat. Thanks to Pablo Lerner for sharing; intellectual conversations, non-intellectual anti-humour, great taste in music, beers on Andra Lång, among many other things. Thanks to my temporary 'parents' Filip and Amanda for letting me stay at your place.

I would finally wish to express my utmost thanks to my family and all of my friends for your support through the roller-coaster of ups and downs that constitute the life of a PhD student.

This work was funded through the Marie Curie FP7 People ITN European Industrial Doctorate (EID) project, IMPACT (Innovative Modelling for Pharmacological Advances through Collaborative Training) (No. 316736) and by the Swedish Foundation for Strategic Research.

Robert Andersson

Gothenburg
August 2017

Declaration

This thesis have been submitted to the University of Warwick in support of Robert Andersson's application for the degree of Doctor of Philosophy. Robert is the sole author of this work and it has not been submitted in any previous applications for any degree.

The data presented in this thesis were collected at AstraZenca, Gothenburg, Sweden. The experimental parts were conducted by Christine Ahlström Ahlström et al. (2011b) under the supervision of Professor Johan Gabrielsson, and by Tobias Kroon Kroon (2016) under the supervision of Doctor Nicholas Oakes and Professor Johan Gabrielsson.

Parts of this thesis have been published by the author:

[A] **Andersson R**., Jirstrand M, Peletier L. A., Chappell M. J., Evans N. D., Gabrielsson J. 2016. Dose-response-time modelling: Second-generation turnover model with integral feedback control. Eur. J. Pharm. Sci. 81, 189-200.

[B] **Andersson R**., Kroon T., Almquist J., Jirstrand M., Oakes N. D., Evans N. D., Chappell M. J., Gabrielsson J. 2017. Modeling of free fatty dynamics: Insulin and NiAc resistance under acute and chronic treatments. J. Pharmacokinet Phar. 44(3) 203-222.

Abstract

The traditional approach to pharmacodynamic modelling relies on knowledge about the pharmacokinetics. A prerequisite for obtaining kinetic information is reliable exposure data. However, in several therapeutic areas, exposure data are unavailable—including when the drug response precedes the systemic exposure (for example pulmonary drug administration) and when the drug is locally administered (for example ophthalmics).

Dose-response-time (DRT) data analysis provides an alternative to exposure-driven pharmacodynamic modelling when exposure data are sparse or lacking. In DRT modelling, the response data are assumed to contain enough information about the drug kinetics, whereby a biophase model can be developed and act as the driver of the pharmacological response.

The following work presents the fundamental principles of DRT modelling. This include the entire procedure of identifying a DRT model, encompassing the assessment of the biophase function and the pharmacodynamic model, extensions to cover population variations, identifiability analysis, parameter estimation, and model validation. To demonstrate the utility of the technique, two extensive pre-clinical DRT studies of the interaction between nicotinic acid (NiAc) and free fatty acids (FFA) are presented. The first study covered the response behaviour following intravenous and oral NiAc dosing in both normal (lean) and diseased (obese) rats. The second study extended the models of the first study to incorporate insulin as a driver of the FFA response. Moreover, data from chronic trials were analysed with the aim to quantitatively understand the adaptive behaviours associated with long-term NiAc treatments.

The aim of this work is to answer the questions of ***when and how*** to use DRT data analysis, and ***what*** the limitations of the method are.

The DRT models of the first study were successfully fitted to all response-time courses in lean rats, with high precision in the parameter estimates (relative standard errors (RSE) $< 25\%$), visual predictive check (VPC) and individual plots that captured the population and subject trends, and ε-shrinkages of less than 10%. The model for the obese rats were less precise, with specific parameters being practically non-identifiable (with, for example, RSE$\sim 250\%$). The results for both lean and obese rats were generally consistent with those of an exposure-driven reference model, albeit with less precision and accuracy in the parameter estimates. Finally, the model was able to describe non-linear biophase kinetics, present at high oral dosages of NiAc.

The DRT models of the second study were able to capture the response-time courses for insulin and FFA on a population and individual level, and for both lean and obese rats. However, many parameters were uncertain (with RSE of, for example, 30-50%) and some were practically non-identifiable (with RSE of $> 100\%$). The estimates were generally less precise and more inaccurate than those obtained in an exposure-driven reference model. Yet, most parameter estimates of the DRT models were within one standard deviation from those of the exposure-driven model. The final model was used to predict steady-state FFA exposures following repeated NiAc dosing for a range of different infusion protocols. The optimal dosing regimens consisted of infusions and wash-out periods were the wash-outs were 2h longer than the infusions. These predictions were consistent with those made by the exposure-driven model. Albeit, the DRT model predicted a slightly lower optimal reduction of FFA exposure.

It is important to recognise that DRT analyses introduce bias and variability in the parameter estimates. To obtain reliable results, it is advisable to have rich pharmacodynamic data, covering drug administration at different routes, rates, and schedules. With these issues taken into account, the technique still performed well in the two extensive studies presented in this work.

In conclusion, DRT data analysis is a modelling technique used in situations when exposure data are unavailable. The method is versatile and can describe a range of different pharmacological behaviours. Precision and accuracy is lost when comparing to an exposure-driven pharmacodynamic modelling approach. Thus, DRT modelling is not to be considered as a replacement of the gold-standard pharmacokinetic-pharmacodynamic framework, but rather as a compliment when exposure data are unavailable.

Keywords: Dose-response-time modelling, Biophase functions, Pharmacodynamic modelling, Nonlinear mixed-effects (NLME), Disease modelling, Tolerance, Adaptation, Feedback

Part I

Introduction

Introduction

This thesis is divided into two parts, each with separate objectives; the first part serves to describe ***what*** dose-response-time (DRT) data analysis and population modelling are and how these techniques are applied. The second part focuses on ***why*** the studies of this PhD project were conducted, and their respective contribution.

Aims and objectives

The aim of this thesis is primarily to answer the following questions:

- When and how do we use DRT data analysis?
- What are the limitations of DRT data analysis?

In order to achieve the aims, an exhaustive literature review and two major data analyses were conducted. A key aspect of this project was to demonstrate how simple biophase structures can be used as the underlying driving mechanism when describing complex pharmacodynamic systems, where lack of pharmacokinetic data prohibits the standard pharmacokinetic-pharmacodynamic modelling practice.

Quantitative pharmacology

Modelling and simulation are crucial in modern pharmaceutical research (Allerheiligen, 2014; Breimer and Danhof, 1997; Burman and Wiklund, 2011; Lalonde et al., 2007; Leil and Bertz, 2014; Manolis et al., 2013; Marshall et al., 2016; Staab et al., 2013). The methods at hand provide quantitative ways to perform pharmacology; applicable when evaluating and comparing drugs, and when designing future experimental protocols (Aarons et al., 2001; Gabrielsson and Weiner, 2010; Rowland and Tozer, 2011). This allows for well-informed

decisions throughout the drug development cycle, from initial *in silico* analyses to post-marketing predictive studies on new populations (Bonate, 2011). In detail, modelling and simulation enable a better understanding of the drug properties, or the *pharmacokinetics* (PK) and *pharmacodynamics* (PD), which are the two main areas of pharmacology (Rowland and Tozer, 2011). PK may in layman's terms be described as *what the body does to the drug*, which encompasses absorption, distribution, metabolism, and elimination of the drug (Benet and Zia-Amirhosseini, 1995; Gibaldi and Perrier, 1982). The kinetic properties are assessed by conducting *in vivo* studies wherein the drug is administered and the corresponding exposure (typically in blood plasma) is measured over time. The experimental data provide the basis for the PK model. A well-designed model may contribute quantitative knowledge of the concentration-elimination relationship, the drug bioavailability, the unbound drug concentration, the volume of distribution of the drug, and so forth.
In contrast to PK, PD represents *what the drug does to the body*. Generally, drugs are designed to alter normal physiological or biochemical processes, inhibit pathological processes, or disrupt parasites or microbes (Lees et al., 2004). Drugs typically function as agonists, antagonists or inverse agonists on a specific receptor (Gabrielsson and Weiner, 2010). By binding to its receptor, and forming a receptor-ligand complex, the drug provokes a stimulating, stabilising or inhibiting action. If the expression of the receptor-ligand complex is measurable, or some downstream biomarker (Aronson, 2005) is measurable, then the PD may be assessed. Measuring exposure and drug effect are done in parallel, whereby the drug concentration-effect relation may be assessed. Traditionally, the PK is analysed first and considered to drive the PD (Holford and Sheiner, 1982). Consequently, the fitted PK model will act as the driving mechanism of the perturbed pharmacological response, and the final PK-PD model will encompass both the kinetic and dynamic properties of the drug and how these are related.

Dose-response-time data analysis

Dose-response-time data analysis is as an alternative to exposure-driven PK-PD modelling when PK data are sparse or lacking, or when it is difficult to relate measured exposure (typically in plasma) to exposure at the target (e.g., in the brain (Andersson et al., 2015; Gabrielsson et al., 2000; Gabrielsson and Peletier, 2014; Jacqmin et al., 2007)). This involves studies where, for example, it is undesirable to perform exposure sampling (e.g., in paediatrics (Tod, 2008)), the drug is locally administered (e.g. in ophthalmics (Audren et al., 2004; Gabrielsson et al., 2000; Smolen, 1971b)), general clinical trials (Abou Hammoud et al., 2009; Buil-Bruna et al., 2014; Ramon-Lopez et al., 2009; Wilbaux and He, 2014), or the pharmacological response precedes the systemic exposure (e.g. pulmonary drug administration (Musuamba et al., 2015; Nielsen et al., 2012; Wu et al., 2011)). In DRT modelling, the pharmacological effect is assumed to be driven by the drug amount at the active site, known as the *biophase* (Schoenwald and Smolen, 1971; Smolen, 1971b; Gabrielsson et al., 2000). The biophase is a conceptual compartment that consists of any type of tissue or

organ, or combinations of tissues and organs. The choice of structure of the biophase depends on how the drug was administered, what characteristics are seen in the response-time data, and the physiological knowledge of the system (Andersson et al., 2015; Gabrielsson and Peletier, 2014).

	Paper I - Dose-response-time modelling	**Paper II** - Modelling of free fatty acid dynamics
What?	Develop a DRT model describing the NiAc-FFA interactions	Develop a PK-PD model describing the NiAc-Insulin-FFA interactions
Why?	Demonstrate the utility of DRT models in describing complex pharmacological systems	Obtain a robust model able to describe acute and chronic treatments
Design/data	Pre-clinical meta-analysis	Pre-clinical meta-analysis
Key findings	Nonlinear biophase needed for saturable absorption	Diseased animals develop full drug resistance
	Integral feedback control describes adaptation	Diseased animals develop insulin resistance
	High parameter precision.	Drug wash-outs necessary
Conclusions	DRT is a versatile modelling approach	Model captured both acute and chronic treatments
	The pharmacodynamic model can describe acute treatments	Integral controller and dynamic efficacy described different adaptations
	Chronic treatment behaviours remain to be assessed	The designed optimal protocols should be experimentally verified

Table I: Summary of published articles that are presented in this thesis.

This work provides the principles of DRT data analysis in a population context; how basic biophase and pharmacodynamic models are constructed, structural and practical identifiability of these models, incorporation of variability, and assessment of the resulting models. The technique is demonstrated by means of two pre-clinical meta-analyses. The data sets for these analyses cover a range of routes, rates, and schedules of drug administration. Both studies were conducted on the complex metabolic system of free fatty acid (FFA) dynamics, under the provocation of the antilipolytic compound nicotinic acid (NiAc) (Carlson, 2005). In the first study, the drug dose-response relations are analysed in an acute setting, using a single-biomarker data set of FFA response-time data. In this study, special emphasis was placed on the selection process of the biophase functions. The modelled biophase amount functioned as the driving-mechanism for a sigmoidal function that acted as an inhibiting force on the turnover of FFA. In the second study, the model was extended to capture chronic dose-response patterns. This was partly done by adding insulin as a second biomarker. Two different types of adaptive behaviours were included in the model; one to describe drug resistance and one to describe insulin resistance. For both studies, PK data were

available, which allowed for a comparison between the DRT analysis and an exposure-driven analysis (Andersson et al., 2017; Tapani et al., 2014). The first chapter of the thesis consists of a thorough literature review of DRT data analysis. This is followed by a Methods and Models chapter where it is demonstrated how a DRT model is constructed. Furthermore, population modelling is introduced and, in particular, the nonlinear mixed-effects framework (Bonate, 2011; Davidian, Marie, 2003). This is followed by a section on parameter estimation and model validation. The second part of the thesis starts with a chapter on the physiology of NiAc-induced antilipolysis and a presentation of the analysed data. Chapters four and five consist of the two major case studies where the potential of DRT data analysis is demonstrated. The majority of the presented scientific contributions have been published separately (Andersson et al., 2015, 2017) which are summarised in Table I.

Chapter 1

Background and literature review

Pharmacokinetic (PK) and pharmacodynamic (PD) modelling are cornerstones in model-based drug development. The modelling techniques serve as a means to understanding and quantifying patterns seen in pharmacological data. This enables the modeller to evaluate the performance of pharmaceutical substances. Furthermore, suitable models can be applied to simulate unobserved pharmacological events and thus predict optimal dosage strategies. In this way, simulations provide valuable input in the design of future experimental trials. The trials, in turn, contribute new data to be analysed. Hence, mathematical modelling and simulation and experiments are used symbiotically to enhance the modeller's knowledge of the pharmacology and physiology. The iterative strategy of using modelling and simulation and experiments advances the pharmacological development process until a drug has been accepted or discontinued.

1.1 PK-PD modelling

The PK-PD modelling procedure is traditionally sequential[1] in that the PK are initially analysed and then considered to be known when assessing the PD. In detail, a PK model

[1]The sequential approach to PK-PD modelling has traditionally been favoured over the simultaneous one as it tends to be less computationally involved and more prone to obtain parameter estimates. However, if the PK model is misspecified, and the PD model is not, the simultaneous approach provide a better PD fit. For more details and a further discussion on the methods and robustness, see Zhang et al. (2003a,b).

is developed and fitted to the exposure-time data (typically drug plasma concentrations). From the generated PK model, a time continuous exposure signal is generated to act as an input to the PD model. Consequently, when assessing the PD, it is assumed that the PK are known and that the simulated PK input corresponds to the true exposure. Given this premise, the PK-PD modelling framework is constrained by the existence of reliable exposure data. PKs is often modelled using compartmental models (Godfrey, 1983). These models consist of ordinary differential equations, where the state variables represent drug concentrations in different physiological compartments. In the simplest possible case, a single-compartment model is used to represent the drug concentration in the plasma (model illustrated in Fig. 1.1a). This concentration, denoted $C(t)$, is given by

$$\frac{\mathrm{d}C(t)}{\mathrm{d}t} = -k \cdot C(t) = -\frac{Cl}{V} \cdot C(t) \quad \text{with} \quad C(0) = 0, \tag{1.1}$$

where k is the elimination rate, Cl the clearance, and V the volume of distribution of the drug (describing the fraction between the drug amount and the drug concentration[2]). Given an intravenous bolus dose D, the initial condition in Eq. (1.1) becomes $C(0) = D/V$. For extravascular drug administration, an intermediate absorption compartment is added to Eq. (1.1) from where the drug is absorbed into the blood plasma compartment (model illustrated in Fig. 1.1b). The drug kinetics are given by

$$\frac{\mathrm{d}A(t)}{\mathrm{d}t} = -k_\mathrm{a} \cdot A(t) \qquad \text{with} \quad A(0) = D, \tag{1.2a}$$

$$\frac{\mathrm{d}C(t)}{\mathrm{d}t} = \frac{F \cdot k_\mathrm{a} \cdot A(t)}{V} - k \cdot C(t) \quad \text{with} \quad C(0) = 0, \tag{1.2b}$$

where A is the drug amount in the absorption compartment, k_a the absorption rate, and F the bioavailability. The bioavailability ranges from 0 to 1 and represents the fraction of dose that reaches plasma intact. Generally, Eq. (1.2a) is solved for $A(t)$ and the system is reduced to, and considered as, a single-compartment model given by

$$\frac{\mathrm{d}C(t)}{\mathrm{d}t} = \frac{D \cdot F \cdot k_\mathrm{a} \cdot e^{-k_\mathrm{a} t}}{V} - k \cdot C(t) \quad \text{with} \quad C(0) = 0. \tag{1.3}$$

These elementary PK models may be expanded to include additional compartments, describing the drug kinetics in other tissues and organs. Such extensions may be required for various reasons; if, for example there are two different phases in the drug plasma kinetics, the drug distributes into different tissues, whereby a peripheral compartment is needed (model illustrated in Fig. 1.1c). In this case, the plasma $C_\mathrm{p}(t)$ and tissue $C_\mathrm{t}(t)$ concentrations after

[2]The volume of distribution is an estimate of how well the drug distributes throughout the body. For example, a high volume of distribution means that a large fraction of the drug distributes outside the plasma.

a bolus dose could be given by

$$\frac{\mathrm{d}C_\mathrm{p}(t)}{\mathrm{d}t} = k_{21} \cdot C_\mathrm{t}(t) - k_{12} \cdot C_\mathrm{p}(t) - k_{10} \cdot C_\mathrm{p}(t) \quad \text{with} \quad C_\mathrm{p}(0) = D/V, \tag{1.4a}$$

$$\frac{\mathrm{d}C_\mathrm{t}(t)}{\mathrm{d}t} = k_{12} \cdot C_\mathrm{p}(t) - k_{21} \cdot C_\mathrm{t}(t) \quad \text{with} \quad C_\mathrm{t}(0) = 0, \tag{1.4b}$$

where k_{10} is the elimination rate from the plasma compartment, k_{12} the distribution rate from the plasma to the tissue compartment, and k_{21} the distribution rate from the tissue to the plasma compartment.

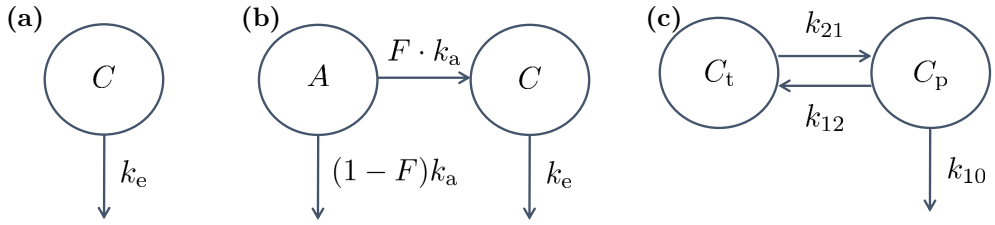

Figure 1.1: Examples of typical PK models: **(a)** represents a one-compartment model with first-order drug elimination; **(b)** a two-compartment model with an absorption and a central drug compartment. The drug is absorbed into, and eliminated from, the central compartment via first-order processes; **(c)** a two-compartment model with a plasma and a tissue compartment. The drug is distributed between plasma and tissue via first-order processes and eliminated from the plasma via a first-order elimination.

The compartmental modelling framework can be expanded to include any number of compartments in order to describe more complex kinetic scenarios. In particular, the physiologically-based PK (PBPK) models consist of multiple compartments and aim at explaining as much as possible of the drug disposition (Rowland et al., 2011). These sophisticated multi-compartment models provide a more general picture of the drug kinetics, and are convenient when, for example, translating results between species. However, the scope of PBPK models often complicates parameter identification (see Section 2.2), and in order for these models to be useful the modeller generally needs prior knowledge of the pharmacology and physiology, and/or exposure assays generated at multiple sites (for a review on PBPK models, see Rowland et al. 2011). As we will see, kinetic information is not always available, whereby PBPK, and simpler PK models, fail.

1.2 Dose-response-time data analysis

Dose-response-time (DRT) data analysis is a modelling approach that is used for assessing the PD response when PK data are lacking or uninformative. PK data may, for example, be difficult to measure if

(i) the turnover of the drug is quick (Uehlinger et al., 1992; Port et al., 1998)

(ii) the concentration of the drug is below the limit of quantification (Lalonde and Gaudreault, 1999)

(iii) the drug is locally administered (e.g., in ophthalmicss (Audren et al., 2004; Smolen, 1971b; Gabrielsson et al., 2000))

Furthermore, in certain clinical trials, it is undesirable to measure drug exposure due to the invasiveness of the sampling methods. Invasiveness is generally an issue in paediatric studies (Tod, 2008) and in situations where the patient is put under considerable distress (e.g., in oncology (Frances et al., 2011; Paule et al., 2012; Wilbaux and He, 2014)). Moreover, if the drug effect precedes the systemic exposure (e.g., for pulmonary drug administration (Musuamba et al., 2015; Nielsen et al., 2012; Wu et al., 2011)), the drug concentration-time series may be uninformative about the unbound drug at the active site. In addition, PK data may be uninformative when there are vast differences between the initial and terminal phase of the drug treatment periods (Lange and Schmidli, 2014, 2015). The traditional PK-PD modelling approach fails in situations where exposure data are lacking or uninformative. In cases like these, DRT data analysis acts as a surrogate (a schematic difference between DRT and PK-PD modelling is illustrated in Fig. 1.2).
DRT modelling is based on the premise that the pharmacological response data contain information about the drug kinetics. This "hidden" information is assumed to be sufficient to determine the drug amount in an intermediate biophase compartment. The biophase represents any organ or tissue where the drug produces its pharmacological effect. From a modelling perspective, the kinetics of the biophase and the pharmacodynamics need to be assessed simultaneously, which is not the case in PK-PD modelling. This is achieved by selecting a possible model that describes the hypothetical drug amount-time course in the biophase. The biophase amount will subsequently act as the driver of a drug-mechanism function—which acts on the pharmacological response.
A summary of published DRT data analyses is given in Table 1.1.

1.2.1 Instantaneous response models

Dose-response-time data analysis dates back to the 1960's and 1970's when Levy (Levy, 1964a,b, 1966; Gibaldi and Levy, 1972) and Smolen (Smolen, 1971b; Schoenwald and Smolen, 1971; Smolen and Schoenwald, 1971; Smolen, 1971a; Smolen and Weigand, 1973; Smolen et al., 1975; Smolen, 1976b,a,c, 1978) introduced the concept. Levy described a relationship between the amount of drug in the body and the corresponding pharmacological effect. Smolen, on the other hand, analysed the dose-response relationship of a mydriatic[3] drug after oral and ophthalmic administration. In the qmydriatic studies, no exposure data were available due to difficulties in assaying the drug in body fluids. Consequently, response

[3]Mydriatic drugs are ones that cause dilation of the pupil.

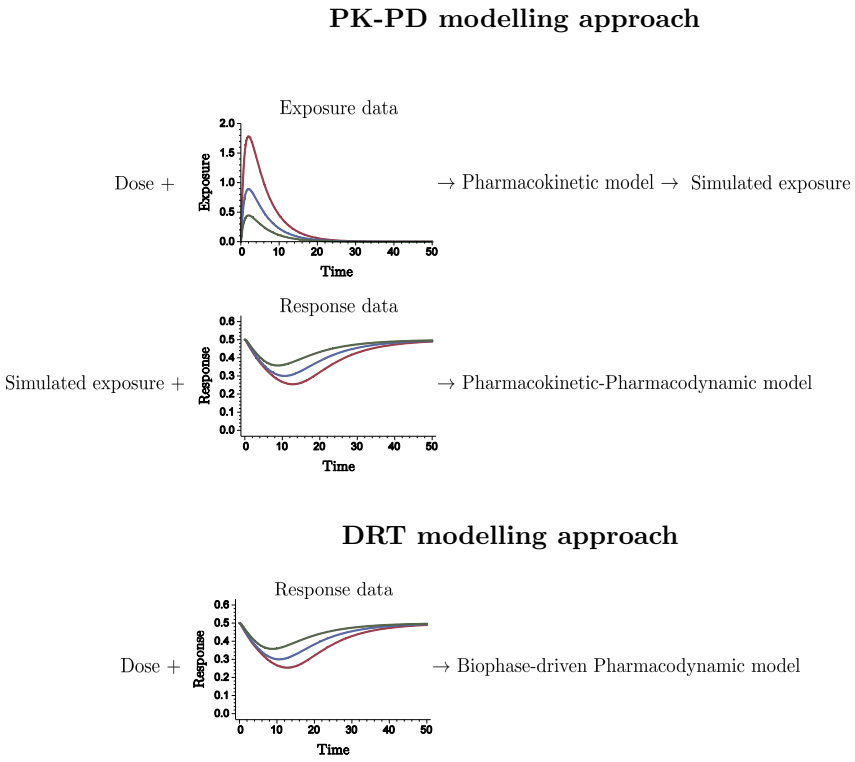

Figure 1.2: Illustration of the conceptual difference between traditional PK-PD modelling and DRT analysis. In traditional pharmacodynamic modelling, the response is assumed to be driven by the pharmacokinetic model. In DRT modelling, the response is driven by the drug amount in the biophase.

data were the sole source of information when quantifying the bioavailability and biokinetic behaviours. Smolen's studies were based on two major assumptions (Smolen, 1976c):

- "The dynamics of the drug's disposition are linear."
- "The intensity of pharmacological response is a single-valued function of the biophasic drug levels."

For example, with a biophase amount of $A_{\mathrm{b}}(t)$, and a pharmacological response of $I(t)$ (mydriatic response intensity, in this case), the functional relationship was assumed to be given by

$$I(t) = f(A_{\mathrm{b}}(t)), \tag{1.5}$$

for some appropriate function f. Now, given the first assumption, a dose vs. effect relationship was used to convert observed intensity-time courses into relative biophase amount-time courses. Combining this with a compartmental model for the biophase dynamics, and multiple relative biophase amount-time courses, the "true" biophase amount was estimated.

Smolen analysed a range of two- and three-compartment biophase models to describe the kinetics of the biophase (the are models illustrated in Fig. 1.3). The corresponding model fits demonstrated the structural and practical identifiability[4] issues associated with multi-compartment biophase models (without making appropriate prior assessments). Nonetheless, when applying an identifiable biophase function, the method was proven to be successful in capturing the pharmacodynamic behaviours and the biophase kinetics. However, the second of Smolen's assumptions heavily constrains the application of the defined technique since many pharmacological processes are non-direct (Dayneka et al., 1993).

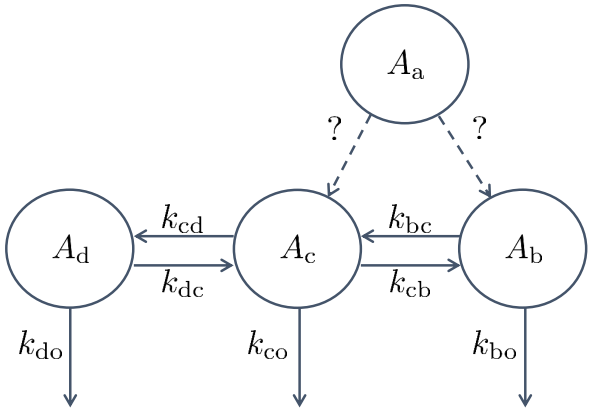

Figure 1.3: Biophase models presented by Smolen (1971b). Smolen used two-compartment models with a biophase A_b, and systemic fluid A_c compartment, and three-compartment models with a biophase A_b, a systemic fluid A_c, and a tissue depot compartment A_d. Moreover, a fourth compartment A_a, corresponding to the site of administration, was included if the drug was not administered systemically.

Since those initial studies, DRT modelling was not applied until the early 1990's when Verotta and Sheiner (1991) further developed the existing techniques. In their study, semi-parametric methods were applied to analyse pharmacodynamic data over a range of different data sets (e.g., verapamil-induced changes in the PR interval of an electrocardiogram). Verotta and Sheiner (1991) made the following model assumptions

- "Both the distribution of the drug and its effect vs. concentration relationship are stationary processes."
- "The distribution of the drug is linear with respect to the input of the drug."
- "The pharmacodynamic response to the drug depends on the concentration of the drug at a single site."
- "The relationship between effect and drug concentration is memoryless."

[4]The identifiability issues were discussed by Smolen. However, no formal identifiability analysis was performed.

The semi-parametric model consisted of an unobserved state X that was proportional to the drug concentration at the active site C_e. The state X was given by the convolution of the input function and a sum of exponentials. Furthermore, the pharmacological effect E was related to X according to a cubic spline. As Verotta and Sheiner had access to PK data in their study, the estimated exposure could be compared with the observed exposure. Here, the uncertainty of the non-parametric technique was made clear, as the worst case estimated exposure profile was far off the observed exposure. Furthermore, the assumption of having stationary processes and a memoryless relationship between the effect and the drug concentration limits the method substantially. However, the study by Verotta and Sheiner inspired subsequent DRT studies. In particular, the response behaviour of the muscle relaxant drug vecuronium was analysed in a range of studies (Bragg et al., 1994; Fisher and Wright, 1997; Fisher et al., 1997; Warwick et al., 1998), where twitch depressions of the muscles were used as the pharmacodynamic biomarker. In these studies, the drug plasma concentration was measurable, but not the concentration at the neuromuscular junction, which is the effective site. Regardless, the studies successfully characterised both the respiratory and adductor pollicis muscle behaviours seen after vecuronium administration. This was done by modelling the biophase concentration Ce (called effective concentration or active concentration in the studies) with a first-order elimination model given by

$$\mathrm{Ce} = k_{\mathrm{eo}} \cdot D \cdot \frac{A \cdot (e^{-\lambda t} - e^{-k_{\mathrm{eo}} t})}{k_{\mathrm{eo}} - \lambda}, \tag{1.6}$$

where k_{eo} is the elimination rate from the plasma compartment to the biophase compartment, D is the dose, A the dose-normalised intercept, and λ the elimination rate from the biophase compartment. This biophase concentration drives the response according to a Hill equation (Gesztelyi et al., 2012)

$$\mathrm{Effect} = \frac{\mathrm{Ce}^{\gamma}}{\mathrm{Ce}^{\gamma} + \mathrm{C}_{50}^{\gamma}}, \tag{1.7}$$

where C_{50} is the steady-state concentration that produces 50% of the effect, and γ is the Hill coefficient. This model was applied to both the respiratory and the adductor pollicis twitch tension data. The models showed that the peak concentration of vecuronium occurred earlier in the respiratory muscles than in the adductor pollicis. This implies a higher peak concentration level and thus explains why the respiratory muscles more frequently experience paralysis than the adductor pollicis after vecuronium exposure. Furthermore, Warwick et al. (1998) showed the potential advantages associated with PK-free PD analysis. In particular, the DRT approach allows for individual predictions of future dosing during anaesthesia. This is not possible using the conventional PK/PD approach due to the time needed to assay the drug. Further usage of DRT data analysis was successfully demonstrated in studies where children were treated with erythropoietin (EPO) for renal anaemia (Uehlinger et al., 1992; Port et al., 1998). Here, the drug-induced haemoglobin (Hb) production was assumed to be

linearly dependent on the EPO dose

$$R = \beta \cdot D, \tag{1.8}$$

where R is the drug-induced Hb production, D the dose, and β the production rate per dose unit. A DRT approach was suitable in these studies since the EPO turnover is rapid in comparison to the response turnover. Consequently, it is hard to relate the concentration-time course of EPO to that of Hb.

1.2.2 Turnover models

Following the DRT studies of the 1990's, the field saw a breakthrough when Gabrielsson et al. (2000), introduced biophase-driven turnover models (Dayneka et al., 1993). In the turnover model framework, the PD response $R(t)$ is given by

$$\frac{\mathrm{d}R(t)}{\mathrm{d}t} = k_{\mathrm{in}} - k_{\mathrm{out}} \cdot R(t) \quad \text{with} \quad R(0) = R_0, \tag{1.9}$$

where k_{in} and k_{out} are the turnover and fractional turnover rate of the response, respectively, and R_0 is the baseline response. For a biophase-driven response, the biophase amount A_{b} will act on the production or elimination of response through a drug-mechanism function $H(A_{\mathrm{b}})$ according to

$$\frac{\mathrm{d}R(t)}{\mathrm{d}t} = k_{\mathrm{in}} \cdot H(A_{\mathrm{b}}) - k_{\mathrm{out}} \cdot R(t) \tag{1.10}$$

or

$$\frac{\mathrm{d}R(t)}{\mathrm{d}t} = k_{\mathrm{in}} - k_{\mathrm{out}} \cdot H(A_{\mathrm{b}}) \cdot R(t). \tag{1.11}$$

The drug-mechanism functions that were applied in the study by Gabrielsson et al. (2000) included nonlinear Hill relations (similar to that of Eq. 1.7) that were either stimulatory

$$H(A_{\mathrm{b}}) = 1 + \frac{E_{\max} \cdot A_{\mathrm{b}}^{\gamma}}{ED_{50}^{\gamma} + A_{\mathrm{b}}^{\gamma}} \tag{1.12}$$

or inhibitory

$$H(A_{\mathrm{b}}) = 1 - \frac{E_{\max} \cdot A_{\mathrm{b}}^{\gamma}}{ED_{50}^{\gamma} + A_{\mathrm{b}}^{\gamma}}. \tag{1.13}$$

where $E_{\max}$ is the efficacy, ED_{50} the potency (based on dose), and γ the Hill coefficient. Turnover models allow for a wide range of response-time behaviours, out of the scope of previous DRT studies (due to their assumptions). The study by Gabrielsson et al. (2000), contained four different cases of biophase-driven turnover models, describing response-time data of miotic response, body temperature, antinociception, and cortisol/ACTH (one example

is illustrated in Fig. 1.4). These case studies showed that DRT models are applicable when the kinetics and/or dynamics behave non-linearly, when there are time-delays in the response data, and when the system contains feedback mechanisms. This heavily expanded the possible applications of DRT models. Beyond the study of Gabrielsson et al. (2000), the

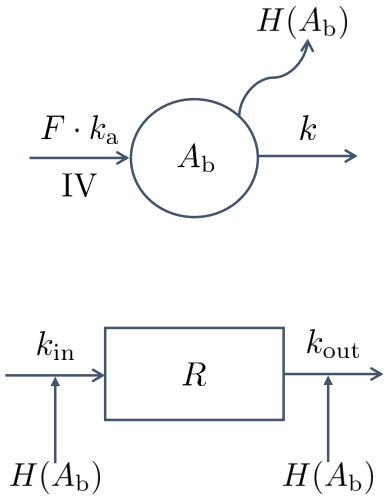

Figure 1.4: Biohase-driven turnover model presented by Gabrielsson et al. (2000). The input into the biophase is either direct (iv administration) or through absorption (oral administration) $F \cdot k_\mathrm{a}$, where F is the biophase availability and k_a is the first-order absorption rate from an absorption compartment into the biophase. The parameter k is the first-order (linear) elimination rate from the biophase. The biophase amount A_b was then driving a drug-mechanism function $H(A_\mathrm{b})$, which can, for example, inhibit the turnover k_in or fractional turnover k_out of the response R.

biophase-driven turnover model was applied across a range of DRT studies in the late 1990's and early 2000's (Lalonde and Gaudreault, 1999; Audren et al., 2004; Gruwez et al., 2005; Tod et al., 2005). In particular, Lalonde and Gaudreault (1999), analysed parathyroid hormone concentrations under treatment by the calcimimetic agent R-568. Since the concentration of the specific agent was below the limits of quantification in more than half of the patient samples, the exposure analysis was excluded and the PD model was assumed to be driven by the drug amount in the biophase. Further, Gruwez et al. (2005) applied a dose-response model to analyse categorical data when they explored the effect of paroxetine and pindolol. Here, the response-time data consisted of total scores on the MADR scale (Montgomery and Åsberg, 1979).

1.2.3 Kinetic-Pharmacodynamic models

In addition to the original DRT-approach by Smolen (1971b), an alternative rate-driven model (K-PD) was suggested by Jacqmin et al. (Gieschke et al., 2001; Goggin et al., 2001; Jacqmin et al., 2001; Pillai et al., 2001). The concepts of the K-PD model are similar to those of the traditional DRT model, except that the 'virtual infusion rate' (biophase turnover

rate) is assumed to be the driver of the pharmacological response, rather than the biophase amount. This is an unconventional approach in pharmacological modelling, where drug exposure (or amounts) are generally assumed to drive the pharmacological effect.
To demonstrate the idea of the K-PD model, assume that the biophase amount $A_{\mathrm{b}}(t)$ has a first-order elimination rate k given by

$$\frac{\mathrm{d}A_{\mathrm{b}}(t)}{\mathrm{d}t} = -k \cdot A_{\mathrm{b}}(t), \tag{1.14}$$

with initial value $A_{\mathrm{b}}(0) = D$. Furthermore, assume that the drug inhibits the turnover of the pharmacodynamic response $R(t)$ according to a nonlinear Hill relation. The response behaviour would then, for the traditional DRT and the K-PD approach, be given by

$$\frac{\mathrm{d}R(t)}{\mathrm{d}t} = k_{\mathrm{in}} \cdot \left(1 - \frac{E_{\max} \cdot A_{\mathrm{b}}^{\gamma}(t)}{ED_{50}^{\gamma} + A_{\mathrm{b}}^{\gamma}(t)}\right) - k_{\mathrm{out}} \cdot R(t) \qquad \text{DRT}, \tag{1.15}$$

and

$$\frac{\mathrm{d}R(t)}{\mathrm{d}t} = k_{\mathrm{in}} \cdot \left(1 - \frac{E_{\max} \cdot IR^{\gamma}(t)}{EDK_{50}^{\gamma} + IR^{\gamma}(t)}\right) - k_{\mathrm{out}} \cdot R(t) \qquad \text{K-PD}, \tag{1.16}$$

with

$$IR(t) = -\frac{\mathrm{d}A_{\mathrm{b}}(t)}{\mathrm{d}t} = k \cdot A_{\mathrm{b}}(t), \tag{1.17}$$

where $IR(t)$ is the virtual infusion rate and EDK_{50} (amount per time unit) the rate that gives half-measured drug-reduced response. As is indicated by Eq. (1.17), the 'drivers' of the DRT and K-PD models are proportional. Thus, the two frameworks only differ by a scaling factor.
K-PD models have been applied in numerous studies (see for example Abou Hammoud et al. (2009); Hamberg et al. (2013); Salem et al. (2016); Wu et al. (2011)) following its introduction by Jacqmin et al. (2001, 2007). However, several studies have misunderstood the original model definition and used the biophase amount as the driving force of the response (see for example Gruwez et al. (2007); Jacobs et al. (2010); Mikaelian et al. (2013); Musuamba et al. (2015); Nielsen et al. (2012)). These studies have in fact applied the traditional DRT approach (Smolen, 1971b).
In a study of chemoradiotherapy-induced thrombocytopenia by Krzyzanski et al. (2015), no biophase kinetics were addressed. Rather, the drug (carboplatin) was assumed to have an on/off effect given by

$$Tx(t) = \begin{cases} K_{\max} & \text{if} \quad t_{\mathrm{j}} \leq t \leq t_{\mathrm{j}} + T_{Tx}, \\ 0 & \text{otherwise}, \end{cases} \tag{1.18}$$

that acted on the elimination of cells. Here, t_{j} represents the starting time of the chemoradiotherapy, T_{Tx} the duration of the toxic effect and $K_{\max}$ is the maximal toxic effect. The study by Krzyzanski et al. (2015) demonstrated that DRT modelling does not necessarily need to include a compartmental biophase.

1.3 Summary and perspectives

DRT data analysis could be an option when the traditional PK-PD approach fails. This occurs when exposure data are lacking or are uninformative, which may be due to:

- Exposure sampling is difficult—quick drug turnover, drug concentrations below limits of quantification, local administration etc.
- Exposure sampling is undesirable—clinical studies, in particular within paediatrics.
- Exposure data are uninformative about the drug exposure—e.g., pulmonary administered drugs or drugs that penetrate the blood-brain barrier.
- Large time differences between the initial and terminal phase—biologics (Morrow and Felcone, 2004).

The technique has been applied for describing drug behaviour in several therapeutic areas (see Table 1.1). In almost all of these studies, simple biophase models were used with first-order elimination and first-order absorption (the latter being applied in cases where drug is not directly administered into the biophase). During recent years, DRT modelling has frequently been applied in clinical oncology (Buil-Bruna et al., 2014; Frances et al., 2011; Parra-Guillen et al., 2013; Paule et al., 2012; Ramon-Lopez et al., 2009; Wilbaux and He, 2014)—a therapeutic area where invasiveness is undesirable. As for clinical oncology studies, invasiveness is an issue in paediatric studies. Thus, DRT modelling is a promising technique when other approaches fails (Tod, 2008).

Drug action or therapeutic area	Drug	Route	Reasons for DRT	Biophase parameters	Reference
Anaesthetics	Phencyclidine and dextroamphetamine	SC	Experimental trial does not allow for exposure sampling	First-order input/output	Jacobs et al. (2010)
Anemia	Induced by ribavirin	PO	No exposure data available	First-order output	Tod et al. (2005)
	Erythropoietin	SC	Exposure kinetics (EPO) are very fast (in comparison to the kinetics of the response (haemoglobin)) and, consequently, hard to relate to the response-time course		Uehlinger et al. (1992); Port et al. (1998)
Antiarrhytmics	Amiodarone	IV bolus + infusion and PO	Sampling amiodarone exposure is not suitable in clinical trials	First-order input(PO)/output	Salem et al. (2016)
Anticoagulants	Warfarin	PO	Exposure data are lacking in most clinical trials of warfarin	First-order output	Wright and Duffull (2011); Hamberg et al. (2010, 2013); Kim et al. (2015)
Antidepressants	Clomipramine and lithium	PO	Exposure data were considered superfluous	First-order output	Gruwez et al. (2007)
	Paroxetine, pindolol	PO	No exposure data	First-order output	Gruwez et al. (2005)
	TC-1734	SC	Demonstrate the utility of DRT	First-order input/output	Gabrielsson and Peletier (2014)
Antilipolytic	NiAc	IV infusion	No exposure data	First-order output	Isaksson et al. (2009); Gabrielsson and Peletier (2014)
	NiAc	IV infusion and PO	Demonstrate the utility of DRT	Michaelis-Menten input (PO)/first-order output	Andersson et al. (2015)
Antinociceptive	Morphine	IV infusion	Morphine is administered with short-time intervals (5 min) where the sedation and pain need to be regularly assessed. This complicates simultaneous exposure assessments	First-order output	Abou Hammoud et al. (2009)
	Experimental	IV and SC	Demonstrate the utility of DRT	First-order input/output, biophaseavailability	Gabrielsson et al. (2000); Gabrielsson and Peletier (2014)

Drug action or therapeutic area	Drug	Route	Reasons for DRT	Biophase parameters	Reference
Arthritis	Fosdagrocorat	PO	No PK model was developed	First-order output of biophase	Shoji et al. (2017)
CNS stimulant	Dexamphetamine	IV bolus and EV	To demonstrate the utility of DRT	First-order input/output	Gabrielsson and Peletier (2014)
	Caffeine	PO	No exposure data	First-order input/output	Ramakrishnan et al. (2013)
	Vecuronium	IV bolus	No exposure data available/needed	First-order output	Bragg et al. (1994); Fisher and Wright (1997); Fisher et al. (1997); Warwick et al. (1998)
COPD	Salmeterol	PUL	Exposure data not available and/or related to the pharmacological response	First-order output of	Musuamba et al. (2015)
	Salmeterol and PF-00610355	PUL	No exposure data	First-order input/output	Nielsen et al. (2012)
	Experimental compound	PUL	No exposure data	First-order input/output	Wu et al. (2011)
COPD and asthma	LABA bronchodilators	PUL	No exposure data	First-order input/output	Agoram et al. (2008)
Cortisol secretion	Adrenocorticotropin	IV infusion	Demonstrate the utility of DRT	No biophase function[a]	Gabrielsson et al. (2000)
Diabetic Macular Edema	Triamcinolone Acetonide	IVI	Exposure sampling at the effective site is arduous	First-order input/output	Audren et al. (2004)
Glaucoma	PF-04475270	IO	Limited exposure data		Luu et al. (2009)
Hyperparathyroidism	R–568	PO	Concentrations of R-568 were below the limit of quantification in more than half of the samples	First-order input/output	Lalonde and Gaudreault (1999)
Hyperphenylalaninemia	Tetrahydrobiopterin	IV infusion	No exposure data	First-order output	Trefz et al. (2015)
Hypotension	Sodium nitroprusside (SNP)	IV infusion	Fast SNP exposure	First-order output	Barrett et al. (2015)
Muscle relaxant	Tubocurarine	IM	No exposure data	First-order output	Levy (1964a)

[a]The drug-mechanism function $H(A_{\mathrm{b}}(t)$ was equal to 1 at a specific drug infusion rate and 2 at another.

Drug action or therapeutic area	Drug	Route	Reasons for DRT	Biophase parameters	Reference
Mydriatics	Tridhexethyl chloride	PO and IO	Exposure sampling at the effective site is arduous	Range of different biophases (see Fig. 1.3)	Smolen (1971b); Schoenwald and Smolen (1971); Smolen and Schoenwald (1971); Smolen and Weigand (1973); Smolen (1976b,a, 1978)
	Latanoprost	IO	Exposure sampling at the effective site is arduous	First-order input/output, lag-time	Gabrielsson et al. (2000)
Myocardial necrosis	Induced in rats through handling	No administration route	Handling effects cannot be measured	First-order output	Mikaelian et al. (2013)
Obesity	PF-05231023	IV infusion	No exposure data	First-order input/output	Thompson et al. (2016)
Oncology	Capecitabine	PO	No exposure data	First-order output	Paule et al. (2012)
	Capecitabine and docetaxel	PO(C) IV(D)	No exposure data	First-order output	Frances et al. (2011)
	Carboplatin, pegylated liposomal doxorubicin and paclitaxel	IV infusion	No exposure data	First-order output	Wilbaux and He (2014)
	Carboplatin, cyclophosphamide and thiotepa	IV infusion	No exposure data	First-order output	Ramon-Lopez et al. (2009)
	Cisplatin, carboplat and etoposide	IV infusion	No exposure data	First-order output	Buil-Bruna et al. (2014)
	CyaA-E7, CpG, cyclophosphamide	IV and IP infusion	No exposure data	First-order output	Parra-Guillen et al. (2013)
	Gemcitabine and carboplatin	IV infusion	No exposure data	First-order output	Tham et al. (2008)
	Irinotecan, MBLI87	IP	No exposure data	First-order output	Sostelly et al. (2014)
	Paclitaxel, nab-paclitaxel, ixabepilone	IV infusion	No exposure data	First-order output	Mehrotra et al. (2017)

Drug action or therapeutic area	Drug	Route	Reasons for DRT	Biophase parameters	Reference
Oncology	Temozolomide	PO	No exposure data	First-order output	Bogdańska et al. (2017); Mazzocco et al. (2015)
Oncology and auto-immune diseases	Monoclonal antibodies (mAbs)[a]	IV and SC	Extensive treatment periods require a very good understanding of the mechanism-of-action (which is not always the case) in order to make use of exposure data	First-order input/output	Lange and Schmidli (2014, 2015)
Osteoporosis	Calcium	PO	No exposure data	First-order output	Ahn et al. (2014)
	Ibandronate	IV infusion and PO	Exposure sampling was avoided to decrease processing time	First-order output	Pillai and Gieschke (2004)
	Bisphosphonate, denosumab	IV infusion and PO	No exposure data	First-order output	van Schaick et al. (2015)
Thermoregualtion	8-OH-DPAT	EV	Demonstrate the utility of DRT	First-order input/output	Gabrielsson et al. (2000)
Thrombocytopenia	Induced by carboplatin and radiation[b]	IV infusion	No exposure data	T_{Tx}—duration of toxic effect	Krzyzanski et al. (2015)
	Romiplostin	SC	No exposure data	First-order output	Perez-Ruixo et al. (2012)

Table 1.1: Summary of published DRT studies—including the drug action or therapeutic area, drug name, administration route, motivation for DRT modelling, and which biophase parameters that were used. The administration routes are abbreviated as follows: IV—intravenous; PO—per os (orally); SC—subcutaneous; EV—extravasuclar; PUL—pulmonary; IVI—intraviteral; IO—intraoccular; IM—intramuscular; IP—intraperitoneally

[a]No specific antibody, but a conceptual article.

[b]Response-time data of platelet counts and endogenous thrombopoietin levels were used.

Chapter 2

Methods and models

This chapter serves to illustrate how to perform dose-response-time (DRT) data analysis. In principle, the study constitutes five fundamental modelling techniques; model selection, identifiability analysis, parameter fitting, sensitivity analysis, and modelevaluation. These techniques will be examined in a logical order—albeit remembering that modelling is an iterative exercise where the modeller goes back and forth until the final model meets some quantitative or qualitative criteria. Since the methods ultimately are designed to be applied in pharmacological studies, particular focus will be on the implementation of the ideas in various examples.

The first section of this chapter covers model selection in a standard DRT data analysis—wherein mean population behaviours are described. Central to these studies is the choice of the biophase function. The biophase generally has a basic structure with, for example, zero- or first-order drug absorption and first-order drug elimination from the biophase. The modelled drug amount in the biophase is subsequently assumed to act as the driver of the pharmacological response via a drug-mechanism function. To successfully choose the PD model with a suitable drug-mechanism function, the response-time data need to be qualitatively analysed and the characteristic response behaviours recognised. The second section of the chapter is devoted to population modelling, where it is demonstrated how a biophase-driven PD model may be extended to incorporate *random effects*. These allow for a quantitative way to assess differences in a population, such as between-subject, inter-study, and inter-occasional variabilities (Bonate, 2011; Davidian, Marie, 2003). To determine such variabilities is of paramount importance in pharmacology since drug behaviours tend

to vary in populations (Mould and Upton, 2012). The section will mainly focus on the nonlinear mixed-effects frameworksince this has been the standard population modelling approach in pharmacology for more than 30 years (Sheiner and Beal, 1980, 1981, 1983). In the subsequent section, the developed models will be subject to an identifiability analysis to verify that the parameter estimation problems are well-posed (Raue et al., 2014). The discussion will encompass both *a priori* and data-based identifiability techniques. The identifiability analysis is followed by a section on different methods for parameter estimation, particularly for nonlinear mixed-effects models. The fourth section will cover sensitivity analysis; a framework that studies how the system output is affected by uncertainties, or perturbations, of the input. Sensitivity analysis techniques will be proven to be useful in both model selection and validation. Finally, tools for validation and diagnostics are examined as ways for quantitative and qualitative evaluation of the analysis.

2.1 Model selection

One of the biggest challenges of developing a DRT model is that the biophase dynamics and the PD need to be assessed simultaneously. Consequently, it may be difficult to distinguish the kinetic and dynamic properties of the drug from each other. More specifically, time-delays in the dose-response data could, for example, be a consequence of rate-limiting absorption or slow onset of the biomarker. To discriminate between the kinetic and dynamic properties, it is important to have a *rich*[1] data set. The data should preferably include multiple dosages and administration routes, as well as careful selection of the dosages (Gabrielsson et al., 2000).

2.1.1 Biophase function

The biophase model is generally simple due to the difficulties associated with identifying a complex kinetic model without exposure data (for identifiability analysis, see Sec. 2.2). More sophisticated biophase models may be used by making prior assessments and fixing some parameter values. The simplicity of the single–compartment biophase model makes it a suitable candidate for describing the biophase dynamics. This model will be slightly modified depending on the drug administration route. If the drug enters directly into the biophase, the input function is that of an intravenous (IV) administration. With a first-order elimination rate from the biophase, denoted by k, the dynamics of the biophase following a direct bolus input or an infusion input are given by

$$\frac{\mathrm{d}A_{\mathrm{b}}(t)}{\mathrm{d}t} = -k \cdot A_{\mathrm{b}}(t) \qquad \text{with} \quad A_{\mathrm{b}}(0) = D \qquad \text{bolus}, \tag{2.1}$$

[1] Obtained from experiments where the system has been properly 'provoked,' thereby revealing the full range of the drug-induced effects.

or

$$\frac{\mathrm{d}A_\mathrm{b}(t)}{\mathrm{d}t} = \mathrm{Inf}(t) - k \cdot A_\mathrm{b}(t) \quad \text{with} \quad A_\mathrm{b}(0) = 0 \qquad \text{infusion,} \tag{2.2}$$

where $A_\mathrm{b}(t)$ is the biophase drug amount, $\mathrm{Inf}(t)$ a function dependent on the infusion protocol, D the drug dose (the models are illustrated in Fig. 2.1a and Fig. 2.1c, respectively). If

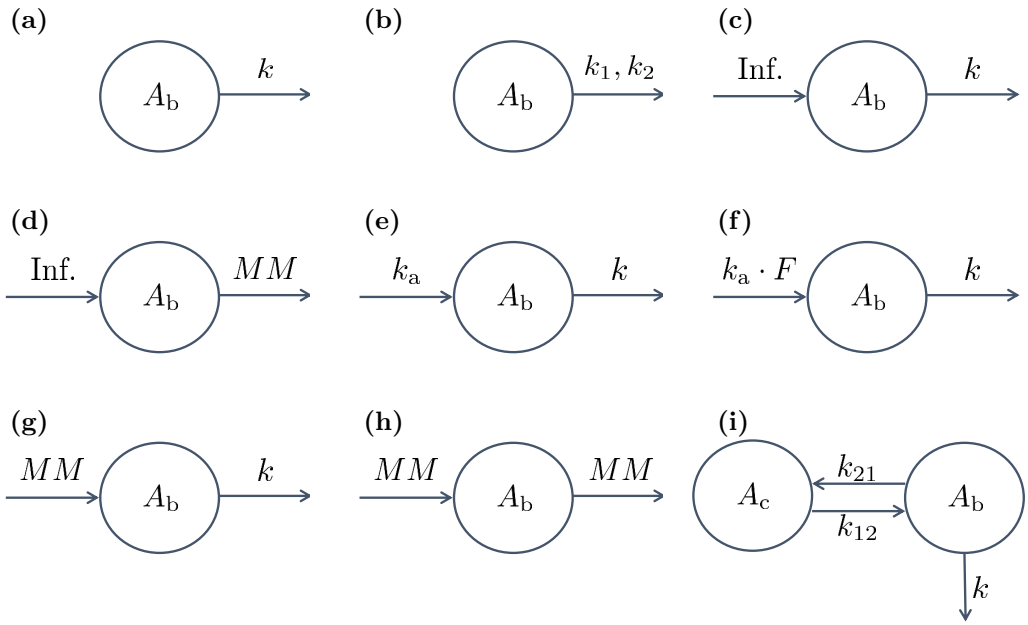

Figure 2.1: Examples drawn from the biophase model library: (a) represents a bolus input and first-order elimination; (b) a bolus input and biphasic first-order elimination; (c) a zero-order input and first-order elimination; (d) a zero-order input and Michaelis-Menten elimination; (e) a first-order input and elimination; (f) a first-order input, scaled by the biophase availability, and first-order elimination; (g) Michaelis-Menten input and first-order elimination; (h) Michaelis-Menten input and elimination; (i) two-compartment model with first-order distribution between the central compartment and the biophase and first-order elimination from the biophase. The parameters A_b, Inf, k, k_a, F and MM represent, respectively, the biophase amount, the constant rate infusion input, the first-order elimination rate constant, the first-order absorption rate constant, the biophase availability and the Michaelis-Menten absorption/elimination process, respectively. All models presented in the library have been applied in published DRT studies (see Table 1.1)

the drug is administered to a peripheral compartment, and subsequently absorbed into the biophase via a first-order process, then the biophase dynamics are given by

$$\frac{\mathrm{d}A_\mathrm{a}(t)}{\mathrm{d}t} = -k_\mathrm{a} \cdot A_\mathrm{a}(t) \qquad \text{with} \quad A_\mathrm{a}(0) = D, \tag{2.3a}$$

$$\frac{\mathrm{d}A_\mathrm{b}(t)}{\mathrm{d}t} = F \cdot k_\mathrm{a} \cdot A_\mathrm{a}(t) - k \cdot A_\mathrm{b}(t) \quad \text{with} \quad A_\mathrm{b}(0) = 0, \tag{2.3b}$$

where $A_{\mathrm{a}}(t)$ is the drug amount in the absorption compartment, k_{a} the first-order absorption rate into the biophase, and F the availability, or the *biophase availability* (Smolen (1971b), model illustrated in Fig. 2.1e). By solving for $A_{\mathrm{a}}(t)$ in Eq. (2.3a), the system can be re-written as

$$\frac{\mathrm{d}A_{\mathrm{b}}(t)}{\mathrm{d}t} = D \cdot F \cdot k_{\mathrm{a}} \cdot e^{-k_{\mathrm{a}}t} - k \cdot A_{\mathrm{b}}(t) \quad \text{with} \quad A_{\mathrm{b}}(0) = 0. \tag{2.4}$$

The aforementioned models are the simplest biophase functions and these have been frequently applied in DRT studies (see Table 1.1). Apart from these models, Andersson et al. (2015) introduced nonlinear absorption/elimination models to describe the biophase dynamics. In their study, an extravascular dose D was absorbed into the biophase via a nonlinear Michaelis-Menten model, which gives the following biophase dynamics

$$\frac{\mathrm{d}A_{\mathrm{a}}(t)}{\mathrm{d}t} = -\frac{V_{\max} \cdot A_{\mathrm{a}}(t)}{K_{\mathrm{m}} + A_{\mathrm{a}}(t)} \qquad \text{with} \quad A_{\mathrm{a}}(0) = D, \tag{2.5a}$$

$$\frac{\mathrm{d}A_{\mathrm{b}}(t)}{\mathrm{d}t} = \frac{V_{\max} \cdot A_{\mathrm{a}}(t)}{K_{\mathrm{m}} + A_{\mathrm{a}}(t)} - k \cdot A_{\mathrm{b}}(t) \quad \text{with} \quad A_{\mathrm{b}}(0) = 0, \tag{2.5b}$$

where $V_{\max}$ is the maximal absorption rate from the absorption compartment and K_{m} the drug amount at which 50% absorption is attained. The biophase elimination could, of course, also be modelled using the nonlinear Michaelis-Menten model. A typical scenario is that the drug amount (or concentration) is measurable in a central compartment (e.g., plasma) but not in the biophase. In cases like these, multi-compartmental biophases could be applied. Such a model could, for example, be characterised in the following way:

$$\frac{\mathrm{d}A_{\mathrm{b}}(t)}{\mathrm{d}t} = k_{12} \cdot A_{\mathrm{c}}(t) - k_{21} \cdot A_{\mathrm{b}}(t) - k \cdot A_{\mathrm{b}}(t) \quad \text{with} \quad A_{\mathrm{b}}(0) = D, \tag{2.6a}$$

$$\frac{\mathrm{d}A_{\mathrm{c}}(t)}{\mathrm{d}t} = k_{21} \cdot A_{\mathrm{b}}(t) - k_{12} \cdot A_{\mathrm{c}}(t) \qquad \text{with} \quad A_{\mathrm{c}}(0) = 0, \tag{2.6b}$$

where $A_{\mathrm{c}}(t)$ is the drug amount in a central compartment, k_{12} and k_{21} are the absorption/elimination rates between the biophase and central compartment, k the elimination rate from the biophase out of the system, and D the drug amount (model illustrated in Fig. 2.1i). Models like the aforementioned have been used by Fisher et al. (1997) among others (Smolen, 1971b; Warwick et al., 1998).

2.1.2 Pharmacodynamic model

The pharmacology literature encompasses a plethora of PD models—aimed at describing different pharmacological phenomena. This section will cover the ones most commonly applied in DRT studies. This includes, for instance, direct and indirect models with linear and nonlinear dose-response relations. For a more thorough discussion on PD modelling, see for example Gabrielsson and Weiner (2010).

The PDs in the DRT framework are assumed to be driven by the biophase amount $A_{\mathrm{b}}(t)$. If there is a rapid equilibrium between the biophase amount and the pharmacological effect then the system can be modelled using a direct response model (Gabrielsson and Weiner,

2010). The simplest possible direct response model assumes a linear effect-amount relation given by

$$E(t) = E_0 \pm \beta \cdot A_{\mathrm{b}}(t), \tag{2.7}$$

where $E(t)$ is the effect, E_0 the baseline, and β the slope parameter. However, the linear dose-response relationship is unbounded and therefore violates basic physiological principles (e.g., a limited receptor pool). The $E_{\max}$ model, on the other hand, has a saturable dose-response relationship as well as physiologically interpretable parameters (Gabrielsson and Weiner, 2010). The standard ($\gamma = 1$) and sigmoidal form of this model are given by

$$E(t) = E_0 \pm \frac{E_{\max} \cdot A_{\mathrm{b}}^{\gamma}(t)}{ED_{50}^{\gamma} + A_{\mathrm{b}}^{\gamma}(t)}, \tag{2.8}$$

where $E_{\max}$ is the maximal drug effect (efficacy), ED_{50} the biophase drug amount at 50% maximal effect (potency), and γ the Hill exponent. The linear and saturable direct response models in Eqs. (2.7) and (2.8) have been applied in several DRT studies (Uehlinger et al., 1992; Port et al., 1998; Bragg et al., 1994; Fisher et al., 1997; Fisher and Wright, 1997; Warwick et al., 1998). To illustrate the connection between the $E_{\max}$-model and ligand-receptor binding, consider the *law of mass action*, which states

$$[L] + [R] \underset{k_{\mathrm{off}}}{\overset{k_{\mathrm{on}}}{\rightleftarrows}} [LR], \tag{2.9}$$

where $[L]$ is the free concentration of a specific ligand, $[R]$ the free concentration of the corresponding receptor, $[LR]$ the free concentration of the receptor-ligand complex, k_{on} the rate constant for association, and k_{off} the rate constant for the dissociation. For the receptor-ligand binding, assume that

- The interaction is reversible.
- The interaction is rapid.
- The receptor has one binding site for the ligand.
- The receptor, ligand, and receptor-ligand complex are in equilibrium.

Under equilibrium, Eq. (2.9) implies that

$$k_{\mathrm{on}}[R][L] = k_{\mathrm{off}}[LR], \tag{2.10}$$

or

$$\frac{[R][L]}{[LR]} = \frac{k_{\mathrm{off}}}{k_{\mathrm{on}}} = K_{\mathrm{d}}, \tag{2.11}$$

where K_{d} is known as the the dissociation constant. Now, assume that a drug-induced effect is proportional to the free concentration of the receptor-ligand complex as

$$E = \alpha \cdot [LR]. \tag{2.12}$$

This implies that the maximal drug-induced effect is given by

$$E_{\max} = \alpha \cdot ([LR] + [R]). \tag{2.13}$$

By taking the fraction of the drug-induced effect and the maximal effect, we get

$$\frac{E}{E_{\max}} = \frac{[LR]}{[LR] + [R]} \tag{2.14}$$

$$= \frac{1}{1 + \frac{[R]}{[LR]}}. \tag{2.15}$$

Using the identity in Eq. (2.11) gives

$$\frac{E}{E_{\max}} = \frac{[L]}{[L] + K_{\mathrm{d}}} \tag{2.16}$$

or

$$E = \frac{E_{\max} \cdot [L]}{[L] + K_{\mathrm{d}}}, \tag{2.17}$$

and we are done. To conclude, under some assumptions, the $E_{\max}$-model may be derived from the law mass action of receptor-ligand binding.

The previous discussion has focused on direct response models. Generally though, the relationship between the biophase drug amount and the pharmacological effect is indirect, whereby turnover models are frequently applied (Dayneka et al., 1993). In a turnover model, the response $R(t)$ is given by

$$\frac{\mathrm{d}R(t)}{\mathrm{d}t} = k_{\mathrm{in}} - k_{\mathrm{out}} \cdot R(t) \quad \text{with} \quad R(0) = R_0, \tag{2.18}$$

where k_{in} and k_{out} are the turnover rate and the fractional turnover rate of the response, respectively, and R_0 the baseline response. Depending on the nature of the drug, its induced effect is typically given by a drug-mechanism function $H(A_{\mathrm{b}}(t))$ that is either stimulatory

$$H(A_{\mathrm{b}}(t)) = S(A_{\mathrm{b}}(t)) = 1 + \frac{S_{\max} \cdot A_{\mathrm{b}}^{\gamma}(t)}{SD_{50}^{\gamma} + A_{\mathrm{b}}(t)^{\gamma}}, \tag{2.19}$$

or inhibitory

$$H(A_{\mathrm{b}}(t)) = I(A_{\mathrm{b}}(t)) = 1 - \frac{I_{\max} \cdot A_{\mathrm{b}}^{\gamma}(t)}{ID_{50}^{\gamma} + A_{\mathrm{b}}^{\gamma}(t)}. \tag{2.20}$$

Here, $S_{\max}$ and $I_{\max}$ represent the maximum stimulatory and inhibitory effect (efficacies), respectively, SD_{50} and ID_{50} are the biophase drug amounts were 50% of the effect is attained (potencies), and γ is the Hill exponent. The stimulatory (displayed in Eq. (2.19)) or inhibitory (displayed in Eq. (2.20)) drug effect acts on the production or loss (or both) of response in Eq. (2.18). For example, a stimulatory effect on the turnover would yield the following relation:

$$\frac{\mathrm{d}R(t)}{\mathrm{d}t} = k_{\mathrm{in}} \cdot S(A_{\mathrm{b}}(t)) - k_{\mathrm{out}} \cdot R(t), \tag{2.21}$$

and an inhibitory effect on the fractional turnover would be given by

$$\frac{\mathrm{d}R(t)}{\mathrm{d}t} = k_{\mathrm{in}} - k_{\mathrm{out}} \cdot I(A_{\mathrm{b}}(t)) \cdot R(t). \tag{2.22}$$

Turnover equations with nonlinear inhibition or stimulation have frequently been applied in DRT studies (see for example Abou Hammoud et al. (2009); Audren et al. (2004); Lalonde and Gaudreault (1999); Gabrielsson et al. (2000); Mikaelian et al. (2013); Wilbaux and He (2014)).

Example 2.1.2.1 Turnover model (Gabrielsson et al., 2000)

In order to illustrate how the characteristic behaviours of a generic response-time data set are extracted, consider the following example where an antinociceptive drug has been given both as an IV bolus (in two different doses of 40 and 80 µg kg^{-1}) and subcutaneously (in three different doses of 50, 100, and 200 µg kg^{-1}) to Sprague-Dawley rats (the data are adapted from Gabrielsson et al. (2000)). Post drug administration, radiant heat is focused on the tail of the rat and the time, in seconds, is measured until the rat removes its tail. The response-time behaviour was observed during 180 min (the data are illustrated in Fig. 2.2). Since the drug was administered via two different routes, we need two separate biophase

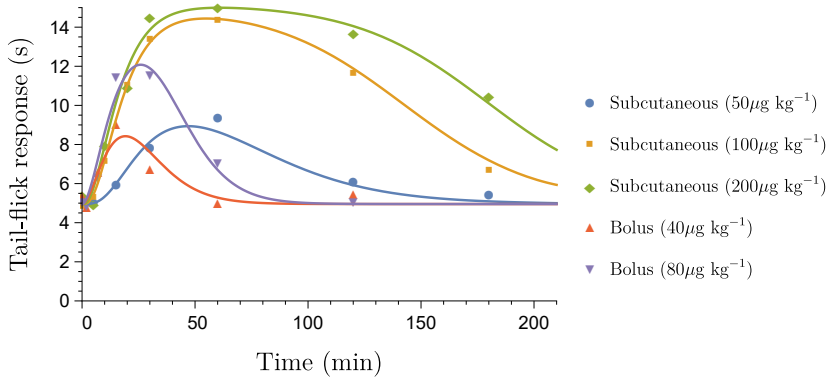

Figure 2.2: Example of response-time data (dots) collected from from five different individuals following IV bolus doses of 40 and 80 µg kg^{-1} and subcutaneous doses of 50, 100, and 200 µg kg^{-1}, respectively, and model simulations of the response (solid lines).

functions. The following functions are selected:

$$\frac{\mathrm{d}A_{\mathrm{b}}(t)}{\mathrm{d}t} = -k \cdot A_{\mathrm{b}}(t) \qquad \text{with} \quad A_{\mathrm{b}}(0) = D_{IV} \qquad \text{bolus}, \tag{2.23}$$

and

$$\frac{\mathrm{d}A_{\mathrm{b}}(t)}{\mathrm{d}t} = D_{SC} \cdot k_{\mathrm{a}} \cdot e^{-k_{\mathrm{a}}t} - k \cdot A_{\mathrm{b}}(t) \qquad \text{with} \quad A_{\mathrm{b}}(0) = 0 \qquad \text{subcut.}, \tag{2.24}$$

where k and k_{a} are the first-order elimination and absorption rates of the biophase, respectively, whilst D_{SC} and D_{IV} represent the subcutaneous and bolus (intravenous) drug dose, respectively. Now, by inspection of the response-time data, there appears to be a constant baseline response. Moreover, the onset of response is not instantaneous, and, thus a turnover model is needed. Furthermore, there is a peak-shift between the two IV doses[2], indicating a nonlinear stimulatory drug-mechanism function. Gabrielsson et al. (2000) concluded that the following PD model is a suitable choice

$$\frac{\mathrm{d}R(t)}{\mathrm{d}t} = k_{\mathrm{in}} \cdot \left(1 + \frac{S_{\max} \cdot A_{\mathrm{b}}^{\gamma}(t)}{SD_{50}^{\gamma} + A_{\mathrm{b}}^{\gamma}(t)}\right) - k_{\mathrm{out}} \cdot R(t) \quad \text{with} \quad R(0) = R_0, \tag{2.25}$$

where k_{in} and k_{out} are the turnover and fractional turnover rates of the response, respectively, R_0 is the baseline response, $S_{\max}$ the efficacy, SD_{50} the potency, and γ the Hill exponent.

In cases where the turnover rate, or fractional turnover rate, is saturable, the standard turnover model of Eq. (2.18) can be expanded to incorporate nonlinear elimination and/or production. In particular, Gabrielsson and Peletier (2014), applied a saturable elimination model to the describe locomotor activity, following treatment with dexamphetamine. In their study, the response was given by

$$\frac{\mathrm{d}R(t)}{\mathrm{d}t} = S(A_{\mathrm{b}}(t)) - k_{\mathrm{out,max}} \frac{R(t)}{K_{\mathrm{m}} + R(t)} \quad \text{with} \quad R(0) = 0, \tag{2.26}$$

where $S(A_{\mathrm{b}}(t))$ is a stimulative drug-mechanism function, $k_{\mathrm{out,max}}$ the maximal fractional turnover of $R(t)$, and K_{m} the response at 50% maximal turnover rate.
Some drugs experience time-delays in their onset. In cases like these, a transduction pathway with additional compartments can be added to the turnover model in Eq. (2.18) to capture the time-delay:

$$\begin{cases} \dfrac{\mathrm{d}R_1(t)}{\mathrm{d}t} = k_{\mathrm{in}} \cdot H(A_{\mathrm{b}}(t)) - k_{\mathrm{out}} \cdot R_1(t) & \text{with} \quad R_1(0) = R_0, \\ \qquad \vdots & \qquad \vdots \\ \dfrac{\mathrm{d}R_i(t)}{\mathrm{d}t} = k_{\mathrm{out}} \cdot (R_{i-1}(t) - R_i(t)) & \text{with} \quad R_i(0) = R_0, \quad i = 2, \ldots, n. \end{cases} \tag{2.27}$$

[2] That is, the peak of the lower IV dose appear to occur after ∼20 min while the peak of the higher dose appear to occur after ∼30 min.

Here, n is the number of steps in the transduction pathway and $R_n(t)$ is the measured response. The transduction compartment model has been used by, for example, Krzyzanski et al. (2015) among others (Gabrielsson and Peletier, 2014; Hamberg et al., 2013; Perez-Ruixo et al., 2012; Ramon-Lopez et al., 2009).
For physiological systems that exhibit feedback behaviours, displayed as rebound and/or overshoot in the response dynamics, a moderator model has been suggested by Gabrielsson et al. (2000) among others (Andersson et al., 2015; Luu et al., 2009; Isaksson et al., 2009; Gabrielsson and Peletier, 2014)). In the moderator model, the response affects the moderator via a first-order process

$$\begin{cases} \dfrac{\mathrm{d}M_1(t)}{\mathrm{d}t} = k_{\mathrm{tol}} \cdot (R(t) - M_1(t)) & \text{with} \quad M_1(0) = M_0, \\ \qquad \vdots & \qquad \vdots \\ \dfrac{\mathrm{d}M_i(t)}{\mathrm{d}t} = k_{\mathrm{tol}} \cdot (M_{i-1}(t) - M_i(t)) & \text{with} \quad M_i(0) = M_0, \quad i = 2, \ldots, n, \end{cases} \tag{2.28}$$

where k_{tol} is the turnover rate of the moderator, M_0 the moderator baseline (typically $M_0 = R_0$), and n the number of moderator compartments (n depends on the magnitude of the feedback mechanisms). The feedback impacts the turnover or fractional turnover (or both) of response in equation (2.18). For example, a feedback mechanism that directly triggers a decrease in the turnover, and slowly triggers an increase in the fractional turnover, of response would be given by

$$\frac{\mathrm{d}R(t)}{\mathrm{d}t} = k_{\mathrm{in}} \cdot \frac{M_0}{M_1} - k_{\mathrm{out}} \cdot \frac{M_n}{M_0} \cdot R(t) \quad \text{with} \quad R(0) = R_0. \tag{2.29}$$

The models presented here and, in the first section, are applicable when the modeller wants to describe a single one-to-one relation between dose and response. This is sufficient if each dose-group comprises a single individual, or when the primary aim is to describe population mean behaviour. However, there are situations in which individual variations in the dose-response relationship need to be quantified (this is specifically relevant in clinical studies). In order to do this, a population modelling framework needs to be applied. The models that have been presented up to know will from here on be referred to as the *base structure* in a population model. The additional components that are introduced in the next section constitute the *statistical model*.

2.1.3 Mixed-effects modelling

Kinetic and dynamic drug properties are prone to vary between individuals with in a population (Mould and Upton, 2012). The distinctive traits of an individual, such as sex, weight, age, etc., affect the physiology and thereby the pharmacology (Bonate, 2011). The extent to which these variations influence the pharmacology needs to be quantified to ensure drug safety and efficacy throughout the population. The naïve approach in establishing between-subject variability is performed in two stages; first, the pharmacological model

is fitted on an individual level, through which parameter estimates are obtained for each subject. In the second stage, some form of regression analysis is performed on the resulting parameter distributions. From this analysis, the modeller may draw statistical inference about the system. This approach is known as the standard two-stage (STS) (Bonate, 2011) method. The disadvantage of using the STS method is that information is lost, and variability added, in the intermediate step. Moreover, the method is constrained by the assumption that individual data are rich enough whereby parameter estimations can be performed in a practically identifiable manner (see Sections 2.2 and 2.3 for parameter identifiability and estimation, respectively). Due to these limitations of the STS method, another framework is often required for quantifying population characteristics.

The nonlinear mixed-effects (NLME) method performs the two stages of the STS method simultaneously, thereby alleviating the problems associated with the STS approach (Bonate, 2011). The title *mixed effects* refers to the fact that the model has both *fixed effects* and *random effects*. The fixed effects refer to parameters that are shared throughout the population, while the random effects introduce between-subject variations. A NLME state-space model is defined in the following way:

$$\dot{\boldsymbol{x}}_i(t) = \boldsymbol{f}(\boldsymbol{x}_i(t), \boldsymbol{u}_i(t), \boldsymbol{\phi}_i) \qquad \text{with} \quad \boldsymbol{x}_i(0) = \boldsymbol{x}_0(\boldsymbol{\phi}_i), \tag{2.30a}$$

$$\boldsymbol{y}_{ij} = \boldsymbol{h}(\boldsymbol{x}_i(t_j), \boldsymbol{u}_i(t_j), \boldsymbol{\phi}_i) + \boldsymbol{e}_{ij} \quad \text{for} \quad i = 1, \ldots, N, \tag{2.30b}$$

where $\boldsymbol{x}_i(t) \in \mathbb{R}^n$ represents the state variables for the ith individual (e.g., biophase amounts, PD responses), $\boldsymbol{y}_{ij} \in \mathbb{R}^m$ the observations of the system at times t_j (i.e., the data), $\boldsymbol{u}_i(t) \in \mathbb{R}^q$ the input functions (e.g., IV or PO doses), $\boldsymbol{\phi}_i \in \mathbb{R}^r$ the parameters, $\boldsymbol{x}_0$ the initial conditions, $\boldsymbol{e}_{ij} \sim \mathcal{N}(\boldsymbol{0}, \boldsymbol{R}(\boldsymbol{x}_i(t_j), \boldsymbol{u}_i(t_j), \boldsymbol{\phi}_i))$ the *residual variabilities* (e.g., measurement noise, model misspecification), and N the number of individuals in the population. The vector-valued function $\boldsymbol{f}(\boldsymbol{x}_i(t), \boldsymbol{u}_i(t), \boldsymbol{\phi}_i)$ describes the dynamics of the system and $\boldsymbol{h}(\boldsymbol{x}_i(t), \boldsymbol{u}_i(t), \boldsymbol{\phi}_i)$ characterises the system observations—both functions are assumed to be smooth. The parameters of the ith individual $\boldsymbol{\phi}_i$ have a functional relation to the fixed effects $\boldsymbol{\theta} \in \mathbb{R}^p$ via

$$\boldsymbol{\phi}_i = \boldsymbol{g}(\boldsymbol{\theta}, \boldsymbol{Z}_i, \boldsymbol{\eta}_i), \tag{2.31}$$

where the $\boldsymbol{Z}_i$ are the individual covariates (e.g., sex, age, weight) and $\boldsymbol{\eta}_i$ the random effects, which are usually assumed to be multivariate Gaussian $\boldsymbol{\eta}_i \sim \mathcal{N}(\boldsymbol{0}, \boldsymbol{\Omega})$ (Grimmett and Stirzaker, 2002) with covariance matrix $\boldsymbol{\Omega} \in \mathbb{R}^{s \times s}$ (s represents the number of random effects). The vector-valued function $\boldsymbol{g}$ is assumed to be smooth with respect to its arguments. As an example, consider a drug with PK properties that vary between subjects. Assume that the clearance of the ith individual is given by

$$Cl_i = \alpha \cdot \text{weight}_i^{\beta}, \tag{2.32}$$

and the volume of distribution given by

$$V_i = V_\mu \cdot e^{\eta_{V_i}}. \tag{2.33}$$

In this example, $Cl_i, V_i \in \boldsymbol{\phi}_i$ are individual parameters, $\alpha, \beta, V_\mu \in \boldsymbol{\theta}$ fixed effects, $\eta_{V_i} \in \boldsymbol{\eta}_i$ a random effect, and $\text{weight}_i \in Z_i$ a covariate. Since η_{V_i} is normally distributed, Eq. (2.33) implies that the volume of distribution is log-normally distributed in the population. This is a common assumption for PK parameters, particularly due to the positive support of the log-normal distribution (Bonate, 2011). Apart from between-subject variability, the NLME framework allows for inter-study and/or inter-occasion variabilities. These variabilities are typically considered in drug trials that are conducted over extended periods of time, and in meta-analyses, wherein data are collected from several studies (Bonate, 2011). Inter-study and inter-occasion variabilities may manifest themselves on either of the fixed or random effects, or both. As an example, assume that data have been collected from S different studies. If a model parameter is log-normally distributed, with standard deviations that vary between the studies (i.e., differences in the random effects), then the parameter of the ith individual ϕ_i is given by

$$\phi_i = \theta_\mu \cdot \exp(\eta_i + \eta_1 \cdot \text{Study}_1 + \ldots + \eta_S \cdot \text{Study}_S) \tag{2.34}$$

where θ_μ is the fixed effect, η_i and $\eta_1, \ldots, \eta_S$ are random effects and

$$\text{Study}_\text{k} = \begin{cases} 1 & \text{if individual } i \text{ is in study group } k \\ 0 & \text{otherwise.} \end{cases} \tag{2.35}$$

Similarly, if the fixed effects differ, but the random effects stay fixed, the parameter for the ith individual is given by

$$\phi_i = (\theta_\mu + \theta_1 \cdot \text{Study}_1 + \ldots + \theta_S \cdot \text{Study}_S) \cdot \exp(\eta_i), \tag{2.36}$$

where θ_μ and $\theta_1, \ldots, \theta_S$ are fixed effects and η_i is a random effect. Inter-occasional variability is modelled in the exact same way as inter-study variability.

The remaining, unexplained discrepancy between the observed and predicted system behaviour is referred to as the *residual variability*. The occurrence of this variability is generally a consequence of model misspecification and measurement noise. Residual variability is modelled in a couple of different ways—often dependent upon the types of observation. With an observed response $R_i(t)$ and predicted response $\widehat{R}_i(t)$, the residual variability is typically additive

$$R_i(t) = \widehat{R}_i(t) + e_i(t) \tag{2.37}$$

or proportional

$$R_i(t) = \widehat{R}_i(t)(1 + e_i(t)) \tag{2.38}$$

or a combination of them

$$R_i(t) = \widehat{R}_i(t)(1 + e_{i1}(t)) + e_{i2}(t). \tag{2.39}$$

As a rule of thumb, the proportional model is applied when the observations vary substantially in magnitude (for example, drug exposure is often measured on a log-scale with 10-fold differences between the maximal and minimal exposure), whilst the additive model is applied when the observations vary little around a constant baseline. The variabilities are assumed to be Gaussian $\boldsymbol{e}_i \sim \mathcal{N}(\boldsymbol{0}, \boldsymbol{R}(\boldsymbol{x}_i(t), \boldsymbol{u}_i(t), \boldsymbol{\phi}_i))$, often uncorrelated and time-independent. This implies that $e_{ik} \sim \mathcal{N}(0, \sigma^2)$, for the kth variability and where σ is the standard deviation. Generally, one assumes that the posed model accurately describes the pharmacology and that any deviations are solely due to noisy data (Leander et al., 2014, 2015). This is a very strong assumption, yet is frequently made (typically for convenience). An alternative way is to try to quantify the model misspecification by applying stochastic differential equations (SDE's) (rather than ordinary differential equations). In the SDE framework, the dynamical model uncertainties are estimated—besides the aforementioned sources of variability (for an introduction to SDE's see Klebaner (2005) and for examples in pharmacology see Leander et al. (2014, 2015)).

2.1.3.1 Modelling random effects

The naïve way of modelling random effects in an NLME model is to assume that all parameters vary between individuals. However, as the number of additional parameters—introduced by including random effects—grow as n^2 (n being the number of random effects) this exhaustive strategy is often infeasible. In fact, the number of random effects is constrained by the quantity and quality of the data and the choice of estimation algorithm (for details on the performance of different estimation algorithms, see Plan et al. (2012)). As data are often limited, a subset of the model parameters needs to be selected for estimation on an individual level. This is a non-trivial task that will be addressed in the following discussion:
In the ideal situation (i.e., in the case of sufficiently rich data and utilising an optimal estimation algorithm), random effects may be included in all of the parameters. The parameter estimation will then reveal if any of the random effects are superfluous. Redundancy is inferred by inspecting the covariance matrix where entries and eigenvalues that are close to zero indicate that the model is (probably) over-parametrised (Pinheiro et al., 1995). With an over-parametrised model, reductions are made by removing the random effects that have corresponding eigenvalues close to zero.
If the data are not sufficiently rich, whereby a full covariance matrix cannot be estimated, a simple diagonal matrix may be applied. The parameters are then estimated and the

correlation between the *empirical Bayes estimates* (EBE) (i.e., the individual parameters ϕ_i) is investigated to determine if any of the random effects are correlated. If correlations are apparent, the corresponding entries in the covariance matrix may be added whereby the matrix, and the other parameters, are re-estimated.
However, the extent of the data often prohibits random effects to be added to all system parameters (even in the case of a simple covariance matrix). In this case, insightful knowledge of the physiology and pharmacology may prove useful. When applying a semi-mechanistic model, it might be biologically justified to keep some parameters fixed in a population and vice versa for varying parameters. However, if the modeller lacks a deeper understanding of the system, an *a priori* sensitivity analysis (see Sec. 2.4)—wherein the impact the respective parameters have on the system output is quantified—often provides a valuable tool. If the model output is sensitive to changes in a specific parameter, this may indicate that this parameter should include a random effect to enhance the model's ability to pick up different variabilities and to make the system more flexible. However, the system sensitivity is analysed at a specific point in the parameter space, which in turn is chosen by graphically analysing the data, from prior physiological knowledge, and/or from model simulations. Consequently, the approach is crude and only holds locally.

Example 2.1.3.2 Mixed-effects turnover model

This example demonstrates how the NLME framework is implemented given a standard response-time data set—generated by simulation. The example is inspired by the study by Urquhart and Li (1969b) on adrenocortisol secretion following administration of the hormone adrenocorticotropin (ACTH). The ACTH affects the secretion rate of cortisol, and has been given for 6 h as constant-rate IV infusion to eight separate individuals. These individuals demonstrate different responses to the drug (the data are illustrated in Fig. 2.3).

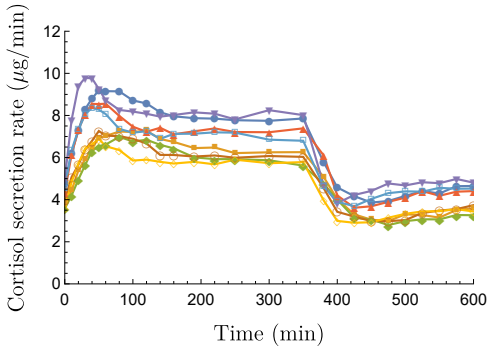

Figure 2.3: Example of cortisol secretion rate response-time data collected from from eight different individuals following IV infusions of ACTH 6 h. The data were simulated (inspired by the study by Urquhart and Li (1969b)).

It is assumed that the drug enters directly into the biophase and that it follows a first-order elimination process. The biophase dynamics are then given by

$$\frac{\mathrm{d}A_{\mathrm{b}}(t)}{\mathrm{d}t} = \mathrm{Inf}(t) - k \cdot A_{\mathrm{b}}(t) \quad \text{with} \quad A_{\mathrm{b}}(0) = 0, \tag{2.40}$$

where k is the first-order elimination rate from the biophase and $\mathrm{Inf}(t)$ the drug infusion function. $\mathrm{Inf}(t)$ is implemented as a step-function with magnitude corresponding to the infusion rate. By inspecting the response-time data it is apparent that the drug effect is stimulative. Furthermore, the initial time-delay suggests an indirect dose-response relationship whilst the post-infusion data indicate that there is a constant baseline. Due to the indirect response, we choose to describe the response dynamics using a turnover model. Now, by inspecting the initial onset and the post-infusion drop in response, there is an apparent tendency for the response to overshoot and rebound. These typical feedback characteristics are implemented using a moderator compartment that will act on the fractional turnover of the response. Thus, the resulting PD model is given by

$$\frac{\mathrm{d}R(t)}{\mathrm{d}t} = k_{\mathrm{in}} \cdot \left(1 + \frac{S_{\max} \cdot A_{\mathrm{b}}(t)}{SD_{50} + A_{\mathrm{b}}(t)}\right) - k_{\mathrm{out}} \cdot \frac{M(t)}{R_0} \cdot R(t) \quad \text{with} \quad R(0) = R_0, \tag{2.41}$$

and

$$\frac{\mathrm{d}M(t)}{\mathrm{d}t} = k_{\mathrm{tol}} \cdot (R(t) - M(t)) \quad \text{with} \quad M(0) = R_0, \tag{2.42}$$

where k_{in} and k_{out} are the turnover and fractional turnover rate, respectively, R_0 the baseline response, SD_{50} the potency, $S_{\max}$ the efficacy, and k_{tol} the moderator turnover rate. The model described by Eqs. (2.40), (2.41), and (2.42) constitutes the base structure of the NLME model. Assuming that $R(t)$ and $M(t)$ initially are at steady-state with $R(t) = R_0$ and $M(t) = R_0$, the turnover rate k_{in} may be eliminated as $\mathrm{d}R/\mathrm{d}t = 0$ implies that

$$0 = k_{\mathrm{in}} \cdot \left(1 + \frac{S_{\max} \cdot A_{\mathrm{b}}(t)}{SD_{50} + A_{\mathrm{b}}(t)}\right) - k_{\mathrm{out}} \cdot \frac{M(t)}{R_0} \cdot R(t), \tag{2.43}$$

and so at $t = 0$

$$0 = k_{\mathrm{in}} - k_{\mathrm{out}} \cdot R_0, \tag{2.44}$$

whereby

$$k_{\mathrm{in}} = k_{\mathrm{out}} \cdot R_0. \tag{2.45}$$

Consequently, the remaining fixed effects $\boldsymbol{\theta}$ are given by the vector

$$\boldsymbol{\theta} = \begin{bmatrix} k \\ k_{\text{out}} \\ R_0 \\ SD_{50} \\ S_{\max} \\ k_{\text{tol}} \end{bmatrix}. \tag{2.46}$$

The statistical part of the NLME model will comprise a number of random effects. Now, efficacy is a drug-specific property that is assumed to be fixed in the population. The remaining parameters are assumed to be log-normally distributed[3]. The individual parameters for the ith individual ($i = 1 \dots 8$) are given by

$$k_i = k \cdot e^{\eta_{ki}} \tag{2.47a}$$

$$k_{\text{out}i} = k_{\text{out}} \cdot e^{\eta_{k_{\text{out}}i}} \tag{2.47b}$$

$$R_{0i} = R_0 \cdot e^{\eta_{R_0 i}} \tag{2.47c}$$

$$SD_{50i} = SD_{50} \cdot e^{\eta_{SD_{50}i}} \tag{2.47d}$$

$$k_{\text{tol}i} = k_{\text{tol}} \cdot e^{\eta_{k_{\text{tol}}i}} \tag{2.47e}$$

where k, k_{out}, R_0, SD_{50}, and k_{tol} are the fixed effects. Let $\boldsymbol{\eta}_i$ be the random effects for the ith individual, given by

$$\boldsymbol{\eta}_i = \begin{bmatrix} \eta_{ki} \\ \eta_{k_{\text{out}}i} \\ \eta_{R_0 i} \\ \eta_{SD_{50}i} \\ \eta_{k_{\text{tol}}i} \end{bmatrix}. \tag{2.48}$$

Then, $\boldsymbol{\eta}_i \sim \mathcal{N}(\mathbf{0}, \boldsymbol{\Omega})$ with

$$\boldsymbol{\Omega} = \begin{bmatrix} \omega_k^2 & \omega_{kk_{\text{out}}} & \omega_{kR_0} & \omega_{kSD_{50}} & \omega_{kk_{\text{tol}}} \\ \omega_{k_{\text{out}}k} & \omega_{k_{\text{out}}}^2 & \omega_{k_{\text{out}}R_0} & \omega_{k_{\text{out}}SD_{50}} & \omega_{k_{\text{out}}k_{\text{tol}}} \\ \omega_{R_0k} & \omega_{R_0k_{\text{out}}} & \omega_{R_0}^2 & \omega_{R_0SD_{50}} & \omega_{R_0k_{\text{tol}}} \\ \omega_{SD_{50}k} & \omega_{SD_{50}k_{\text{out}}} & \omega_{SD_{50}R_0} & \omega_{SD_{50}}^2 & \omega_{SD_{50}k_{\text{tol}}} \\ \omega_{k_{\text{tol}}k} & \omega_{k_{\text{tol}}k_{\text{out}}} & \omega_{k_{\text{tol}}R_0} & \omega_{k_{\text{tol}}SD_{50}} & \omega_{k_{\text{tol}}}^2 \end{bmatrix}. \tag{2.49}$$

As covariance matrices are symmetric, the off-diagonal entries (i.e., the correlations) will satisfy $\omega_{k_{\text{out}}R_0} = \omega_{R_0k_{\text{out}}}$, $\omega_{k_{\text{out}}SD_{50}} = \omega_{SD_{50}k_{\text{out}}}$, and so forth.

[3] This parameter distribution is chosen due to its positive support, which is generally expected for the parameters of a turnover model.

Finally, since the response-time relationship experiences relatively small deviations around a constant baseline, an additive residual error model is chosen. Consequently, the observations are assumed to relate to the model response $R(t)$ as

$$y_{ij} = R(t_j) + e_{ij} \quad \text{where} \quad i = 1, \ldots, 8, \quad j = 1, \ldots, n_i, \tag{2.50}$$

and $e_{ij} \sim \mathcal{N}(0, \sigma^2)$.
The chosen NLME model comprises several parameters. In particular, the covariance matrix alone has 10 unique ones. It remains to examine if all of these can be estimated given the quality and quantity of the data available. However, before that, it must be ensured that the parameters are identifiable.

2.2 Parameter identifiability

In order for a parameter estimation problem to be well-posed, the parameters need to be uniquely defined by the input-output relation[4] of the model. A model for which this holds is known to be *structural identifiable*. For a formal definition, consider a state-space model given by

$$\dot{\boldsymbol{x}}(t) = \boldsymbol{f}(\boldsymbol{x}(t), \boldsymbol{u}(t), \boldsymbol{\theta}) \quad \text{with} \quad \boldsymbol{x}(0) = \boldsymbol{x}_0 = \boldsymbol{g}(\boldsymbol{\theta}), \tag{2.51a}$$

$$\boldsymbol{y}(t) = \boldsymbol{h}(\boldsymbol{x}(t), \boldsymbol{u}(t), \boldsymbol{\theta}), \tag{2.51b}$$

where $\boldsymbol{x}(t) \in \mathbb{R}^n$ represents the state variables (e.g., biophase amounts, PD responses), $\boldsymbol{y}(t) \in \mathbb{R}^m$ the observations of the system (i.e. the data), $\boldsymbol{u}(t) \in \mathbb{R}^q$ the input functions (e.g., IV or PO doses), $\boldsymbol{\theta} \in \boldsymbol{\Theta} \subset \mathbb{R}^p$ the system parameters (e.g., potencies, efficacies, turnover rates—here, $\boldsymbol{\Theta}$ is the feasible parameter space), and where the vector-valued functions $\boldsymbol{f}, \boldsymbol{g}$ and $\boldsymbol{h}$ are smooth with respect to their respective arguments. Assuming ideal, noise free observations, the system defined by Eqs. (2.51a) and (2.51b) is said to be *structurally globally identifiable* at $\boldsymbol{\theta} \in \boldsymbol{\Theta}$ if $\bar{\boldsymbol{\theta}} \in \boldsymbol{\Theta}$ and $\boldsymbol{y}(t, \boldsymbol{\theta}) = \boldsymbol{y}(t, \bar{\boldsymbol{\theta}})$ (for all t) imply that $\boldsymbol{\theta} = \bar{\boldsymbol{\theta}}$. If this property holds in a neighbourhood of $\boldsymbol{\theta}$ then the model is said to be *locally identifiable* at $\boldsymbol{\theta}$ (Anguelova et al., 2012; Raue et al., 2014; Yates et al., 2009). Moreover, the model itself is said to be *structurally globally/locally identifiable* if the previous statements hold for any generic $\boldsymbol{\theta} \in \boldsymbol{\Theta}$. If this is not the case, the model is *structurally non-identifiable* (or *unidentifiable*).

Example 2.2.0.1 Non-identifiable PK model

A well-known example of an unidentifiable PK model is the one-compartment absorption model following oral administration. Given a dose D, the concentration of the central

[4] Provided that the input and output functions satisfy some conditions of 'persistence of excitation' (see Bellman and Åström, 1970 (Bellman and Åström, 1970)).

compartment $C(t)$ is given by

$$V \cdot \frac{\mathrm{d}C(t)}{\mathrm{d}t} = D \cdot F \cdot k_\mathrm{a} \cdot e^{-k_\mathrm{a} t} - Cl \cdot C(t) \quad \text{with} \quad C(0) = 0, \tag{2.52}$$

where F is the bioavailability, k_a the absorption rate, Cl the clearance, and V the volume of distribution. This equation can be solved analytically as

$$C(t) = \frac{D \cdot F \cdot k_\mathrm{a}}{V \cdot (k_\mathrm{a} - k_\mathrm{e})}(e^{-k_\mathrm{e} t} - e^{-k_\mathrm{a} t}), \tag{2.53}$$

where $k_\mathrm{e} = Cl/V$. Given the relation between D and $C(t)$ in Eq. (2.53), it is trivial to see that the degrees of freedom of the system can be reduced, without any loss of generality, by replacing the fraction F/V with a parameter α. Hence, the individual parameters F and V (but not their fraction) are non-identifiable, as is the model (by definition). Yet, the parameters k_a and k_e are locally identifiable, and the model as a whole is structurally identifiable if re-parameterised with α or by fixating any of the parameters F or V. Given a non-identifiable model, multiple sets of parameters will yield the same response behaviour, rendering any interpretations of the estimates futile. Even if the estimation procedure converges and an optimal solution is found—with high accuracy and precision in the parameter estimates—the model might still be non-identifiable (Janzén, 2016). Thus, convergence is not a guarantee for identifiability and an *a priori* analysis is advised. Model non-identifiability may be resolved by, for example, fixing some of the parameters or by performing additional measurements or experiments (Janzén, 2016). In the case of the one-compartment absorption model given by Eq. (2.53), identifiability may be attained by, for example, fixing the bioavailability to one. Alternatively, additional experiments with IV drug administration may be conducted.

Although structural identifiability is a necessary condition for parameter identification, it is not sufficient to guarantee a successful estimation. In fact, the model might still be *practically non-identifiable* (Raue et al., 2009; Janzén, 2016), i.e., the parameter estimates cannot be determined—with acceptable precision and accuracy—given the available data. Practical non-identifiability can occur when, for example, the quality of the data is low and/or when the system has not been sufficiently 'excited' [5] (Raue et al., 2014).

2.2.1 Identifiability methods

Identifiability analysis can be performed using various methods and software (Raue et al., 2014). The following discussion will cover the fundamental concepts of two different *a priori* identifiability analysis approaches, with corresponding references to software where these are implemented. An additional data-driven identifiability method will be discussed in Sec. 2.3.

[5] The system could have been challenged with poorly chosen dosages (for example, exposures way below or way above the drug potency).

2.2.1.1 Input-output relation

Assume a general state-space model, as presented in Eqs. (2.51a) and (2.51b), with functional dependencies $\boldsymbol{f}$, $\boldsymbol{g}$, and $\boldsymbol{h}$ that are rational or polynomial in their respective arguments. By repeatedly differentiating the output function, the state variables of this model can be eliminated to obtain an input-output representation of the system, depending only on $\boldsymbol{u}(t)$ and $\boldsymbol{y}(t)$ and their derivatives. This representation can be expressed as a polynomial, with monomials that are algebraically dependent and arise from a differential ring (Bellu et al., 2007) generated by the output functions $\boldsymbol{y}(t)$. This polynomial is in turn parametrised by rational expressions in $\boldsymbol{\theta}$. By introducing an auxiliary parameter $\bar{\boldsymbol{\theta}}$ in the input-output relation, the coefficients of the monomials can be pair-wise compared to establish if they are linearly independent and that $\boldsymbol{\theta} = \bar{\boldsymbol{\theta}}$, which will imply global identifiability of the model.

Example 2.2.1.2 Identifiable turnover model

As an example, we derive the input-output relation of the following DRT model

$$\frac{\mathrm{d}A_\mathrm{b}(t)}{\mathrm{d}t} = -k \cdot A_\mathrm{b} \quad \text{with} \quad A_\mathrm{b}(0) = D, \tag{2.54}$$

and

$$\frac{\mathrm{d}R(t)}{\mathrm{d}t} = k_\mathrm{in} - (1 + \alpha \cdot A_\mathrm{b}(t)) \cdot k_\mathrm{out} \cdot R(t) \quad \text{with} \quad R(0) = R_0, \tag{2.55}$$

where $A_\mathrm{b}(t)$ is the biophase amount, $R(t)$ the PD response, k the biophase turnover rate, k_in and k_out the turnover and fractional turnover rate of the response, respectively, α the slope parameter, R_0 the baseline response, and D the bolus drug dose. In this case, D is the known input and $y(t) = R(t)$ is the measured output. It is trivial to see that the parameter R_0 is identifiable as $y(0) = R_0$. We will therefore exclude R_0 in the following input-output analyis. Now, by replacing $R(t)$ with $y(t)$ in Eq. (2.55) and differentiating we get

$$\ddot{y}(t) = -\alpha \cdot \dot{A}_\mathrm{b}(t) \cdot k_\mathrm{out} \cdot y(t) - (1 + \alpha \cdot A_\mathrm{b}(t)) \cdot k_\mathrm{out} \cdot \dot{y}(t). \tag{2.56}$$

Eqs. (2.54) and (2.55) allow us to re-write $A_\mathrm{b}(t)$ and $\dot{A}_\mathrm{b}(t)$ in terms of $R(t)$, and thereby in terms of $y(t)$, as

$$A_\mathrm{b}(t) = \frac{k_\mathrm{in} - \dot{y}(t) - k_\mathrm{out} \cdot y(t)}{k_\mathrm{out} \cdot \alpha \cdot y(t)}, \tag{2.57}$$

and

$$\dot{A}_\mathrm{b}(t) = -k \cdot \frac{k_\mathrm{in} - \dot{y}(t) - k_\mathrm{out} \cdot y(t)}{k_\mathrm{out} \cdot \alpha \cdot y(t)}. \tag{2.58}$$

Substitution of Eqs. (2.57) and (2.58) in Eq. (2.56) gives

$$\ddot{y}(t) \cdot y(t) + (k_{\text{in}} - \dot{y}(t)) \cdot \dot{y}(t) + k \cdot \dot{y}(t) \cdot y(t) + k \cdot k_{\text{out}} \cdot y(t)^2 - k \cdot k_{\text{in}} \cdot y(t) = 0, \quad (2.59)$$

which represents a reduced output relation[6], independent of the remaining state variables. Assume that there exists another set of parameters $\bar{\boldsymbol{\theta}}$ given by

$$\bar{\boldsymbol{\theta}} = \{\bar{k}, \bar{k}_{\text{in}}, \bar{k}_{\text{out}}, \bar{\alpha}\}, \quad (2.60)$$

that satisfies Eq. (2.59). By comparing the coefficients of the corresponding monomials we obtain

$$k = \bar{k}, \quad (2.61a)$$

$$k_{\text{in}} = \bar{k}_{\text{in}}, \quad (2.61b)$$

$$k \cdot k_{\text{out}} = \bar{k} \cdot \bar{k}_{\text{out}}, \quad (2.61c)$$

$$\vdots$$

From the Eqs. (2.61a) to (2.61c) it follows that k, k_{in}, and k_{out} are uniquely identifiable. Knowing this, Eq. (2.55) yields that α also is uniquely identifiable. Thus, the model is globally structurally identifiable.

The advantages of the input-output method are that it can be applied to determine global, local, or non-identifiability. Furthermore, the method performs *a priori* identifiability, where no data are needed (Janzén, 2016). However, the method is very computationally expensive for high dimensional nonlinear systems, in terms of calculation time (Raue et al., 2014). An implemented MAPLE version have been presented by Forsman (1991) and Evans et al. (2013). Moreover, the approach has been implemented in similar way in the software DAISY (Differential Algebra for Identifiability of SYstems) (Bellu et al., 2007).

2.2.1.3 Exact arithmetic rank approach

Before presenting the exact arithmetic rank (EAR) method, we will consider an alternative way of defining local identifiability (based on system observability (Sedoglavic, 2002)). Recall that the system output $\boldsymbol{y}(t)$ can be written as a vector-valued function of the states $\boldsymbol{x}(t)$, the input functions $\boldsymbol{u}(t)$, and the parameters $\boldsymbol{\theta}$ as

$$\boldsymbol{y}(t) = \boldsymbol{h}(\boldsymbol{x}(t), \boldsymbol{u}(t), \boldsymbol{\theta}). \quad (2.62)$$

[6]Reduced in the sense that this expression only includes the output function and its derivatives (note that the input function is only present in the initial condition for $A_{\text{b}}(t)$).

Define the extended *Lie derivative* differential operator $\mathcal{L}_f$ as

$$\mathcal{L}_f := \sum_{i=1}^{m} f_i \frac{\partial}{\partial x_i} + \sum_{j \in \mathbb{N}} \sum_{i=1}^{q} u_i^{(j+1)} \frac{\partial}{\partial u_i^{(j)}}, \tag{2.63}$$

and let $\mathcal{L}_f^{(k)}$ denote the k:th repeated Lie derivative, i.e., $\mathcal{L}_f^{(k)} = \overbrace{\mathcal{L}_f \circ \cdots \circ \mathcal{L}_f}^{k \text{ times}}$. Now, assume that $\boldsymbol{y}(t)$ is analytic on an open interval around an arbitrary initial time-point t_0. This allows us to evaluate repeated differentiations of $\boldsymbol{y}(t)$ at t_0. From the functional relationship given in Eq. (2.62) and the definition of the Lie derivative in Eq. (2.63), it follows that

$$\boldsymbol{y}^{(k)}(t) = \mathcal{L}_f^{(k)} \boldsymbol{h}(\boldsymbol{x}(t), \boldsymbol{u}(t), \boldsymbol{\theta}). \tag{2.64}$$

It can be shown that the $n + p - 1$ first repeated time-derivatives of $\boldsymbol{y}(t)$ (where n and p are the dimensions of the state space and parameter space, respectively) are algebraically independent. Any further differentiations of $\boldsymbol{y}^{(n+p-1)}(t)$ will yield terms that are algebraically dependent on the previous ones (for details, see Sedoglavic (2002)). The $n + p - 1$ first repeated time-derivatives of $\boldsymbol{y}(t)$ will generate a system of algebraic equations given by

$$\begin{aligned}
\boldsymbol{y}(t_0) &= \boldsymbol{h}(\boldsymbol{x}(t_0), \boldsymbol{u}(t_0), \boldsymbol{\theta}), && \text{(2.65a)} \\
\dot{\boldsymbol{y}}(t_0) &= \mathcal{L}_f^{(1)} \boldsymbol{h}(\boldsymbol{x}(t_0), \boldsymbol{u}(t_0), \boldsymbol{\theta}), && \text{(2.65b)} \\
&\vdots \\
\boldsymbol{y}^{(n+p-1)}(t_0) &= \mathcal{L}_f^{(n+p-1)} \boldsymbol{h}(\boldsymbol{x}(t_0), \boldsymbol{u}(t_0), \boldsymbol{\theta}). && \text{(2.65c)}
\end{aligned}$$

By definition, the system in Eqs. (2.51a) and (2.51b) is said to be locally identifiable if the system of algebraic equations given by Eqs. (2.65a) to (2.65c) has solutions $\boldsymbol{x}(t_0)$ and $\boldsymbol{\theta}$ that are locally unique almost everywhere[7].

Now, the left-hand side of the system in Eqs. (2.65a) to (2.65c) constitutes time-derivatives $\boldsymbol{y}^{(k)}(t_0)$—which are known for any $k = 0, 1, \ldots, n + p - 1$. The right-hand side represents expressions in $\boldsymbol{x}(t_0)$, $\boldsymbol{\theta}$, and $\boldsymbol{u}(t_0)$ (with the latter being known). Using vector notation, the right-hand side may be expressed as $\mathcal{Y}(\boldsymbol{x}(t_0), \boldsymbol{u}(t_0), \boldsymbol{\theta})$. It follows from the inverse function theorem that Eqs. (2.51a) and (2.51b) have a locally unique solution $\boldsymbol{x}(t_0)$ and $\boldsymbol{\theta}$ if and only if the Jacobian defined by

$$J(\boldsymbol{x}(t_0), \boldsymbol{u}(t_0), \theta) = \left. \frac{\partial \mathcal{Y}(\boldsymbol{x}(t), \boldsymbol{u}(t), \boldsymbol{\theta})}{\partial (\boldsymbol{x}, \boldsymbol{\theta})} \right|_{t=t_0}, \tag{2.66}$$

has full rank.

The EAR method is based on performing a rank test on the Jacobian in Eq. (2.66) (Pohjanpalo, 1978; Sedoglavic, 2002; Karlsson et al., 2012). Since identifiability is a generic property that

[7] Almost everywhere means that the condition holds with potential exception on a set of measure 0 (for more on measure theory, see Folland (Folland, 1999)).

holds almost everywhere[8] in $\boldsymbol{\Theta}$, the rank of the Jacobian may be evaluated numerically by selecting a random integer representation of the parameters and the initial conditions. Moreover, the symbolic complexity of calculating the entries of the Jacobian may be avoided by performing power series expansions in $\boldsymbol{x}_0$ and $\boldsymbol{\theta}$ of the partial derivatives. The complexity is further enhanced by performing all calculations modulo a large prime, preventing the switch to slow arithmetics for large integers.

Example 2.2.1.4 Identifiable feedback turnover model

The following example demonstrates how the model of Example 2.1.3.2 can be proven to be (at least) structurally locally identifiable, using the EAR method. The method is implemented in the MATHEMATICA application `IdentifiabilityAnalysis` (Karlsson et al., 2012). The following MATHEMATICA code was used:

```
In[1]:= Get["IdentifiabilityAnalysis`"];

In[2]:= system = {Ab'[t] == input[t] - kb*Ab[t],
        R'[t] == kout*R0*(1 + Smax*Ab[t] /(SD50 + Ab[t])) -
                 (M[t]/R0)*kout*R[t],
        M'[t] == ktol (R[t] - M[t]),
        Ab[0] == 0, R[0] == R0, M[0] == R0};

In[3]:= output = {R[t]};

In[4]:= parameters = {kb, Smax, SD50, kout, R0, ktol};

In[5]:= states = {Ab, R, M};

In[6]:= iad =  IdentifiabilityAnalysis[{system, output}, states,
                          parameters, t, input]

Out[6]= "IdentifiabilityAnalysisData[True, <>]"
```

The calculations in the analysis were performed in a matter of seconds, and it can be concluded from `"IdentifiabilityAnalysisData[True, <>]"` that the model is structurally locally identifiable.

2.3 Parameter estimation

Estimating the parameters of a dose-response-time (DRT) model amounts to minimise, using some metric, the difference between the model predicted and the observed behaviour (Bonate, 2011). In theory, this is achievable given continuous, noise-free observations of the system, and a structurally identifiable model (Raue et al., 2009; Janzén, 2016). Practically, the

[8] I.e., except possibly on a set of measure zero.

success of a parameter estimation tends to depend on several determinants such as quantity and quality of data, choice of estimator, desired accuracy and precision, selecting suitable initial estimates and so forth (Rice, 1988; Nocedal and Wright, 2006; Bonate, 2011). The following section will address different aspects of parameter estimation, provided models of varying complexity; including simple linear models, nonlinear (fixed-effects) models, and nonlinear mixed-effects models.
The estimation theory that is presented in this section has been adapted from *Mathematical Statistics and Data Analysis* by Rice (1988) and *Pharmacokinetic-Pharmacodynamic Modeling and Simulation* by Bonate (2011). The optimisation theory has been adapted from *Numerical Optimization* by Nocedal and Wright (2006). The reader is referred to those texts for further theory around estimation and optimisation.

2.3.1 Linear models

In the case of simple linear regression, the *method of (ordinary) least squares* is the benchmark technique for parameter estimation. To demonstrate the method, consider a linear model of the following form

$$\boldsymbol{y} = \boldsymbol{X}\boldsymbol{\beta} + \boldsymbol{\varepsilon}, \tag{2.67}$$

where $\boldsymbol{y}$ represents an $n \times 1$ vector[9] of dependent variables (i.e, the observations), $\boldsymbol{X}$ is an $n \times (p+1)$ *design matrix* of independent variables given by

$$\boldsymbol{X} = \begin{bmatrix} 1 & x_{11} & \cdots & x_{1p} \\ 1 & x_{21} & \cdots & x_{2p} \\ \vdots & \vdots & \ddots & \vdots \\ 1 & x_{n1} & \cdots & x_{np} \end{bmatrix}, \tag{2.68}$$

$\boldsymbol{\beta}$ is the $(p+1) \times 1$ vector of model parameters

$$\boldsymbol{\beta} = \begin{bmatrix} \beta_0 \\ \beta_1 \\ \vdots \\ \beta_p \end{bmatrix}, \tag{2.69}$$

and $\boldsymbol{\varepsilon}$ is an $n \times 1$ vector of independent, normally distributed residuals with $\varepsilon_i \sim \mathcal{N}(0, \sigma^2)$ for $i = 1, \ldots, n$. The term $\boldsymbol{X}\boldsymbol{\beta}$ is often referred to as the *expectation function* since

$$\mathrm{E}[\boldsymbol{y}] = \mathrm{E}[\boldsymbol{X}\boldsymbol{\beta} + \boldsymbol{\varepsilon}] = \mathrm{E}[\boldsymbol{X}\boldsymbol{\beta}] + \mathrm{E}[\boldsymbol{\varepsilon}] = \boldsymbol{X}\boldsymbol{\beta}, \tag{2.70}$$

[9] In this definition, we consider a single observation. The framework may readily be extended to include an arbitrary number of observations.

where we have used the linearity of the expected value, the fact that $\mathrm{E}[\boldsymbol{\varepsilon}] = 0$, and that $\boldsymbol{X}$ and $\boldsymbol{\beta}$ are deterministic. The method of least squares finds an estimate $\hat{\boldsymbol{\beta}}$ of the true parameter $\boldsymbol{\beta}$ by minimising the squared difference between the expectation function and the observations. We define the sum of squares as

$$S_n(\boldsymbol{\beta}) = \sum_{i=1}^{n} (y_i - \hat{y}_i)^2, \tag{2.71}$$

where $\hat{y}_i$ is the predicted response at the ith time-point, given by

$$\hat{y}_i = \sum_{j=0}^{p} X_{ij} \hat{\beta}_j, \tag{2.72}$$

and n is the number of observations. Thus, the estimation problem may be stated as

$$\arg\min_{\boldsymbol{\beta}} S_n(\boldsymbol{\beta}). \tag{2.73}$$

It turns out that there is a closed-form solution to Eq. (2.91) in the linear case. To obtain the solution, note that the partial derivatives of $S_n(\boldsymbol{\beta})$ evaluated at $\hat{\boldsymbol{\beta}}$ need to satisfy

$$\left. \frac{\partial S_n(\boldsymbol{\beta})}{\partial \beta_j} \right|_{\boldsymbol{\beta}=\hat{\boldsymbol{\beta}}} = 0 \quad \text{for} \quad j = 0, \ldots, p. \tag{2.74}$$

Thus, we have

$$2 \sum_{i=1}^{n} \left(y_i - \sum_{j=0}^{p} X_{ij} \hat{\beta}_j \right) (-X_{ik}) = 0 \quad \text{for} \quad k = 0, \ldots, p, \tag{2.75}$$

or

$$\sum_{i=1}^{n} \sum_{j=0}^{p} X_{ik} X_{ij} \hat{\beta}_j = \sum_{i=1}^{n} X_{ik} y_i \qquad \text{for} \quad k = 0, \ldots, p, \tag{2.76}$$

which in matrix notation is

$$\boldsymbol{X}^{\mathrm{T}} \boldsymbol{X} \hat{\boldsymbol{\beta}} = \boldsymbol{X}^{\mathrm{T}} \boldsymbol{y}, \tag{2.77}$$

known as the *normal equations*. Hence, the solution is given by

$$\hat{\boldsymbol{\beta}} = (\boldsymbol{X}^{\mathrm{T}} \boldsymbol{X})^{-1} \boldsymbol{X}^{\mathrm{T}} \boldsymbol{y}. \tag{2.78}$$

2.3.1.1 Accuracy and precision of the estimates

The estimate of $\boldsymbol{\beta}$ conveys little information about the *true value* unless the accuracy and precision of the estimate are quantified. In statistical analysis, accuracy and precision are

commonly referred to as *bias* and *variability*. Bias is a measure of how the expected value of an estimate differs from the true value. Variability, on the other hand, quantifies the spread of the empirical distribution of the estimate. In other words, how much separate realizations of the true parameter differ (Taylor, 1996). By definition, a parameter estimate is unbiased if its expected value is the true value. This is indeed the case for the estimate derived by the least squares method (given by Eq. (2.78)) since

$$\mathrm{E}[\hat{\boldsymbol{\beta}}] = \mathrm{E}[(\boldsymbol{X}^{\mathrm{T}}\boldsymbol{X})^{-1}\boldsymbol{X}^{\mathrm{T}}\boldsymbol{y}] = (\boldsymbol{X}^{\mathrm{T}}\boldsymbol{X})^{-1}\boldsymbol{X}^{\mathrm{T}}\,\mathrm{E}[\boldsymbol{y}] = (\boldsymbol{X}^{\mathrm{T}}\boldsymbol{X})^{-1}\boldsymbol{X}^{\mathrm{T}}\boldsymbol{X}\boldsymbol{\beta} = \boldsymbol{\beta}. \tag{2.79}$$

Here, we have used the linearity of the expected value and the assumption that the residuals are independent and normally distributed with $\mathrm{E}[\boldsymbol{\varepsilon}] = 0$.
The variability of an estimate is often expressed in its *coefficient of variation* (CV), also known as the *relative standard error* (RSE) or *relative standard deviation* (RSD) (Bonate, 2011). The CV is defined as

$$\mathrm{CV} = \frac{\sigma}{\mu} \times 100\%, \tag{2.80}$$

where σ represents the standard deviation and μ the mean of the estimate. For an estimate $\hat{\boldsymbol{\beta}}$, the CV is given by

$$\mathrm{CV}_{\hat{\beta}_j} = \frac{\sqrt{\mathrm{Var}\,(\hat{\beta}_j)}}{|\hat{\beta}_j|} \times 100\% \quad \text{for} \quad j = 0, \ldots, p. \tag{2.81}$$

The estimated variance $\mathrm{Var}\,(\hat{\beta}_j)$ of the jth parameter is obtianed from the covariance matrix

$$\mathrm{Cov}(\hat{\boldsymbol{\beta}}) = \sigma^2(\boldsymbol{X}^{\mathrm{T}}\boldsymbol{X})^{-1}, \tag{2.82}$$

where σ^2 is the true variance of the residuals, which of course is an unknown quantity. However, an unbiased estimate of σ^2, denoted s^2, is obtained as

$$s^2 = \frac{\boldsymbol{e}^{\mathrm{T}}\boldsymbol{e}}{n - p - 1}, \tag{2.83}$$

where $\boldsymbol{e}$ represents the observed residuals

$$\boldsymbol{e} = \boldsymbol{y} - \hat{\boldsymbol{y}}. \tag{2.84}$$

Example 2.3.1.2 Parameter estimation of linear model (Lefèvre et al., 1997)

The following example is based on the work by Lefèvre et al. (1997), who investigated how renal impairment affects the pharmacokinetics and pharmacodynamics of the anticoagulant desirudin. Here, desirudin clearance is the measured effect, as a function of creatinine clearance (lowered creatinine clearance is a sign of mild renal failure). The data are obtained from the Lefèvre et al. (1997) study, and are illustrated in Fig. 2.4.

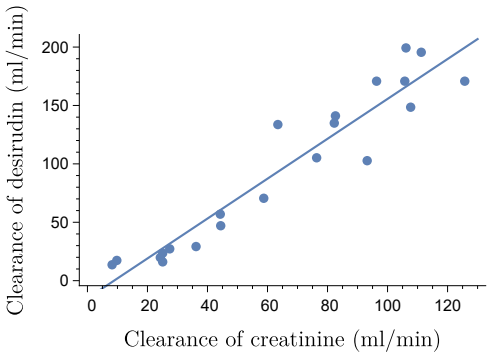

Figure 2.4: Plasma clearance of desirudin in relation to creatinine clearance in patients of various level of renal failure. The dots represent the data and the line the linear fit. The data are obtained from the study by Lefèvre et al. (1997).

When plotting the data, there appears to be a linear relation between the clearance of desirudin and that of creatinine. Consequently, we choose to model the relationship as

$$Cl_{\text{de}} = \beta_0 + \beta_1 \cdot Cl_{\text{cr}}, \tag{2.85}$$

where Cl_{de} and Cl_{cr} are the clerance of desirudin and creatinine, respectively, β_0 is the intercept and β_1 the slope parameter. Applying the least squares method, closed-form estimates of β_0 and β_1 are obtained as

$$\hat{\boldsymbol{\beta}} = \begin{bmatrix} \hat{\beta}_0 \\ \hat{\beta}_1 \end{bmatrix} = (\boldsymbol{X}^{\mathrm{T}}\boldsymbol{X})^{-1}\boldsymbol{X}^{\mathrm{T}}\boldsymbol{y}, \tag{2.86}$$

where

$$\boldsymbol{X} = \begin{bmatrix} 1 & 8.22 \\ 1 & 9.79 \\ 1 & 25.07 \\ 1 & 24.28 \\ 1 & 25.07 \\ 1 & 27.42 \\ 1 & 36.19 \\ 1 & 44.41 \\ 1 & 44.26 \\ 1 & 58.75 \\ 1 & 63.45 \\ 1 & 76.37 \\ 1 & 82.25 \\ 1 & 82.64 \\ 1 & 93.21 \\ 1 & 96.34 \\ 1 & 107.70 \\ 1 & 105.74 \\ 1 & 106.14 \\ 1 & 111.23 \\ 1 & 125.72 \end{bmatrix} \quad \text{and} \quad \boldsymbol{y} = \begin{bmatrix} 13.61 \\ 17.33 \\ 16.09 \\ 19.8 \\ 23.51 \\ 27.23 \\ 29.21 \\ 47.03 \\ 56.93 \\ 70.54 \\ 133.66 \\ 105.2 \\ 134.9 \\ 141.09 \\ 102.72 \\ 170.79 \\ 148.51 \\ 170.79 \\ 199.26 \\ 195.54 \\ 170.79 \end{bmatrix}. \tag{2.87}$$

Thus, by solving Eq. (2.86) we obtain

$$\hat{\boldsymbol{\beta}} = \begin{bmatrix} -15.1 \\ 1.71 \end{bmatrix}, \tag{2.88}$$

with the corresponding covariance matrix given by

$$\mathrm{Cov}(\hat{\boldsymbol{\beta}}) = \begin{bmatrix} 92.3 & -1.09 \\ -1.09 & 0.0168 \end{bmatrix}. \tag{2.89}$$

Hence, the variability of the parameter estimates, expressed in CV%'s, are found to be

Parameter	CV%
$\hat{\beta}_0$	$\frac{\sqrt{92.3}}{15.2} \times 100 = 63.6$
$\hat{\beta}_1$	$\frac{\sqrt{0.0168}}{1.71} \times 100 = 7.59$

Table 2.1: Uncertainty in the parameter estimates, expressed in CV%'s.

The relative standard error for $\hat{\beta}_0$ is high, while $\hat{\beta}_1$ is relatively small. Thus, there is high uncertainty in the estimate for the intercept.

2.3.2 Nonlinear models

Consider a nonlinear regression model given by

$$\boldsymbol{y} = h(\boldsymbol{x}; \boldsymbol{\theta}) + \boldsymbol{\varepsilon}, \tag{2.90}$$

where $\boldsymbol{y}$ represents the observations, h is the expectation function (which is assumed to be differentiable with respect to its arguments), $\boldsymbol{\theta}$ the model parameters, $\boldsymbol{x}$ the state variables, and $\boldsymbol{\varepsilon}$ independent, normally distributed residuals. As for linear regression, the objective is to find an estimate $\hat{\boldsymbol{\theta}}$ of the true parameters $\boldsymbol{\theta}$ such that the model optimally (by means of some measure) fits the data. This estimation problem can be approached in a similar way to the linear case, i.e, by finding

$$\arg\min_{\boldsymbol{\theta}} S_n(\boldsymbol{\theta}), \tag{2.91}$$

where $S_n(\boldsymbol{\theta})$ is the sum of squares given by

$$S_n(\boldsymbol{\theta}) = \sum_{i=1}^{n} (y_i - h(\boldsymbol{x}_i|\boldsymbol{\theta}))^2. \tag{2.92}$$

This estimation method is the *nonlinear least squares estimator*. An alternative approach is to use *maximum likelihood* (ML) estimation; wherein the aim is to find the "most likely" parameter estimates, given the observed data. In terms of probability, this is equivalent

to maximising the conditional probability of the data, given the parameters. Let $L(\boldsymbol{\theta}; \boldsymbol{y})$ represent the *likelihood function*, defined as

$$L(\boldsymbol{\theta}; \boldsymbol{y}) = f(\boldsymbol{y}|\boldsymbol{\theta}). \tag{2.93}$$

where f is the *joint conditional probability density function*. Assuming that the observations are independent, the joint probability density may be written as a product of the probability densities of the separate observations. Moreover, since the residuals of the nonlinear model are assumed to be normally distributed, the probability density functions are *Gaussian*. Thus, we have

$$f(\boldsymbol{y}|\boldsymbol{\theta}) = \prod_{i=1}^{n} f(y_i|\boldsymbol{\theta}) = \prod_{i=1}^{n} \frac{1}{\sqrt{2\pi}\sigma} \exp\left(-\frac{(y_i - h(\boldsymbol{x}_i; \boldsymbol{\theta}))^2}{2\sigma^2}\right), \tag{2.94}$$

where σ is the standard deviation of the residuals[10]. It is often convenient to consider the logarithm of the likelihood function, rather than the function itself[11]. Since the logarithm is monotonically increasing, a log-transformation will preserve the stationary points of the likelihood function. Consequently, the likelihood function and the *log-likelihood function* have the same maxima. Let $l(\boldsymbol{\theta}; \boldsymbol{y})$ denote the log-likelihood function, given by

$$l(\boldsymbol{\theta}; \boldsymbol{y}) = \log L(\boldsymbol{\theta}; \boldsymbol{y}) = \sum_{i=1}^{n} \log f(y_i|\boldsymbol{\theta}) = -\frac{n}{2} \log 2\pi\sigma^2 - \frac{1}{2\sigma^2} \sum_{i=1}^{n} \left(y_i - h(\boldsymbol{x}_i; \boldsymbol{\theta})\right)^2. \tag{2.95}$$

The ML estimation now amounts to determining

$$\arg\max_{\boldsymbol{\theta}} l(\boldsymbol{\theta}; \boldsymbol{y}), \tag{2.96}$$

which in fact is equivalent to

$$\arg\min_{\boldsymbol{\theta}} \sum_{i=1}^{n} (y_i - f(\boldsymbol{x}_i|\boldsymbol{\theta}))^2 = \arg\min_{\boldsymbol{\theta}} S_n(\boldsymbol{\theta}). \tag{2.97}$$

Consequently, under the assumption that the residuals are normally distributed, ML estimation and nonlinear least squares estimation are equivalent[12].

The optimisation problems in Eqs. (2.96) and (2.97) do not typically have closed-form solutions in the nonlinear case. Rather, approximate solutions are found numerically by iteratively refining the estimates until convergence occurs. There are several optimisation methods designed for this task, where one of the most well-known is *Newton's method*.

[10] Note that f represents two different probability densities in this identity; the former being a multivariate normal distribution and the latter being univariate one. Yet, for convenience, we use the same notation for the two densities (and will do so in similar cases later in this section).

[11] The logarithm will, for example, transform the product of the likelihood function into a sum.

[12] We introduce ML estimation since it is a benchmark method within estimation theory. Moreover, the Hessian of the objective function (used in the gradient methods of the optimisation) of the ML method is related to the *Fisher information* (see Sec. 2.3.2.6), which will prove to be of importance when quantifying the estimation errors.

2.3.2.1 Newton's method

In Newton's method, the objective function is locally approximated by its quadratic Taylor-expansion. For the log-likelihood function[13], this approximation around the iterative $\boldsymbol{\theta}_k$ is given by

$$l(\boldsymbol{\theta}_k + \boldsymbol{p}_k) \approx l(\boldsymbol{\theta}_k) + \nabla l(\boldsymbol{\theta}_k)^{\mathrm{T}} \boldsymbol{p}_k + \frac{1}{2} \boldsymbol{p}_k^{\mathrm{T}} H[l(\boldsymbol{\theta}_k)] \boldsymbol{p}_k =: m_k(\boldsymbol{p}_k), \tag{2.98}$$

where $\boldsymbol{p}_k$ is the *search direction*, $H[l(\boldsymbol{\theta}_k)]$ the Hessian of l evaluated at $\boldsymbol{\theta}_k$, and $m_k(\boldsymbol{p}_k)$ the kth *model function* evaluated at $\boldsymbol{p}_k$ (defined as the second-order expansion of l). The idea behind Newton's method is to choose $\boldsymbol{p}_k$ such that $m_k(\boldsymbol{p}_k)$ is a stationary point, satisfying

$$\nabla m_k(\boldsymbol{p}_k) = \nabla l(\boldsymbol{\theta}_k) + H[l(\boldsymbol{\theta}_k)] \boldsymbol{p}_k = 0, \tag{2.99}$$

or

$$\boldsymbol{p}_k^{\mathrm{N}} = -H[l(\boldsymbol{\theta}_k)]^{-1} \nabla l(\boldsymbol{\theta}_k), \tag{2.100}$$

which specifices the *Newton step* $\boldsymbol{p}_k^{\mathrm{N}}$. Alternatively, the step length is scaled by $\gamma_k \in (0, 1)$ such that

$$\boldsymbol{p}_k^{\mathrm{N}} = -\gamma_k H[l(\boldsymbol{\theta}_k)]^{-1} \nabla l(\boldsymbol{\theta}_k), \tag{2.101}$$

where an appropriate step length is found by imposing some form of conditions. A typical choice are the *Wolfe conditions* (Wolfe, 1969, 1971), defined as

$$l(\boldsymbol{\theta}_k + \gamma_k \boldsymbol{p}_k^{\mathrm{N}}) \leq l(\boldsymbol{\theta}_k) + c_1 \gamma_k \nabla l(\boldsymbol{\theta}_k)^{\mathrm{T}} \boldsymbol{p}_k^{\mathrm{N}} \tag{2.102a}$$

$$\nabla l(\boldsymbol{\theta}_k + \gamma_k \boldsymbol{p}_k^{\mathrm{N}})^{\mathrm{T}} \boldsymbol{p}_k^{\mathrm{N}} \geq c_2 \nabla l(\boldsymbol{\theta}_k)^{\mathrm{T}} \boldsymbol{p}_k^{\mathrm{N}}, \tag{2.102b}$$

where $0 < c_1 < c_2 < 1$. Here, c_1 is typically chosen to be very small ($\approx 10^{-4}$) and c_2 is near 1 (Nocedal and Wright, 2006).

2.3.2.2 The Gauss-Newton method

A major drawback of Newton's method is that the inversion of the Hessian in Eq. (2.100) tends to be complicated, error prone, and costly. However, this inversion is avoided in many gradient methods by employing some form of approximation of the Hessian.

[13] For the sake of convenience, the dependence on $\boldsymbol{y}$ in the log-likelihood function is disregarded, i.e, $l(\boldsymbol{\theta}) = l(\boldsymbol{\theta}|\boldsymbol{y})$.

Consider the gradient and Hessian of the sum of squares $S_n(\boldsymbol{\theta})$, which are given by

$$\nabla S_n(\boldsymbol{\theta}) = \sum_{i=1}^{n} r_i \nabla r_i \tag{2.103}$$

$$H[S_n(\boldsymbol{\theta})] = \sum_{i=1}^{n} \nabla r_i^{\mathrm{T}} \nabla r_i + r_i \nabla^2 r_i, \tag{2.104}$$

where r_i represents the residual

$$r_i = y_i - h(\boldsymbol{x}_i|\boldsymbol{\theta}) \quad \text{for} \quad i = 1, \ldots, n. \tag{2.105}$$

The *Gauss-Newton* method finds parameter estimates in nonlinear least squares problems, using Newton's method with an approximated Hessian. In this approximation, the second-order terms in Eq. (2.104) are excluded such that

$$B_k = \sum_{i=1}^{n} \nabla r_i^{\mathrm{T}} \nabla r_i = J_k^{\mathrm{T}} J_k, \tag{2.106}$$

where B_k is the approximated Hessian of the kth iteration in the Gauss-Newton method, and J_k is the Jacobian of S_n, evaluated at $\boldsymbol{\theta}_k$. Thus, the Gauss-Newton step $\boldsymbol{p}_k^{\mathrm{GN}}$ becomes

$$\boldsymbol{p}_k^{\mathrm{GN}} = -(J_k^{\mathrm{T}} J_k)^{-1} J_k^{\mathrm{T}} \boldsymbol{r}_k, \tag{2.107}$$

where

$$\boldsymbol{r}_k = \boldsymbol{y} - h(\boldsymbol{x}|\boldsymbol{\theta}_k). \tag{2.108}$$

As for Newton's method, this step may be scaled by a factor γ_k such that, for example, the Wolfe conditions are satisfied.
It is straightforward to show that the Gauss-Newton step is taken in a descent direction (provided that the Jacobian has full rank and the gradient is non-zero) since

$$\boldsymbol{p}_k^{\mathrm{GN}} \nabla S_n(\boldsymbol{\theta}_k) = \boldsymbol{p}_k^{\mathrm{GN}} J_k^{\mathrm{T}} \boldsymbol{r}_k = -\boldsymbol{p}_k^{\mathrm{GN}} J_k^{\mathrm{T}} J_k \boldsymbol{p}_k^{\mathrm{GN}} = -||J_k \boldsymbol{p}_k^{\mathrm{GN}}||^2 \leq 0, \tag{2.109}$$

where we have used the definition of the gradient ($\nabla S_n(\boldsymbol{\theta}_k) = J_k \boldsymbol{r}_k$) and the Gauss-Newton step in Eq. (2.107). Thus, provided that the step length is *sufficiently small*, the value of the objective function will decrease in the kth iteration. Another advantage of the Gauss-Newton method is that the Jacobian is often known from the calculation of the gradient. Hence, no additional computations need to be performed when approximating the Hessian. Moreover, in many situations, the first-order term of the Hessian dominates the second-order term—rendering the latter insignificant. This typically occurs when the problem is "almost linear" or if the residuals are "small". In cases like these, the Gauss-Newton method is expected to be efficient. Finally, the identity in Eq. (2.107) is equivalent to that of the linear

least squares solution in Eq. (2.78). Thus, the Gauss-Newton step could be regarded as the solution to the linear problem

$$\min_{\boldsymbol{p}_k^{\mathrm{GN}}} \left\| J_k \boldsymbol{p}_k^{\mathrm{GN}} + \boldsymbol{r}_k \right\|^2 . \tag{2.110}$$

The advantage of viewing the Gauss-Newton approach as a linear problem, defined by Eq. (2.110), is that the computation of the approximated Hessian $J_k^T J_k$ is not required to solve this problem. Rather, the problem in Eq. (2.110) may be solved by using, for example, *Cholesky* or *SVD* decomposition, or *QR* factorisation. (Heath, 2002).

2.3.2.3 Levenberg-Marquardt method

The Gauss-Newton method may have convergence issues if the Jacobian is (or nearly is) locally rank-deficient. Problems like these may be alleviated by *damping* the approximated Hessian. Given that the step size of the kth iteration is insufficient, the step in Eq. (2.107) may be damped according to

$$\boldsymbol{p}_k = (J_k^{\mathrm{T}} J_k + \lambda_k \mathbf{1})^{-1} J_k^{\mathrm{T}} \boldsymbol{r}_k, \tag{2.111}$$

for some $\lambda_k > 0$. If λ_k is large, the relation in Eq. (2.111) approaches that of the *steepest descent*. Conversely, $\lambda_k \approx 0$ results in the Gauss-Newton step. By adjusting λ_k in each iteration, it is ensured that the objective is reduced. This method is known as the *Levenberg-Marquardt* approach (Levenberg, 1944; Marquardt, 1963). Like the Gauss-Newton method, the problem in Eq. (2.111) may be regarded as a linear problem, given by

$$\min_{\boldsymbol{p}_k^{\mathrm{LN}}} \left\| \begin{bmatrix} J_k \\ \sqrt{\lambda}\mathbf{1} \end{bmatrix} \boldsymbol{p}_k^{\mathrm{LN}} + \begin{bmatrix} \boldsymbol{r}_k \\ \mathbf{0} \end{bmatrix} \right\|^2 , \tag{2.112}$$

where $\boldsymbol{p}_k^{\mathrm{LN}}$ is the Levenberg-Marquardt step. Typically, λ_k is initially large and subsequently reducued in each iteration if the step size is sufficiently small (thereby approaching Gauss-Newton in convergence). If the step is insufficient, λ_k is generally increased in the following iteration. For details and suitable choices of λ_k, see Marquardt (1963).

2.3.2.4 Quasi-Newton methods

The aforementioned Gauss-Newton and Levenberg-Marquardt methods are designed to find optima in nonlinear least squares problems. The following section will introduce more general techniques, known as *quasi-Newton* methods, which can be applied to optimise any real-valued function. The quasi-Newton methods rely on approximations of the full Hessian, and therefore tend to be better suited (than Gauss-Newton or Levenberg-Marquardt) for nonlinear least squares problems (or equivalently, maximum likelihood problems) that are non-smooth or highly nonlinear.

In order to derive the quasi-Newton methods, consider a general optimisation problem given by

$$\begin{aligned} &\underset{\boldsymbol{x}}{\text{minimize}} \quad g(\boldsymbol{x}) \\ &\text{subject to} \quad \boldsymbol{x} \in \boldsymbol{X}. \end{aligned} \tag{2.113}$$

As in Newton's method, f is locally approximated by its second-order Taylor expansion, given by

$$g(\boldsymbol{x}_k + \boldsymbol{p}_k) \approx m_k(\boldsymbol{p}_k) = g(\boldsymbol{x}_k) + \nabla g(\boldsymbol{x}_k)^{\mathrm{T}} \boldsymbol{p}_k + \frac{1}{2} \boldsymbol{p}_k^{\mathrm{T}} B_k \boldsymbol{p}_k, \tag{2.114}$$

where $\boldsymbol{x}_k$ is the iterate, $\boldsymbol{p}_k$ the search direction, m_k the approximated quadratic model function, and B_k the approximated Hessian. The iterations are intitiated with an initial point $\boldsymbol{x}_0$ and a positive definite, symmetric Hessian approximation B_0 (typically chosen to be the identity matrix). Given $\boldsymbol{x}_0$ and B_0, a search direction $\boldsymbol{p}_0$ can be found through Newton's equation

$$B_0 \boldsymbol{p}_0 = \nabla g(\boldsymbol{x}_0). \tag{2.115}$$

The subsequent Hessian approximation will then be chosen such that the gradient of the model function is the same in the two last iterates. For a general iteration $k+1$, this implies that

$$\begin{aligned} \nabla m_{k+1}(0) = \nabla g(\boldsymbol{x}_{k+1}) = \\ \nabla m_{k+1}(-\alpha_{k+1} \boldsymbol{p}_{k+1}) = \nabla g(\boldsymbol{x}_k) - \alpha_{k+1} B_{k+1} \boldsymbol{p}_{k+1}, \end{aligned} \tag{2.116}$$

or

$$\nabla g(\boldsymbol{x}_{k+1}) = \nabla g(\boldsymbol{x}_k) - \alpha_{k+1} B_{k+1} \boldsymbol{p}_{k+1} \tag{2.117}$$

if and only if

$$\nabla g(\boldsymbol{x}_k) - \nabla g(\boldsymbol{x}_{k+1}) = B_{k+1}(\boldsymbol{x}_{k+1} - \boldsymbol{x}_k). \tag{2.118}$$

where α_{k+1} is the step length (which again may be imposed by, e.g., the Wolfe conditions). By introducing the notation

$$\boldsymbol{s}_k = \boldsymbol{x}_{k+1} - \boldsymbol{x}_k, \tag{2.119}$$

and

$$\boldsymbol{y}_k = \nabla g(\boldsymbol{x}_{k+1}) - \nabla g(\boldsymbol{x}_k), \tag{2.120}$$

we can express the relation in Eq. (2.118) as

$$B_{k+1}\boldsymbol{s}_k = \boldsymbol{y}_k, \tag{2.121}$$

which is known as the *secant equation*. Furthermore, we assume that B_{k+1} is as close as possible to B_k, and that B_{k+1} is symmetric. Thus, finding the next iteration of the Hessian amounts to finding

$$\begin{aligned} &\min_B \|B - B_k\| \\ \text{subject to} \quad &B = B^{\mathrm{T}} \quad \text{and} \quad B\boldsymbol{s}_k = \boldsymbol{y}_k. \end{aligned} \tag{2.122}$$

The solution of the system in Eq. (2.122) gives rise to the *Davidon-Fletcher-Powell* (DFP) algorithm. However, it turns out that a better choice for the updated Hessian is obtained by letting the inverse Hessian $H_{k+1} = B_{k+1}^{-1}$ satisfy the system in Eqs. (2.122). This will give rise to the *Broyden-Fletcher-Goldfarb-Shanno* (BFGS) algorithm, which is one of the most prominent quasi-Newton methods. By solving the system in Eq. (2.122) for the inverse of the Hessian, we get

$$B_{k+1} = B_k + \frac{\boldsymbol{y}_k\boldsymbol{y}_k^{\mathrm{T}}}{\boldsymbol{y}_k^{\mathrm{T}}\boldsymbol{p}_k} - \frac{B_k\boldsymbol{p}_k(B_k\boldsymbol{p}_k)^{\mathrm{T}}}{\boldsymbol{p}_k^{\mathrm{T}}B_k\boldsymbol{p}_k}. \tag{2.123}$$

The updated Hessian is then employed to find the next search direction $\boldsymbol{p}_{k+1}$, thus re-initiates the iterative procedure.

2.3.2.5 Convergence analysis

The optimisation methods presented in this chapter are only ensured to converge globally under certain circumstances. In detail, given a twice continuously differentiable function f, an initial point $\boldsymbol{x}_0$, and a symmetric positive definite initial Hessian H, the level set Ω, defined as

$$\Omega = \{\boldsymbol{x} \in \mathbb{R}^n : g(\boldsymbol{x}) \leq g(\boldsymbol{x}_0)\}, \tag{2.124}$$

needs to be *convex*[14] and there must exist positive constants M and m such that

$$m\|\boldsymbol{z}\| \leq \boldsymbol{z}^{\mathrm{T}}H(\boldsymbol{x})\boldsymbol{z} \leq M\|\boldsymbol{z}\| \tag{2.125}$$

for all $z \in \mathbb{R}^n$ and all $\boldsymbol{x} \in \Omega$ ($\|\cdot\|$ represents the Eucledian norm (Folland, 1999)). The stated conditions imply that g is convex on Ω and that the optimum $x^* \in \Omega$ is unique. Clearly, these conditions are strong and tend not to be satisfied. Under slightly weaker conditions, the methods ensure local convergence. If $g(\boldsymbol{x})$ is a quadratic function, then the optimum is reached in a single iteration in Newton's method. Otherwise, the method converges quadratically under the following conditions:

[14] A set $\Omega \subset \mathbb{R}^n$ is said to be convex if $\sum_{i=1}^n \lambda_i\boldsymbol{x}_i \in \Omega$ for any list of vectors $\boldsymbol{x}_1, \ldots, \boldsymbol{x}_n \in \Omega$ and $\lambda_1, \ldots, \lambda_n \in [0, 1]$ such that $\sum_{i=1}^n \lambda_i = 1$ (i.e., the set is closed under convex summation).

(i) $g(\boldsymbol{x})$ is twice continuously differentiable.

(ii) The Hessian is *Lipschitz continuous* in a neighbourhood of the optimum $\boldsymbol{x}^*$.

(iii) $\boldsymbol{x}_0$ is sufficiently close to $\boldsymbol{x}^*$ (for details, see Nocedal and Wright (2006)).

Under the same conditions, the BFGS converges superlinearly (Nocedal and Wright, 2006). Thus, Newton's method has a higher rate of convergence than the BFGS. However, depending on the complexity of the problem, the BFGS may be faster and more stable. For the Gauss-Newton method, local convergence is guaranteed if

(i) The resiudal functions $r_i(\boldsymbol{x})$, $i = 1, \ldots, n$, are Lipschitz continuously differentiable in a neighbourhood U of the level set Ω.

(ii) The Jacobian $J(\boldsymbol{x})$ satisfies the *uniform full-rank condition*[15].

Similar conditions apply for the Levenberg-Marquardt method (for details, see Nocedal and Wright (2006)). The rate of convergence of both the Gauss-Newton and Levenberg-Marquardt methods depends on the significance of the second-order derivatives in the true Hessian or, in other words, how good the approximation is. In the best case scenario, the convergence of these methods is approached quadratically (indeed, the convergence is quadratic in limit). As a final note, the convergence criteria demonstrate the importance of selecting sound initial estimates. This is to decrease the risk of converging to a saddle point or suffering from bad numerics.

2.3.2.6 Bias and variability of the estimates

The ML method has asymptotic properties that generally provide valid error estimates for large sample sizes (Rice, 1988). Specifically, an estimate $\hat{\boldsymbol{\theta}}_{\mathrm{ML}}$ satisfies

$$\hat{\boldsymbol{\theta}}_{\mathrm{ML}} \overset{d}{\sim} \mathcal{N}(\boldsymbol{\theta}_0, [\mathcal{I}(\hat{\boldsymbol{\theta}}_{\mathrm{ML}})]^{-1}) \tag{2.126}$$

i.e, it converges in distribution to the normal distribution, centred at the true value $\boldsymbol{\theta}_0$ (Rice, 1988). Here, $\mathcal{I}(\hat{\boldsymbol{\theta}}_{\mathrm{ML}})$ represents the *observed Fisher information matrix*, evaluated at $\hat{\boldsymbol{\theta}}_{\mathrm{ML}}$ (Rice, 1988). For a formal definition of the Fisher information matrix, let $\boldsymbol{X} \in \mathbb{R}^n$ be an observable random variable and $f(\boldsymbol{X}|\boldsymbol{\theta})$ the corresponding probability density function, conditioned on the distribution parameters $\boldsymbol{\theta}$. Then, the Fisher information matrix is the $p \times p$ (p being the number of parameters) matrix defined as

$$\mathcal{I}(\boldsymbol{\theta}) = \mathrm{E}\left[\left(\frac{\partial}{\partial \boldsymbol{\theta}} \log f(\boldsymbol{X}|\boldsymbol{\theta})\right)^2\right] = \int \left(\frac{\partial}{\partial \boldsymbol{\theta}} \log f(\boldsymbol{x}|\boldsymbol{\theta})\right)^2 f(\boldsymbol{x}|\boldsymbol{\theta}) \, \mathrm{d}\boldsymbol{x}. \tag{2.127}$$

It turns out that the Fisher information matrix is related to the curvature of the log-likelihood function, which is described by the Hessian of the log-likelihood function. In fact, the expected

[15] I.e., there exist $\xi > 0$ such that $\left\|J(\boldsymbol{x})\boldsymbol{z}\right\| > \xi \left\|\boldsymbol{z}\right\|$ for all $\boldsymbol{z} \in \mathbb{R}^n$ and all $\boldsymbol{x} \in U$.

Hessian of the log-likelihood is given by

$$\begin{aligned}
\mathrm{E}\left[H_{ij}(f(\boldsymbol{y}|\boldsymbol{\theta}))\right] &= \mathrm{E}\left[D_{ij}\log f(\boldsymbol{y}|\boldsymbol{\theta})\right] && (2.128)\\
&= \mathrm{E}\left[D_i\left(\frac{D_j f(\boldsymbol{y}|\boldsymbol{\theta})}{f(\boldsymbol{y}|\boldsymbol{\theta})}\right)\right] && (2.129)\\
&= \mathrm{E}\left[\frac{D_{ij}f(\boldsymbol{y}|\boldsymbol{\theta})}{f(\boldsymbol{y}|\boldsymbol{\theta})} - \frac{D_i f(\boldsymbol{y}|\boldsymbol{\theta})}{f(\boldsymbol{y}|\boldsymbol{\theta})}\frac{D_j f(\boldsymbol{y}|\boldsymbol{\theta})}{f(\boldsymbol{y}|\boldsymbol{\theta})}\right] && (2.130)\\
&= \mathrm{E}\left[(D_i\log f(\boldsymbol{y}|\boldsymbol{\theta}))(D_j\log f(\boldsymbol{y}|\boldsymbol{\theta}))\right] && (2.131)\\
&= -\mathcal{I}_{ij}(\boldsymbol{\theta}) && (2.132)
\end{aligned}$$

where we have used the identity $D_i \log f(\boldsymbol{y}|\boldsymbol{\theta}) = D_i f(\boldsymbol{y}|\boldsymbol{\theta})/f(\boldsymbol{y}|\boldsymbol{\theta})$ and the fact that

$$\mathrm{E}\left[\frac{D_{ij}f(\boldsymbol{y}|\boldsymbol{\theta})}{f(\boldsymbol{y}|\boldsymbol{\theta})}\right] = \int D_{ij}f(\boldsymbol{y}|\boldsymbol{\theta})\,\boldsymbol{y} = D_{ij}1 = 0. \tag{2.133}$$

Here, we have interchanged the order of the derivative and the integral. This is valid if the integrand is *Lebesgue integrable*, bounded, and that its derivative exists almost everywhere; conditions that are generally satisfied for probability density functions (Folland, 1999; Rice, 1988). The relation between the Hessian and the Fisher information matrices implies that

$$\mathcal{I}(\hat{\boldsymbol{\theta}}_{\mathrm{ML}}) = -H[f(\boldsymbol{y}|\boldsymbol{\theta}_{\mathrm{ML}})], \tag{2.134}$$

which is utilised in combination with Eq. (2.126) to estimate the covariance of the estimates and approximate confidence intervals for the point estimates. In conclusion, by applying, for example, a quasi-Newton method in combination with the maximum likelihood measure, the model parameters may be determined. Moreover, the approximated Hessian in the quasi-Newton method can be utilised to quantify the variability and bias of the estimates. An alternative approach to estimating the bias of the estimates is to use some form of bootstrapping technique (Davison and Hinkley, 1997).
Naturally, the question arises as to how to interpret the quantified bias and variability? There is no clear answer to this issue since what is 'acceptable', regarding bias and variability, depends on the application of the model. Bonate (2011) suggests that, as a rule of thumb, a pharmacodynamic estimate is considered to be precise if its CV is below 25%.

Example 2.3.2.7 Parameter estimation of nonlinear model (Schulte et al., 1991)

The following example is based on a study by Schulte et al. (1991) on the pharmacokinetic and pharmacodynamic properties of the drug AF-DX 116. The drug has a positive effect on the heart rate. The increase in heart rate was measured for various plasma concentrations of AF-DX 116. The results are illustrated on a log-linear scale in Fig. 2.5a.

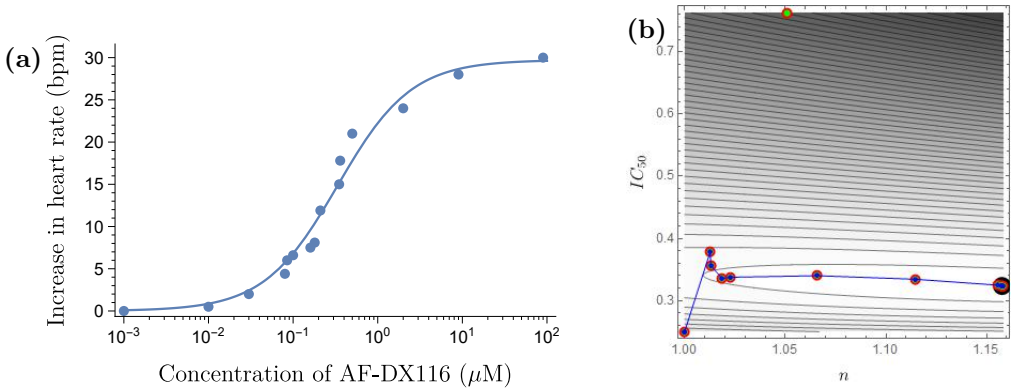

Figure 2.5: Response-concentration course of heart rate increase as a function of AF-DX 116 plasma concentration in (a). The dots represent the data and the line the fitted $E_{\max}$-model. The data are adapted from Schulte et al. (1991). (b) illustrates the path taken by Newton's method in the parameter estimation, starting at $n = 1$ and $IC_{50} = 0.25$.

By analysing the data, it appears that there is a nonlinear, saturable relationship between concentration and response. We therefore propose the following pharmacodynamic model

$$E(t) = \frac{E_{\max} \cdot C(t)^n}{IC_{50}^n + C(t)^n} \quad \text{with} \quad E(0) = 0. \tag{2.135}$$

To simplify the problem, we set $E_{\max} = 30$. We now want to estimate the unknown parameters n and IC_{50}. Let the objective function be the MSE given by

$$g(n, IC_{50}) = \frac{1}{m} \sum_{i=1}^{m} \left(y_i - \frac{E_{\max} \cdot C(t)^n}{IC_{50}^n + C(t)^n} \right)^2, \tag{2.136}$$

where y_i represents the measured response in the ith time-point. The optimisation problem is given by

$$\arg\min_{n, IC_{50}} g(n, IC_{50}). \tag{2.137}$$

This problem can be solved by using Newton's method and a suitable initial estimate. A visual inspection of the data suggests that $n \approx 1$ and $IC_{50} \approx 0.25$; these are used as our initial estimates. In 10 steps, the method finds the optimum at $n = 1.16$ and $IC_{50} = 0.271$. The parameter estimation was performed in MATHEMATICA using the Levenberg-Marquardt method. Finally, by inverting the Hessian of the objective function, standard errors of the estimates were approximated with the following result:

Parameter	CV%
n	$\frac{\sqrt{0.000532}}{0.271} \times 100 = 8.50$
IC_{50}	$\frac{\sqrt{0.0121}}{1.16} \times 100 = 9.50$

Table 2.2: Uncertainty in the parameter estimates, expressed in CV%'s.

Hence, with the guidelines suggested by Bonate (2011), the estimates are precise.

2.3.3 Nonlinear mixed-effects models

The following section will address parameter estimation for nonlinear mixed-effects models. As for nonlinear regression, the parameter estimation is performed using the maximum likelihood (ML) method. To apply the ML method, we need to derive an expression for the *population likelihood function* $L(\boldsymbol{\theta}, \boldsymbol{\Omega}, \boldsymbol{R}; \boldsymbol{y})$, which is defined as

$$L(\boldsymbol{\theta}, \boldsymbol{\Omega}, \boldsymbol{R}; \boldsymbol{y}) = f(\boldsymbol{y}|\boldsymbol{\theta}, \boldsymbol{\Omega}, \boldsymbol{R}). \tag{2.138}$$

For simplicity, the individuals are considered to be independent. Consequently, the population likelihood can be expressed as a product of the individual likelihoods according to

$$f(\boldsymbol{y}|\boldsymbol{\theta}, \boldsymbol{\Omega}, \boldsymbol{R}) = \prod_{i=1}^{N} f(\boldsymbol{y}_i|\boldsymbol{\theta}, \boldsymbol{\Omega}, \boldsymbol{R}). \tag{2.139}$$

The underlying model is dependent on the unobserved random effects $\boldsymbol{\eta}_i$. By marginalising on $\boldsymbol{\eta}_i$, the individual likelihoods can be expressed as

$$f(\boldsymbol{y}_i|\boldsymbol{\theta}, \boldsymbol{\Omega}, \boldsymbol{R}) = \int f(\boldsymbol{y}_i, \boldsymbol{\eta}_i|\boldsymbol{\theta}, \boldsymbol{\Omega}, \boldsymbol{R}) \, \mathrm{d}\boldsymbol{\eta}_i. \tag{2.140}$$

Furthermore, the definition of *conditional probability*, $P(A, B) = P(A|B)P(B)$, is used to rewrite the joint probability density as

$$f(\boldsymbol{y}_i, \boldsymbol{\eta}_i|\boldsymbol{\theta}, \boldsymbol{\Omega}, \boldsymbol{R}) \, \mathrm{d}\boldsymbol{\eta}_i = f(\boldsymbol{y}_i|\boldsymbol{\eta}_i, \boldsymbol{\theta}, \boldsymbol{R}) f(\boldsymbol{\eta}_i|\boldsymbol{\Omega}) \, \mathrm{d}\boldsymbol{\eta}_i, \tag{2.141}$$

where $f(\boldsymbol{y}_i|\boldsymbol{\eta}_i, \boldsymbol{\theta}, \boldsymbol{R})$ is the conditional density function of $\boldsymbol{y}_i$, given $\boldsymbol{\eta}_i$, and $f(\boldsymbol{\eta}_i|\boldsymbol{\Omega})$ is the marginal distribution of $\boldsymbol{\eta}_i$. Both of these density functions are Gaussian with

$$f(\boldsymbol{y}_i|\boldsymbol{\eta}_i, \boldsymbol{\theta}, \boldsymbol{R}) = \exp\left[-\frac{1}{2} \sum_{j=1}^{n_i} \left(\boldsymbol{\varepsilon}_{ij}^{\mathrm{T}} \boldsymbol{R}_{ij}^{-1} \boldsymbol{\varepsilon}_{ij} + \log|2\pi \boldsymbol{R}_{ij}| \right) \right], \tag{2.142}$$

and

$$f(\boldsymbol{\eta}_i|\boldsymbol{\Omega}) = \exp\left[-\frac{1}{2} \left(\boldsymbol{\eta}_i^{\mathrm{T}} \boldsymbol{\Omega}^{-1} \boldsymbol{\eta}_i + \log|2\pi \boldsymbol{R}_{ij}| \right) \right]. \tag{2.143}$$

Here, $\boldsymbol{\varepsilon}_{ij}$ represents the jth residual of the ith individual and $\boldsymbol{R}_{ij}$ the covariance of the corresponding residual. Let l_i denote the *individual joint log-likelihoods* such that

$$L(\boldsymbol{\theta}, \boldsymbol{\Omega}, \boldsymbol{R}; \boldsymbol{y}) = \prod_{i=1}^{N} \int \exp(l_i(\boldsymbol{\eta}_i)) \, \mathrm{d}\boldsymbol{\eta}_i \tag{2.144}$$

The integral over $\boldsymbol{\eta}_i$ seldom has a closed-form solution for nonlinear systems. Moreover, solving this integral numerically is commonly computationally heavy. To overcome this issue, we will use the *Laplacian approximation* of the log-likelihoods around the point $\boldsymbol{\eta}_{i0}$. This approximation will render a closed-form solution of the integral. We have

$$l(\boldsymbol{\eta}_i) \approx l(\boldsymbol{\eta}_{i0}) + \nabla l(\boldsymbol{\eta}_{i0})(\boldsymbol{\eta}_i - \boldsymbol{\eta}_{i0}) + \frac{1}{2}(\boldsymbol{\eta}_i - \boldsymbol{\eta}_{i0})^{\mathrm{T}} \Delta l(\boldsymbol{\eta}_{i0})^{-1} (\boldsymbol{\eta}_i - \boldsymbol{\eta}_{i0}). \tag{2.145}$$

In order to eliminate the first-order term of the Laplacian approximation, we choose $\boldsymbol{\eta}_{i0}$ to be the mode of the log-likelihoods, denoted $\boldsymbol{\eta}_i^*$, since it satisfies $\nabla l(\boldsymbol{\eta}_i^*) = 0$. Now, the zero-order term in the approximation is independent of $\boldsymbol{\eta}_i$, which allows us to place it outside the integral and obtain

$$L(\boldsymbol{\theta}, \boldsymbol{\Omega}, \boldsymbol{R}; \boldsymbol{y}) = \prod_{i=1}^{N} \exp(l_i(\boldsymbol{\eta}_i^*)) \int \exp\left[\frac{1}{2}(\boldsymbol{\eta}_i - \boldsymbol{\eta}_i^*)^{\mathrm{T}} \Delta l(\boldsymbol{\eta}_i^*)^{-1} (\boldsymbol{\eta}_i - \boldsymbol{\eta}_i^*)\right] \mathrm{d}\boldsymbol{\eta}_i. \tag{2.146}$$

The remaining integral is known as a *Gaussian* (or *Euler-Poisson*) (Persson and Böiers, 2005) integral, and has the following closed-form solution

$$\int \exp\left[\frac{1}{2}(\boldsymbol{\eta}_i - \boldsymbol{\eta}_i^*)^{\mathrm{T}} \Delta l(\boldsymbol{\eta}_i^*)^{-1} (\boldsymbol{\eta}_i - \boldsymbol{\eta}_i^*)\right] \mathrm{d}\boldsymbol{\eta}_i = \left| \frac{-\Delta l(\boldsymbol{\eta}_i^*)}{(2\pi)^p} \right|^{-1/2}, \tag{2.147}$$

where p is the dimension of $\boldsymbol{\eta}_i$. Thus, we arrive at the following expression for the population likelihood

$$L(\boldsymbol{\theta}, \boldsymbol{\Omega}, \boldsymbol{R}; \boldsymbol{y}) = \prod_{i=1}^{N} \exp(l_i(\boldsymbol{\eta}_i^*)) \left| \frac{-\Delta l(\boldsymbol{\eta}_i^*)}{(2\pi)^p} \right|^{-1/2}. \tag{2.148}$$

For convenience, we consider the logarithm of the likelihood (this is motivated in Section 2.3.2), which is given by

$$l(\boldsymbol{\theta}, \boldsymbol{\Omega}, \boldsymbol{R}; \boldsymbol{y}) = \log L(\boldsymbol{\theta}, \boldsymbol{\Omega}, \boldsymbol{R}; \boldsymbol{y}) = \sum_{i=1}^{N} l_i(\boldsymbol{\eta}_i^*) - \frac{1}{2} \log \left| \frac{-\Delta l(\boldsymbol{\eta}_i^*)}{(2\pi)^p} \right|. \tag{2.149}$$

The Hessian $\Delta l(\boldsymbol{\eta}_i^*)$ in Eq. (2.149) contains second-order partial derivatives of the log-likelihoods with respect to η_{ik} $(k = 1, \ldots, p)$. These second-order derivatives are often neglected for computational reasons and because they are generally insignificant in comparison to the first-order terms. Consequently, we arrive at the following first-order approximation

of the Hessian:

$$H_{ikl} = -\frac{1}{2}\sum_{j=1}^{n_i}\left[2\left(\frac{\mathrm{d}\boldsymbol{\varepsilon}_{ij}^{\mathrm{T}}}{\mathrm{d}\eta_{ik}} - \boldsymbol{\varepsilon}_{ij}^{\mathrm{T}}\boldsymbol{R}_{ij}^{-1}\frac{\mathrm{d}\boldsymbol{R}_{ij}}{\mathrm{d}\eta_{ik}}\right)\boldsymbol{R}_{ij}^{-1}\left(\frac{\mathrm{d}\boldsymbol{\varepsilon}_{ij}^{\mathrm{T}}}{\mathrm{d}\eta_{il}} - \boldsymbol{\varepsilon}_{ij}^{\mathrm{T}}\boldsymbol{R}_{ij}^{-1}\frac{\mathrm{d}\boldsymbol{R}_{ij}}{\mathrm{d}\eta_{il}}\right)^{\mathrm{T}} + \mathrm{tr}\left[-\boldsymbol{R}_{ij}^{-1}\frac{\mathrm{d}\boldsymbol{R}_{ij}}{\mathrm{d}\eta_{ik}}\boldsymbol{R}_{ij}^{-1}\frac{\mathrm{d}\boldsymbol{R}_{ij}}{\mathrm{d}\eta_{il}}\right]\right] - \boldsymbol{\Omega}_{kl}^{-1} \quad \text{for} \quad k,l = 1,\ldots,p. \tag{2.150}$$

This version of the Laplacian approximation is known as the *first-order conditional estimation with interactions* (FOCEI). A common assumption is that the residual matrix $\boldsymbol{R}_{ij}$ is independent of $\boldsymbol{\eta}_i$. This is known as the first-order conditional estimation *without interactions* (FOCE).
As described in Section 2.3.2, gradient methods like Newton's method or the quasi-Newton method are applied to find the optimum of the individual likelihoods.

2.3.3.1 Expectation-Maximisation

Returning to the population log-likelihood function, given by

$$l(\boldsymbol{\psi};\boldsymbol{y}) = \log f(\boldsymbol{y}|\boldsymbol{\psi}), \tag{2.151}$$

where $\boldsymbol{\psi} = (\boldsymbol{\theta}, \boldsymbol{\Omega}, \boldsymbol{R})$. Maximum likelihood (ML) estimation of $l(\boldsymbol{\psi};\boldsymbol{y})$ tends to be involved here since the underlying model is dependent on the unobserved random effects $\boldsymbol{\eta}$. Consequently, the likelihood function needs to be marginalised with respect to $\boldsymbol{\eta}$ according to

$$\log f(\boldsymbol{y}|\boldsymbol{\psi}) = \int \log f(\boldsymbol{y},\boldsymbol{\eta}|\boldsymbol{\psi})\,\mathrm{d}\boldsymbol{\eta}, \tag{2.152}$$

where the integral over $\boldsymbol{\eta}$ is computed for every evaluation of $l(\boldsymbol{\psi};\boldsymbol{y})$. This computation can be simplified by utilising a Laplacian approximation of the log-likelihoods (as is down in the previously mentioned FOCE and FOCEI methods). As a consequence of applying the Laplacian approximation, the integral becomes Gaussian, and thus has an analytic solution. Nonetheless, the Hessian of the log-likelihoods still needs to be computed, which may be costly, error prone and complicated.
The aforementioned estimation is a form of *incomplete data problem*, as $\boldsymbol{y}$ is observed but not $\boldsymbol{\eta}$. A probabilistic approach to problems constituting incomplete data is to compute the expected value of the unobserved data, conditioned on the posterior distribution—which is assumed to be known. These values will subsequently be used to find ML estimates, from which the expected value of the unobserved data can be re-computed. This iterative scheme is known as the *Expectation-Maximisation* (EM) method (Dempster et al., 1977). To

demonstrate the algorithm, define the *Q-function* as

$$Q(\boldsymbol{\psi}|\boldsymbol{\psi}_k) = \mathrm{E}_{f(\cdot|\boldsymbol{y},\boldsymbol{\psi}_k)}[\log f(\boldsymbol{X}|\boldsymbol{\psi})] = \int \log f(\boldsymbol{x}|\boldsymbol{\psi}) f(\boldsymbol{x}|\boldsymbol{y},\boldsymbol{\psi}_k)\,\mathrm{d}\boldsymbol{x}, \tag{2.153}$$

where $\boldsymbol{x} = (\boldsymbol{y}, \boldsymbol{z})$ is the complete data ($\boldsymbol{y}$ being the incomplete, observed data, and $\boldsymbol{z}(= \boldsymbol{\eta})$ the unobserved data) and $p(\boldsymbol{x}|\boldsymbol{y},\boldsymbol{\psi}_k)$ the posterior distribution (conditioned on the observed data and current iterate $\boldsymbol{\psi}_k$). Computing the Q-function is the *expectation step* in the EM algorithm. In the subsequent *maximisation step*, the Q-function is maximised with respect to $\boldsymbol{\psi}$ as

$$\boldsymbol{\psi}_{k+1} = \arg\max_{\boldsymbol{\psi}} Q(\boldsymbol{\psi}|\boldsymbol{\psi}_k). \tag{2.154}$$

To show that the EM algorithm improves the likelihood, note that

$$l(\boldsymbol{\psi}_{k+1};\boldsymbol{y}) - l(\boldsymbol{\psi}_k;\boldsymbol{y}) = \log f(\boldsymbol{y}|\boldsymbol{\psi}_{k+1}) - \log f(\boldsymbol{y}|\boldsymbol{\psi}_k), \tag{2.155}$$

which by taking the expected value, conditioned on $\boldsymbol{y}$ and $\boldsymbol{\psi}_k$, yields

$$\begin{aligned} l(\boldsymbol{\psi}_{k+1};\boldsymbol{y}) - l(\boldsymbol{\psi}_k;\boldsymbol{y}) &= \mathrm{E}_{f(\cdot|\boldsymbol{y},\boldsymbol{\psi}_k)}[\log f(\boldsymbol{y}|\boldsymbol{\psi}_{k+1})] \\ &\quad - \mathrm{E}_{f(\cdot|\boldsymbol{y},\boldsymbol{\psi}_k)}[\log f(\boldsymbol{y}|\boldsymbol{\psi}_k)], \end{aligned} \tag{2.156}$$

since the left hand side is a constant. Moreover, as $P(A|C) = P(A,B|C)/P(B|A,C)$, it follows that

$$\begin{aligned} l(\boldsymbol{\psi}_{k+1};\boldsymbol{y}) - l(\boldsymbol{\psi}_k;\boldsymbol{y}) &= \mathrm{E}_{f(\cdot|\boldsymbol{y},\boldsymbol{\psi}_k)}\left[\log\left(\frac{f(\boldsymbol{X}|\boldsymbol{\psi}_{k+1})}{f(\boldsymbol{Z}|\boldsymbol{y},\boldsymbol{\psi}_{k+1})}\right)\right] \\ &\quad - \mathrm{E}_{f(\cdot|\boldsymbol{y},\boldsymbol{\psi}_k)}\left[\log\left(\frac{f(\boldsymbol{X}|\boldsymbol{\psi}_k)}{f(\boldsymbol{Z}|\boldsymbol{y},\boldsymbol{\psi}_k)}\right)\right], \end{aligned} \tag{2.157}$$

rearranging the terms gives

$$\begin{aligned} l(\boldsymbol{\psi}_{k+1};\boldsymbol{y}) - l(\boldsymbol{\psi}_k;\boldsymbol{y}) &= Q(\boldsymbol{\psi}_{k+1}|\boldsymbol{\psi}_k) - Q(\boldsymbol{\psi}_k|\boldsymbol{\psi}_k) \\ &\quad + \mathrm{E}_{f(\cdot|\boldsymbol{y},\boldsymbol{\psi}_k)}\left[-\log\left(\frac{(\boldsymbol{Z}|\boldsymbol{y},\boldsymbol{\psi}_{k+1})}{f(\boldsymbol{Z}|\boldsymbol{y},\boldsymbol{\psi}_k)}\right)\right]. \end{aligned} \tag{2.158}$$

Moreover, since the negative logarithm is convex, *Jensen's inequality* gives

$$\mathrm{E}_{f(\cdot|\boldsymbol{y},\boldsymbol{\psi}_k)}\left[-\log\left(\frac{f(\boldsymbol{Z}|\boldsymbol{y},\boldsymbol{\psi}_{k+1})}{f(\boldsymbol{Z}|\boldsymbol{y},\boldsymbol{\psi}_k)}\right)\right] \geq -\log \mathrm{E}_{f(\cdot|\boldsymbol{y},\boldsymbol{\psi}_k)}\left[\frac{f(\boldsymbol{Z}|\boldsymbol{y},\boldsymbol{\psi}_{k+1})}{f(\boldsymbol{Z}|\boldsymbol{y},\boldsymbol{\psi}_k)}\right] = 0. \tag{2.159}$$

Thus, by choosing $\boldsymbol{\psi}_{k+1}$ such that

$$Q(\boldsymbol{\psi}_{k+1}|\boldsymbol{\psi}_k) \geq Q(\boldsymbol{\psi}_k|\boldsymbol{\psi}_k), \tag{2.160}$$

we get

$$l(\boldsymbol{\psi}_{k+1};\boldsymbol{y}) - l(\boldsymbol{\psi}_k;\boldsymbol{y}) \geq Q(\boldsymbol{\psi}_{k+1}|\boldsymbol{\psi}_k) - Q(\boldsymbol{\psi}_k|\boldsymbol{\psi}_k) \geq 0 \tag{2.161}$$

which imply

$$l(\boldsymbol{\psi}_{k+1};\boldsymbol{y}) \geq l(\boldsymbol{\psi}_k;\boldsymbol{y}). \tag{2.162}$$

Thus, the likelihood has been improved in the iterate $\boldsymbol{\psi}_{k+1}$, relative $\boldsymbol{\psi}_k$, which shows that the EM algorithm improves the likelihood.

2.3.3.2 Monte Carlo and Stochastic Approximation of the Expectation-Maximisation

The integral computed in the expectation step of Eq. (2.153) does not necessarily have a closed-form solution. If this is the case, *Monte Carlo* integration may be used to find an approximation of the Q-function. The expectation step is then replaced by a *simulation step* where n_k realisations of the posterior distribution are generated at the kth iteration, and the Q-function is approximated according to

$$\widehat{Q}(\boldsymbol{\psi}|\boldsymbol{\psi}_k) = \frac{1}{n_k}\sum_{i=1}^{n_k} \log f(\boldsymbol{X}_i|\boldsymbol{\psi}), \tag{2.163}$$

where $\boldsymbol{X}_i \sim f(\cdot|\boldsymbol{y},\boldsymbol{\psi}_k)$ for $i = 1,\ldots,n_k$. This modification of the EM approach is known as the Monte Carlo EM (MCEM). In situations where it is difficult to generate random samples from the posterior distribution, an alternative distribution may be used according to the *importance sampling* method. Importance sampling relies on the premise that

$$\begin{aligned}
\mathrm{E}_{f(\cdot|\boldsymbol{y},\boldsymbol{\psi}_k)}[\log f(\boldsymbol{X}|\boldsymbol{\psi})] &= \int \log f(\boldsymbol{x}|\boldsymbol{\psi}) f(\boldsymbol{x}|\boldsymbol{y},\boldsymbol{\psi}_k)\,\mathrm{d}\boldsymbol{x} && (2.164)\\
&= \int \log f(\boldsymbol{x}|\boldsymbol{\psi}) \frac{f(\boldsymbol{x}|\boldsymbol{y},\boldsymbol{\psi}_k)}{g(\boldsymbol{x}|\boldsymbol{y},\boldsymbol{\psi}_k)} g(\boldsymbol{x}|\boldsymbol{y},\boldsymbol{\psi}_k)\,\mathrm{d}\boldsymbol{x} && (2.165)\\
&= \mathrm{E}_{g(\cdot|\boldsymbol{y},\boldsymbol{\psi}_k)}\left[\log f(\boldsymbol{X}|\boldsymbol{\psi}) \frac{f(\boldsymbol{X}|\boldsymbol{y}|\boldsymbol{\psi}_k)}{g(\boldsymbol{X}|\boldsymbol{y},\boldsymbol{\psi}_k)}\right]. && (2.166)
\end{aligned}$$

Thus, n_k samples can be drawn from $g(\cdot|\boldsymbol{y},\boldsymbol{\psi}_k)$[16], rather than from $f(\cdot|\boldsymbol{y},\boldsymbol{\psi}_k)$, and the Q-function approximated as

$$\widehat{Q}(\boldsymbol{\psi}|\boldsymbol{\psi}_k) = \frac{1}{n_k}\sum_{i=1}^{n_k} \log f(\boldsymbol{X}_i|\boldsymbol{\psi}) \frac{f(\boldsymbol{X}_i|\boldsymbol{y}|\boldsymbol{\psi}_k)}{g(\boldsymbol{X}_i|\boldsymbol{y},\boldsymbol{\psi}_k)}. \tag{2.167}$$

[16]The probability distribution g does not necessarily have to be dependent on $\boldsymbol{y}$ or $\boldsymbol{\psi}_k$.

The distribution $g(\cdot|\boldsymbol{y}, \boldsymbol{\psi}_k)$ is preferably chosen to mimic the posterior distribution $f(\boldsymbol{x}|\boldsymbol{y}, \boldsymbol{\psi}_k)$. In this way, the frequencies of the samples correspond to their weights $\log f(\boldsymbol{X}|\boldsymbol{\psi}) \frac{f(\boldsymbol{X}|\boldsymbol{y}|\boldsymbol{\psi}_k)}{g(\boldsymbol{X}|\boldsymbol{y}, \boldsymbol{\psi}_k)}$ — thus, favouring the "important" samples. By the *inverse sampling method*, it is possible to generate samples as long as the proposed density has an injective cumulative distribution. Moreover, the performance of the method may be improved[17] by applying a quasi-random method, such as *Sobol sequences*, to generate the random sample—known as the *Quasi-Random Parametric Expectation-Maximisation* (QRPEM) method.
Finally, another popular modification of the EM algorithm is *Stochastic Approximation* (SAEM). Here, a simulation step, where n_k samples are drawn from the posterior distribution, replaces the expectation step. However, the approximation of the Q-function is

$$\widetilde{Q}(\boldsymbol{\psi}|\boldsymbol{\psi}_k) = \widetilde{Q}(\boldsymbol{\psi}|\boldsymbol{\psi}_{k-1}) + \gamma_k \left(\frac{1}{n_k} \sum_{i=1}^{n_k} \log p(\boldsymbol{X}_i|\boldsymbol{\psi}) - \widetilde{Q}(\boldsymbol{\psi}|\boldsymbol{\psi}_{k-1}) \right), \tag{2.168}$$

where $\{\gamma_k\}_{k\geq 1}$ is a decreasing sequence of positive numbers. For details on the convergence of the EM methods, see lDelyon et al. (1999).

2.3.4 Profile likelihood

Profile likelihood is a tool for structural and practical identifiability analysis. The premise of the method is that parameter non-identifiability manifests itself as flat hypersurfaces of the likelihood function (Raue et al., 2009). The profile of these surfaces can be analysed before the parameter estimation, without any real data, by studying the likelihood obtained from a randomly generated realisation of the system. Since identifiability is a generic property of a model structure (i.e., independent of the parameter values), the identifiability holds even if the generated parameters are infeasible.
Consider a maximum likelihood estimation problem with the log-likelihood function $l(\boldsymbol{\theta}, \boldsymbol{y})$ and a random sample $\hat{\boldsymbol{\theta}}$, drawn from the parameter space $\boldsymbol{\Theta}$. By fixing all but one parameter $\hat{\theta}_i$, $(i = 1, \ldots, p)$, the profile likelihood is readily visualised as a function of a single parameter according to

$$\mathrm{PL}(\hat{\theta}_i) = \max_{\hat{\theta}_{j\neq i}} l(\hat{\boldsymbol{\theta}}; \boldsymbol{y}). \tag{2.169}$$

Thus, for each value θ_i, the profile likelihood is found by optimising the likelihood. Potential local parameter non-identifiability manifests itself by a flat profile likelihood curve. By analysing one parameter at a time, the profile likelihood can be used to find specific parameters, or parameter combinations (by examining a multidimensional profile likelihood), that are non-identifiable.
In the posterior profile likelihood analysis, non-identifiability characterises itself as high uncertainty in the parameter estimates. Unlike the prior analysis, this analysis also ensures

[17] Improved performance in the sense of decreased sample size and increased accuracy.

practical local (non-)identifiability.

2.3.5 Software

The NLME modelling and simulations, and the identifiability analysis in this thesis, were performed using Wolfram Mathematica (Wolfram Research, Inc., Mathematica, Version 11.1, Champaign, IL (2017)). Mathematica is a powerful mathematical programming language which supports multiple programming paradigms and is powerful for symbolic computations and visualisations. The estimation was computed by maximising the FOCE approximation of the population likelihood. This was done using a method developed at the Fraunhofer-Chalmers Research Centre for Industrial Mathematics (Gothenburg, Sweden) (Almquist et al., 2015), which combines exact gradients of the FOCE likelihood based on the so-called sensitivity equations with the Boyden-Fletcher-Goldfarb-Shanno optimisation algorithm (Nocedal and Wright, 2006). Parameter standard errors were derived using the Hessian of the approximate population likelihood with respect to the parameters, evaluated at the point estimate. The Hessian was computed using finite differences of the exact gradients.
When performing numerical calculations with plenty of data, MATLAB (The MathWorks Inc., Natick, MA) is an alternative to Mathematica. MATLAB is a user-friendly software, which compromises a plethora of toolboxes—designed for a range of different mathematical problems. The language is highly efficient when handling linear algebraic problems.

2.3.5.1 Nonlinear mixed-effects estimation

There exists a variety of software for parameter estimation in nonlinear mixed-effects models. Sheiner and Beal (Sheiner et al., 1977; Sheiner and Beal, 1980, 1981, 1983) developed the most frequently used NONMEM (ICON Development Solutions, Ellicott City, MD, USA) software in the 80's. Some other commonly used software in practise today are the Monolix (Lixoft, Orsay, France) and Phoenix NLME (Pharsight Corporation, St Louis, MO, USA) tools, based on the SAEM and QRPEM algorithm, respectively.

2.4 Sensitivity analysis

Sensitivity analysis (SA) constitutes a modelling and simulation framework in which the aim is to quantify the sensitivity and robustness of a modelled system output concerning variations in the input. SA strives to answer the following important questions:

- Redundancy—are there parts of the model which are unnecessary?
- Prioritisation—are there specific components of the system that need to more thoroughly analysed to ensure robustness?
- Hidden relationships—in particular, do they make sense from a biological or pharmacological point-of-view?

- If changes occur in the system—how will this affect the output?
- Critical values—e.g., what are the maximum possible responses?
- Design and communication—is the system particularly sensitive at some instance? Knowledge like this is informative when designing future experiments (to, for example, decide when to sample during the experiments).

2.4.1 Methods

There are several ways to approach an SA. One method is *one-at-a-time*, where all but one of the input signals or parameters are held fixed while the particular signal is moved throughout feasible values. An alternative method is *local sensitivity analysis*. For an expected response $h(\boldsymbol{x}, \boldsymbol{u}, \boldsymbol{\phi})$ and a local point in the parameter space $\boldsymbol{\phi}^0$ (e.g., the optimal solution), we analyse

$$\left.\frac{\partial h(\boldsymbol{x}, \boldsymbol{u}, \boldsymbol{\phi})}{\partial \phi_i}\right|_{\boldsymbol{\phi}^0}, \tag{2.170}$$

or

$$\left.\frac{\partial h(\boldsymbol{x}, \boldsymbol{u}, \boldsymbol{\phi})}{\partial u_i}\right|_{\boldsymbol{\phi}^0}, \tag{2.171}$$

for one parameter ϕ_i, or input signal u_i, at-a-time.
For more SA techniques and details, see Clemson et al. (1995) or Greenland (1996).

2.5 Model evaluation

The derived and estimated regression models (whether they are linear, nonlinear, or nonlinear mixed-effects) rely on some fundamental assumptions. It is crucial to recognise these assumptions, question their validity, and understand their implications. It is assumed that:

- The proposed model captures all vital components of the system without incorporating any redundancy.
- Individuals are independent.
- The residuals are independent, identically normally distributed with mean zero and time-invariant standard deviation.

In many ways, the first assumption represents the core objective of model identification; to find an accurate mathematical representation of, in our case, a pharmacological system. The question of what constitutes vital components of the system depends on the purpose of the model, rightly stated before the modelling procedure. The assumption that the individuals are independent is strong, and generally, does not hold. Still, it may prove to be

a valid representation of reality since the dependencies tend to be negligible. Assuming that individuals are independent often simplifies computations without introducing too much bias. The last assumption is central when deriving the maximum likelihood estimator.
The following discussion will aim to verify the validity of the stated assumptions. Moreover, we will discuss how to assess the performance of the model, as well as introduce methods for comparisons of separate models. A central theme will be the concepts of *bias* and *variability*. With a finite data set, model bias is inversely proportional to the variability. Thus, there is a trade-off between having an accurate model and a precise model, which is a well-known phenomenon in mathematical and statistical modelling (Myers, 2000). An estimation with high accuracy, but low precision, is known to be *overfitted*, and one with low accuracy and high precision is *underfitted*. What characterises overfitted models is that they describe the available data well, but lack the generality needed to, for example, predict future experimental trials. Underfitted models, on the other hand, lack the ability to capture all of the important aspects of the system.
A standard approach in model identification, if data are abundant, is to divide the data into training and test sets. The training set serves to derive and estimate the model, while the test set acts to assess the performance of the model. As a rule of thumb, 80% of the data are assigned as training data and 20% test data—either by randomization or by a deterministic division of the data (Bonate, 2011). However, this modelling approach requires a sufficient amount of data to uphold practical identifiability. The data in pharmacological studies are often sparse, specifically in pre-clinical studies. Thus, the method is not always applicable.
The following discussion on model validation presents a range of *quantitative* and *qualitative* tools. Quantitative validations provide a direct measure of the performance of the model, while qualitative validations rely on graphical representations of the results, which are interpreted by the modeller.

2.5.1 Quantitative analysis

The most obvious quantitative measure of how well a model fits a set of data is the uncertainty of the parameter estimates. As discussed previously, there is a trade-off between bias and variability of the parameter estimates. As a rule of thumb, we consider parameter estimates to be precise if the corresponding CV% is less than 25% (Bonate, 2011). Besides the precision of the parameter estimates, we will introduce the concept of *shrinkage* as a quantitative measure of the variability of the residuals and the Empirical Bayes Estimates (EBE). Shrinkage serves as a valuable tool for validating the graphical results. Finally, we discuss information criteria as measures of the model fit, and thereby its quality in comparison to other possible candidate models.

2.5.1.1 Shrinkage analysis

Assume a nonlinear mixed-effects model. The *individual predictions* (sometimes referred to as the IPRED) for individual i at time-point t_j is given by

$$\hat{\boldsymbol{y}}_{ij} = \boldsymbol{h}(\boldsymbol{x}_i(t_j), \boldsymbol{u}_i, \boldsymbol{\phi}_i), \tag{2.172}$$

where $\boldsymbol{h}$ are the expectation functions, which characterise the system behaviour, $\boldsymbol{x}_i$ are the state variables, $\boldsymbol{u}_i$ the input functions, and $\boldsymbol{\phi}_i$ the system parameters. Define the *individual weighted residual* as

$$\text{IWRES}_{ij} = \frac{\boldsymbol{y}_{ij} - \hat{\boldsymbol{y}}_{ij}}{\sigma}, \tag{2.173}$$

where $\boldsymbol{y}_{ij}$ are the observed data for individual i at time-point j, and σ is the standard deviation of the residuals. The *ε-shrinkage* is then defined as

$$\varepsilon_{\text{shrinkage}} \coloneqq 1 - \text{SD}(\text{IWRES}_{ij}) \tag{2.174}$$

As the individual predictions tend toward the dependent variable, the distribution of the IWRES shrinks towards 0, and the $\varepsilon_{\text{shrinkage}}$ tends to 1. A shrinking distribution of IWRES indicates that the model is overfitted. On the other hand, a high $\varepsilon_{\text{shrinkage}}$ expresses an underfitted model.
In contrast to ε-shrinkage, η-shrinkage describes the variability of the Empirical Bayes Estimates (EBE). Given that a random effect has the estimated standard error ω, its corresponding η-shrinkage is given by

$$\eta_{\text{shrinkage}} \coloneqq 1 - \frac{\text{SD}(\eta_{\text{EBE}})}{\sqrt{\omega^2}}. \tag{2.175}$$

The η-shrinkage describes the information in the data on an individual level. If data are uninformative on an individual level, the standard deviation of the EBEs will shrink towards 0, giving an η-shrinkage near 1.
In the presence of shrinkage the diagnostics, involving EBEs and residuals, may lose their validity and distort the true relationships. For example, high levels of ε-shrinkage may result in the residual distribution deviating from a Gaussian distribution, even if the underlying model is correct (or vice versa). Similarly, high levels of η-shrinkage may result in misleading correlations between the EBEs and the covariates (or may fail to show existing correlations). It has been shown that at shrinkage levels of 20-30%, the results may start to be misleading (Savic and Karlsson, 2009).

2.5.1.2 Information criterion

Consider a scenario with two, or more, candidate models that describe an observed system. The natural question that arises is what model produces the 'best fit'? In general, the more

complex the model, the higher the accuracy. On the other hand, a complex model will introduce variability. The *Akaike information criterion* (AIC) is a measure of the fit of a model—based on the premise that the criterion rewards accuracy but penalise complexity. This criterion serve as tools for model comparison, as it do not require the models to have the same parameters, the same state variables, or even the same response relation.
In order to derive the AIC, assume a sample of observations $\boldsymbol{y} = y_1, \ldots, y_n$ from the true underlying density function $g(\boldsymbol{y})$. Consider a set of potential models denoted by $\mathcal{M}$. A model, $M_i \in \mathcal{M}$, will be known as a candidate model. Each candidate model has a corresponding class of probability density functions defined as

$$\mathcal{F}_k = \{f(\boldsymbol{y}|\boldsymbol{\theta}_k) : \boldsymbol{\theta}_k \in \boldsymbol{\Theta}_k\}, \tag{2.176}$$

where k is the dimension of the parameter vector $\boldsymbol{\theta}_k$ and $\boldsymbol{\Theta}_k$ is the set of potential parameter vectors of dimension k.

2.5.1.3 Akaike information criterion

Consider the *Kullback-Leibler information* $I_{\mathrm{KL}}(\boldsymbol{\theta})$[18] defined as

$$I_{\mathrm{KL}}(\boldsymbol{\theta}) = \mathrm{E}\left[\log\left(\frac{g(\boldsymbol{y})}{f(\boldsymbol{y}|\boldsymbol{\theta})}\right)\right], \tag{2.177}$$

where the expected value is taken over the density $g(\cdot)$. The Kullback-Leibler information is a measure of how much $f(\boldsymbol{y}|\boldsymbol{\theta})$ diverges from $g(\boldsymbol{y})$, and it will be positive unless $f(\boldsymbol{y}|\boldsymbol{\theta}) = g(\boldsymbol{y})$ almost everywhere. Consider the re-written relation

$$2I_{\mathrm{KL}}(\boldsymbol{\theta}) = D_{\mathrm{KL}}(\boldsymbol{\theta}) - \mathrm{E}[-2\log g(\boldsymbol{y})], \tag{2.178}$$

where

$$D_{\mathrm{KL}}(\boldsymbol{\theta}) = \mathrm{E}[-2\log(f(\boldsymbol{y}|\boldsymbol{\theta}))], \tag{2.179}$$

is known as the *Kullback divergence*. Note that the term $\mathrm{E}[-2\log g(\boldsymbol{y})]$ is independent of the candidate model. Hence, minimising the Kullback-Leibler information is equivalent to maximising the Kullback divergence. We will consider the Kullback divergence, evaluated at the MLE estimate $\hat{\boldsymbol{\theta}}$, for model comparisons. This would seem to be an appropriate measure of the fit of a model. Yet, $D_{\mathrm{KL}}(\hat{\boldsymbol{\theta}})$ cannot be directly computed as the underlying density $g(\boldsymbol{y})$ is unknown. However, we will see that the following term

$$\mathrm{AIC} := -2l(\hat{\boldsymbol{\theta}}|\boldsymbol{y}) + 2k, \tag{2.180}$$

[18] The index k of $\boldsymbol{\theta}_k$ will be dropped for the sake of convenience.

is an unbiased estimator of $D_{\mathrm{KL}}(\hat{\boldsymbol{\theta}})$ (here, k is the dimension of $\boldsymbol{\theta}$). To show this, assume that the true distribution belongs to model M_i[19]. In that case, $g(\boldsymbol{y}) = f(\boldsymbol{y}|\boldsymbol{\theta}_0)$ for some $\boldsymbol{\theta}_0 \in \boldsymbol{\Theta}_k$. The expected Kullback divergence can be expressed as

$$\begin{aligned} \mathrm{E}[D_{\mathrm{KL}}(\hat{\boldsymbol{\theta}})] &= \mathrm{E}[-2\log f(\boldsymbol{y}|\hat{\boldsymbol{\theta}})] && (2.181)\\ &+ (\mathrm{E}[-2\log f(\boldsymbol{y}|\boldsymbol{\theta}_0] - \mathrm{E}[-2\log f(\boldsymbol{y}|\hat{\boldsymbol{\theta}})]) && (2.182)\\ &+ (\mathrm{E}[D_{\mathrm{KL}}(\hat{\boldsymbol{\theta}})] - \mathrm{E}[-2\log f(\boldsymbol{y}|\boldsymbol{\theta}_0]). && (2.183) \end{aligned}$$

By applying the second-order expansion of $\log f(\boldsymbol{y}|\boldsymbol{\theta}_0)$ about $\hat{\boldsymbol{\theta}}$, we get

$$\mathrm{E}[-2\log f(\boldsymbol{y}|\boldsymbol{\theta}_0)] = \mathrm{E}[-2\log f(\boldsymbol{y}|\hat{\boldsymbol{\theta}})] - \mathrm{E}[(\hat{\boldsymbol{\theta}} - \boldsymbol{\theta}_0)^{\mathrm{T}} H[f(\boldsymbol{y}|\hat{\boldsymbol{\theta}})]^{-1}(\hat{\boldsymbol{\theta}} - \boldsymbol{\theta}_0)] + O(1), \quad (2.184)$$

or

$$\mathrm{E}[-2\log f(\boldsymbol{y}|\boldsymbol{\theta}_0)] = \mathrm{E}[-2\log f(\boldsymbol{y}|\hat{\boldsymbol{\theta}})] + \mathrm{E}[(\hat{\boldsymbol{\theta}} - \boldsymbol{\theta}_0)^{\mathrm{T}} \mathcal{I}(\boldsymbol{y}|\hat{\boldsymbol{\theta}})^{-1}(\hat{\boldsymbol{\theta}} - \boldsymbol{\theta}_0)] + O(1), \quad (2.185)$$

where $\mathcal{I}(\boldsymbol{y}|\hat{\boldsymbol{\theta}})$ is the expected Fisher Information matrix and where the first-order term disappears since the likelihood is maximised over $\hat{\boldsymbol{\theta}}$. Note the expected Fisher information is related to the Hessian as $H[f(\boldsymbol{y}|\hat{\boldsymbol{\theta}})] = -\mathcal{I}(\boldsymbol{y}|\hat{\boldsymbol{\theta}})$. Furthermore, by applying a second-order expansion of $d(\hat{\boldsymbol{\theta}})$ about $\boldsymbol{\theta}_0$, we obtain

$$\mathrm{E}[d(\hat{\boldsymbol{\theta}})] = \mathrm{E}[-2\log f(\boldsymbol{y}|\boldsymbol{\theta}_0)] + \mathrm{E}[(\hat{\boldsymbol{\theta}} - \boldsymbol{\theta}_0)^{\mathrm{T}} \mathcal{I}(\boldsymbol{y}|\boldsymbol{\theta}_0)^{-1}(\hat{\boldsymbol{\theta}} - \boldsymbol{\theta}_0)] + O(1), \quad (2.186)$$

where $\mathcal{I}(\boldsymbol{y}|\boldsymbol{\theta}_0)$ is the observed Fisher Information matrix and where the first-order term again disappears since $d(\boldsymbol{\theta})$ is maximised over $\boldsymbol{\theta}_0$. Thus, we have

$$\begin{aligned} \mathrm{E}[d(\hat{\boldsymbol{\theta}})] &= \mathrm{E}[-2\log f(\boldsymbol{y}|\hat{\boldsymbol{\theta}})] && (2.187)\\ &+ \mathrm{E}[(\hat{\boldsymbol{\theta}} - \boldsymbol{\theta}_0)^{\mathrm{T}} \mathcal{I}(\boldsymbol{y}|\hat{\boldsymbol{\theta}})^{-1}(\hat{\boldsymbol{\theta}} - \boldsymbol{\theta}_0)] && (2.188)\\ &+ \mathrm{E}[(\hat{\boldsymbol{\theta}} - \boldsymbol{\theta}_0)^{\mathrm{T}} \mathcal{I}(\boldsymbol{y}|\boldsymbol{\theta}_0)^{-1}(\hat{\boldsymbol{\theta}} - \boldsymbol{\theta}_0)] + O(1). && (2.189) \end{aligned}$$

However, as $\boldsymbol{\theta}_0 \in \boldsymbol{\Theta}_k$, we have

$$(\hat{\boldsymbol{\theta}} - \boldsymbol{\theta}_0)^{\mathrm{T}} \mathcal{I}(\boldsymbol{y}|\hat{\boldsymbol{\theta}})^{-1}(\hat{\boldsymbol{\theta}} - \boldsymbol{\theta}_0) \xrightarrow{d} \chi^2(k), \quad (2.190)$$

i.e., the second-order term converges in distribution to a χ^2 distributed variable with k degrees of freedom. As $\mathrm{E}[\chi^2(k)] = k$ we obtain

$$\begin{aligned} \mathrm{E}[d(\hat{\boldsymbol{\theta}})] &= \mathrm{E}[-2\log f(\boldsymbol{y}|\hat{\boldsymbol{\theta}})] + 2k + O(1) = && (2.191)\\ &= -2l(\hat{\boldsymbol{\theta}}|\boldsymbol{y}) + 2k + O(1), && (2.192) \end{aligned}$$

[19] This is obviously a strong assumption. For details on how this assumption affects the conclusion, see Cavanaugh et al. (Cavanaugh and Neath, 2011).

and we are done.

2.5.2 Qualitative analysis

The following discussion will introduce graphical tools for assessing the fit of a model in a population, as well as at an individual, level. Moreover, we will discuss techniques for verifying the prior assumptions of, for example, normally distributed residuals and EBE's.

2.5.2.1 Visual predictive check plots

The *visual predictive check* (VPC) plots capture many of the important features of a model. A VPC typically includes the observed data, the estimated population mean or median, a simulation-based confidence interval for the mean or median, observed quantiles, a model predicted quantile-quantile span that, for example, covers 90% of the predicted behaviour (i.e., a band is plotted between the 5% and 95% quantiles), simulation-based confidence interval for the quantiles (for details, see Bergstrand et al. (2011)). An example, generated from the model and data from Example 2.1.3.2, is illustrated in Fig 2.6.

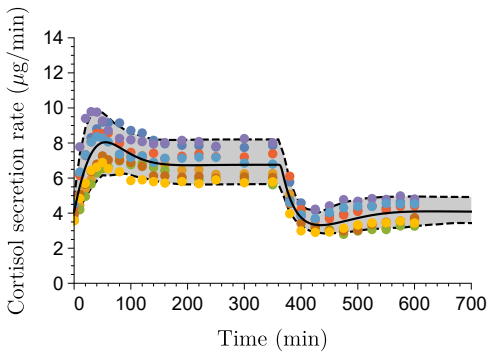

Figure 2.6: Visual predictive check plot generated from Example 2.1.3.2. The dots represent the data, with colours indicating separate individuals, the black line the estimated median individual, and the grey area the 90% population prediction interval.

2.5.2.2 Individual fits

Individual plots serve to demonstrate the ability of the model to capture the between-subject variability seen in the population. The plots involve the observed data of an individual along with the IPRED. Two examples, generated from the model and data of Example 2.1.3.2, are illustrated in Fig 2.7. The individual plots suggest that the model captures between-subject variability well.

2.5.2.3 Scatter and probability plots

Scatter plots illustrate pair-wise comparisons between two quantities, typically the observed and predicted behaviours. Fig. 2.8b shows an example of a scatter plot with the observed and

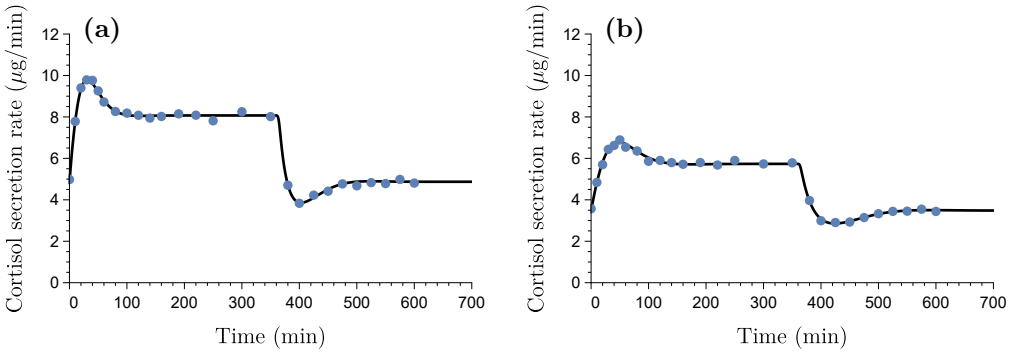

Figure 2.7: Individual predicted response behaviour of two individuals taken from Example 2.1.3.2. The blue dots represent the data and the the black line the model predicted behaviour.

the predicted response from Example 2.1.3.2. The example illustrates a linear relationship between the two quantities along the line $y = x$, which shows that the model captures the observed behaviour well. Probability plots refer to *quantile-quantile* (Q-Q) plots or *probability-probability* (percent-percent) (P-P) plots, which are particular instances of scatter plots. In Q-Q plots, two *cumulative distribution functions* (CDF) are outlined against each other. Typically, one of the CDF's is a theoretical (predicted) distribution and the other an empirical (data) distribution. The quantiles of the theoretical distribution can be selected in various ways. Given a set of n data points, one common approach is to chose the k/n quantiles, where $k = 1, \ldots, n$, in which the n/n is the 100% quantile. Alternatively, the $(k - 0.5)/n$ quantiles are chosen, where $k = 1, \ldots, n$. In contrast to Q-Q plots, P-P plots represent the CDF's themselves, rather than their quantiles. The P-P plot is a slightly less common probability plot due its features; whereas a Q-Q plot is weighted to provide additional information about the outliers (which often are of most interest when assessing the difference between, for example, an empirical and theoretical CDF), the P-P plots are weighted to be denser near the medians. The Q-Q plot of the empirical and theoretical distributions from Example 2.1.3.2 are illustrated in Fig. 2.8c and the corresponding P-P plot is illustrated in Fig. 2.8d. The P-P plot indicates a nearly perfect fit between the observed and theoretical probabilities while the Q-Q plot suggests a somewhat higher kurtosis (heavier tails) of the observed distribution.

2.5.2.4 Histograms

A histogram represents an estimation of the underlying *probability density function* (PDF) of, for example, the data. Histograms are constructed by dividing the range of the PDF into equally sized bins[20], and then plot a bar for each bin, whose size corresponds to the number of observations in the given interval of the bin. There are many different approaches

[20] Using equally sized bins are the standard approach when constructing histograms. The bins may vary in size (Freedman et al., 2007).

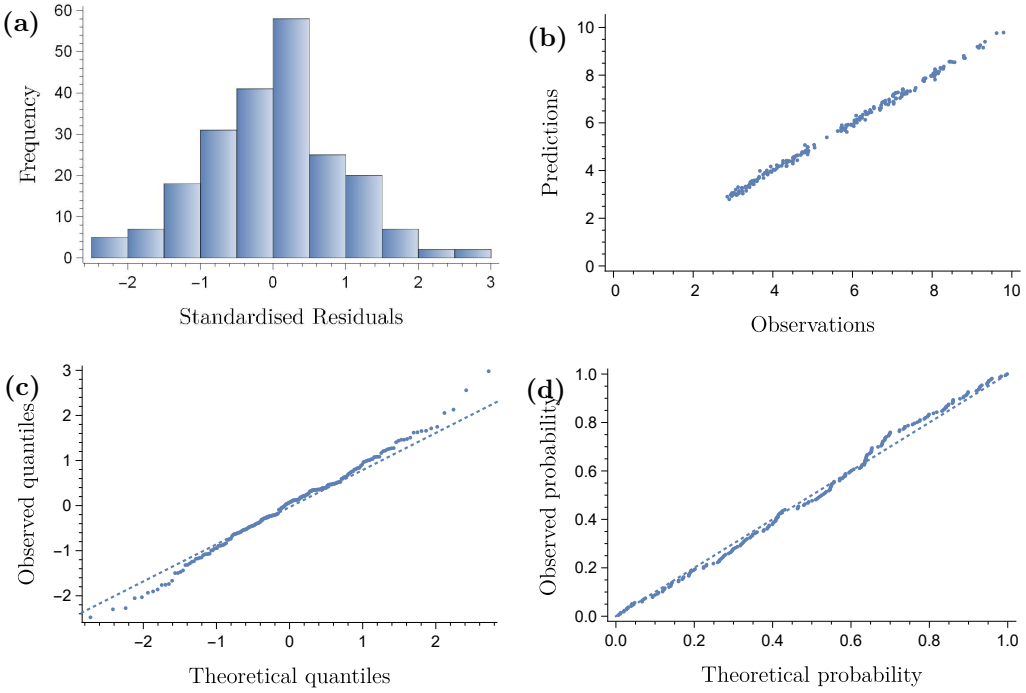

Figure 2.8: Plot of results in Example 2.1.3.2. Fig. (a) illustrates the distribution of the standardised residuals in the form of a histogram, (b) a scatter plot of the observations vs. the predicted values, (c) a Q-Q plot of the observed vs. the predicted residuals, and (d) a P-P plot of the observed vs. the predicted residuals.

to choose the number of bins. For a tutorial, see Freedman et al. (2007). An example of a histogram is illustrated in Fig. 2.8a. The histogram suggests that a normal distribution is possible for the standardised residuals.

2.6 Summary

This chapter has served to illustrate the dose-response-time model identification procedure. Starting by investigating the data, a suitable pharmacodynamic model, as well as driving biophase function, are selected. The biophase function is typically simple in its structure, consisting of few parameters, and the choice of biophase depends on the route of administration. For the pharmacodynamic model, this chapter has demonstrated a range of different structures, able to describe the direct and indirect response, nonlinear drug-response behaviour, feedback mechanisms, adaptation and so forth. Dependent on the type of data and the aim of the model, the structure may be extended to capture between-subject variability. This is done by applying a nonlinear mixed-effects modelling framework. Here, it was demonstrated how to choose fixed and random effects as well as the covariance structure of the random effects. For the selected model to make sense, and for the parameters to be uniquely

determined by the data, the model needs to be structurally identifiable. Three different a priori identifiability methods and one a posteriori method were presented for determining structural and practical identifiability, respectively. Given that the model is structurally identifiable, the parameter estimation may be initiated. Here, different approaches were demonstrated depending on the type of model. In the linear case, the parameters may be found analytically by solving the linear system for the parameters and then evaluating the solution at the observed data points. In the case of a nonlinear model, the parameters are estimated numerically. The estimation is typically done by applying some form of Newton's method. Here, the quasi-Newton methods, in particular, the Broyden-Fletcher-Goldfarb-Shanno algorithm, and the Levenberg-Marquardt method were discussed. This includes convergence analysis for the different methods. Further, parameter estimation for nonlinear mixed-effects models was examined. Here, the population likelihood function was derived and a range of software, designed for parameter estimation of nonlinear mixed-effects models, was presented. Following the discussion on parameter estimation, sensitivity analysis was introduced, both from an *a priori* and an *a posteriori* perspective. Finally, model validation, from both a quantitative and qualitative perspective, were considered to verify the results obtained from the parameter estimation.

Although the different methods were presented logically, where each method represented a natural continuation of the modelling procedure, it is important to recognise that model identification is not typically a linear process. The different steps are often iterated and, for example, practical non-identifiability may require the model structure to be modified, which in turn leads to an updated structural identifiability analysis (unless the modified model is a simplified version of the original), after that the parameters may be re-estimated.

Part II

Analysis and results

Chapter 3

Background

The dose-response-time (DRT) modelling framework will be demonstrated by two extensive meta-analyses of the nicotinic acid (NiAc) interaction with free fatty acids (FFA). Since the pharmacokinetic properties of NiAc have been thoroughly characterised by Ahlström et al. (2011b), the results of the two meta-analyses can be compared to those of exposure-driven analyses.
This chapter serves to provide a brief description of the drug; comprising the underlying physiology of antilipolysis, the pharmacokinetics of NiAc, and the data analysed in the two studies.

3.1 Nicotinic acid-induced antilipolysis

Nicotinic acid (NiAc; or niacin; or vitamin B_3) is an organic compound with a long clinical history in the treatment of dyslipidemia (Altschul and Hoffer, 1960; Carlson and Orö, 1962). When administered in large doses (1-3 g/day), NiAc improves the plasma lipid profile by reducing total cholesterol, triglycerides, low-density lipoprotein cholesterol, and very-low-density lipoprotein cholesterol, while increasing levels of high-density lipoprotein cholesterol (Kendall et al., 2002). Furthermore, by binding to the G-protein coupled receptor GPR109A, NiAc potently inhibits lipolysis in adipose tissue, resulting in decreased plasma free fatty acid (FFA) concentrations (Offermanns, 2006; Tunaru et al., 2003). The mechanisms of NiAc-induced antilipolysis have been thoroughly analysed by Heemskerk et al. (2014) among others (Chen et al., 2015; Li et al., 2011; Oh et al., 2011). Chronically

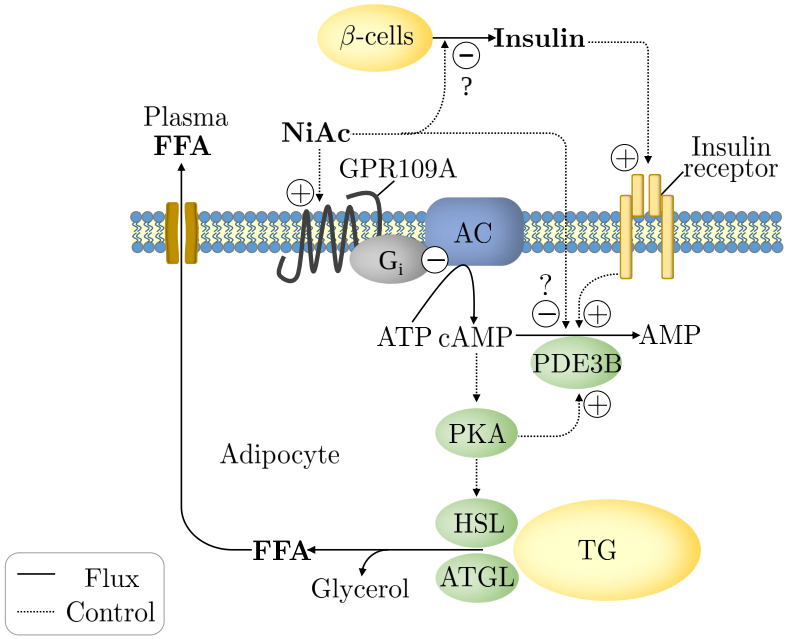

Figure 3.1: Mechanisms of nicotinic acid (NiAc) and insulin induced antilipolysis in adipose tissue. NiAc binds and activates the inhibitory G-protein (G_i) coupled receptor GPR109A, abundantly expressed in adipose tissue. Following activation, GPR109A inhibits adenylate cyclase (AC), a membrane-bound enzyme that hydrolyses adenosine triphosphate (ATP) into cyclic adenosine monophosphate (cAMP), resulting in reduced intracellular cAMP concentrations. Consequently, the activity of the cAMP-dependent protein kinase A (PKA) is reduced. The rate limiting step in free fatty acid (FFA) and glycerol mobilization from intracellular triglyceride (TG) stores involves TG hydrolysis by adipocyte lipases; primarily hormone sensitive lipase (HSL) and adipocyte triglyceride lipase (ATGL). The activity of these lipases is governed by PKA. Thus, failed PKA-mediated lipase phosphorylation results in attenuated lipolysis and subsequently reduced release of FFA into the circulation. Insulin is a potent inhibitor of adipocyte lipolysis. Activation of the insulin receptor results in a series of enzyme phosphorylations, ultimately activating phosphodiesterase 3B (PDE3B), an enzyme that breaks down cAMP into AMP. Thus, insulin disrupts cAMP-mediated signalling pathways and hence lipolysis. PKA may also activate PDE3B, thus regulating its own activity. NiAc has also been suggested as an inhibitor of glucose-stimulated insulin secretion via binding of the GPR109A receptor in pancreatic β-cells. Long-term NiAc exposure may also be involved in down-regulation of PDE3B gene expression.

elevated plasma FFA concentrations are associated with several metabolic diseases, including insulin resistance (Eckel et al., 2005; Krauss, 2004; Morita et al., 2012). The hypothesis is that NiAc-induced FFA lowering could ameliorate these conditions. However, the clinically applied dosing regimens are designed for treating dyslipidemia, and not for reducing FFA levels (Carlson, 2005).

Although acute administration of NiAc results in rapid reduction in FFA concentrations (Ahlström

et al., 2013a; Carlson and Orö, 1962), sustained treatments are associated with tolerance development (drug resistance) and plasma FFA concentrations returning to pre-treatment levels (complete adaptation) (Kroon et al., 2015). Moreover, abrupt cessation of the NiAc infusions produces an FFA rebound that overshoots the pre-infusion levels (Kroon et al., 2015; Oh et al., 2011). Numerous studies have sought to quantitatively determine the acute concentration-response relationship between NiAc and FFA (Ahlström, 2011; Ahlström et al., 2013a, 2011a, 2013b, 2011b; Andersson et al., 2015; Isaksson et al., 2009; Leander et al., 2015; Tapani et al., 2014). Although the current pharmacokinetic/pharmacodynamic (PK/PD) models are successful in characterising the acute NiAc-induced FFA response, the associated chronic behaviour has not been successfully captured. Thus, an improved model is required to predict optimal treatment regimens, aimed to achieve durable NiAc-induced FFA lowering.

3.2 Pharmacokinetics of NiAc

The pharmacokinetic properties of NiAc have been thoroughly characterised in previous studies (Ahlström, 2011; Ahlström et al., 2013a, 2011a, 2013b, 2011b; Isaksson et al., 2009; Iwaki et al., 1996; Leander et al., 2015; Tapani et al., 2014). Ahlström (2011) introduced a two-compartment disposition model with parallel nonlinear (Michaelis-Menten) elimination for lean Sprague-Dawley rats, and a one-compartment model with a single nonlinear elimination for obese Zucker rats (the model structures are illustrated in Fig. 3.2).

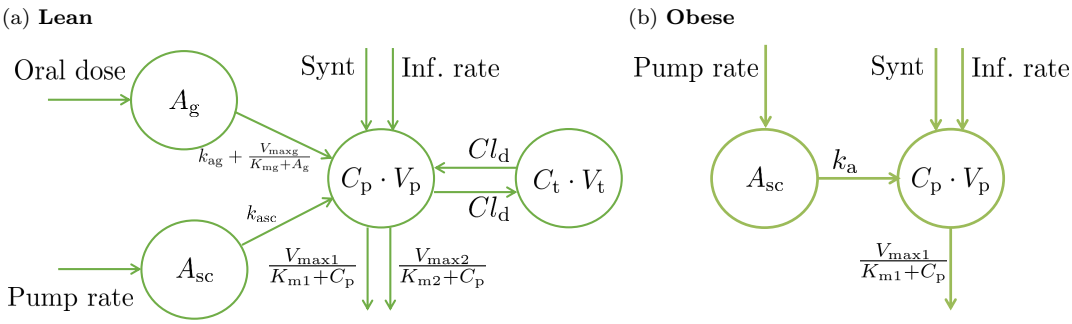

Figure 3.2: NiAc disposition models for lean Sprague-Dawley (a) and obese Zucker rats (b). NiAc is either infused directly into the central compartment (intravenous administration) or absorbed via a subcutaneous compartment (subcutaneous administration via an implanted mini-pump) or absorbed from the gut (oral administration).

3.2.0.1 Lean rats

A model for the NiAc disposition in lean Sprague-Dawley rats is given by

$$\begin{aligned} V_{\mathrm{p}} \cdot \frac{\mathrm{d}C_{\mathrm{p}}(t)}{\mathrm{d}t} &= \mathrm{Input}(t) + \mathrm{Synt} - \frac{V_{\mathrm{max1}} \cdot C_{\mathrm{p}}(t)}{K_{\mathrm{m1}} + C_{\mathrm{p}}(t)} \\ &\quad - \frac{V_{\mathrm{max2}} \cdot C_{\mathrm{p}}(t)}{K_{\mathrm{m2}} + C_{\mathrm{p}}(t)} - Cl_{\mathrm{d}} \cdot C_{\mathrm{p}}(t) \\ &\quad + Cl_{\mathrm{d}} \cdot C_{\mathrm{t}}(t), \end{aligned} \tag{3.1}$$

$$V_{\mathrm{t}} \cdot \frac{\mathrm{d}C_{\mathrm{t}}(t)}{\mathrm{d}t} = Cl_{\mathrm{d}} \cdot C_{\mathrm{p}}(t) - Cl_{\mathrm{d}} \cdot C_{\mathrm{t}}(t), \tag{3.2}$$

where $C_{\mathrm{p}}(t)$ is the observed NiAc concentration in the central *plasma* compartment and $C_{\mathrm{t}}(t)$ is the concentration in the peripheral *tissue* compartment (both measured in µM), and V_{p} and V_{t} (both measured in l) are the volumes of distribution of the plasma and tissue compartments, respectively. The parameters V_{max1} ($\mu\mathrm{mol\,min^{-1}\,kg^{-1}}$) and K_{m1} (µM) are the maximal elimination rate and the Michaelis constant of the first pathway, and V_{max2} ($\mu\mathrm{mol\,min^{-1}\,kg^{-1}}$) and K_{m2} (µM) are the maximal elimination rate and the Michaelis constant of the second pathway (low and high affinity pathway, respectively). Furthermore, Cl_{d} ($\mathrm{l\,min^{-1}\,kg^{-1}}$) represents the inter-compartmental distribution and Synt ($\mu\mathrm{mol\,min^{-1}\,kg^{-1}}$) the endogenous NiAc synthesis. To derive the initial conditions of the plasma and tissue compartments, we propose that the system given in Eqs.(3.1) and (3.2) is at steady-state at $t = 0$, and after 10 min of constant rate infusion (Ahlström et al., 2011b), with $\frac{\mathrm{d}C_{\mathrm{p}}(t)}{\mathrm{d}t} = 0$. Consequently, we can solve for the steady-state concentration $C_{\mathrm{pss}} (= C_{\mathrm{tss}})$ as

$$\begin{aligned} V_{\mathrm{c}} \cdot \frac{\mathrm{d}C_{\mathrm{pss}}}{\mathrm{d}t} &= \underbrace{\mathrm{input} + \mathrm{Synt}}_{=\alpha} - \frac{V_{\mathrm{max1}} \cdot C_{\mathrm{pss}}}{K_{\mathrm{m1}} + C_{\mathrm{pss}}} \\ &\quad - \frac{V_{\mathrm{max1}} \cdot C_{\mathrm{pss}}}{K_{\mathrm{m1}} + C_{\mathrm{pss}}} + \underbrace{Cl_{\mathrm{d}} \cdot C_{\mathrm{tss}} - Cl_{\mathrm{d}} \cdot C_{\mathrm{pss}}}_{=0} \\ &= 0. \end{aligned} \tag{3.3}$$

This gives rise to a quadratic equation with positive real root

$$C_{\mathrm{pss}} = \frac{-b + \sqrt{b^2 - 4ac}}{2a}, \tag{3.4}$$

where

$$a = \alpha - V_{\mathrm{max1}} - V_{\mathrm{max2}} \tag{3.5}$$

$$b = \alpha \cdot (K_{\mathrm{m1}} + K_{\mathrm{m2}}) - V_{\mathrm{max1}} \cdot K_{\mathrm{m2}} - V_{\mathrm{max2}} \cdot K_{\mathrm{m1}}, \tag{3.6}$$

and

$$c = \alpha \cdot K_{\mathrm{m1}} \cdot K_{\mathrm{m2}}. \tag{3.7}$$

Consequently, the initial steady-state concentration is given by Eqn, 3.4 with Const. = Synt and the steady-state attained after 10 min of infusion is given by Eqn. 3.4 with Const. = input + Synt. The term Input(t) in (3.1) is a time-dependent function determined by the route of administration according to

$$\mathrm{Input}(t) = \begin{cases} \text{Inf. rate} & \text{Intravenous infusion} \\ k_{\mathrm{asc}} \cdot A_{\mathrm{sc}}(t) & \text{Subcutaneous infusion} \\ k_{\mathrm{ag}} \cdot A_{\mathrm{g}}(t) + \frac{V_{\mathrm{maxg}} \cdot A_{\mathrm{g}}(t)}{K_{\mathrm{mg}} + A_{\mathrm{g}}(t)} & \text{Oral dose,} \end{cases} \tag{3.8}$$

where Inf. rate (μmol min^{-1} kg^{-1}) is the infusion rate, $A_{\mathrm{sc}}(t)$ (μmol kg^{-1}) the amount of drug in the subcutaneous compartment, k_{asc} (min^{-1}) the absorption rate from the subcutaneous compartment to plasma, $A_{\mathrm{g}}(t)$ (μmol kg^{-1}) the amount of drug in the gut, k_{ag} (min^{-1}) the absorption rate from the gut to plasma of the linear translocation pathway, V_{maxg} (μmol min^{-1} kg^{-1}) the maximal absorption rate from the gut to plasma of the nonlinear translocation pathway, and K_{mg} the amount in the gut corresponding to 50% absorption from the gut to plasma of the nonlinear translocation pathway. The rate of change of $A_{\mathrm{sc}}(t)$ is given by

$$\frac{\mathrm{d}A_{\mathrm{sc}}(t)}{\mathrm{d}t} = \text{Pump rate} - k_{\mathrm{asc}} \cdot A_{\mathrm{sc}}(t), \tag{3.9}$$

with initial condition $A_{\mathrm{sc}}(0) = 0$. Here, Pump rate represents the infusion rate from a subcutaneous mini-pump. Surgical implantation of the mini-pump occurred seven days before the final acute experiment. During this period, when the pump was not infusing, interstitial tissue fluid could diffuse into the tip of the catheter, diluting the NiAc dosing solution. Therefore a concentration gradient may have formed, resulting in an apparently lower initial infusion rate compared to the pre-programmed setting. To capture this, the pump infusion rate is modelled as

$$\text{Pump rate} = \text{Inf. rate} \cdot \mathrm{erf}\left(\frac{t \cdot \delta}{\sqrt{t_0}}\right), \tag{3.10}$$

where Inf. rate is the programmed infusion rate of the pump, δ (min$^{-1/2}$) is a lumped diffusion parameter, and t_0 is the pump inactivation time (in this case 7 days). Here erf is the error function (Andrews, 1997), defined as

$$\mathrm{erf}(t) = \frac{2}{\sqrt{\pi}} \int_0^t e^{-\tau^2}\, \mathrm{d}\tau. \tag{3.11}$$

The concentration gradient, described by Eq. (3.10), is derived by viewing the catheter as a one-dimensional diffusion problem and applying Fick's law. The one-dimensional fluid equation has the solution

$$c(x,t) = c_0 \cdot \text{erfc}\left(\frac{x}{2\sqrt{\hat{\delta}t}}\right), \tag{3.12}$$

where c_0 is the concentration at the boundary (of where the fluid diffuses from), x the diffusion direction, t the time, δ the diffusion parameter, and erfc the complementary error function (Andrews, 1997). Given that the intestinal fluids take the form given in Eq. (3.12), the NiAc concentration in the catheter will, due to symmetry, be scaled by the factor

$$\text{erf}\left(\frac{x}{2\sqrt{\hat{\delta}t}}\right), \tag{3.13}$$

where erf is the error function (Andrews, 1997). Now, we assume that the diffusion is negligible after the infusion has started. Consequently, only the time between the implantation and the initiation of the pump, given by t_0, affects the concentration gradient. Then the infusion rate will be scaled by the factor in Eq. (3.12), with $t = t_0$. The direction can be expressed as $x = v \cdot t$, where v is the infusion velocity and t the time after the infusion has started. The velocity is fixed in the experiment and can be lumped with the factor $\frac{1}{2\sqrt{\hat{\delta}}}$ as

$$\delta = \frac{v}{2\sqrt{\hat{\delta}}}, \tag{3.14}$$

and the rate is scaled by

$$\text{erf}\left(\frac{t \cdot \delta}{\sqrt{t_0}}\right) \tag{3.15}$$

where the parameter δ is estimated from the data.
For simplicity, the bioavailability from the subcutaneous compartment was assumed to be equal to unity. The rate of change of $A_\text{g}(t)$ is given by

$$\frac{\text{d}A_\text{g}(t)}{\text{d}t} = -k_\text{ag} \cdot A_\text{g}(t) - \frac{V_\text{maxg} \cdot A_\text{g}(t)}{K_\text{mg} + A_\text{g}(t)}, \tag{3.16}$$

with initial condition $A_\text{g}(0) = D$.

3.2.0.2 Obese rats

For obese Zucker rats, the NiAc disposition is given by

$$V_\text{p} \cdot \frac{\text{d}C_\text{p}(t)}{\text{d}t} = \text{Input}(t) + \text{Synt} - \frac{V_\text{max1} \cdot C_\text{p}(t)}{K_\text{m1} + C_\text{p}(t)}, \tag{3.17}$$

where $C_{\mathrm{p}}(t)$ is the NiAc concentration in the central plasma compartment, V_{c} the volume of distribution, V_{max1} the maximal elimination rate, K_{m1} the Michaelis constant, and Synt the endogenous synthesis. The term Input(t) is the same as for the lean rats (the relations given in Eqs. 3.8, 3.9 and 3.10).

3.3 Data

The data sets used in the two meta-analyses of this thesis consist of FFA (and insulin for study DRT II) response-time series obtained from experiments on lean (normal) Sprague-Dawley rats and obese (diseased) Zucker rats under provocation of NiAc. The NiAc was administered at different rates, routes, and modes. A detailed outline of the experiments of DRT study I can be found in the thesis by Ahlström (2011). The data of this study are given in Table 3.1.

				Number of rats	
Admin. route	Dose (μmol kg^{-1})	Acute exp. (min)	Inf. rate (μmol kg^{-1} min^{-1})	Lean rats	Obese rats
Infusion	0	30	0	10	2
	1		0.033	4	-
	5		0.170	8	-
	20		0.660	9	7
	0	300	0	8	2
	5		0.017	9	-
	10		0.033	8	-
	51		0.170	7	8
	0	210[a]	0-0.170	1	-
	20		0	5	-
	0	240[b]	0-0.170	1	-
	25		0	5	-
Oral	0	-	-	6	-
	24.4	-	-	6	-
	81.2	-	-	6	-
	812	-	-	6	-

Table 3.1: Study I data characteristics—including route of administration, dose, duration of experiment, infusion rate, and the number of lean (a total of 95) and obese (a total of 19) rats within each experiment.

[a] Constant rate infusion at 0.17 μmol kg^{-1} min^{-1} for 30 min, followed by a step-wise decrease every 10 min for 180 min to an infusion rate of 0 μmol kg^{-1} min^{-1}.

[b] Constant rate infusion at 0.17 μmol kg^{-1} min^{-1} for 30 min, followed by a step-wise decrease every 10 min for 180 min to an infusion rate of 0 μmol kg^{-1} min^{-1}, followed by another 30 min constant rate infusion at 0.17 μmol kg^{-1} min^{-1}.

The data of DRT study II are given in Table 3.2.

3.3.1 Outline of experimental procedures

The following section will present a detailed outline of how the data of DRT study II were obtained.

					Number of rats	
	Admin. route	Pre-treat.(h)	Acute exp.(h)	Protocol	Lean rats	Obese rats
Conscious	Subcutaneous	0	5	NiAc Naïve	7(2)	7(5)
animals	inf.	120	5	Cont. NiAc	6(2)	8(2)
		120	5	Inter. NiAc	6(2)	8(3)
Anaesthetised	Intravenous	0	1	NiAc Off 1 h	4(3)	5(3)
animals	inf.	0	1	NiAc Stp-Dwn 1 h	5(2)	5(2)
	Subcutaneous	0	12	NiAc Off 12 h	5(2)	4(2)
	inf.	0	12	NiAc Stp-Dwn 12 h	5(3)	4(3)

Table 3.2: Study II data characteristics—including conscious or anaesthetised state, route of administration, duration of experiment, protocol name, and the number of lean (a total of 54) and obese (a total of 61) rats within each experiment (the numbers of saline infused controls given in parenthesis).

3.3.1.1 Animals

Male Sprague Dawley (lean) and Zucker rats (fa/fa, obese) were purchased from (conscious groups) Harlan Laboratories B.V. (The Netherlands) or (anesthetized groups) Charles River Laboratories (USA). Experimental procedures were approved by the local Ethics Committee for Animal Experimentation (Gothenburg region, Sweden). Rats were housed in an Association for Assessment and Accreditation of Laboratory Animal Care accredited facility with environmental control: 20-22° C, relative humidity 40-60%, and 12 h light-dark cycle. During acclimatization ($\geq$5 days), animals were housed in groups of 5 with free access to both water and standard rodent chow (R70, Laktamin AB, Stockholm, Sweden).

3.3.1.2 Surgical preparations

To prevent potential infections in conjunction with surgery, oral antibiotics were given 1 day before pump/catheter surgery and then once daily for 3 days (sulfamethoxazole and trimethoprim 40 mg mL^{-1} + 8 mg mL^{-1}; Bactrim®, 0.2 mL/animal, Roche Ltd, Basel, Switzerland). Surgery was performed under isoflurane (Forene®, Abbott Scandinavia AB, Solna, Sweden) anesthesia, with body temperature maintained at 37°C. For NiAc/saline administration, a programmable mini pump (iPrecio® SMP200 Micro Infusion Pump, Primetech Corporation, Tokyo, Japan) was implanted subcutaneously, via a dorsal skin incision. To allow blood sampling during the terminal experiment (conscious animals only), a polyurethane catheter (Instech Laboratories Inc, Plymouth Meeting, PA USA) was placed in the right jugular vein via an incision in the neck. In order to maintain its patency up to the acute experiment, the jugular catheter was filled with sterile 45.5% (wt/wt) PVP (polyvinylpyrrolidone, K30, MW ~40 000 Fluka, Sigma-Aldrich, Sweden) dissolved in a sodium-citrate solution (20.6 mmol), sealed and exteriorized at the nape of the neck. Each animal received a post-operative, subcutaneous analgesic injection (buprenorphine, Temgesic®, 1.85 µg kg^{-1}, RB Pharmaceuticals Ltd, Berkshire, GB). Animals were then housed individually and allowed three days of recovery before the start of the pre-programmed pump infusion. Throughout the study, body weight and general health status were monitored

and recorded daily.

3.3.1.3 Nicotinic acid exposure selection and formulation

A key aspect of the study design was to achieve plateau plasma nicotinic acid (NiAc) concentrations corresponding to therapeutically relevant levels in the rat (∼1 µM), based on the relationship between plasma NiAc levels and FFA lowering (Ahlström, 2011). For intravenous infusions (i.v.), NiAc (pyridine-3-carboxylic acid, Sigma-Aldrich, St. Louis, MO, USA) was dissolved in sterile saline. For subcutaneous (s.c.) infusions, NiAc was dissolved in sterile water and adjusted to physiological pH using sodium hydroxide. Vehicle, for control animals, consisted of sodium chloride solutions at equimolar concentrations. Freshly prepared formulations were loaded into the infusion pump (see below) via a 0.2 µm sterile filter (Acrodisc®, Pall Corporation, Ann Arbor, MI, USA) just before pump implantation.

3.3.1.4 Experimental protocols

Conscious animals (NiAc naïve, Cont. NiAc and Inter. NiAc groups)

Both lean and obese animals were divided into 3 dose groups and NiAc was given either acutely (NiAc naïve) or following 5 days of either continuous (Cont. NiAc) or intermittent (Inter. NiAc) administration. Each dose group was matched with corresponding saline infused controls. NiAc infusions were given subcutaneously at 170 nmol min^{-1} kg^{-1}. The intermittent infusion protocol was programmed as a 12 h on-off cycle (infusion on at 13:00). Following overnight fast, in the morning of the acute experimental day, the jugular catheter was connected to a swivel system to enable blood sampling in unrestrained animals. Jugular catheter patency was maintained by continuous infusion (5 µmol min^{-1}) of sodium-citrate solution (20.6 mM). After a 3-4 h adaptation period, at ∼12:00, the basal phase of the acute experiment commenced with 2-3 blood samples drawn between -60 and -5 min, relative to start of NiAc/saline infusion (note that, in the Cont. NiAc groups, infusion pumps were on throughout this sampling period). Blood samples (16-17/animal) were drawn under an 8 h experimental period. Samples, 30-150 µl (with total loss less than 5% of blood volume), were collected in potassium-EDTA tubes, centrifuged and plasma stored at 80°C pending analysis for NiAc, FFA and insulin.

Anaesthetised animals (NiAc Off and NiAc Stp-Dwn 12 h infusion groups)

Before the infusions began, lean and obese rats were fasted for 8 h. On the day of the acute study, at 01:00 (corresponding to time=0 h), the implanted pre-programmed pump began infusing NiAc at a constant rate of 170 nmol min^{-1} kg^{-1} for 12 h. At 8.5 h animals were anaesthetised (Na-thiobutabarbitol, Inactin®, 180 mg kg^{-1}, i.p., RBI, Natick, MA, USA), underwent a tracheotomy with PE 240 tubing, and breathed spontaneously. One catheter (PE 50 tubing) was placed in the left carotid artery for blood sampling and for recording

arterial blood pressure and heart rate. One catheter (PE 10 tubing) was placed in the right external jugular vein to infuse top-up doses of anaesthetic. The arterial catheter patency was maintained by continuous infusion of sodium-citrate (20.6 mM in saline, 5 µl min^{-1}) from shortly after carotid catheterising until the experiment ended. Body temperature was monitored using a rectal thermocouple and maintained at 37.5°C by means of servo controlled external heating. After surgery, animals were allowed a stabilization period of at least 1.5 h and blood sampling began at 11.0 h. At 12.0 h, NiAc infusion was either programmed to switch off (NiAc Off) or to decrease in a step-wise manner, with final switch-off at 15.5 h (NiAc Stp-Dwn). The step-down NiAc infusion rates were 88.9, 58.3, 43.7, 34.0, 24.3, 17.0, and 9.7 nmol min^{-1} kg^{-1}. All NiAc protocols were matched with saline-infused controls. Blood samples (18/animal) were drawn during a 6 h experimental period. Samples, 30-150 µl (with total loss less than 5% of blood volume), were collected in potassium-EDTA tubes, centrifuged, and plasma was stored at 80°C pending analysis for NiAc, FFA and insulin.

Anaesthetised animals (NiAc Off and NiAc Stp-Dwn 1 h infusion groups)

After an overnight fast, lean and obese rats were anaesthetize and surgically prepared, as described above. They were allowed a stabilization period after surgery of at least 1.5 h. Two basal blood samples were obtained, after which an i.v. NiAc infusion was given at a constant rate (170 nmol min^{-1} kg^{-1}) for 1.0 h (the start of infusion was taken as time=0 h). The NiAc infusion was then either switched off (NiAc-Off 1 h) or decreased in a step-wise manner, with final switch-off at 4.5 h (NiAc Stp-Dwn 1 h). The step-down NiAc infusion rates were: 31.1, 20.4, 15.3, 11.9, 8.50, 5.95 and 3.40 nmol min^{-1} kg^{-1}. All NiAc protocols were matched with saline infused controls. Blood samples (13-18/animal) were drawn during a 6 h experimental period. Samples, 30-150 µl (with total loss less than 5% of blood volume), were collected in potassium-EDTA tubes, centrifuged, and plasma was stored at 80°C pending analysis for NiAc, FFA, and insulin.

3.3.1.5 Analytical methods

Plasma FFA was analysed using an enzymatic colorimetric method (Wako Chemicals GmbH, Neuss, Germany). Plasma insulin from obese rats was analysed with a radioimmunoassay kit (rat insulin RIA kit, Millipore Corporation, St. Charles, Missouri, USA). Plasma insulin concentrations from lean rats were determined using a colorimetric ELISA kit (Ultra Sensitive Rat Insulin ELISA Kit, Crystal Chem INC, Downers Grove, IL, USA). The ELISA was used for lean rats to minimize blood sample volume (only 5 µl plasma required vs. ∼50 µl plasma for RIA). The RIA was used for the obese rats because their high lipid levels in plasma interfere with the ELISA but not the RIA measurement. Due to the hyperinsulinemia in the obese rats only 5 µl of plasma was required. For lean-rat plasma (with low lipid levels) the absolute insulin measurements are equivalent for the RIA and ELISA assays, according to an in-house comparison. Plasma NiAc concentrations were analysed using LC-MS/MS with a hydrophilic interaction liquid chromatography (HILIC) approach, separated on a 50×2.1 mm

Biobasic AX column, with 5 µm particles (Thermo Hypersil-Keystone, Runcorn, Cheshire, UK) as previously described by Ahlström (2011).

Chapter 4

DRT I - Free fatty acid dynamics

The first study presents a dose-response-time (DRT) analysis based on an extensive preclinical biomarker data set on the nicotinic acid-induced (NiAc) reduction of free fatty acids (FFA). The data constitute FFA-time courses, collected from studies that examined different rates, routes, and modes of NiAc provocations on lean (normal) and obese (diseased) rats. All information regarding the exposure to NiAc was excluded to demonstrate the utility of a DRT model. The study emphasised the selection process of the biophase function. An inhibitory $I_{\max}$-model, driven by the biophase amount, acted on the turnover rate of FFA. A second generation NiAc-FFA model, which encompasses integral (slow build-up of tolerance) and moderator (rapid and oscillatory) feedback control, was simultaneously fitted to all time courses. The results of the study were compared to an exposure-driven analysis to assess the performance of the DRT analysis.

4.1 Model development

In contrast to the traditional pharmacokinetic-pharmacodynamic modelling approach—where the kinetic and dynamic properties of the drug can be assessed sequentially[1]—the biophase

[1] Although PK-PD modelling traditionally have been performed sequentially, simultaneous fitting of the models is preferable in many cases (Zhang et al., 2003a,b), and has indeed been done in several studies (see, for example, Standing et al. (2010)).

and pharmacodynamics need to be determined simultaneously in dose-response-time (DRT) modelling. Thus, the evolution of the biophase, described in the following section, acted in parallel with the development of the pharmacodynamic model.
A fundamental assumption for this study was that systems for the lean and obese rats could be described with the same DRT model. As the data generated from experiments on lean rats were more extensive than those for the obese rats, those data were analysed when developing the model. When a satisfactory DRT model was selected and fitted to the data for the lean rats, the model was fitted to the data for the obese rats.

4.2 The biophase function

Dose-response-time (DRT) data analysis relies on the assumption that the pharmacological response contains enough information about the kinetics to develop a biophase, which in turn acts as a 'driving' function for the pharmacological response. Depending on the route of administration, the input is either approximated to be directly into the biophase (intravenous dosing) or absorbed into the biophase (oral dosing).

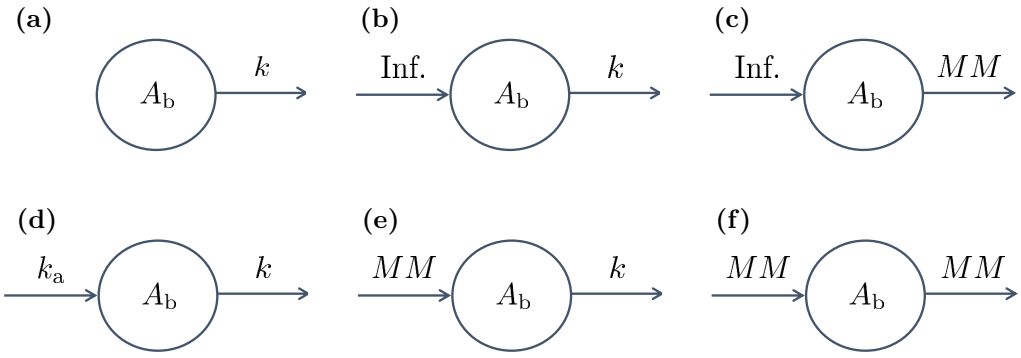

Figure 4.1: Examples drawn from the biophase model library: (a) bolus input and first-order elimination; (b) zero-order input and first-order elimination; (c) zero-order input and Michaelis-Menten elimination; (d) first-order input and elimination; (e) Michaelis-Menten input and first-order elimination; (f) Michaelis-Menten input and elimination. The parameters A_b, Inf., k, k_a, and MM represent, respectively, the biophase amount, the constant rate infusion input, the first-order elimination rate constant, the first-order absorption rate constant, and the Michaelis-Menten absorption/elimination process.

4.2.1 Selection process of biophase models

Developing the biophase model was done sequentially, starting with the simplest data (intravenous administration). In a pair-wise accept-reject procedure, two candidate models were qualitatively and quantitatively analysed and compared, and the best fit was selected and further challenged with more complex data (see Table 4.1). In detail, the goodness-of-fit

was assessed by the Akaike information criterion (AIC) and by graphical inspection of the visual predictive check (VPC), and individual, plots.

Step I The first biophase model evaluated consists of a zero-order input into, and first-order elimination from, the biophase (Fig. 4.1b). The analysed data consist of response-time courses, derived from constant-rate intravenous infusion experiments.

Step	Model	Description	Data
I	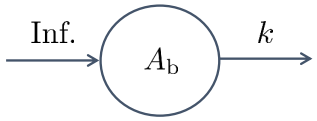	Zero-order input First-order elimination	Intravenous
II	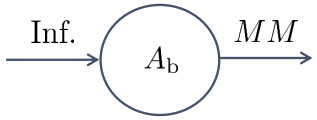	Zero-order input Michaelis-Menten elimination	Intravenous
Pair-wise accept-reject procedure between the models in Step I and Step II. The model in Step I was considered the better model.			
III	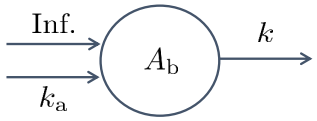	Zero-order input (IV[a]) First-order input (PO[b]) First-order elimination	Intravenous and oral
IV	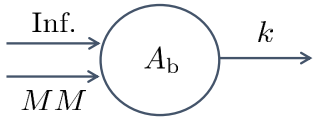	Zero-order input (IV[a]) Michaelis-Menten input (PO[b]) First-order elimination	Intravenous and oral
Pair-wise accept-reject procedure between the models in Step III and Step IV. The model in Step IV was considered the better model.			

[a] Intravenous
[b] Oral

Table 4.1: Evolution of the biophase model structure. The table depicts Steps I-IV, a description of the biophase function, the data used for the regression analysis, and the pair-wise accept/reject procedures applied when addressing the biophase disposition and absorption.

Step II The next biophase model evaluated consists of a zero-order input into, and Michaelis-Menten elimination from, the biophase (Fig. 4.1c). The analysed data were the same as in step I.

The model that best describes (regarding goodness-of-fit) the dynamics of the dose-response-time data was kept for the later stages of the biophase evolution. In this case, the models in steps I and II had close to similar likelihood and were indistinguishable by graphical inspection of the VPC's. Nonetheless, by the AIC, the simpler model was consider to be the best fit.

Step III Given a model for the biophase elimination, response-time data derived from experiments for oral administration were analysed to address the biophase absorption. The first biophase absorption model evaluated consists of first-order input into, and first-order elimination from, the biophase (Fig. 4.1d).

Step IV The final absorption model evaluated consists of Michaelis-Menten input into, and first-order elimination from, the biophase (Fig 4.1e). The analysed data are the same as in step III.

The model in step IV was selected in accordance with the AIC.

4.2.2 The final biophase model

The biophase model is given by

$$\frac{\mathrm{d}A_{\mathrm{b}}(t)}{\mathrm{d}t} = \mathrm{Input}(t) - k \cdot A_{\mathrm{b}}(t) \quad \text{with} \quad A_{\mathrm{b}}(0) = 0, \tag{4.1}$$

where $A_{\mathrm{b}}(t)$ ($\mu\mathrm{mol\,kg^{-1}}$) represents the biophase drug amount, k ($\mathrm{min^{-1}}$) the biophase elimination rate, and $\mathrm{Input}(t)$ a time-dependent function determined by the route of administration according to

$$\mathrm{Input}(t) = \begin{cases} \text{Inf. rate} & \text{Intravenous administration} \\ \frac{V_{\mathrm{maxg}} \cdot A_{\mathrm{g}}(t)}{K_{\mathrm{mg}} + A_{\mathrm{g}}(t)} & \text{Oral administration,} \end{cases} \tag{4.2}$$

where Inf. rate ($\mu\mathrm{mol\,kg^{-1}\,min^{-1}}$) is the infusion rate to the biophase, $A_{\mathrm{g}}(t)$ ($\mu\mathrm{mol\,kg^{-1}}$) the drug amount in the gut, V_{max} ($\mu\mathrm{mol\,kg^{-1}\,min^{-1}}$) the maximal absorption rate from the gut to the biophase, and K_{mg} ($\mu\mathrm{mol\,kg^{-1}}$) the amount in the gut corresponding to 50% absorption rate from the gut to the biophase. The infusion rate is modelled as a either a constant, or a stepwise decreasing, Heaviside function to mimic the infusion regimens used in the experiments. The rate of change of $A_{\mathrm{g}}(t)$ is given by

$$\frac{\mathrm{d}A_{\mathrm{g}}(t)}{\mathrm{d}t} = -\frac{V_{\mathrm{max,g}} \cdot A_{\mathrm{g}}(t)}{K_{\mathrm{m,g}} + A_{\mathrm{g}}(t)} \quad \text{with} \quad A_{\mathrm{g}}(0) = D, \tag{4.3}$$

where D ($\mu\mathrm{mol\,kg^{-1}}$) is the oral drug dose.

4.3 The pharmacodynamic model

The free fatty acid (FFA) dynamics are characterised by a turnover equation according to

$$\frac{\mathrm{d}F(t)}{\mathrm{d}t} = \widetilde{k}_{\mathrm{in}}(t) - \widetilde{k}_{\mathrm{out}}(t) \cdot F(t) \quad \text{with} \quad F(0) = F_0, \tag{4.4}$$

where $F(t)$ denotes the observed FFA level, F_0 the baseline FFA level, both expressed in mM, and $\widetilde{k}_{\mathrm{in}}(t)$ and $\widetilde{k}_{\mathrm{out}}$ are functions describing the lumped effects of NiAc, insulin, and other hormones, on the turnover and fractional turnover of FFA, respectively. The NiAc-induced action on FFA is described by means of an inhibitory drug-mechanism function given by

$$I(A_{\mathrm{b}}(t)) = 1 - \frac{I_{\max} \cdot A_{\mathrm{b}}(t)^{\gamma}}{ID_{50}^{\gamma} + A_{\mathrm{b}}(t)^{\gamma}}, \tag{4.5}$$

where $I_{\max}$ (unitless[2]) denotes the efficacy, ID_{50} ($\mu\mathrm{mol\,kg}^{-1}$) the potency, and γ the Hill exponent. Furthermore, the FFA level is affected by a chain of moderator compartments $M_1, \ldots, M_8$. These moderator compartments represent a conglomerate of insulin, and other hormonal, regulators of the FFA disposition. Insulin, for example, acts as a dual regulator on the FFA level via rapid inhibition of the lipolysis and slow re-esterification of FFA to triglycerides (Frayn et al., 1994; Sadur and Eckel, 1982; Strålfors et al., 1984). The rapid inhibition is captured by the dynamics of the first moderator M_1 and the re-esterification by the last moderator M_8. The moderators dynamics are given by

$$\begin{aligned}
\frac{\mathrm{d}M_1(t)}{\mathrm{d}t} &= k_{\mathrm{tol}} \cdot (F(t) - M_1(t)) \\
\frac{\mathrm{d}M_2(t)}{\mathrm{d}t} &= k_{\mathrm{tol}} \cdot (M_1(t) - M_2(t)) \\
&\vdots \\
\frac{\mathrm{d}M_8(t)}{\mathrm{d}t} &= k_{\mathrm{tol}} \cdot (M_7(t) - M_8(t)),
\end{aligned} \tag{4.6}$$

where k_{tol} (min^{-1}) is the fractional turnover rate of the moderators. Consequently, all moderator compartments have the same transit time of $1/k_{\mathrm{tol}}$ (min). The moderators are initially assumed to be in equilibrium with the response with

$$M_1(0) = \ldots = M_8(0) = F_0. \tag{4.7}$$

The number of moderator compartments selected has previously been discussed by Ahlström et al. (2011b). Long-term exposure to NiAc has proven to induce insulin resistance in adipocytes (Fabbrini et al., 2010; Poynten et al., 2003). The resistance is believed to be a consequence of down-regulated gene expressions of the insulin and β-adrenergic pathways in

[2]Notation will from hereon be omitted for unitless parameters.

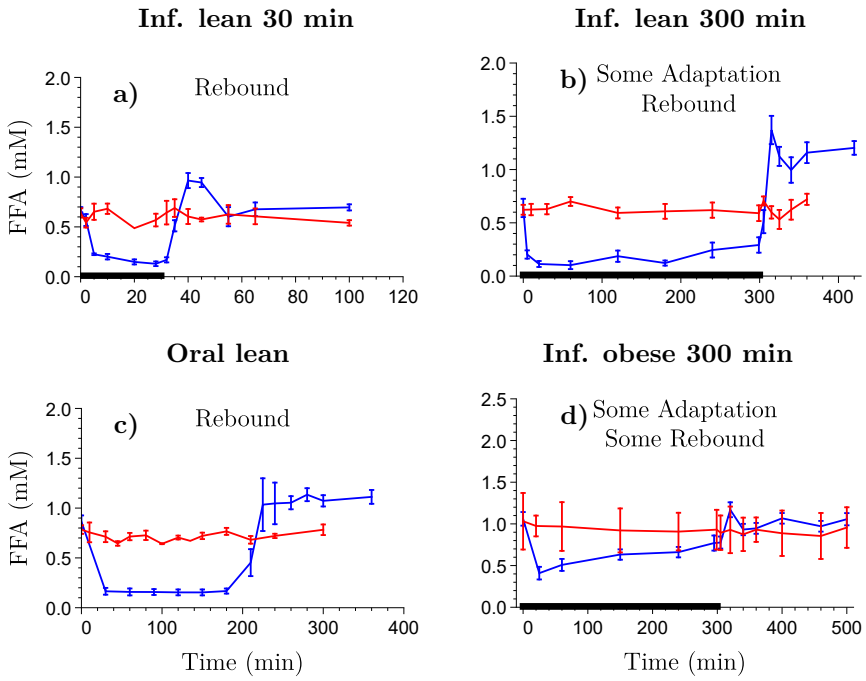

Figure 4.2: Example of FFA-time course data under intravenous and oral NiAc dosing. (a) represents 30 min NiAc infusion and (b) 300 min NiAc infusion, both for lean rats. (c) represents oral NiAc dosing for lean rats. (d) represents 300 min NiAc infusion for obese rats. The blue lines represent the NiAc treated animals, the red lines the vehicle control group, and the black lines the infusion periods.

adipose tissue (Heemskerk et al., 2014). Insulin resistance ultimately leads to full systemic adaptation with an FFA level that returns to its baseline within a few days (Oh et al., 2011). This slow and complete adaptation is captured by an integral feedback controller, with output $u(t)$, that slowly forces deviating FFA levels back towards their baseline F_0, despite persistent perturbations such as a constant rate infusion of NiAc (the adaptation can partly be seen in Fig. 4.2b and Fig. 4.2d). The integral controller is given by

$$u(t) = K_\mathrm{i} \int_0^t \left(1 - \frac{F(\tau)}{F_0}\right) \mathrm{d}\tau, \tag{4.8}$$

where K_i represents the integral gain parameter (hereafter referred to as the adaptation rate).

The integral controller may also be expressed as a rate equation

$$\frac{\mathrm{d}u}{\mathrm{d}t} = K_\mathrm{i} \cdot \left(1 - \frac{F(t)}{F_0}\right), \tag{4.9}$$

with initial condition

$$u(0) = 0. \tag{4.10}$$

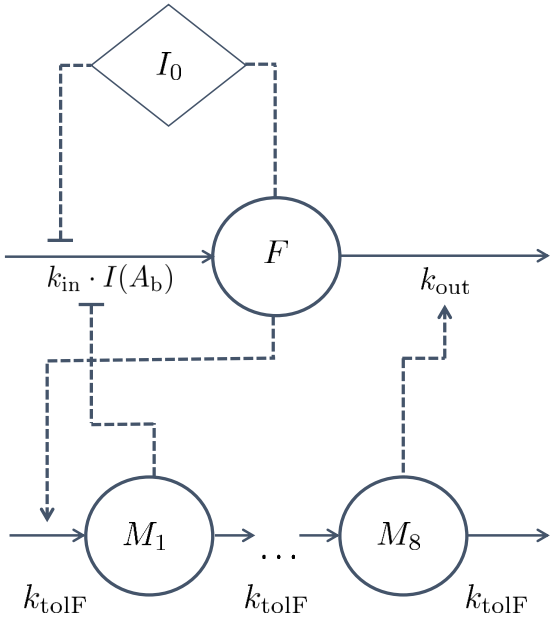

Figure 4.3: Schematic structure of the pharmacodynamics of the DRT feedback model. The pharmacodynamic model structure consists of a turnover equation coupled with a chain of moderator compartments, with slow and rapid feedback, as well as a slow integral control feedback. Here k_{in} denotes the turnover rate of FFA, k_{out} the fractional turnover rate of FFA, k_{tol} the turnover rate of the moderators, p the amplification factor, $I(A_{\text{b}})$ the drug-mechanism function, and M_1 and M_8 the first and last moderator, respectively. Solid lines represent fluxes whilst the dashed lines represent flow of information (i.e., how the different entities affect one another)

With all model components introduced, the expanded turnover equation of FFA under NiAc provocation is modelled by

$$\begin{aligned}\frac{\mathrm{d}F(t)}{\mathrm{d}t} &= k_{\text{in}} \cdot \big(1 + u(t)\big) \cdot \frac{1}{\left(\frac{M_1(t)}{F_0}\right)^p} \cdot I(A_{\text{b}}(t)) \\ &\quad - k_{\text{out}} \cdot \left(\frac{M_8(t)}{F_0}\right) \cdot F(t),\end{aligned} \tag{4.11}$$

with initial condition

$$F(0) = F_0, \tag{4.12}$$

where $F(t)$ denotes the FFA level, k_{in} ($\mathrm{mM\,min^{-1}}$) the basal turnover rate, k_{out} ($\mathrm{min^{-1}}$) the basal fractional turnover rate, F_0 the FFA baseline, $u(t)$ the integral controller, p the amplification factor, and $M_1(t)$ and $M_8(t)$ the first and last moderator, respectively (all moderators have unit mM). The moderators are normalised in the turnover Eq. (4.11) with the baseline FFA value F_0. The levels of the moderators follow the concentration of the FFA according to Eq. (4.6). In turn, the first moderator $M_1(t)$ modifies the turnover rate

k_{in}, amplified with the exponent p, whilst the last moderator $M_8(t)$ modifies the fractional turnover rate k_{out}. These feedback mechanisms represent the fast inhibition of lipolysis and the slower re-esterification of FFA to triglycerides, triggered by insulin and other hormones, that strive to dampen fluctuations in the FFA level (these physiological processes manifest themselves as, for example, rebound in the FFA dynamics post drug infusion—a feature seen in all data (see Fig. 4.2)). Furthermore, when the FFA level drops below the baseline level, the integral controller, given by Eq. (4.8), will accumulate and provide a positive contribution to the turnover rate k_{in} of FFA (this adaptation can be seen in, for example, Fig. 4.2b and Fig. 4.2d). Similarly, when the FFA level increases and rises above the baseline level, the integral controller will accumulate and provide a negative contribution to the turnover rate. The pharmacodynamic model structure is illustrated in Fig. 4.3.

4.3.1 Structural identifiability

The model structure, summarised in Table 4.2 (including the biophase function, the pharmacodynamic model, the parameters, and the input-output), was proven to be structurally locally identifiable. Identifiability was tested using the Exact Arithmetic Rank (EAR) approach (presented in Sec. 2.2.1.3, see Anguelova et al. (2012); Karlsson et al. (2012); Raue et al. (2014) for details). EAR requires that the functions of the system of differential equations are rational polynomial expressions in their variables and parameters. In this study, the inhibitory drug-mechanism function and the feedback function of the first moderator compartment in Eq. (4.5) and Eq. (4.11), respectively, do not fulfil this requirement since the state variables are raised to the powers of γ and p, respectively (which are real-valued). However, by introducing auxiliary variables, the system may be re-written in rational form (Lindskog, 1996). As an example, let

$$B(t) = A_{\text{b}}^{\gamma}(t), \tag{4.13}$$

with

$$B(0) = B_0 \,(= A_{\text{b}}^{\gamma}(0)). \tag{4.14}$$

Then we have that

$$\frac{\mathrm{d}B}{\mathrm{d}t} = \gamma \frac{B(t)}{A_{\text{b}}(t)} \cdot \frac{dA_{\text{b}}}{dt}, \tag{4.15}$$

and by introducing the parameter $\widetilde{ID}_{50}(=ID_{50}^{\gamma})$ the non-rational functions in the inhibitory drug-mechanism function can be written as

$$1 - \frac{I_{\max} \cdot B(t)}{\widetilde{ID}_{50} + B(t)}, \tag{4.16}$$

which is a rational expression of the parameters and the variables. The MATHEMATICA code used for the identifiability analysis can be found in the Appendix A.

4.3.2 Modelling between-subject variability

The data were analysed in a nonlinear mixed-effects framework in order to quantify between-subject variability. Individual model fitting and an *a priori* sensitivity analysis (see Sec. 2.4) were applied to identify parameters with a significant spread in the population or high sensitivity. These parameters were selected to vary in the population. The remaining parameters were considered to be fixed effects. The fixed effects were V_{maxg}, K_{mg}, $I_{\max}$, ID_{50}, γ, and p. The parameters with a population distribution were k, K_{i}, F_0, k_{out}, and k_{tol}. These parameters were assumed to be uncorrelated (to simplify the model) and log-normally distributed (to keep the parameters positive). Thus, for example, the individual biophase elimination rate k_i of subject i is given by

$$k_i = k \cdot \exp \eta_i, \tag{4.17}$$

where k is the population median of the biophase elimination rate and η_i the associated random effect of subject i. If $\boldsymbol{\eta}_i$ is the vector of all random effects of subject i, we have $\boldsymbol{\eta}_i \sim \mathcal{N}(\mathbf{0}, \boldsymbol{\Omega})$, where

$$\boldsymbol{\Omega} = \begin{bmatrix} \omega_{11} & 0 & 0 & 0 & 0 \\ 0 & \omega_{22} & 0 & 0 & 0 \\ 0 & 0 & \omega_{33} & 0 & 0 \\ 0 & 0 & 0 & \omega_{44} & 0 \\ 0 & 0 & 0 & 0 & \omega_{55} \end{bmatrix}. \tag{4.18}$$

Here, ω_{11}, ω_{22}, ω_{33}, ω_{44}, and ω_{55} are the standard devations of the population parameters. The individual parameter estimates, or the Empirical Bayes Estimates (EBEs), provide model diagnostics. The validity of the diagnostics is quantified by the corresponding η-shrinkage of the EBEs (Savic and Karlsson, 2009; Bonate, 2011).

4.4 Parameter estimation

The parameter estimation of the DRT model in this study was performed using a mixed effects modelling framework implemented in Mathematica, developed at the Fraunhofer-Chalmers Research Centre for Industrial Mathematics (Gothenburg, Sweden Almquist et al. (2015)). A summary of the model structure, the model parameters, the input, and output is given in Table 4.2.
The MATHEMATICA code used for the parameter estimation can be found in the Appendix B.

4.4.1 Initial parameter estimates

At time zero, before administration of NiAc, the system is in steady-state with the moderators set at F_0. Consequently, the turnover equation Eq. (4.11) pre-NiAc administration is given

Dose-response-time model						
			Parameters			
Biophase function	Pharmacodynamic model	State variables	Fixed effects	Mixed effects[a]	Input	Output
$\frac{\mathrm{d}A_\mathrm{b}}{\mathrm{d}t} = \mathrm{Input}(t) - k \cdot A_\mathrm{b}$ $A_\mathrm{b}(0) = 0$ $\mathrm{Input}(t) = \begin{cases} \text{Inf. rate} & \text{IV} \\ \frac{V_\mathrm{maxg} \cdot A_\mathrm{g}}{K_\mathrm{mg} + A_\mathrm{g}} & \text{Oral} \end{cases}$ $\frac{\mathrm{d}A_\mathrm{g}}{\mathrm{d}t} = -\frac{V_\mathrm{maxg} \cdot A_\mathrm{g}}{K_\mathrm{mg} + A_\mathrm{g}}$ $A_\mathrm{g}(0) = D$	$\frac{\mathrm{d}F}{\mathrm{d}t} = k_\mathrm{in} \cdot (1+u) \cdot \frac{1}{\left(\frac{M_1}{F_0}\right)^p} \cdot I(A_\mathrm{b}) - k_\mathrm{out} \cdot \left(\frac{M_8}{F_0}\right) \cdot F$ $F(0) = F_0$ $\frac{\mathrm{d}u}{\mathrm{d}t} = K_\mathrm{i} \cdot (1 - \frac{F}{F_0})$ $u(0) = 0$ $\frac{\mathrm{d}M_1}{\mathrm{d}t} = k_\mathrm{tol} \cdot (F - M_1)$ $M_1(0) = F_0$ $\frac{\mathrm{d}M_i}{\mathrm{d}t} = k_\mathrm{tol} \cdot (M_{i-1} - M_i)$ $M_i(0) = F_0 \quad i = 2, \ldots, 8$ $I(A_\mathrm{b}) = 1 - \frac{I_\mathrm{max} \cdot A_\mathrm{b}^\gamma}{ID_{50}^\gamma + A_\mathrm{b}^\gamma}$	A_b F M_1 $\vdots$ M_8 u	V_maxg K_mg I_max ID_{50} γ p	k K_i F_0 k_out k_tol	Inf. rate D	F

Table 4.2: Summary of the dose-response-time model used in this study, including the biophase function, the pharmacodynamic model, the state variables, the fixed and random effects, the input, and the ouput.

[a] To be specific, these fixed effects are associated with random effects. For example, the individual k_i for subject i is given by $k_i = k \cdot \exp \eta_i$.

by

$$\frac{\mathrm{d}F(t)}{\mathrm{d}t} = k_{\mathrm{in}} - k_{\mathrm{out}} \cdot F_0 = 0. \tag{4.19}$$

A simple rearrangement gives the relation

$$F_0 = \frac{k_{\mathrm{in}}}{k_{\mathrm{out}}}. \tag{4.20}$$

Hence the system may be simplified by removing one of the parameters F_0, k_{in}, or k_{out} in the parameter estimation. Here, k_{in}[3] was estimated as a secondary parameter from the product of F_0 and k_{out}. The initial estimate of the FFA baseline level F_0 was taken as the mean response at time zero. Since the minimum FFA level is close to zero, initially for high NiAc dosages, we conclude that NiAc has a high efficacy and that I_{max} is close to 1. Furthermore, for high NiAc infusion rates, the inhibitory drug-mechanism function becomes saturated while the moderators are initially in steady-state with the response. Using this, and the initial estimate of I_{max} Eq. (4.11), can be approximated as

$$\frac{\mathrm{d}F(t)}{\mathrm{d}t} \approx -k_{\mathrm{out}} \cdot F(t), \tag{4.21}$$

or

$$F(t) \cong F_0 e^{-k_{\mathrm{out}} t}. \tag{4.22}$$

Using this relation, k_{out} can be estimated from the initial slope of the response-time course, taken on a semi-logarithmic scale. The initial estimate for the Hill exponent γ and the amplification factor p were set to 1. Simulations of the system were used to find suitable initial estimates for the remaining parameters.

4.5 Results and validation

Visual predictive check (VPC) plots for the FFA levels, constituting the observed data, the model predicted median, and 90% Monte Carlo prediction intervals (Robert and Casella, 2004) are illustrated in Fig. 4.4 for lean and obese rats. The FFA concentrations were suppressed in all animals receiving NiAc. Adaptation towards the FFA baseline was seen for the individuals that received a 300 min constant rate infusion of NiAc (see Fig. 4.4f and 4.4m). The adaptation was more pronounced the higher the infusion rate. All infusion regimens give rise to a rebound effect, i.e., the FFA level overshoots the initial baseline after the infusions stopped. The rebound effect was more pronounced the higher the infusion rate. Apparent oscillations around the FFA baseline level followed after the rebound. Oscillations were more pronounced the higher the NiAc doses and the longer the infusion regimens. The rats that received an oral dose of NiAc experienced an FFA drop followed by an approximately constant FFA level (Fig. 4.4i, 4.4j, and 4.4k). The higher the dose, the longer the rats stayed

[3]Note that since F_0 and k_{out} are assumed to be log-normally distributed, k_{in} also becomes log-normally distributed.

	Lean Sprague-Dawley rats			Obese Zucker rats		
Parameter	Estimate	Half-life	90% PI[a]	Estimate	Half-life	90% PI[a]
k_{out} (min^{-1})	0.31	2.3	$[1.3, 4.0]$	0.191	3.6	[1.6,6.2]
k_{tol} (min^{-1})	0.024	29	$[15, 51]$	0.0116	60	[29,95]
K_{i} (min^{-1})	0.0017	400	$[210, 710]$	0.0000645	11000	[0.95,5 000 000]

Table 4.3: Estimated system rate constants with corresponding half-lives (in minutes) with 90% non-parametric bootstrap prediction intervals for lean Sprague-Dawley and obese Zucker rats, respectively.

[a]90% non-parametric bootstrap prediction interval

at a suppressed FFA level. Rebound and oscillations followed the FFA suppression. The suppression of FFA, the occurrence of rebound, and the extent of the oscillations were more pronounced the higher the oral dose. Individual observed FFA response-time data, with individually fitted FFA response levels, are illustrated in Fig. 4.5 for one individual per administration route and rate. The individual behaviour was captured by the model for all provocations. The estimated population biophase amount-time courses are illustrated in Fig. 4.6. For the constant rate NiAc infusions, the biophase amount quickly reached steady-state. The wash-out kinetics were rapid with a half-life of around 2 min. For the highest oral doses, the biophase amount declined in a non-linear fashion post-peak due to the absorption rate-limited elimination of NiAc. Here, both a linear and non-linear biophase absorption model were fitted, with the latter providing the best fit. The fitted population parameters and inter-individual variations with corresponding relative standard errors for the full system are illustrated in Table 4.4. The biophase elimination rate constant k and the fractional turnover rate of FFA, k_{out}, are of the same order of magnitude (for both lean and obese rats), indicating little to no time-delay between biophase kinetics and FFA dynamics. Since the absorption into the biophase is non-linear, we observed typical absorption rate-limited elimination at higher oral doses of NiAc. The estimated $K_{\text{m,g}}$ of about 40 µmol kg^{-1} implies that the two higher oral doses (81.2 and 812 µmol kg^{-1}) approach and exceed saturation. The efficacy parameter I_{max} was estimated as 0.893 and $0.694 < 1$ for lean and obese rats, respectively; therefore, NiAc cannot completely suppress FFA levels. The estimated biophase potency ID_{50} shows that the drug-mechanism function (Eq. 4.5) will be saturated at the highest infusions and for all of the oral doses (Fig. 4.6). The estimated Hill exponent γ indicates a steep NiAc biophase amount—FFA response relationship at equilibrium (for both lean and obese rats). The estimated FFA baseline was higher for the obese rats, and the turnover of FFA slower. The rate constants k_{out}, k_{tol}, and K_{i} all have different orders of magnitude, and thus act over different time-scales. Half-lives for these three rate constants with 90% non-parametric bootstrap prediction intervals (Davison and Hinkley, 1997) are given in Table 4.3. All processes acted slower in the obese rather than the lean rats. However, the parameter K_i for the obese rats is practically non-identfiable given the current data (indicated by the extreme uncertainty in the point estimate).

		Lean Sprague-Dawley rats		Obese Zucker rats	
Parameter	Definition	Estimate (RSE%)	BSV[a] (RSE%)	Estimate (RSE%)	BSV[a] (RSE%)
$V_{\mathrm{max,g}}$ ($\mu\mathrm{mol\,kg^{-1}\,min^{-1}}$)	Max. elimination rate from gut	5.37(0.97)	-	-	-
$K_{\mathrm{m,g}}$ ($\mu\mathrm{mol\,kg^{-1}}$)	Amount in gut at half $V_{\mathrm{max,g}}$	37.1(3.4)	-	-	-
k ($\mathrm{min^{-1}}$)	Biophase elimination rate	0.446(5.8)	45.1(23)	0.207(22)	19.6(15)
F_0 ($\mathrm{mmol\,l^{-1}}$)	Baseline FFA conc.	0.705(2.3)	21.1(37)	0.952(4.3)	16.1(9.2)
k_{out} ($\mathrm{min^{-1}}$)	Fractional turnover rate	0.306(8.1)	42.4(47)	0.191(30)	47.2(37)
k_{tol} ($\mathrm{min^{-1}}$)	Turnover rate of moderator	0.0242(5.2)	24.4(98)	0.0116(30)	41.0(47)
K_{i} ($\mathrm{min^{-1}}$)	Adaptation rate	0.00174(25)	90.6(23)	0.0000645(250)	540(640)
p	Amplification factor	0.819(4.7)	-	0.415(47)	-
I_{max}	Efficacy	0.881(2.8)	-	0.697(30)	-
ID_{50} ($\mu\mathrm{mol\,kg^{-1}}$)	Potency	0.0456(6.8)	-	0.641(28)	-
γ	Hill exponent	2.96(8.6)	-	2.03(35)	-

Table 4.4: DRT model parameter estimates and between-subject variability, expressed in CV%, with corresponding relative standard errors (RSE%), and η-shrinkages

[a]Between-subject variability expressed in CV%, calculated as $100 \times \sqrt{\omega^2}$.

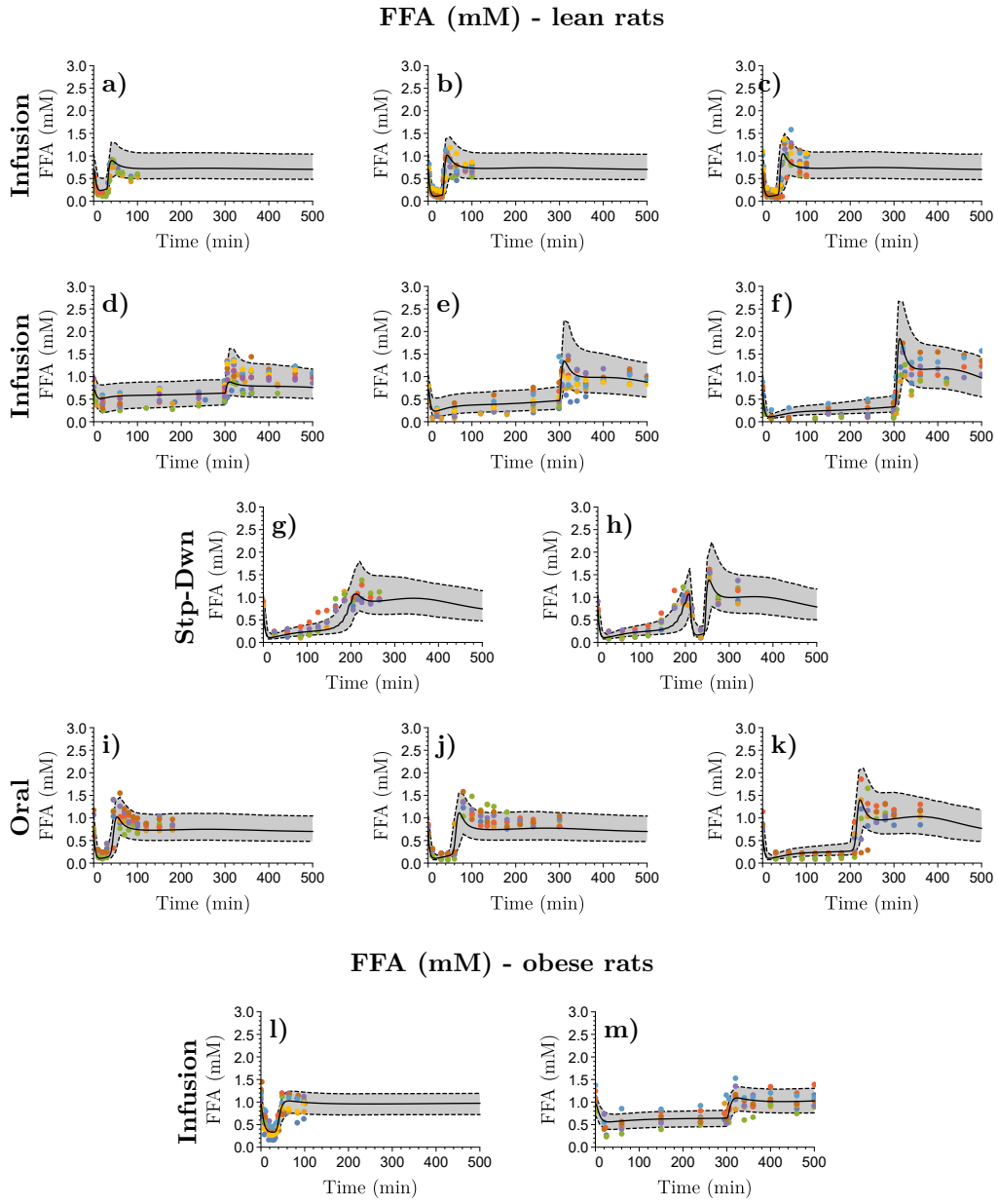

Figure 4.4: Visual predictive checks (VPC) of the FFA levels (in mM) for all experiments. The first row represents 30 min infusions of NiAc (rates of 0.033, 0.17, and 0.67 µmol min^{-1} kg^{-1}, respectively), the second 300 min infusions (rates of 0.017, 0.033, and 0.017 µmol min^{-1} kg^{-1}, respectively), the third step-down protocol (from 0.17 to 0 µmol min^{-1} kg^{-1}[a] with an additional 30 min infusion of 0.17 µmol min^{-1} kg^{-1} in (h)), the fourth oral dosing (doses of 24.4, 81.2, and 812 µmol kg^{-1}, respectively), and the fifth 30 repectively 300 min infusions (rates of 0.17 µmol min^{-1} kg^{-1}) for obese rats (experiments are detailed in Sec. 3.3). The dots represent the data, with colours indicating separate individuals, the black line the estimated median individual, and the grey area the 90% population prediction interval.

[a]The details of the protocols are given in Sec. 3.3

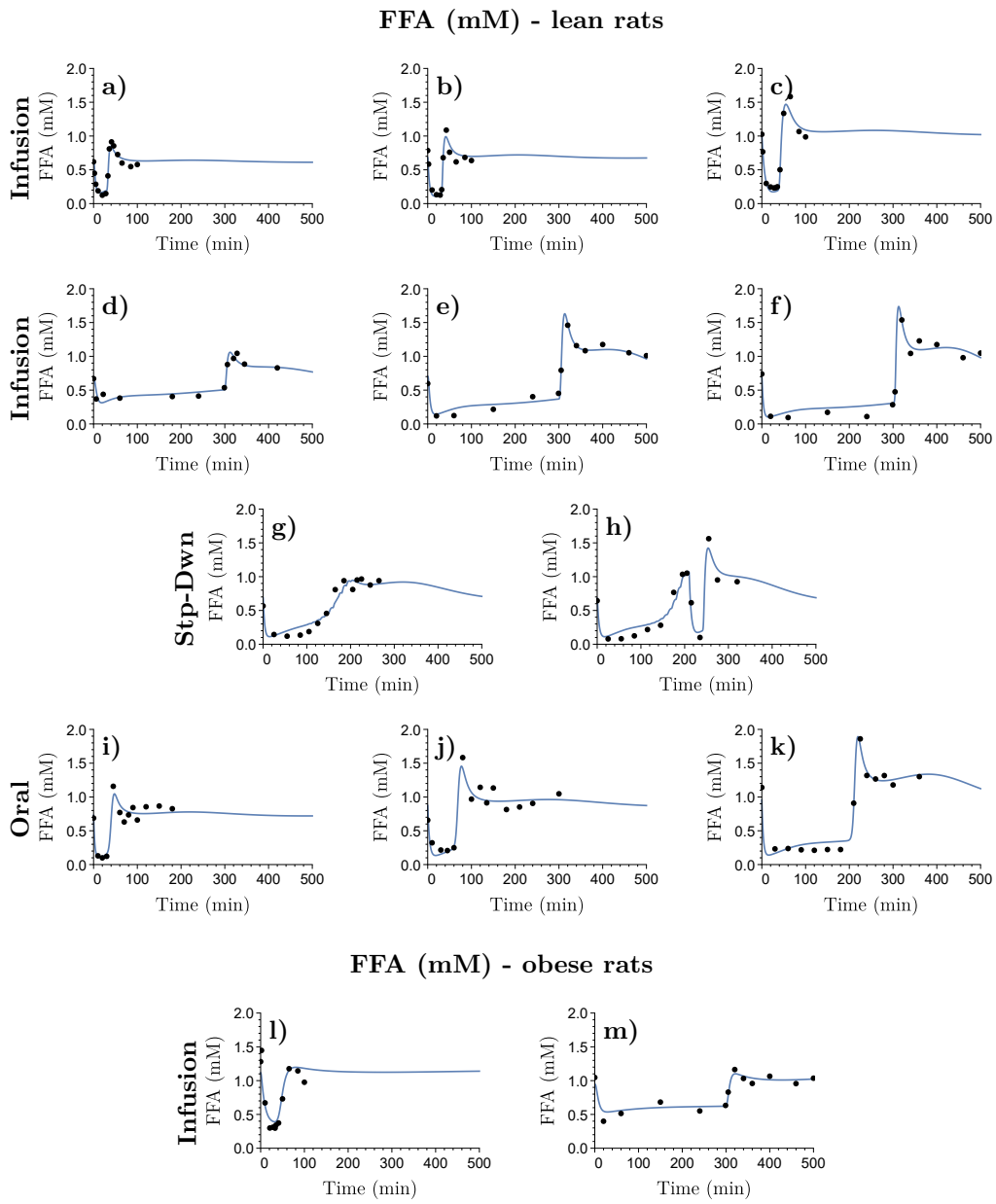

Figure 4.5: Individually fitted FFA response-time courses. The first row represents 30 min infusions of NiAc (rates of 0.033, 0.17, and 0.67 µmol min^{-1} kg^{-1}, respectively), the second 300 min infusions (rates of 0.017, 0.033, and 0.017 µmol min^{-1} kg^{-1}, respectively), the third step-down protocol (from 0.17 to 0 µmol min^{-1} kg^{-1} [a] with an additional 30 min infusion of 0.17 µmol min^{-1} kg^{-1} in (h)), the fourth oral dosing (doses of 24.4, 81.2, and 812 µmol kg^{-1}, respectively), and the fifth 30 repectively 300 min infusions (rates of 0.17 µmol min^{-1} kg^{-1}) for obese rats (experiments are detailed in Sec. 3.3). The dots represent the data and the black lines the estimated individual behaviour.

[a] The details of the protocols are given in Sec. 3.3

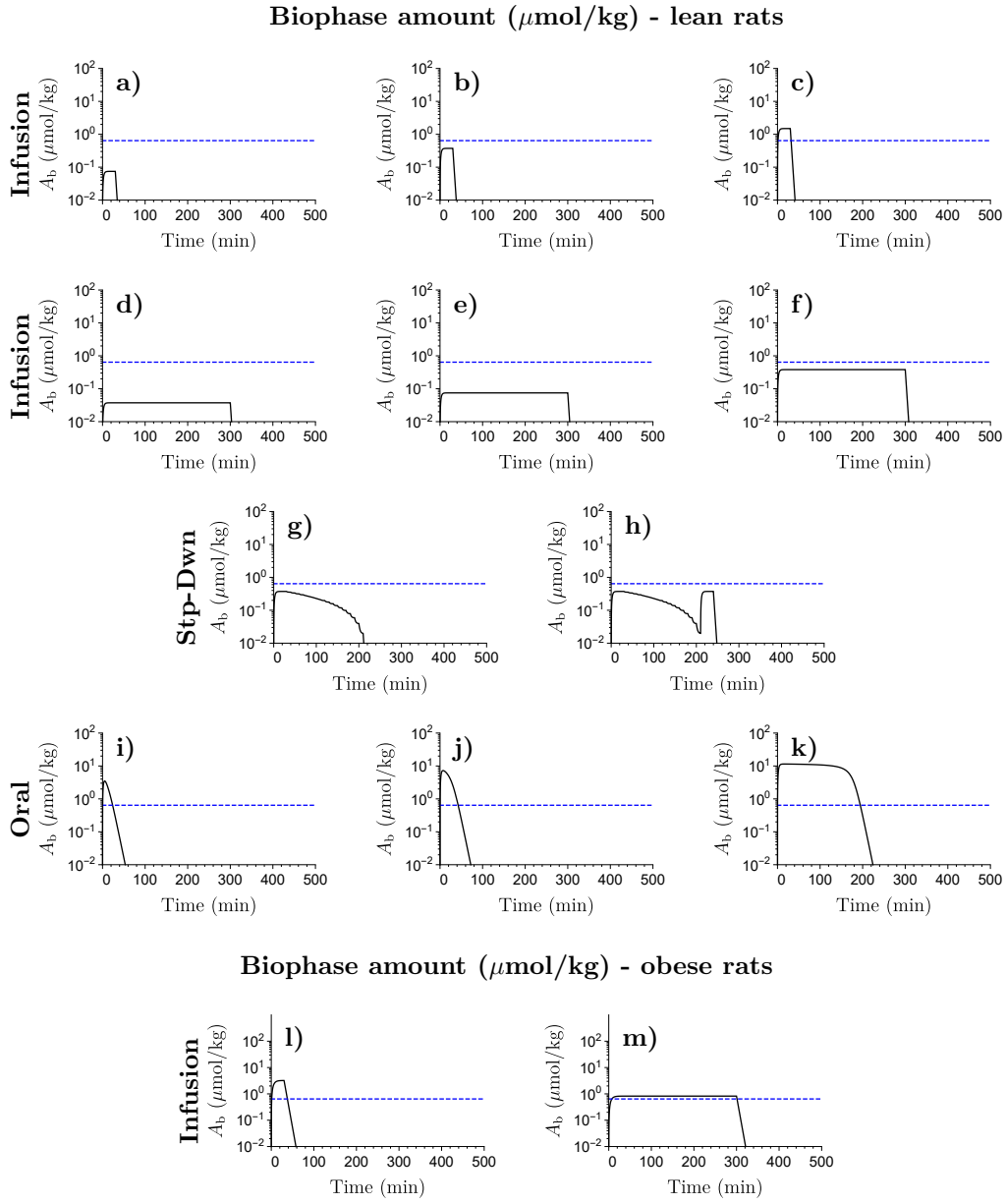

Figure 4.6: Population model predicted biophase drug amounts. The first row represents 30 min infusions of NiAc (rates of 0.033, 0.17, and 0.67 µmol min^{-1} kg^{-1}, respectively), the second 300 min infusions (rates of 0.017, 0.033, and 0.017 µmol min^{-1} kg^{-1}, respectively), the third step-down protocol (from 0.17 to 0 µmol min^{-1} kg^{-1} [a] with an additional 30 min infusion of 0.17 µmol min^{-1} kg^{-1} in (h)), the fourth oral dosing (doses of 24.4, 81.2, and 812 µmol kg^{-1}, respectively), and the fifth 30 repectively 300 min infusions (rates of 0.17 µmol min^{-1} kg^{-1}) for obese rats (experiments are detailed in Sec. 3.3). The black line represent the predicted biophase amount and the dashed blue line the predicted drug potency.

[a]The details of the protocols are given in Sec. 3.3

4.5.1 Model predictions

By using the predicted population parameters, we explored the long-term effects of NiAc provocation on FFA level for the infusion rate of 0.17 µmol kg^{-1} min^{-1}(Fig. 4.7), aiming at a therapeutic plasma concentration of NiAc of 1 µmol (Ahlström et al., 2013a). The model predicted 90% adaptation within approximately ten days of constant NiAc exposure for lean rats, and about 80% adaptation in obese rats during the same period. The effect of the first moderator (M_1) feedback can be seen immediately after the initial drop, where the system rapidly returns towards the baseline. The effect of the slower moderator feedback (M_8) is seen as a slower terminal return with oscillations in the FFA level. The effect of the integral feedback controller is seen as the slow return to baseline over time.

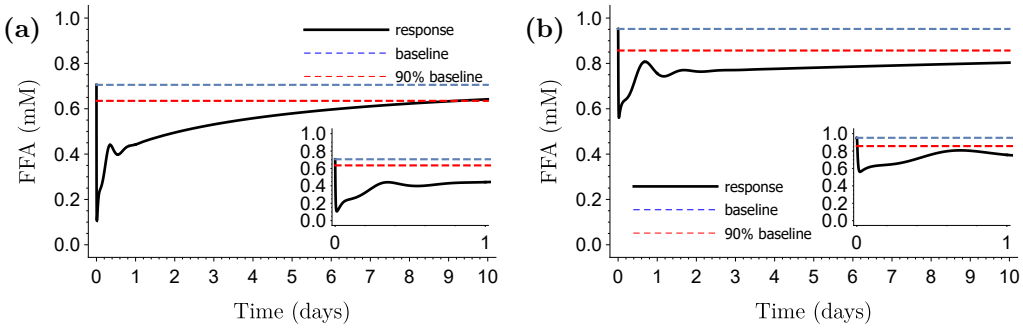

Figure 4.7: The long-term FFA response under constant rate infusions in lean (left figure) and obese rats (right figure). Here, the infusion rate is set to 0.17 µmol kg^{-1} min^{-1} (aiming at a therapeutic NiAc concentration of 1 µmol (Ahlström et al., 2013a)) and the infusions last for 10 days. The inserted figure shows in more detail the dynamics during the first day of the NiAc provocation.

Some of the pivotal parameters were compared to previously published estimates based on a meta-analysis of NiAc concentration–FFA response data (Tapani et al., 2014). These results are given in Table 4.5.

	Lean Sprague Dawley rats		Obese Zucker rats	
Parameter	DRT study	Tapani et al.	DRT study	Tapani et al.
k_{out} (min^{-1})	0.306(8.1)	0.316(9.8)	0.191(30)	0.343(31)
k_{tol} (min^{-1})	0.0242(5.2)	0.0239(1.9)	0.0116(30)	0.0245(2.0)

Table 4.5: Pharmacodynamic parameter comparison between this dose-response-time analysis (DRT) and the PK-PD analysis by Tapani et al. (2014) for lean Sprague-Dawley and obese Zucker rats, respectively. The parameter estimates are given with corresponding relative standard errors (RSE%) in parentheses.

4.5.2 Shrinkage analysis

Shrinkage analysis was used to quantify the parameter assumptions (log-normality) and to assess the model fits (Savic and Karlsson, 2009). The η-shrinkage of the EBEs are given in Table 4.7. The standard deviation of the residual additive error and the ε-shrinkage for the infusion and oral data are presented in Table 4.6.

	Lean Sprague-Dawley rats		Obese Zucker rats	
Data	Residual add. error σ	ε-shrinkage	Residual add. error σ	ε-shrinkage
Infusion	0.0982(14)	9.5%	0.112(5.2)	7.3%
Oral	0.149(5.0)	7.7%	-	-

Table 4.6: Model residual additive errors with corresponding relative standard errors (RSE%) and ε-shrinkage for lean Sprague-Dawley rats (infusion and oral data) and obese Zucker rats (infusion data), respectively.

Parameter	Sprague-Dawley	Obese Zucker
k (min^{-1})	21.4	24.9
F_0 (mM)	4.2	1.03
k_{out}(min^{-1})	46	33.5
k_{tol} (min^{-1})	52	67.2
K_{i} (min^{-1})	58	98.5

Table 4.7: Estimated η-shrinkage of the EBEs to the corresponding parameters k, F_0, k_{out}, k_{tol}, and K_{i}.

4.5.3 Sensitivity analysis

A local sensitivity analysis was performed to examine which of the model parameters affect the FFA response the most. The local analysis was conducted at the maximum likelihood estimate $\hat{\boldsymbol{\theta}}_{\mathrm{ML}}$ on a system perturbed by a 300 min constant rate infusion of NiAc with the infusion rate of 0.17 $\mu\mathrm{mol}\,\mathrm{min}^{-1}\,\mathrm{kg}^{-1}$. The sensitivity of, for example, the parameter F_0 is given by

$$\left.\frac{\partial F(t)}{\partial F_0}\right|_{\hat{\boldsymbol{\theta}}_{\mathrm{ML}}}. \tag{4.23}$$

The results of the analysis are seen in Fig. 4.8 at the maximum likelihood estimates obtained from the study of the lean and the obese rats. The parameters K_{i} and k_{tol} had the greatest impact on the system output, while the parameters γ and p had the least significiant impact. This holds around both the lean and the obese parameter estimates.

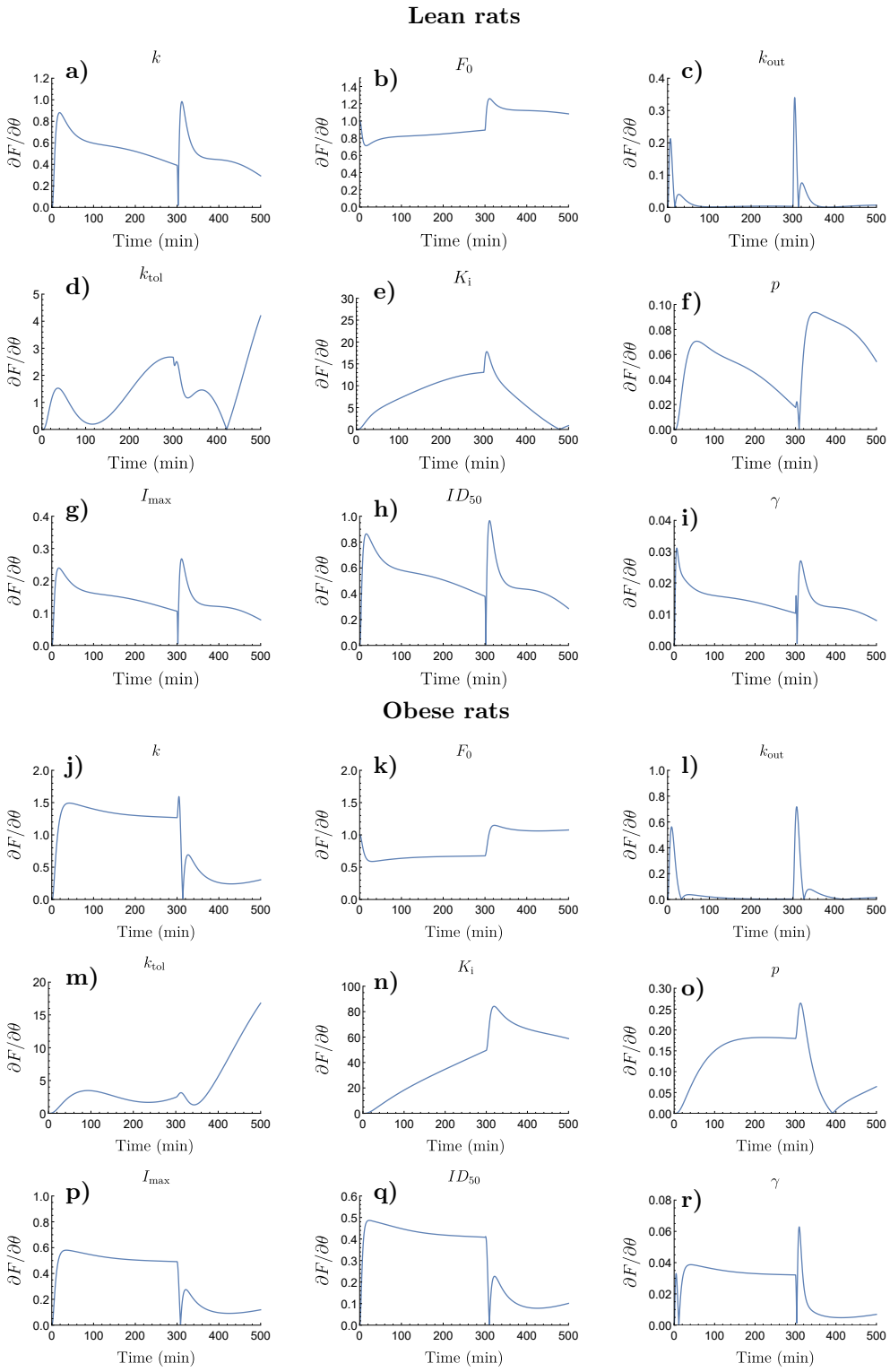

Figure 4.8: Local sensitivity analysis. The impact of each of the model parameters on the output is examined during a 300 min infusion of NiAc at an infusion rate of 0.17 µmol min^{-1} kg^{-1}. The analysis was performed at the maximum likelihood estimate, obtained from the analysis of the lean rats (upper plots) and the obese rats (lower plots).

4.5.4 Goodness-of-fit plots

The empirical distribution of the standardised residuals was investigated to assess the assumption of normality. This is illustrated in the form of a histogram in Fig. 4.9a and Fig. 4.9b for lean and obese rats, respectively. The standardised residuals were also plotted against time, seen in Fig. 4.9d and Fig. 4.9d. The assumption of normality was further assessed by investigating the quantile-quantile relationship of the theoretical and observed distributions of the standardised residuals. These are illustrated in Fig. 4.9e and Fig. 4.9f for lean and obese rats, respectively. Finally, the predicted vs. observed behaviour was investigated to determine if the performance of the model was consistent for all FFA levels. These dependencies are illustrated as scatter plots in Fig. 4.9g and Fig. 4.9h for lean and obese rats, respectively.

4.6 Discussion

DRT data analysis has previously proved to be a viable alternative to exposure-driven modelling when exposure data are sparse or absent (Bragg et al., 1994; Fisher and Wright, 1997; Fisher et al., 1997; Warwick et al., 1998; Gabrielsson et al., 2000; Gabrielsson and Peletier, 2014; Jacqmin et al., 2007; Luu et al., 2009; Wu et al., 2011). The technique has been successful in studies where the pharmacodynamic response behaves non-linearly, where time-lags are present in the data, and when the system displays potential feedback mechanisms (Gabrielsson et al., 2000). The present study has shown the utility of a non-linear biophase model (as a linear model were not sufficient in describing the absroption kinetics), permitting the description of more complex absorption kinetics.
Although DRT analyses cannot completely replace exposure-driven modelling, particularly when safety is an issue, DRT modelling can be considered even in studies where exposure assays are available (Hamberg et al., 2010). By avoiding drug plasma measurements, the pharmacological analysis becomes more biomarker oriented, focusing on the drug effect, provided time-series of the pharmacological response are available (Jacqmin et al., 2007). The non-invasiveness of DRT data analysis makes it useful in cases where invasive procedures are undesired, as in paediatric studies (Tod, 2008).

4.6.1 DRT modelling

In contrast to exposure-driven pharmacodynamic modelling, the biophase kinetics and the pharmacodynamic properties of a DRT model must be estimated simultaneously. Consequently, there may be difficulties in discriminating whether specific artefacts in the data originate from the concentration-time course or the response-time course.

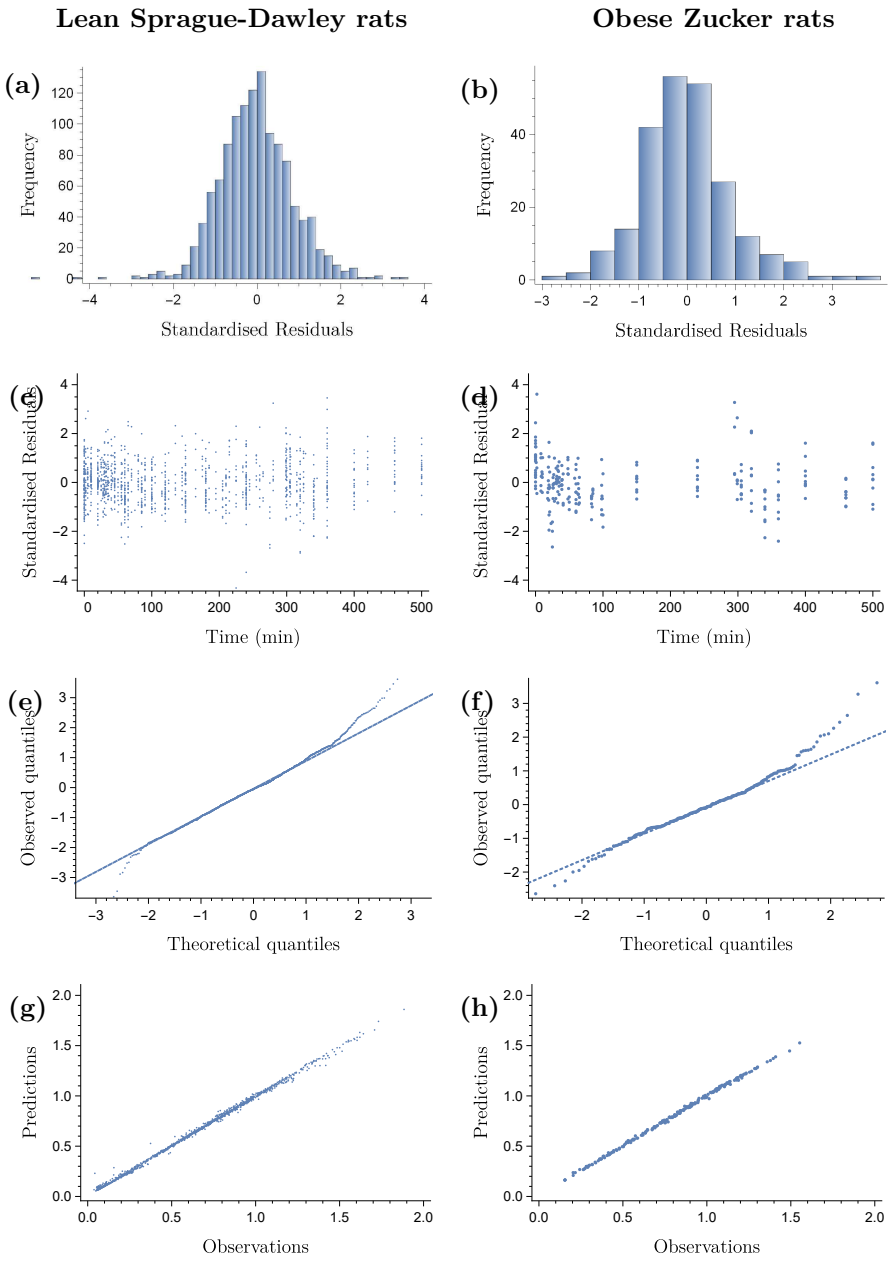

Figure 4.9: Histogram of the standardised residuals in (a) and (b), the standardised residuals over time in (c) and (d), Q-Q plots of the observed residuals vs. the theoretical residuals in (e) and (f), and scatter plots showing the relationships between the observed and predicted responses in (g) and (h). The left column represents lean Sprague-Dawley rats and the right obese Zucker rats.

4.6.2 Strategy when selecting the biophase model

The biophase model structure is preferably derived in a series of steps where data from different administration routes are sequentially analysed, and the biophase structure refined

if necessary (Table 4.1). In this way, different properties, for example, elimination rate and absorption rate, can be addressed separately.
In this study, the intravenous data were initially analysed to address the biophase disposition. Both a linear first-order and a Michaelis-Menten elimination model were successfully fitted to the data. The two models had approximately the same likelihood and fitted the data equally well when the function plots were inspected graphically. However, when the AIC was applied, the simpler model was preferred and therefore selected. The similarity between the linear first-order and Michaelis-Menten elimination models was due to the high estimate of the Michaelis-Menten constant (Table 4.4), in comparison to the biophase amounts (see Figs. 4.6), rendering an approximately linear elimination rate at all dose levels.
When the disposition model was selected, oral data were included to assess the absorption process into the biophase. Both a first-order and nonlinear Michaelis-Menten absorption model were analysed (Table 4.1). The first-order absorption model failed to capture the full dynamic behaviour of the data—as the model systematically overpredicted the response-time course for the highest oral dose ($812\,\mu mol\,kg^{-1}$). However, the Michaelis-Menten absorption model captured the absorption rate-limited elimination.

4.6.3 DRT model

The model captures the general trends of the populations, and the Monte Carlo prediction intervals cover approximately 90% of the individuals (see Figs. 4.4).
The integral feedback control, moderator feedback, and the turnover of FFA are shown to act over different time-scales (Table 4.3). Turnover of FFA occurs within minutes, the feedback triggered by insulin and other hormones operates within 30 min and 60 min for lean and obese rats, respectively, while the slow build-up of NiAc tolerance occurs within a couple of hours for lean rats and within a week for obese rats. However, the integral feedback control had extreme uncertainty for the obese rats, indicating practical non-identifiability (Table 4.4). Furthermore, the sensitivity of the system output, with respect to K_i, was high (Fig. 4.8e and 4.8n). Thus, the high sensitivity, yet extreme uncertainty, suggest that the data obtained from the experiments on the obese rats did not provide enough information about the build-up of tolerance. This adaptation, for the obese rats, is most likely occurring over a larger time-span. In conclusion, more data, preferably from long-term experiments, are needed to identify K_i for the obese rats.
The model predicts full system adaptation for long-term constant rate infusions with the therapeutic infusion rate of $0.17\,\mu mol\,kg^{-1}\,min^{-1}$ (Fig. 4.7). This homoeostatic behaviour has been proven experimentally in studies of long-term NiAc provocation (Oh et al., 2011). However, 90% of adaptation typically occurs within 24 h at therapeutic concentrations of NiAc. As mentioned, a better estimate for the adaptation K_i is expected when longitudinal data are generated and added to the analysis.
The standardised residuals fits the standard normal distribution well (see Fig. 4.9a and Fig. 4.9b), yet with slightly heavier tails (see Fig. 4.9e and Fig. 4.9f). There is no apparent

trend in the standardised residuals over time for normal rats (Fig. 4.9c). For obese rats, the standardised residuals seem to be systematically biased, specifically around the rebound (Fig. 4.9d). The prediction vs. observed values are consistent over the entire range of FFA levels (see Fig. 4.9g and Fig. 4.9h).
The disease impact was manifested by higher baseline levels of FFA (Table 4.4) and systematically slower rate processes (biophase elimination rate as well as turnover of FFA and the moderators) (Table 4.5) in the obese rats rather than in the lean rats.
In general, there is high consistency between our derived parameter estimates and exposure-driven model parameter estimates (Tapani et al., 2014) for lean rats, but not for the obese rats (see Table 4.5). For the lean study, the data consisted of 95 individuals taken from experiments of different rates, routes, and modes of NiAc provocations. The obese study only included 19 rats, taken from experiments of intravenous NiAc administration at only two different rates. These results illustrate the importance of having rich data (generated from experiments of different rate and route of drug administration) when performing DRT modelling, to obtain reliable results.
The models used for the infusion (lean and obese) and oral (lean) data resulted in relatively low levels of ε-shrinkages, less than 10%, indicating that the models describe the data without being over-fitted (Table 4.6).
This study has demonstrated the utility of DRT modelling in developing biophase-driven pharmacodynamic models. Given extensive data (with different rates, routes, and modes of administration), the biophase structure can be assessed even though the data demonstrate time-lags, feedback mechanisms, functional adaptation, and rebound phenomena.
We envisage that DRT data analysis will have great significance with regard to pharmacological responses (biomarkers) used in the future assessment of dynamics. DRT analysis has proven to be an acceptable alternative to exposure-driven PD modelling in situations where plasma concentrations are sparse or missing, or if extreme differences are seen for the initial and terminal disposition phases in plasma (such as with oligonucleotides, where rate and extent of exposure vary significantly between tissues (Callies et al., 2011; Heemskerk et al., 2010)).

4.6.4 Control theory

In this study, techniques from systems and control theory were utilised to describe feedback mechanisms and systemic adaptation. By applying integral feedback control, the system demonstrated full adaptation under constant long-term NiAc pressure (see Fig. 4.7). In fact, integral feedback control is a prerequisite for perfect adaptation in systems that experience constant disturbance (Ang et al., 2010; Sontag, 2003).
Many biological systems, experiencing adaptation when put under external disturbance, have been successfully modelled using control theory techniques, including metabolic networks (Bates and Cosetino, 2011; He et al., 2013), synthetic biology (Cosentino and Bates, 2011), the osmoregulation in yeast (Gennemark et al., 2006; Muzzey et al., 2009), and bacterial

chemotaxis (Barkai and Leibler, 1997; Yi et al., 2000). El-Samad et al. (2002) showed how integral feedback control could, for example, be derived from enzymatic relations when the goal is to address the control of plasma calcium levels. Control theory techniques have been used sparsely within PK-PD modelling and mostly in dose control (Schwildren et al., 1987; Stone and Howell, 2002; Urquhart and Li, 1969a; Vožch and Steimer, 1985; Veng-Pedersen and Modi, 1993). Control theory methods have a definite potential in modelling intrinsic control and feedback systems.

4.6.5 Inter-individual and intra-individual variability

In the initial stage, when the data were fitted on an individual level to assess parameter spread in the population, no parametric model (e.g., normal or log-normal) was successfully matched to the distributions of the EBEs. Nonetheless, a log-normal distribution was chosen to model the EBEs spread due to its positive range, a feature expected in the parameters. Fitting a log-normal distribution to the EBEs resulted in high levels of shrinkage for some of the parameters. While F_0 and k had low η-shrinkages, indicating that the log-normal assumption on the parameter distributions might be reasonable, the remaining three parameters had high η-shrinkages of $30-100\%$, suggesting that the standard deviation of the EBEs had shrunk to 0 and that the log-normal distribution did not fit the corresponding distribution of the EBEs. Consequently, one should be careful in interpreting the behaviour of the EBEs—like, for example, examining EBE vs. EBE plots or EBE vs. covariate plots. These are not reliable under high levels of shrinkage and, for that reason, omitted in this study. However, the estimated random effects are still useful when describing the data and when extrapolating to, for example, other dosing regimens.

Chapter 5

DRT II - Free fatty acid and insulin dynamics

The second study sought to extend the dose-response-time (DRT) model used in the previous analysis to obtain a more general, NiAc-FFA interaction model—applicable to a broad set of dosing regimens and NiAc exposure durations. The model aimed at quantitatively determining the impact of disease on the FFA-insulin system and to provide predictions for optimal drug delivery. A meta-analysis on an extensive pre-clinical data set of the interaction between NiAc and FFA, as well as insulin, was conducted in a nonlinear mixed-effects (NLME) modelling framework. Using various routes and modes of NiAc provocations, concentration-time course data of insulin and FFA was collected. All information regarding the exposure to NiAc was excluded to demonstrate the utility of a DRT model. Experiments were done both in lean Sprague-Dawley and obese Zucker rats—to evaluate the impact of the disease. Furthermore, by including insulin as a covariate of the FFA response, we could quantitatively analyse the endogenous antilipolytic effects of insulin (Arner et al., 1981) under NiAc provocations. Two forms of systemic adaptation were discovered—covering both NiAc and insulin resistance. Moreover, optimal dosing regimens, consisting of constant rate infusion periods followed by washout periods, were investigated. Finally, the results were compared to those for an exposure-driven analysis to assess the performance of the DRT model.

5.1 Model development

The dynamics of the two biomarkers, insulin and FFA, were described by separate DRT models. We assumed that NiAc inhibits the release of both insulin and FFA and that insulin inhibits the release of FFA (due to its antilipolytic effects). This assumption allows for a sequential approach to the model development; starting by fitting the insulin DRT model to the data, the resulting parameters estimated could then act as covariates in the ensuing FFA DRT model. This approach was adopted in the current study—including both the fixed effects (population parameters) and the Empirical Bayes Estimates (individual parameters) from the insulin model as covariates in the subsequent FFA model. Fig. 5.1b illustrates the interactions between the two DRT models (insulin and FFA) and Fig. 5.1a illustrates model interactions of previously published NiAc-FFA DRT models (Andersson et al., 2015).

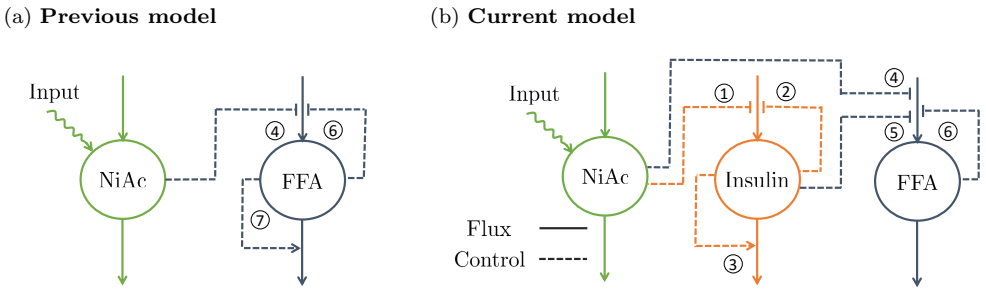

Figure 5.1: Schematic illustration of how the dependency between NiAc and FFA was modelled in previous studies (a) and how the dependencies between NiAc, insulin, and FFA were modelled in this study (b). Solid lines represent fluxes while dashed lines represent control. NiAc inhibits the turnover of insulin (1). Insulin, in turn, has feedback mechanisms that inhibit its turnover (2) and stimulates its fractional turnover (3). Both NiAc (4) and insulin (5) inhibit the turnover of FFA. In this study, FFA has a single feedback mechanism which inhibits its turnover (6), while in previous studies, FFA was modelled using an additional feedback mechanism which stimulates its fractional turnover (7).

5.1.1 Disease modelling and inter-study variability

The pharmacodynamics (PD) were significantly different between lean (normal) and obese (diseased) rats. Consequently, the parameter estimation for lean and obese rats was performed separately. Moreover, varying experimental conditions (separate time periods, anaesthetized vs. conscious animals) may have provoked different dynamic behaviours. Therefore, inter-study variability was included the models in the form of fixed-study effects (Laporte-Simitidis et al., 2000).

5.1.2 Notation conventions

To simplify for the reader, and differentiate between separate sub-model parameters, the model parameters are labelled with a subscript, indicating to which model they belong. For example, the turnover rate of FFA will be referred to as k_{inF} while the turnover rate of insulin is k_{inI} (i.e., F for FFA and I for insulin). Parameters that link the biophase NiAc amount, insulin, and FFA will be labelled with both sub-model subscripts (e.g., the potency of NiAc as an FFA inhibitor will be called $ID_{50\mathrm{NF}}$—N for NiAc and F for FFA).

5.2 The biophase function

Suitable biophase functions for NiAc have been developed previously for intravenous and oral administration (Andersson et al., 2015). The proven biophase function for intravenous administration was adopted in this study, while a new biophase function was developed for subcutaneous drug administration. The biophase dynamics are given by

$$\frac{\mathrm{d}A_{\mathrm{b}}(t)}{\mathrm{d}t} = \mathrm{Input}(t) - k \cdot A_{\mathrm{b}}(t) \quad \text{with} \quad A_{\mathrm{b}}(0) = 0, \tag{5.1}$$

where $A_{\mathrm{b}}(t)$ represents the biophase drug amount (expressed in $\mu\mathrm{mol\,kg^{-1}}$), k ($\mathrm{min^{-1}}$) the biophase elimination rate, and $\mathrm{Input}(t)$ a time-dependent function determined by the route administration according to

$$\mathrm{Input}(t) = \begin{cases} \text{Inf. rate} & \text{Intravenous administration} \\ k_{\mathrm{a}} \cdot A_{\mathrm{sc}}(t) & \text{Subcutaneous administration,} \end{cases} \tag{5.2}$$

where Inf. rate ($\mu\mathrm{mol\,kg^{-1}\,min^{-1}}$) is the infusion rate, A_{sc} ($\mu\mathrm{mol\,kg^{-1}}$) is the drug amount in the subcutaneous compartment, and k_{a} ($\mathrm{min^{-1}}$) the absorption rate from the subcutaneous compartment to the biophase. The infusion rate is modelled as either a constant, or stepwise decreasing Heaviside function to mimic the infusion regimens used in the experiments. The rate of change of $A_{\mathrm{sc}}(t)$ is given by

$$\frac{\mathrm{d}A_{\mathrm{sc}}(t)}{\mathrm{d}t} = \text{Inf. rate} - k_{\mathrm{sc}} \cdot A_{\mathrm{sc}}(t) \quad \text{with} \quad A_{\mathrm{sc}}(0) = 0. \tag{5.3}$$

The biophase functions are illustrated in Fig. 5.2.

5.3 The pharmacodynamics of insulin

The primary aim of the insulin model was to establish smooth trajectories that would accurately describe the insulin-time courses under various provocations of NiAc, rather than explain all of the mechanistic aspects of insulin dynamics. To this end, the model structure chosen was as simple as possible. The insulin model could subsequently be used to provide

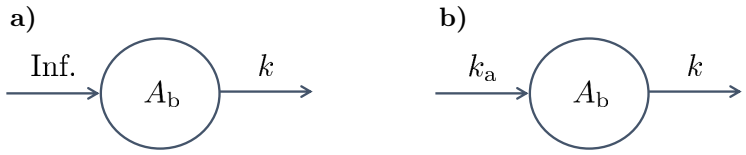

Figure 5.2: Illustration of the biophase models used in this case study. Fig. (a) represents a zero-order input into, and first-order elimination from, the biophase—used for modelling intravenous drug administration. Fig. (b) represents a first-order absorption into, and a first-order elimination from, the biophase—used for modelling subcutaneous administration.

input to the FFA model, enabling a quantitative analysis of the antilipolytic effects of insulin. Given this premise, we applied a phenomenologically based modelling approach. Under the assumption that NiAc perturbs insulin, the characteristics seen in the data were used to establish an insulin model with NiAc as input. The characteristic behaviour of the data for acute and long-term NiAc provocations in lean and obese rats is illustrated in Fig. 5.3. Attributes seen include indirect action, tolerance, rebound, and complete adaptation. Data with similar properties to those observed in the acute experiments (Figs. 5.3a and 5.3c) have been modelled using turnover equations with moderator feedback control (Ahlström et al., 2013a; Gabrielsson and Peletier, 2007). Furthermore, to capture the different long-term adaptive behaviours with (Fig. 5.3b), and without (Fig. 5.3d) rebound, a 'NiAc action compartment' was included, as well as an integral feedback control (a schematic illustation of the model is shown in Fig. 5.4).
The insulin dynamics are given by

$$\begin{aligned}\frac{\mathrm{d}I(t)}{\mathrm{d}t} &= k_{\mathrm{inI}} \cdot R_\mathrm{I}(t) \cdot H_\mathrm{NI}(A_\mathrm{b}(t)) \cdot \frac{M_{0\mathrm{I}}}{M_{1\mathrm{I}}(t)} \\ &\quad - k_{\mathrm{outI}} \cdot \frac{M_{2\mathrm{I}}(t)}{M_{0\mathrm{I}}} \cdot I(t), \qquad (5.4)\\ \frac{\mathrm{d}M_{1\mathrm{I}}(t)}{\mathrm{d}t} &= k_{\mathrm{tolI}} \cdot \big(I(t) - M_{1\mathrm{I}}(t)\big)\,, \qquad (5.5)\\ \frac{\mathrm{d}M_{2\mathrm{I}}(t)}{\mathrm{d}t} &= k_{\mathrm{tolI}} \cdot \big(M_{1\mathrm{I}}(t) - M_{2\mathrm{I}}(t)\big)\,, \qquad (5.6)\end{aligned}$$

with initial conditions

$$I(0) = I_0, \qquad (5.7)$$

and

$$M_{1\mathrm{I}}(0) = M_{2\mathrm{I}}(0) = M_{0\mathrm{I}} = I_0, \qquad (5.8)$$

where $I(t)$ denotes the observed insulin level (expressed in nM), $A_\mathrm{b}(t)$ the biophase amount, and $M_{1\mathrm{I}}(t)$ and $M_{2\mathrm{I}}(t)$ the first and second moderator compartments, respectively (both

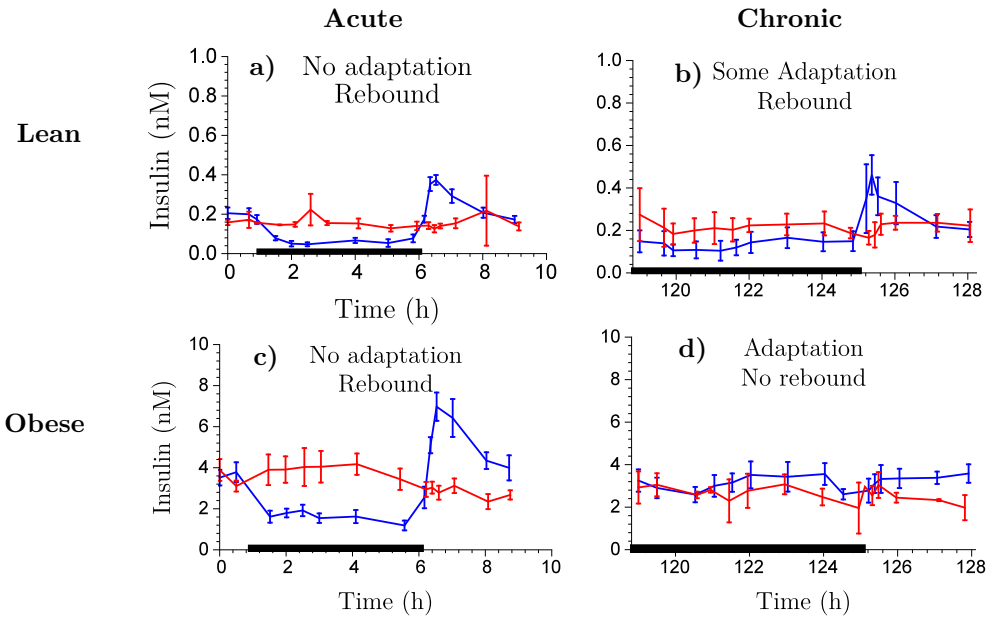

Figure 5.3: Example of insulin-time course data during acute NiAc dosing (a) and (c), and chronic NiAc dosing (continuous infusion) (b) and (d) for lean and obese rats, respectively. The blue lines represent the NiAc treated animals and the red lines the vehicle control group.

expressed in nM). The parameters k_{inI} ($\text{nM}\,\text{min}^{-1}$) and k_{outI} (min^{-1}) are the turnover rate and fractional turnover rate of insulin, respectively, and k_{tolI} (min^{-1}) is the fractional turnover rate of the moderators. The regulator $R_{\text{I}}(t)$ compartment is given by

$$\frac{\text{d}R_{\text{I}}(t)}{\text{d}t} = k_{\text{inRI}} - k_{\text{RI}} \cdot I(t) \quad \text{with} \quad R_{\text{I}}(0) = 1, \tag{5.9}$$

where k_{inRI} (min^{-1}) is the turnover rate, k_{outRI} ($\text{min}^{-1}\,\text{nM}^{-1}$) the fractional turnover rate, and $I(t)$ the insulin concentration. The regulator is initially at steady-state with

$$\frac{\text{d}R_{\text{I}}(0)}{\text{d}t} = k_{\text{inRI}} - k_{\text{outRI}} \cdot I_0 = 0 \tag{5.10}$$

or

$$I_0 = \frac{k_{\text{inRI}}}{k_{\text{outRI}}}. \tag{5.11}$$

By integrating Eq. (5.9), the dynamics of $R_{\text{I}}(t)$ can be expressed as

$$R_{\text{I}}(t) = 1 + \int_0^t k_{\text{inRI}} - k_{\text{outRI}} \cdot I(\tau)\,\text{d}\tau. \tag{5.12}$$

Hence, by construction, $R_{\text{I}}(t)$ represents the output of an insulin-driven integral feedback controller (Glad and Ljung, 2000) with I_0 as the set-point and k_{outRI} as the integral gain

parameter (k_{outRI} will from hereon be referred to as the integral gain parameter). The integral feedback controller ensures that insulin levels return to the baseline I_0, despite persistent external effects on insulin turnover and fractional turnover. The inhibitory NiAc function for insulin is given by

$$H_{\text{NI}}(A_{\text{b}}(t)) = 1 - E_{\text{NI}}(N_{\text{I}}(t)) \cdot \frac{A_{\text{b}}^n(t)}{ID_{50\text{NI}}^n + A_{\text{b}}^n(t)}, \tag{5.13}$$

where $ID_{50\text{NI}}$ ($\mu\text{mol}\,\text{kg}^{-1}$) is the potency of NiAc on insulin and n the Hill coefficient of the inhibitory function. The term $E_{\text{NI}}(N_{\text{I}}(t))$ represents the drug efficacy, which is fixed for lean rats and dependent on the concentration in a hypothetical NiAc action compartment, $N_{\text{I}}(t)$ ($\mu\text{mol}\,\text{kg}^{-1}$), for obese rats, according to

$$E_{\text{NI}}(N_{\text{I}}(t)) = \begin{cases} I_{\text{maxNI}} & \text{lean} \\ I_{\text{maxNI}} \left(1 - \frac{S_{\text{NI}} \cdot N_{\text{I}}^{\gamma}(t)}{N_{50\text{I}}^{\gamma} + N_{\text{I}}^{\gamma}(t)}\right) & \text{obese,} \end{cases} \tag{5.14}$$

where I_{maxNI} is the initial efficacy of NiAc for insulin, $N_{50\text{I}}$ ($\mu\text{mol}\,\text{kg}^{-1}$) the potency of the NiAc action compartment, S_{NI} the long-term NiAc efficacy loss, and γ the corresponding Hill coefficient of the efficacy relation. The dynamics of N_{I} are in turn given by

$$\frac{\text{d}N_{\text{I}}(t)}{\text{d}t} = k_{\text{NI}} \cdot (A_{\text{b}}(t) - N_{\text{I}}(t)), \tag{5.15}$$

with $N_{\text{I}}(0) = A_{\text{b}}(0)$. Here k_{NI} (min^{-1}) is the turnover rate of the NiAc action concentration. The NiAc action compartment is initially at steady-state with the biophase NiAc amount A_{b}. As infusions are initiated, and the biophase amount increases, $N_{\text{I}}(t)$ increases until it reaches the steady-state biophase NiAc amount $N_{\text{ss}}(t) = A_{\text{bss}}$. With increasing levels in the NiAc action compartment, $E(N_{\text{I}}(t))$ decreases to a minimum of $1 - S_{\text{NI}}$ and, consequently, the efficacy of NiAc as an insulin inhibitor is down-regulated. In other words, the system has developed tolerance to the drug. The turnover rate k_{NI} determines the rate at which tolerance develops.

Assuming that the system in Eq. (5.4) is at an initial steady-state with $\frac{\text{d}I}{\text{d}t} = 0$ and knowing that the initial biophase drug amount is zero, i.e., $A_{\text{b}}(0) = 0$, the inhibitory NiAc function for insulin is $H_{\text{NI}}(A_{\text{b}}(0)) = 1$ and we obtain

$$\left.\frac{\text{d}I}{\text{d}t}\right|_{t=0} = k_{\text{inI}} - k_{\text{outI}} \cdot I_0 = 0, \tag{5.16}$$

or

$$k_{\text{inI}} = k_{\text{outI}} \cdot I_0. \tag{5.17}$$

Thus, we can eliminate k_{inI} from the estimation procedure and obtain an estimate for this parameter from Eq. 5.17.

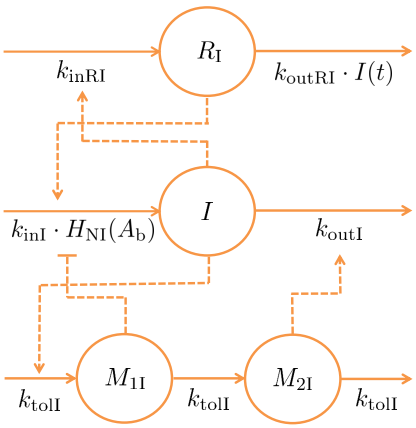

Figure 5.4: Mechanisms of insulin dynamics. The parameters k_inI and k_outI represent the turnover rate and fractional turnover rate, respectively. The turnover of insulin is inhibited by the NiAc action function $H_\mathrm{NI}(A_\mathrm{b})$. Tolerance and rebound are captured by the moderator compartments M_1I and M_2I, which act on the turnover rate and fractional turnover rate of insulin, respectively. The integral feedback controller acts on the turnover rate of insulin, in that it strives to maintain the insulin baseline, I_0, despite persistent external effects on the turnover.

5.3.0.1 Between-subject, inter-study, and residual variability

The insulin data illustrate individual variations (as can be seen in Fig. 5.3), which were described by incorporating random effects in the model and allow the parameters I_0, k_tolI, and $ID_{50\mathrm{NI}}$ to vary in the population. These parameters were assumed to be log-normally distributed. Thus, for example, the insulin baseline level I_{0i} of subject i is given by

$$I_{0i} = I_0 \cdot \exp \eta_i, \tag{5.18}$$

where I_0 is the median population insulin baseline level and η_i is the corresponding random effect of subject i. The covariance matrix of the random effects was assumed to be diagonal in order to simplify the estimations. Hence, the vector of random effects $\boldsymbol{\eta}_i$ of subject i is normally distributed $\boldsymbol{\eta}_i \sim \mathcal{N}(\mathbf{0}, \boldsymbol{\Omega})$ where

$$\boldsymbol{\Omega} = \begin{bmatrix} \omega_{11} & 0 & 0 \\ 0 & \omega_{22} & 0 \\ 0 & 0 & \omega_{33} \end{bmatrix}. \tag{5.19}$$

Here, ω_{11}, ω_{22}, and ω_{33} are the standard deviations of the random effects. The choice of these parameters was guided by an *a priori* sensitivity analysis (see Sec. 2.4 or Saltelli et al. (2008); Saltelli (2002) for more details). Moreover, the parameters I_0 and k_tolI varied over study groups according to fixed-study effects on both the mean and individual parameter distributions (Laporte-Simitidis et al., 2000). In other words, for S the number of groups,

the parameter I_0 for an individual j was modelled as

$$I_{0j} = (I_{01} \cdot \text{Study}_1 + \ldots + I_{0S} \cdot \text{Study}_S) \cdot \tag{5.20}$$

$$\exp(\eta_1 \cdot \text{Study}_1 + \ldots + \eta_S \cdot \text{Study}_S), \tag{5.21}$$

where $\text{Study}_k = 1$ if individual j is in group k and 0 otherwise. The residual variability was modelled using an additive model (with normally distributed errors).

5.4 The pharmacodynamics of FFA

The model suggested in this study is founded on preceding approaches (Ahlström et al., 2013a,b; Andersson et al., 2015; Tapani et al., 2014); however here, insulin has been included as the primary endogenous regulator of FFA as it provides a homoeostatic force on the system—thereby keeping FFA levels in the vicinity of its baseline concentration. Further, the NiAc efficacy is dynamic in that it is decreasing during long-term infusions, which allows for full systemic adaptation—a feature apparent in the data (Fabbrini et al., 2010; Poynten et al., 2003). The characteristic behaviour of the data, for acute and chronic NiAc provocations in lean and obese rats, is illustrated in Fig. 5.5. Attributes observed include indirect response, tolerance, rebound, and full adaptation. The behaviour observed in the acute experiment (Fig. 5.5a and Fig. 5.5c) has been described by turnover equations with moderator feedback (as described for the insulin system). The long-term behaviour, and in particular the adaptations with, and without, rebound, is captured by dynamic NiAc efficacy and an insulin integral controller (a schematic illustation of the model is shown in Fig. 5.6). The FFA model is given by

$$\begin{aligned}\frac{\mathrm{d}F(t)}{\mathrm{d}t} &= k_{\text{inF}} \cdot R_{\text{F}}(t) \cdot H_{\text{NF}}(A_{\text{b}}(t)) \cdot \frac{M_{0\text{F}}}{M_{\text{F}}(t)} \\ &\quad - k_{\text{outF}} \cdot F(t),\end{aligned} \tag{5.22}$$

with initial condition

$$F(0) = F_0. \tag{5.23}$$

Here, $F(t)$ denotes the observed FFA level (expressed in mM), $A_{\text{b}}(t)$ the biophase amount, k_{inF} ($\text{mM}\,\text{min}^{-1}$) the turnover rate, and k_{outF} (min^{-1}) the fractional turnover rate. The moderator compartment M_{F} (mM) is given by

$$\frac{\mathrm{d}M_{\text{F}}(t)}{\mathrm{d}t} = k_{\text{tolF}} \cdot \big(F(t) - M_{\text{F}}(t)\big)\,, \tag{5.24}$$

with initial condition

$$M_{\text{F}}(0) = M_{0\text{F}} = F_0, \tag{5.25}$$

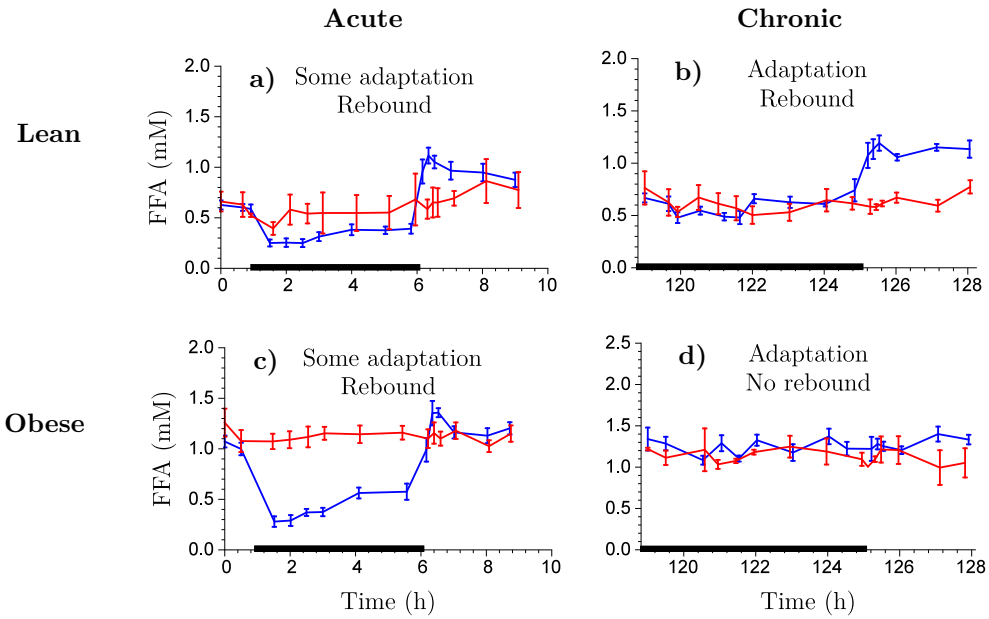

Figure 5.5: Example of FFA-time course data under acute NiAc dosing (a) and (c), and chronic NiAc dosing (continuous infusion) (b) and (d) for lean and obese rats, respectively. The blue lines represent the NiAc treated animals and the red lines the vehicle control group.

where the parameter k_{tolF} (min^{-1}) represents the turnover rate of the moderator compartment. The moderator compartment provides a feedback mechanism for the turnover of FFA, that strives to dampen deviations from the baseline response. The regulator compartment $R_{\text{F}}(t)$, that links the insulin dynamics to FFA release, is similar to that for the insulin model in Eq. (5.26) and is given by

$$\frac{\text{d}R_{\text{F}}(t)}{\text{d}t} = k_{\text{inRF}} - k_{\text{outRF}} \cdot I(t), \quad R_{\text{F}}(0) = 1, \tag{5.26}$$

where k_{inRF} (min^{-1}) is the turnover rate, k_{outRF} ($\text{nM}\,\text{min}^{-1}$) the fractional turnover rate, and $I(t)$ (nM) the insulin concentration. As for the insulin regulator, $R_{\text{F}}(t)$ represents the output of an insulin-driven integral controller with I_0 (nM) as the set-point and k_{outRF} as the integral gain parameter. The contribution of this integral controller during acute and chronic NiAc treatments in lean and obese rats is illustrated in Fig. 5.13b. The inhibitory NiAc function on FFA (similar to that for the insulin model in Eq. (5.13)), is given by

$$H_{\text{NF}}(A_{\text{b}}(t)) = 1 - E_{\text{NF}}(N_{\text{F}}(t)) \cdot \frac{A_{\text{b}}^m(t)}{ID_{50\text{NF}}^m + A_{\text{b}}^m(t)}, \tag{5.27}$$

where $ID_{50\text{NF}}$ ($\mu\text{mol}\,\text{kg}^{-1}$) is the potency of NiAc as an inhibitor of FFA release and m is the Hill coefficient. The drug efficacy is dynamic and changes (down-regulates) during

long-term infusions of NiAc. The efficacy is given by

$$E_{\mathrm{NF}}(N_{\mathrm{F}}(t)) = I_{\mathrm{maxNF}} \cdot \left(1 - \frac{S_{\mathrm{NF}} \cdot N_{\mathrm{F}}^{\phi}(t)}{N_{50\mathrm{F}}^{\phi} + N_{\mathrm{F}}^{\phi}(t)}\right), \tag{5.28}$$

where I_{maxNF} is the initial efficacy of NiAc on FFA, $N_{50\mathrm{F}}$ the potency of the NiAc action compartment, S_{NF} the long-term NiAc efficacy loss, ϕ the Hill coefficient, and $N_{\mathrm{F}}(t)$ the concentration in the NiAc action compartment. The dynamics of the NiAc action compartment are in turn described by

$$\frac{\mathrm{d}N_{\mathrm{F}}(t)}{\mathrm{d}t} = k_{\mathrm{NF}} \cdot (A_{\mathrm{b}}(t) - N_{\mathrm{F}}(t)), \tag{5.29}$$

with initial condition $N_{\mathrm{F}}(0) = A_{\mathrm{b}}(0)$. Here, the parameter k_{NF} is the turnover rate of the NiAc action state.

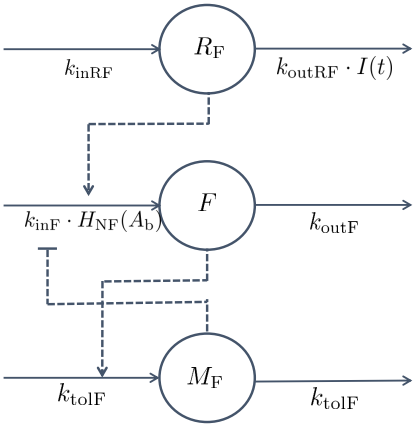

Figure 5.6: Mechanisms of FFA dynamics. The parameters k_{inF} and k_{outF} represent the turnover rate and fractional turnover rate, respectively. The turnover of FFA is inhibited by the NiAc action function $H_{\mathrm{NF}}(A_{\mathrm{b}})$. Tolerance and rebound are captured by the moderator compartment M_{F}, which acts on the turnover rate of FFA. The upper control arrow represents the insulin-driven integral controller with set-point I_0.

Assuming that the system in Eq. (5.22) is at an initial steady-state with $\frac{\mathrm{d}F}{\mathrm{d}t} = 0$ and that the initial biophase drug amount is zero, then the inhibitory NiAc function for insulin is $H_{\mathrm{NF}}(A_{\mathrm{b}}(0)) = 1$ and we obtain

$$\left.\frac{\mathrm{d}F}{\mathrm{d}t}\right|_{t=0} = k_{\mathrm{inF}} - k_{\mathrm{outF}} \cdot F_0 = 0, \tag{5.30}$$

or

$$k_{\mathrm{inF}} = k_{\mathrm{outF}} \cdot F_0. \tag{5.31}$$

Thus, we can eliminate k_{inF} from the estimation procedure and obtain an estimate for this

parameter from Eq. (5.31).

5.4.0.1 Between-subject, inter-study, and residual variability

Random effects were again selected using an a priori sensitivity analysis (see Sec. 2.4) (Saltelli et al., 2008; Saltelli, 2002). The analysis was performed around a local point in the parameter space around which the optimal solution was assumed to be found. Here, the parameters that affected the system output the most, and thus having the highest sensitivity, were assumed to vary in the population. The parameters that varied in the population were F_0, k_{tolF}, and $ID_{50\text{NF}}$ (according to a log-normal distribution). The covariance matrix of the random effects was chosen to be diagonal in order to simplify the estimations. Moreover, inter-study variability was incorporated in the model according to a fixed-study effect (as described for the insulin model). The parameters that varied between experimental groups were F_0 and k_{tolF} (only for the obese rats). The residual variability was modelled using an additive model (with normally distributed errors), which is often sufficient in pharmacodynamic modelling (rather than using, for example, a proportional residual error model or a combination of additive and proportional residual error (Mould and Upton, 2013)).

5.4.1 Structural identifiability

All population model structures analysed in this study were proven to be structurally locally identifiable in a fixed effects setting (identifiability of the population model (fixed effects) implies identifiability of the statistical model (random effects) (Janzén, 2016)) (a summary of the models—including fixed and random effects, input, and output—can be found in Table 5.1). The identifiability analysis was performed using the Exact Arithmetic Rank (EAR) approach (Anguelova et al., 2012; Karlsson et al., 2012; Raue et al., 2014)—implemented in the IdentifiabilityAnalysis Wolfram Mathematica package, developed by the Fraunhofer-Chalmers Centre (see Sec. 2.2.1.3 and Appendix C for an example code for the Mathematica package). The EAR algorithm requires that all states and system parameters are rational functions of their arguments. This requirement is not fulfilled in the insulin and FFA systems (for example, the state space variable A_{b} is raised to the power of n in Eq. (5.13)). We will now provide an illustrative example of how this requirement can be achieved by rewriting the system in a rational form.

5.4.1.1 System on rational form

The insulin system, given by Eqs. (5.4) to (5.15), with the NiAc biophase amount A_{b} as input and the insulin level I as output, does not fulfill the requirement that all states and system parameters must be rational functions of their arguments (for example, the state space variable $A_{\text{b}}(t)$ is raised to the power of n in Eq. (5.13)). This issue is overcome by

introducing the auxiliary state variable $B(t) = A_{\mathrm{b}}^{n}(t)$ (Lindskog, 1996) with

$$\frac{\mathrm{d}B(t)}{\mathrm{d}t} = n \cdot A_{\mathrm{b}}^{n-1}(t) \cdot \frac{\mathrm{d}A_{\mathrm{b}}(t)}{\mathrm{d}t} = n \cdot \frac{B(t)}{A_{\mathrm{b}}(t)} \cdot \frac{\mathrm{d}A_{\mathrm{b}}(t)}{\mathrm{d}t}, \tag{5.32}$$

and the parameter B_0 as the initial condition

$$B(0) = B_0 \, (= A_{\mathrm{b}}^{n}(0)). \tag{5.33}$$

Furthermore, we introduce IB_{50} as $IB_{50} = ID_{50\mathrm{NI}}^{n}$. Given these transformations, the drug mechanism function in Eq. (5.13) becomes

$$H_{\mathrm{NI}}(B(t)) = 1 - E_{\mathrm{NI}}(N(t)) \frac{B(t)}{IB_{50} + B(t)}, \tag{5.34}$$

and the augmented insulin system, with Eq. (5.32) to (5.34) with parameters B_0 and IB_{50} included, will fulfil the requirements of the EAR algorithm (this augmented system is equivalent to the original one). Now, explicit relations such as $B_0 = A_{\mathrm{b}}^{n}(0))$ cannot be included in the algorithm. This leaves B_0 structurally locally unidentifiable and, consequently, IB_{50} structurally locally unidentifiable. However, all other parameters are structurally locally identifiable and the number of degrees of freedom of the system, given by the algorithm, is 1. Given that we can identify n and that we know the initial input $A_{\mathrm{b}}(0)$, we can identify B_0 from $B_0 = A_{\mathrm{b}}^{n}(0))$. Hence, we can also identify IB_{50} (since the degree of freedom was 1), and the system is structurally locally identifiable.

5.5 Parameter estimation

The parameter estimation of the DRT model in this study was performed using a mixed effects modelling framework implemented in Mathematica, developed at the Fraunhofer-Chalmers Research Centre for Industrial Mathematics (Gothenburg, Sweden) (Almquist et al., 2015). This framework is described in Sec. 2.3.5. Diagonal covariance matrices were chosen to simplify the parameter estimation. From the steady-state relations in the insulin and FFA models, dependencies were derived which enabled the parameters k_{inI}, k_{inF}, k_{inRI}, and k_{inRF} to be expressed in terms of other model parameters. Consequently, these parameters were redundant and could be replaced in the parameter estimation. Furthermore, some parameters were initially estimated to be very close to their physiological limit (e.g. $I_{\mathrm{maxNI}} = 0.9999 \approx 1$ for obese rats) and were consequently fixed for numerical stability. Finally, to simplify the parameter estimation, some parameters were fixed (e.g., $S_{\mathrm{NI}} = 1$ for obese rats—this is motivated by the full systemic adaptation apparent in the long-term insulin-time data, implying that S_{NI} must be 1). A full summary of the models can be found in Table 5.1.
The MATHEMATICA code used for the parameter estimation of the FFA model in DRT study I can be found in the Appendix B. The code used for this model is omitted as the codes are practically the same.

Dose-response-time model						
			Parameters			
Biophase function	Pharmacodynamic model	State variables	Fixed effects	Mixed effects[a]	Input	Output
	Insulin model					
$\frac{\mathrm{d}A_\mathrm{b}}{\mathrm{d}t} = \mathrm{Input}(t) - k \cdot A_\mathrm{b}$ $A_\mathrm{b}(0) = 0$ $\mathrm{Input}(t) = \begin{cases} \text{Inf. rate} & \text{IV} \\ k_\mathrm{sc} \cdot A_\mathrm{sc}(t) & \text{Subcut.} \end{cases}$ $\frac{\mathrm{d}A_\mathrm{sc}}{\mathrm{d}t} = \text{Inf. rate} - k_\mathrm{a} \cdot A_\mathrm{sc}$ $A_\mathrm{sc}(0) = 0$	$\frac{\mathrm{d}I}{\mathrm{d}t} = k_\mathrm{inI} \cdot R_\mathrm{I} \cdot H_\mathrm{NI}(A_\mathrm{b}(t)) \cdot \frac{M_\mathrm{0I}}{M_\mathrm{1I}(t)} - k_\mathrm{outI} \cdot \frac{M_\mathrm{2I}(t)}{M_\mathrm{0I}} \cdot I(t)$ $I(0) = I_0$ $\frac{\mathrm{d}M_\mathrm{1I}(t)}{\mathrm{d}t} = k_\mathrm{tolI} \cdot \left(I(t) - M_\mathrm{1I}(t)\right),$ $M_\mathrm{1I}(0) = I_0,$ $\frac{\mathrm{d}M_\mathrm{2I}(t)}{\mathrm{d}t} = k_\mathrm{tolI} \cdot \left(M_\mathrm{1I}(t) - M_\mathrm{2I}(t)\right),$ $M_\mathrm{2I}(0) = I_0,$ $\frac{\mathrm{d}R_\mathrm{I}(t)}{\mathrm{d}t} = k_\mathrm{inRI} - k_\mathrm{RI} \cdot I(t),$ $R_\mathrm{I}(0) = 1,$ $H_\mathrm{NI}(A_\mathrm{b}(t)) = 1 - E_\mathrm{NI}(N_\mathrm{I}(t)) \cdot \frac{A_\mathrm{b}^n(t)}{ID_\mathrm{50NI}^n + A_\mathrm{b}^n(t)},$ $E_\mathrm{NI}(N_\mathrm{I}(t)) = \begin{cases} I_\mathrm{maxNI} & \text{lean} \\ I_\mathrm{maxNI}\left(1 - \frac{S_\mathrm{NI} \cdot N_\mathrm{I}^\gamma(t)}{N_\mathrm{50I}^\gamma + N_\mathrm{I}^\gamma(t)}\right) & \text{obese,} \end{cases}$ $\frac{\mathrm{d}N_\mathrm{I}(t)}{\mathrm{d}t} = k_\mathrm{NI} \cdot (A_\mathrm{b}(t) - N_\mathrm{I}(t)),$ $N_\mathrm{I}(0) = 0$	A_b A_sc I M_1I M_2I R_I N_I	k k_sc k_outI I_maxNI n k_tolI k_outRI k_NI N_50I γ S_NI	I_0 ID_50NI k_tolI	Inf. rate	I

[a]To be specific, these fixed effects are associated with random effects. For example, the individual k_i for subject i is given by $k_i = \cdot \exp \eta_i$.

FFA model

$$\frac{\mathrm{d}A_\mathrm{b}}{\mathrm{d}t} = \mathrm{Input}(t) - k \cdot A_\mathrm{b}$$
$$A_\mathrm{b}(0) = 0$$
$$\mathrm{Input}(t) = \begin{cases} \text{Inf. rate} & \text{IV} \\ k_\mathrm{sc} \cdot A_\mathrm{sc}(t) & \text{Subcut.} \end{cases}$$
$$\frac{\mathrm{d}A_\mathrm{sc}}{\mathrm{d}t} = \text{Inf. rate} - k_\mathrm{a} \cdot A_\mathrm{sc}$$
$$A_\mathrm{sc}(0) = 0$$

$$\frac{\mathrm{d}F}{\mathrm{d}t} = k_\mathrm{inF} \cdot R_\mathrm{F} \cdot H_\mathrm{NF}(A_\mathrm{b}(t)) \cdot \frac{M_\mathrm{0F}}{M_\mathrm{F}(t)} - k_\mathrm{outI} \cdot F(t)$$
$$F(0) = F_0$$
$$\frac{\mathrm{d}M_\mathrm{F}(t)}{\mathrm{d}t} = k_\mathrm{tolF} \cdot \left(F(t) - M_\mathrm{1F}(t)\right),$$
$$M_\mathrm{F}(0) = F_0,$$
$$\frac{\mathrm{d}R_\mathrm{F}(t)}{\mathrm{d}t} = k_\mathrm{inRF} - k_\mathrm{RF} \cdot I(t)^{a},$$
$$R_\mathrm{F}(0) = 1,$$
$$H_\mathrm{NF}(A_\mathrm{b}(t)) = 1 - E_\mathrm{NF}(N_\mathrm{F}(t)) \cdot \frac{A_\mathrm{b}^m(t)}{ID_\mathrm{50NF}^m + A_\mathrm{b}^m(t)},$$
$$E_\mathrm{NF}(N_\mathrm{F}(t)) = I_\mathrm{maxNF}\left(1 - \frac{S_\mathrm{NF} \cdot N_\mathrm{F}^\phi(t)}{N_\mathrm{50f}^\phi + N_\mathrm{F}^\phi(t)}\right),$$
$$\frac{\mathrm{d}N_\mathrm{F}(t)}{\mathrm{d}t} = k_\mathrm{NF} \cdot (A_\mathrm{b}(t) - N_\mathrm{F}(t)),$$
$$N_\mathrm{F}(0) = 0$$

A_b	k			
A_sc	k_sc			
F	k_outF	F_0		
M_F	I_maxNF	ID_50NF	Inf. rate	F
R_F	m	k_tolF	I	
N_F	k_tolF			
	k_outRF			
	k_NF			
	N_50F			
	ϕ			
	S_NF			

Table 5.1: Summary of the dose-response-time model used in this study, including the biophase function, the pharmacodynamic model, the state variables, the fixed and random effects, the input, and the ouput.

[a] The insulin model was fitted prior to the FFA fitting and the insulin input acted as a known input.

5.6 Results and validation

The parameter estimation for the two DRT models (insulin and FFA) was performed sequentially, as described in the Model development section 5.1. The estimates and between-subject variabilities (expressed in CV%), both with corresponding relative standard errors (RSE%), for normal Sprague-Dawley rats and obese Zucker rats are given in Table 5.3. Weighted summaries (Laporte-Simitidis et al., 2000) are presented for the parameters that varied between studies. The resulting models were qualitatively evaluated using visual predictive check (VPC) plots (Bergstrand et al., 2011); illustrating the data, the model predicted median individual, and 90% Monte Carlo prediction intervals generated from the models (Bergstrand et al., 2011; Post et al., 2008). The VPC's are shown in Fig. 5.7 for lean Sprague-Dawley rats and in Fig. 5.10 for obese Zucker rats. The VPCs were generated from the insulin and FFA models for all provocations of NiAc. Individually fitted insulin-time courses and FFA-time courses are illustrated in Fig. 5.8 for lean rats and in Fig. 5.11 for obese rats. Predicted biophase amounts from the insulin and FFA DRT models for lean and obese rats are illustrated in Fig. 5.9 and Fig. 5.12, respectively.

5.6.1 Biophase dynamics

The driving biophase functions were estimated for each submodel, both insulin and FFA, and for lean and obese rats. The biophase elimination and absorption rates are given in Table 5.3. The biophase amount reached steady-state quickly for all infusions, seen in Fig. 5.9 and Fig. 5.12. The wash-out kinetics were predicted to have a half-life of between 4 and 12 min for lean rats and between 2.5 and 3.2 min for obese rats (the ranges are derived from the estimates obtained from the insulin and FFA DRT models).

5.6.2 Insulin model

The insulin concentration was suppressed below its baseline value for all provocations of NiAc. The suppression was more pronounced at an early stage of the infusions; at later stages, the insulin concentrations drifted back towards their baselines. After the infusions were terminated, the insulin concentrations rebounded before reaching their baseline values. The individuals receiving the 12 h Off protocols (Fig. 5.7d and Fig. 5.10d) had the highest rebound, while individuals receiving step-down protocols had less pronounced rebound (Figs. 5.7e, 5.7g, 5.10e, and 5.10g). The insulin concentrations returned to their baselines after long-term infusions of NiAc in the obese rats (Fig. 5.10c). No rebound was observed after the extended infusions were terminated (Fig. 5.10c).

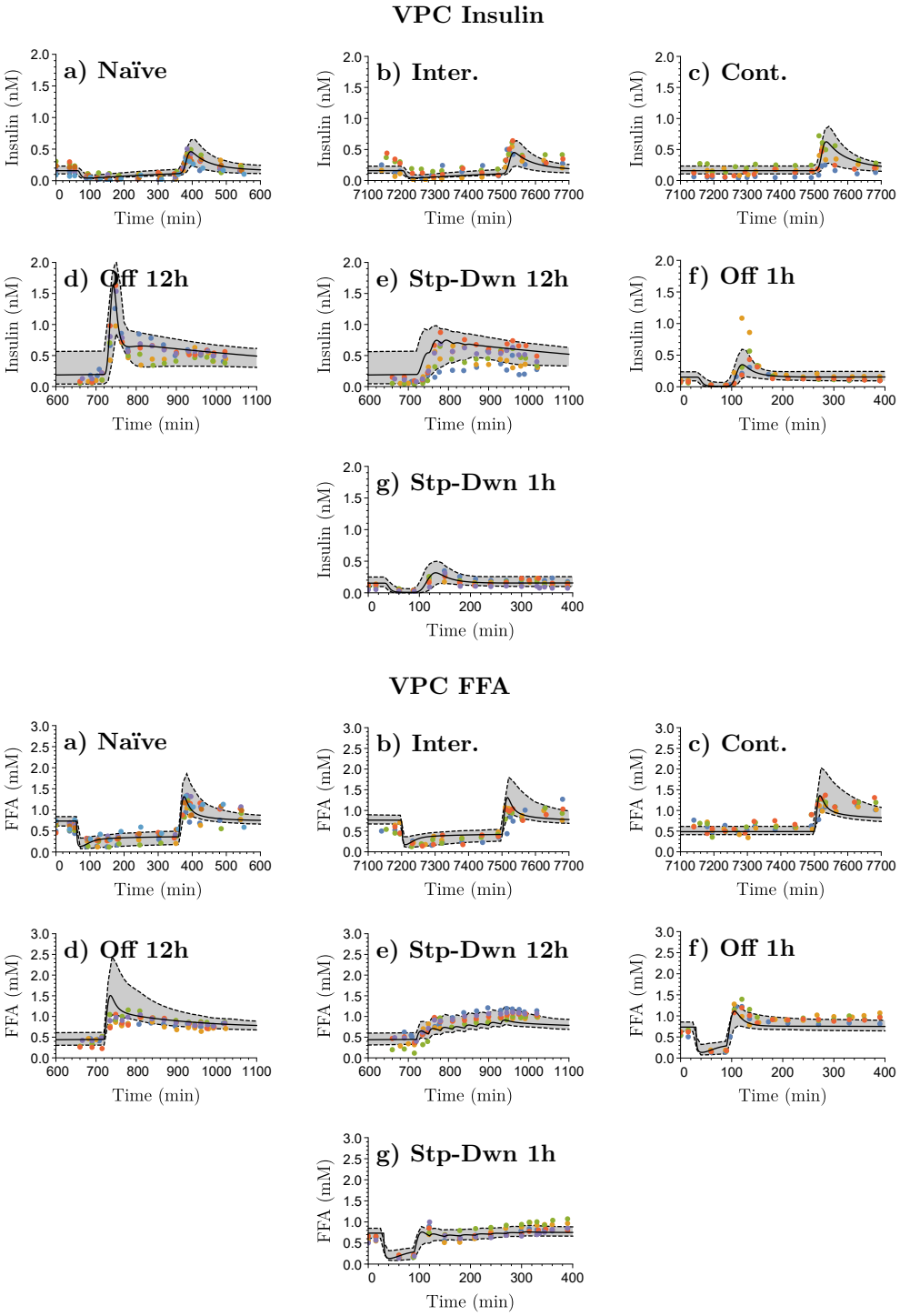

Figure 5.7: Visual predictive checks for **lean Sprague-Dawley rats**. The upper seven illustrations show the insulin fits, the lower seven the FFA fits. The dots represent the data, with colours indicating separate individuals, the black lines the estimated median individual, and the grey area the 90% population prediction interval.

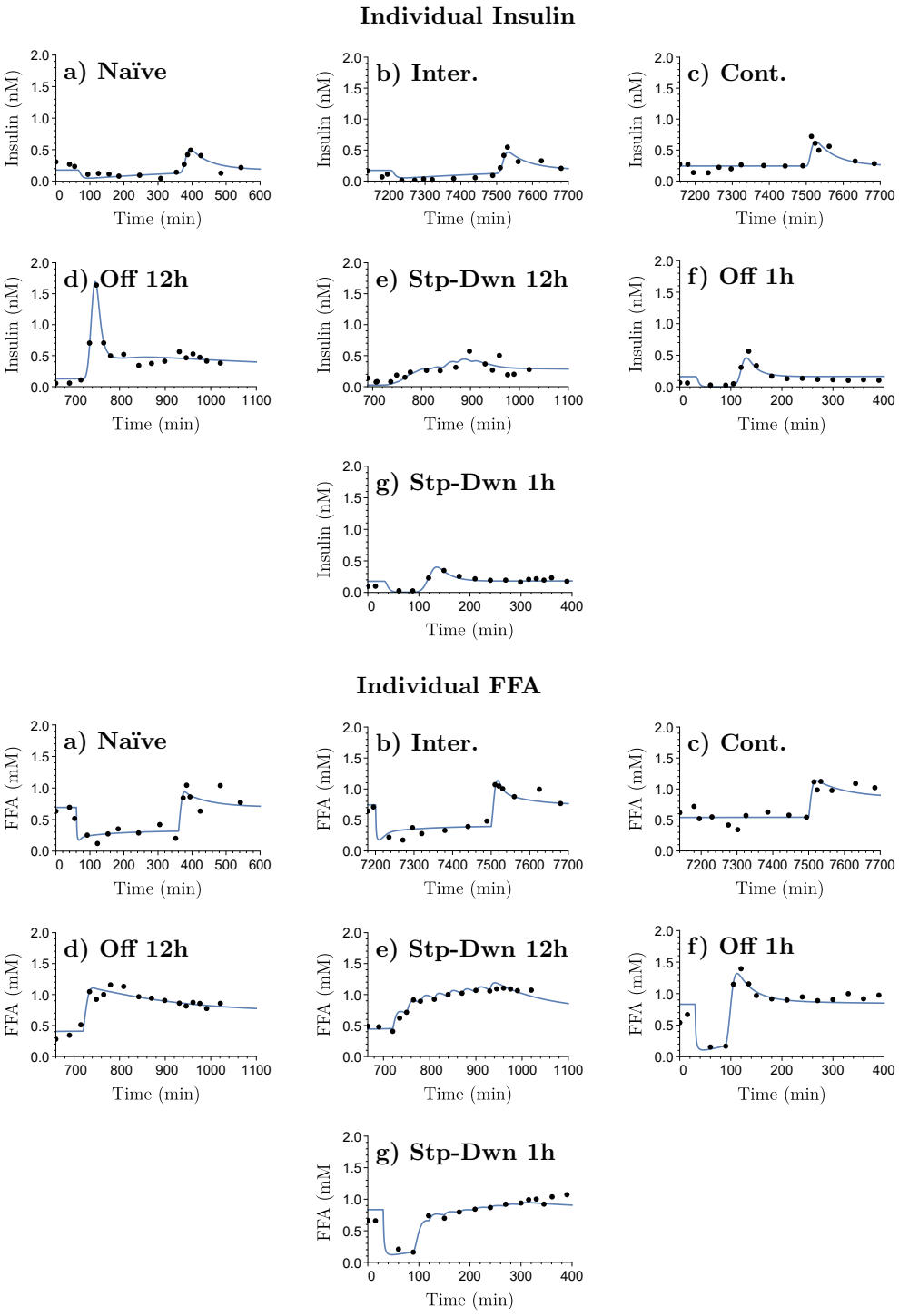

Figure 5.8: Individual fits for **lean Sprague-Dawley rats**. The upper seven illustrations show the insulin fits, the lower seven the FFA fits. The dots represent the data and the black lines the estimated individual behaviour.

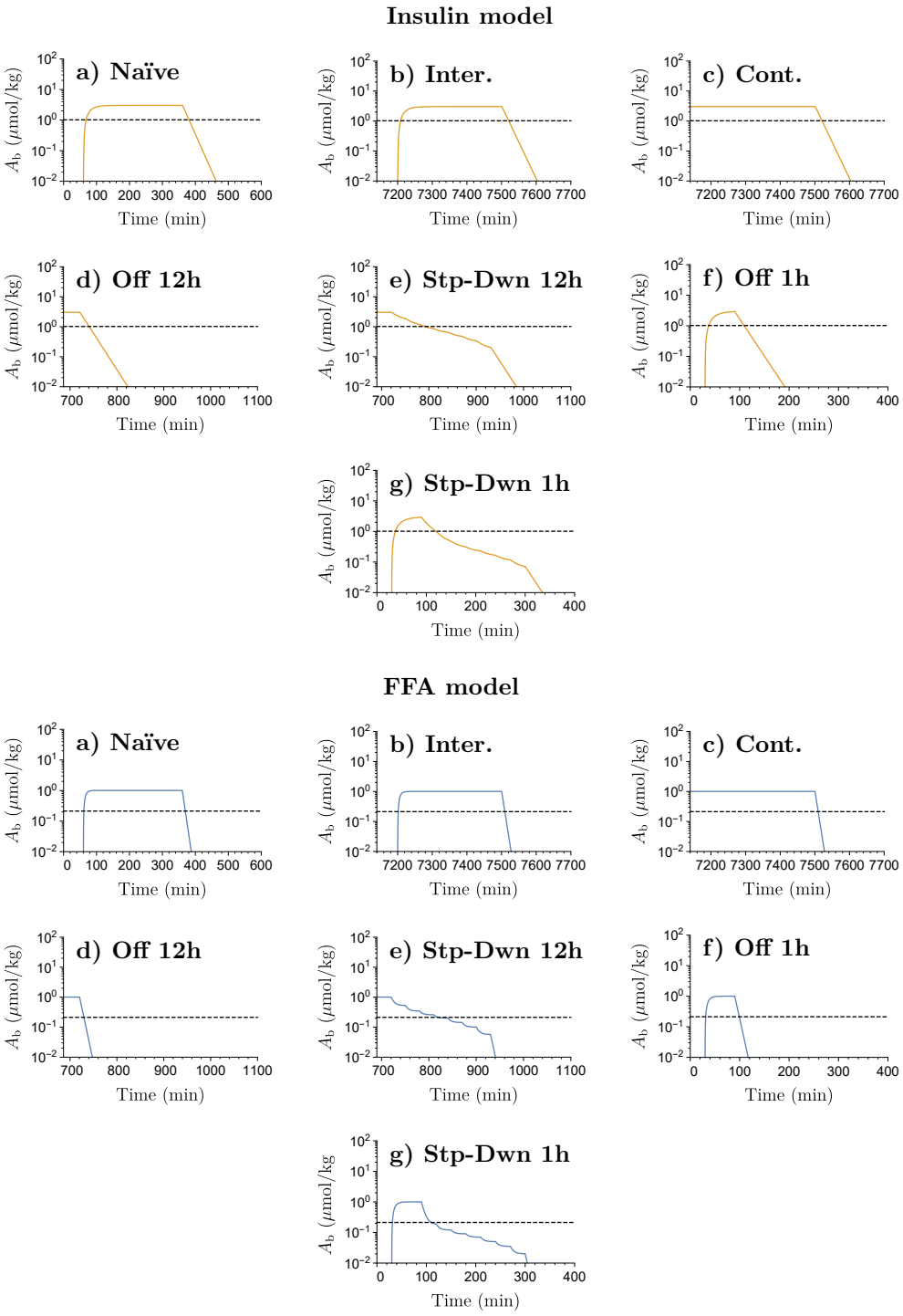

Figure 5.9: Fitted biophase amounts for the insulin and FFA DRT models for **lean Sprague-Dawley rats**. The upper seven illustrations show the fitted biophase amounts for the insulin model, the lower seven for the FFA model. The dashed lines represent the potency of NiAc to inhibit insulin (upper) and FFA (lower), respectively.

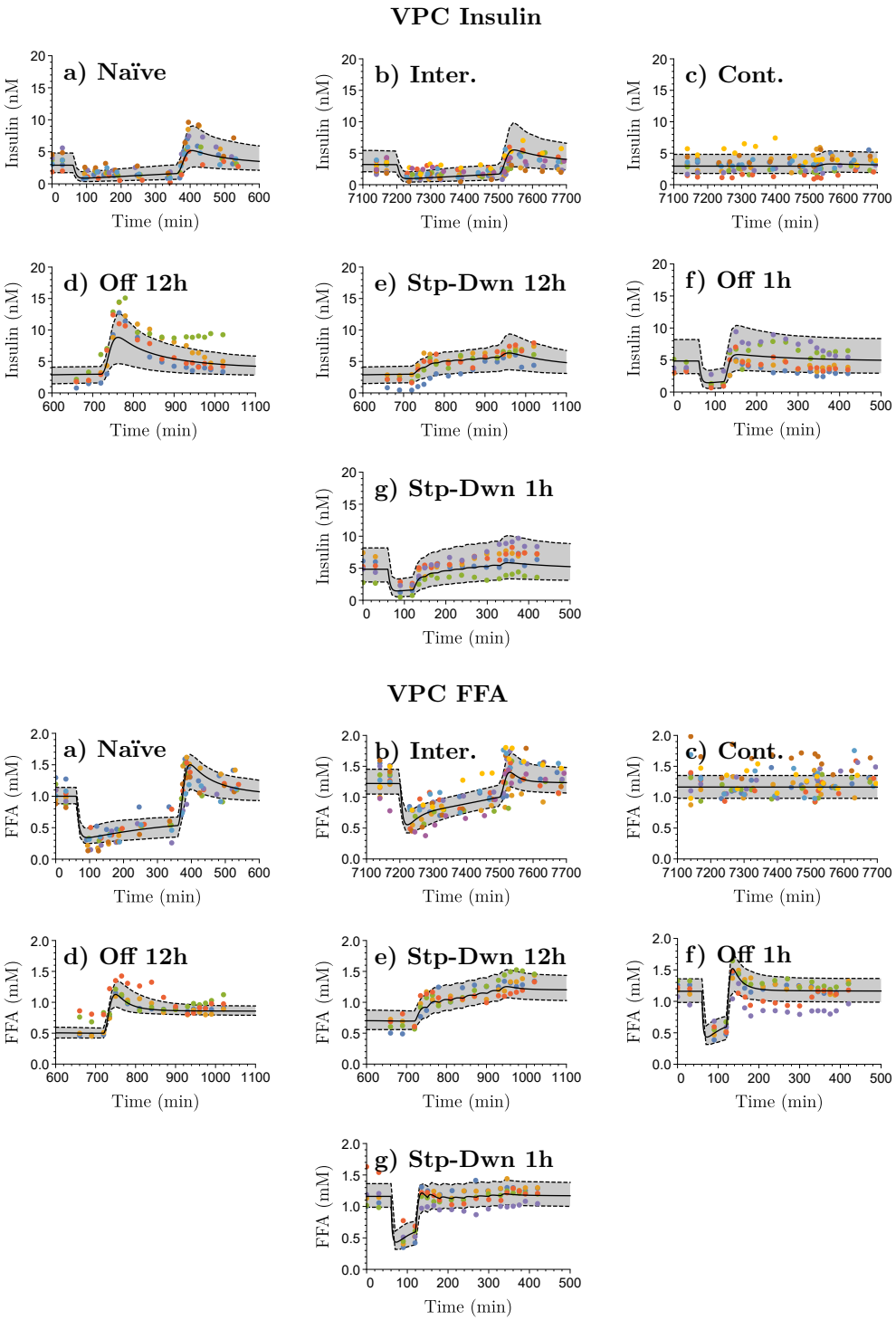

Figure 5.10: Visual predictive checks for **obese Zucker rats**. The upper seven illustrations show the insulin fits, the lower seven the FFA fits. The dots represent the data, with colours indicating separate individuals, the black lines the estimated median individual, and the grey area the 90% population prediction interval.

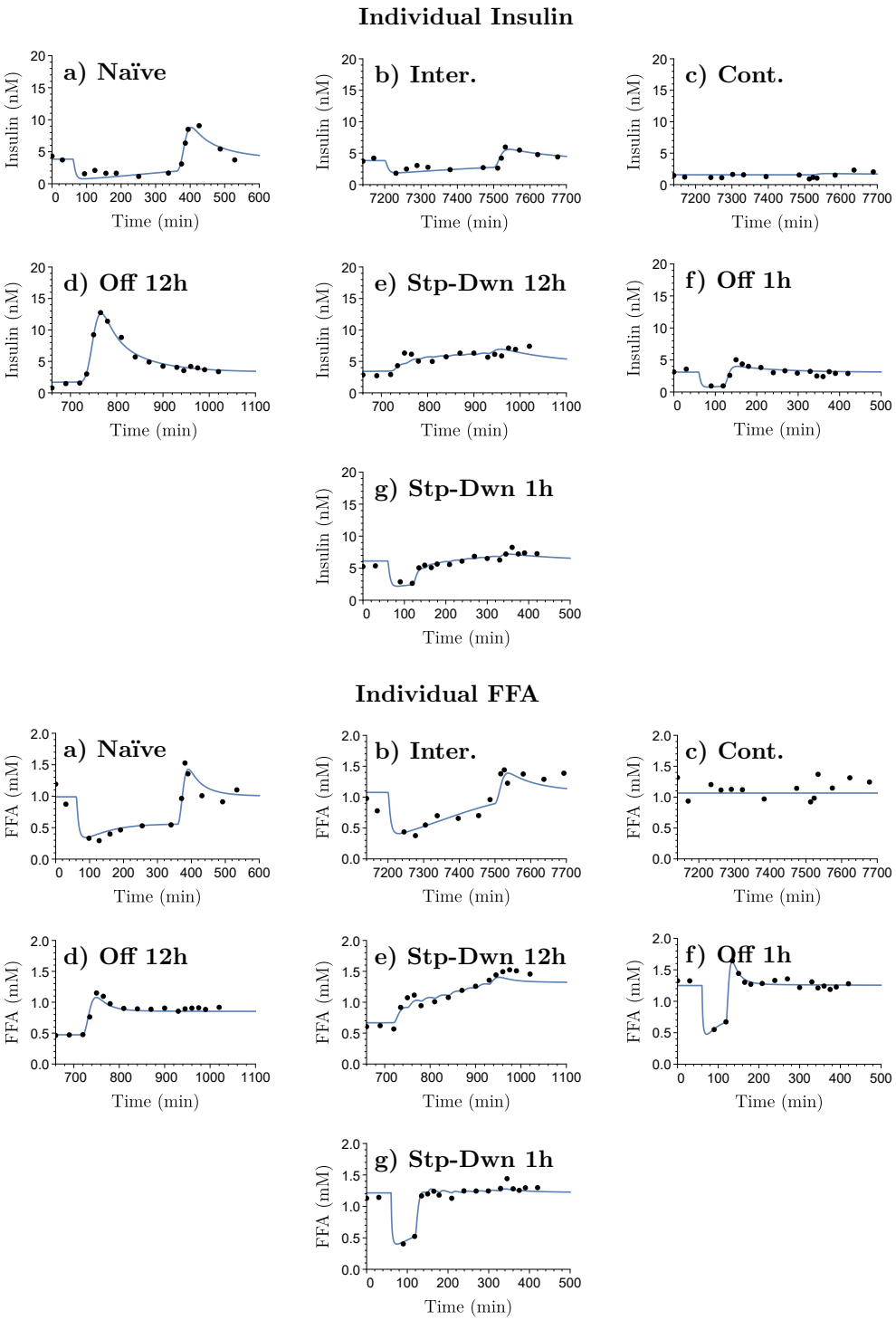

Figure 5.11: Individual fits for **obese Zucker rats**. The upper seven illustrations show the insulin fits, the lower seven the FFA fits. The dots represent the data and the black lines the estimated individual behaviour.

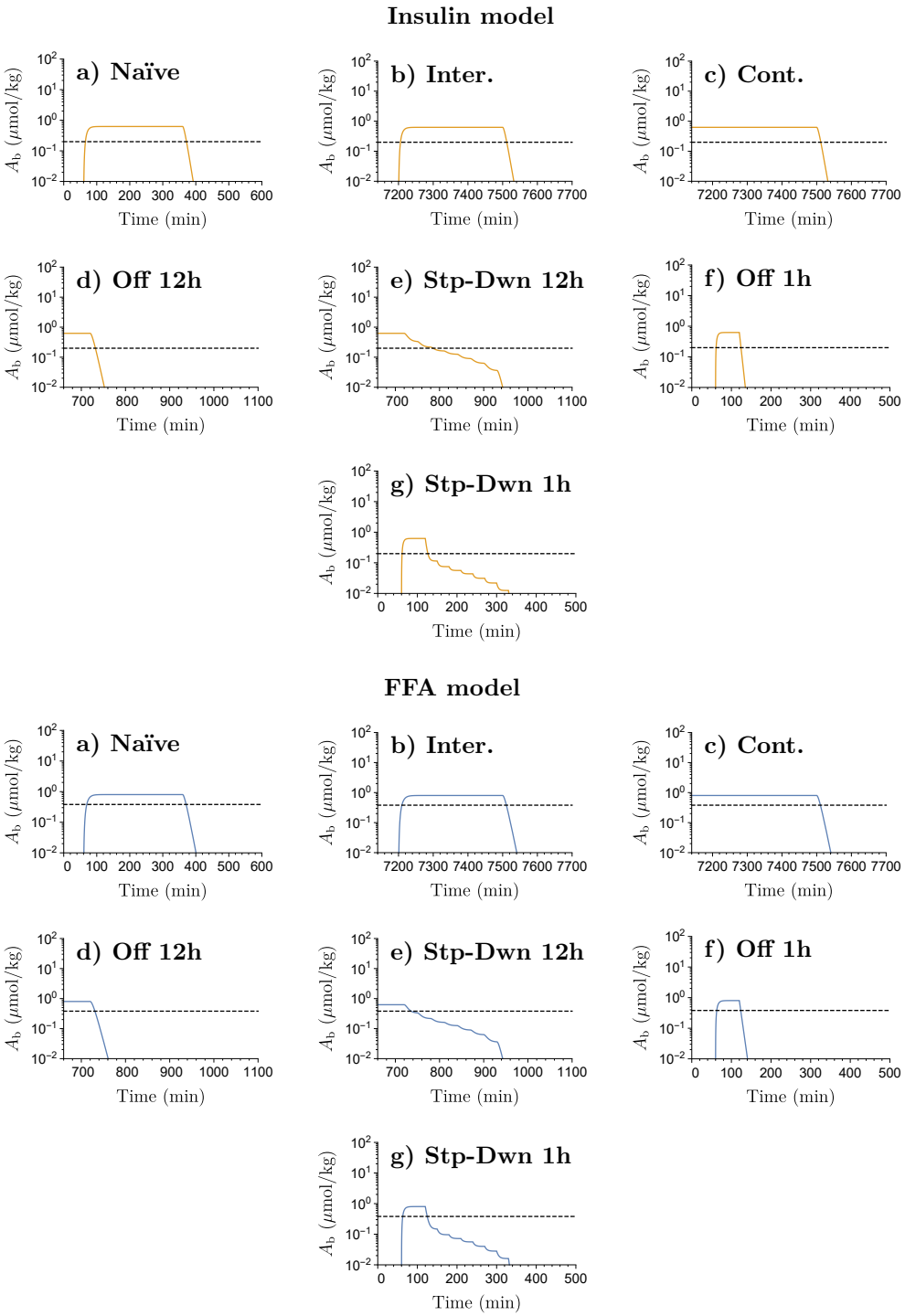

Figure 5.12: Fitted biophase amounts for the insulin and FFA DRT models for **obese Zucker rats**. The upper seven illustrations show the fitted biophase amounts for the insulin model, the lower seven for the FFA model. The dashed lines represent the potency of NiAc to inhibit insulin (upper) and FFA (lower), respectively.

The median baseline concentrations of insulin across groups were 0.206 nM and 3.74 nM for lean and obese rats, respectively. The estimates for the individual groups ranged between 0.152-0.346 nM for the lean rats and 2.91-4.85 nM for the obese rats. The median turnover half-lives of insulin, for the moderator, the integral controller, and the NiAc action level for lean and obese rats are given in Table 5.2. For **lean rats**, the efficacy of NiAc on insulin inhibition, I_{maxNI}, was estimated to be 0.805; consequently, NiAc cannot completely inhibit insulin release. The established NiAc biophase amount was approximately $1\,\mu\mathrm{mol\,kg^{-1}}$ for both the insulin and FFA DRT models, which is approximately three times the NiAc potency related to inhibition of insulin ($ID_{50\mathrm{NI}}$ =$1.02\,\mu\mathrm{mol\,kg^{-1}}$). This implies that the inhibitory function was saturated at steady-state. The estimated Hill coefficient n indicates a steep NiAc concentration-insulin response relationship at steady-state. Furthermore, for **obese rats**, the efficacy was fixed to 1 (motivated in the Parameter estimation section 5.5), and the corresponding potency was high with low $ID_{50\mathrm{NI}}$ in comparison to the NiAc steady-state biophase amount. However, since the estimated Hill coefficient was $0.817 < 1$, indicating a gentle NiAc biophase amount-insulin response relationship at steady state, the NiAc biophase amount never reached high enough levels to saturate the inhibitory function. The estimated $N_{50\mathrm{I}}$ of the NiAc action compartment was lower than the steady-state NiAc biophase amount ($0.607 < A_{\mathrm{bss}}(\approx 1)$) and the Hill coefficient for the dynamic efficacy γ was estimated to be 55.6 (suggesting an all or non-response). This implies that the efficacy was completely down-regulated at the end of the long-term experiments in obese rats, implying no NiAc inhibition on insulin release. However, the estimates for $N_{50\mathrm{I}}$ and γ were highly uncertain, with RSE% values of 170 and 180, respectively, suggesting practical non-identifiability.

	Half-lives (min)			
	Lean rats		Obese rats	
Turnover	Insulin	FFA	Insulin	FFA
Biomarker	1.81	0.0716	2.61	0.149
Moderator	7.24	21.8	262	73.0
Controller	10.1	4.85	1660	4620
NiAc action	-	8570	231	1160

Table 5.2: Turnover half-lives (expressed in min) in the insulin and FFA model for lean and obese rats of the biomarkers (insulin or FFA—corresponding rate constant k_{out}), the moderator (rate constant k_{tol}), the integral controller (rate constant k_{outR}), and the NiAc action (rate constant k_{N}).

5.6.3 FFA model

The FFA concentration was suppressed below its baseline value for all provocations of NiAc. The suppression of the FFA was more pronounced initially during NiAc infusions. FFA concentrations then drifted back towards their baselines (cf. Fig. 5.7h to Fig. 5.7j or Fig. 5.10h to Fig. 5.10j). After the infusions were terminated, the FFA concentrations rebounded before reaching their baselines. The step-down protocols resulted in less rebound.

The FFA concentrations returned to their baselines during extended exposure of NiAc in both the lean and the obese rats (Fig. 5.7j and Fig. 5.10j, respectively). However, as the long-term exposure was terminated, rebound was seen in the lean rats, but not in the obese rats (Fig. 5.7j and Fig. 5.10j).

The median FFA baseline concentrations across groups were 0.734 mM and 1.01 mM for the lean rats and the obese rats, respectively, with corresponding ranges between studies of 0.834-1.16 mM for the obese rats. The median turnover half-lives of the FFA, the moderator, the integral controller, and the NiAc action level are given in Table 5.2. The estimated turnovers for the moderator, the integral controller, and the NiAc action level were extremly uncertain for the FFA model for lean rats, suggesting practical non-identifiability.

Model simulations of the acute and chronic action of NiAc ($H_{\mathrm{NF}}(A_{\mathrm{b}}(t))$), the insulin-driven integral controller ($R_{\mathrm{F}}(t)$—also referred to as the insulin-controlled regulator), and the moderator feedback ($M_{0\mathrm{F}}/M_{\mathrm{F}}(t)$) on the FFA turnover are illustrated in Fig. 5.13 with the corresponding acute and chronic FFA responses. The turnover rate of FFA was initially inhibited about 80 % (lean) and 70 % (obese) by the NiAc infusion (Fig. 5.13a). Upon the extended exposure to NiAc (120 h) the inhibitory action for the turnover rate was decreased by approximately 13 % due to intrinsic tolerance mechanisms (Eq. D.5). In the obese rats the NiAc action totally vanished (Fig. 5.13a). The insulin-driven controller Eq. (5.26) provides a stimulatory action on the FFA turnover rate as insulin concentrations fall below the baseline (Fig. 5.13b). The positive (stimulatory) action increases from 100 % (at baseline) to approximately 200 % after extended (120 h) exposure to NiAc in the lean rats. The insulin action is totally abolished at equilibrium (120 h) in the obese rats (Fig. 5.13b). The positive impact of the moderator is seen acutely in both the lean rats and the obese rats, whereas the moderator action has receded in the obese rats at equilibrium (Fig. 5.13c). In the lean rats the combined inhibitory (NiAc) and stimulatory (insulin, moderator) action for the FFA turnover rate causes a rebound in FFA response upon cessation of the NiAc infusion (Fig. 5.13d). This is not seen in the obese rats since all of the NiAc, insulin, and moderator actions return to baseline levels at equilibrium (120 h). The potency of the NiAc action compartment was low ($N_{50\mathrm{F}} > N(t)$) for the lean rats and high ($N_{50\mathrm{F}} < N(t)$) for the obese rats at equilibrium (120 h). Consequently, the loss of efficacy was low, respectively high, in the lean rats and the obese rats at equilibrium. Furthermore, the estimated of Hill coefficient, $\phi = 10.9$, for the obese rats suggests an all or none-efficacy loss in the obese rats.

Parameter	Definition	Normal Sprague-Dawley rats		Obese Zucker rats	
		Estimate (RSE%)	BSV[a] (RSE%)	Estimate (RSE%)	BSV[a] (RSE%)
		Insulin model parameters			
k (min^{-1})	Biophase elimination rate	0.0562(8.4)	-	0.272(27)	-
k_{sc} (min^{-1})	Absorption rate to biophase	0.835(62)	-	0.154(12)	-
I_0 (nM)	Baseline insulin conc.	0.206(11)	27.8(22)	3.74(7.8)	10.1(8.2)
k_{outI} (min^{-1})	Fractional turnover rate insulin	0.382(16)	-	0.266(45)	-
I_{maxNI}	Efficacy - NiAc on insulin	0.805(11)	-	1[b]	-
$ID_{50\mathrm{NI}}$ ($\mu\mathrm{mol\,kg}^{-1}$)	Potency - NiAc on insulin	1.02(12)	111(67)	0.199(31)	53.8(48)
n	Hill coefficient - NiAc on insulin	4.05(6.9)	-	0.817(7.2)	-
k_{tolI} (min^{-1})	Turnover rate moderator	0.0149(30)	93.9(20)	0.00265(6.0)	33(31)
k_{outRI} ($\mathrm{nM}^{-1}\,\mathrm{min}^{-1}$)	Integral gain parameter	0.0684(16)	-	0.000417(54)	-
k_{NI} (min^{-1})	Turnover rate NiAc action comp.	-	-	0.00229(170)	-
$N_{50\mathrm{I}}$ ($\mu\mathrm{mol\,kg}^{-1}$)	Potency NiAc action compartment	-	-	0.607(27)	-
γ	Hill coefficient	-	-	55.6(180)	-
S_{NI}	Long-term NiAc effect loss	-	-	1[a]	-
σ_{addI}(nM)	Residual additive error	0.0680(3.4)	-	0.763(3.2)	-

[a]Between-subject variability expressed in CV%, calculated as $100 \times \sqrt{\omega^2}$.
[b]Fixed in the estimations.

		Free fatty acid model parameters			
k (min^{-1})	Biophase elimination rate	0.169(64)	-	0.212(8.3)	-
k_{sc} (min^{-1})	Absorption rate to biophase	3.27(19)	-	0.131(10)	-
F_0 (mM)	Baseline FFA conc.	0.734(5.9)	11.4(22)	1.01(5.5)	18.9(25)
k_{outF} (min^{-1})	Fractional turnover rate FFA	9.68(0.82)	-	4.64(150)	-
I_{maxNF}	Efficacy - NiAc on FFA	1^a	-	1^a	-
$ID_{50\mathrm{NF}}$ ($\mu\mathrm{mol\,kg}^{-1}$)	Potency - NiAc on FFA	0.213(110)	30.2(36)	0.381(10)	12.1(11)
m	Hill coefficient - NiAc on FFA	1.30(5.8)	-	1.07(6.5)	-
k_{tolF} (min^{-1})	Turnover rate moderator	0.0318(1000)	286(22)	0.00950(4.3)	88.4(61)
k_{outRF} ($\mathrm{nM}^{-1}\,\mathrm{min}^{-1}$)	Integral gain parameter	0.143(300)	-	0.000150(58)	-
k_{NF} (min^{-1})	Turnover rate NiAc action comp.	0.0000809(330)	-	0.000600(24)	-
$N_{50\mathrm{F}}$ ($\mu\mathrm{mol\,kg}^{-1}$)	Potency NiAc action compartment	4.95(7.8)	-	0.402(8.7)	-
ϕ	Hill coefficient	1^a	-	10.9(39)	-
S_{NF}	Long-term NiAc effect loss	1^a	-	1^a	-
σ_{addF}(mM)	Residual additive error	0.116(4.7)	-	0.131(3.0)	-

Table 5.3: Estimates of parameter median values and between-subject variabilities with corresponding relative standard errors (RSE%) for normal Sprague-Dawley rats and obese Zucker rats.

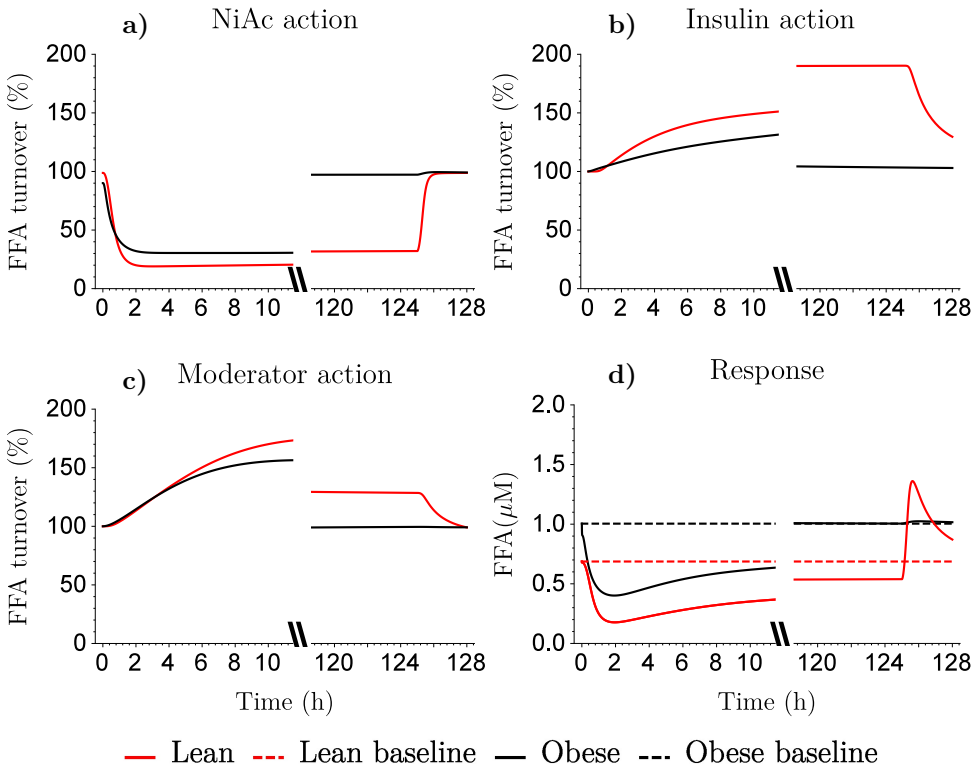

Figure 5.13: Model simulations of acute and chronic action of NiAc exposure H_{NF} (a), insulin-driven integral control (b), and moderator feedback (c) on the FFA turnover. Acute and chronic FFA response (d). Red lines show lean rats and black lines obese rats. The dashed lines show the baseline FFA response.

5.6.4 Shrinkage analysis

Shrinkage analysis was used to assess the distributions of the residuals and the EBEs. The standard deviations of the residual additive errors and the ε-shrinkages for the different DRT models are presented in Table 5.4.

	Lean Sprague-Dawley rats		Obese Zucker rats	
Data	Residual add. error σ	ε-shrinkage	Residual add. error σ	ε-shrinkage
Insulin	0.0677(14)	6.3%	0.763(3.2)	6.3%
FFA	0.116(4.7)	6.3%	0.131(3.0)	-0.14%

Table 5.4: Insulin and FFA model residual additive errors with corresponding relative standard errors (RSE%) and ε-shrinkage for lean Sprague-Dawley rats and obese Zucker rats, respectively.

The η-shrinkages of the EBEs are given in Table 5.5.

Parameter	Sprague-Dawley	Obese Zucker
I_0 (nM)	5.98	1.46
k_{tolI} (min^{-1})	-3.33	20.4
$ID_{50\text{NI}}$ (µM)	6.95	8.06
F_0 (mM)	-8.91	-8.53
k_{tolF} (min^{-1})	22.9	33.1
$ID_{50\text{NF}}$ (µM)	9.01	44.9

Table 5.5: Estimated η-shrinkage of the EBEs to the corresponding parameters I_0, k_{tolI}, $ID_{50\text{NI}}$, F_0, k_{tolF}, and $ID_{50\text{NF}}$.

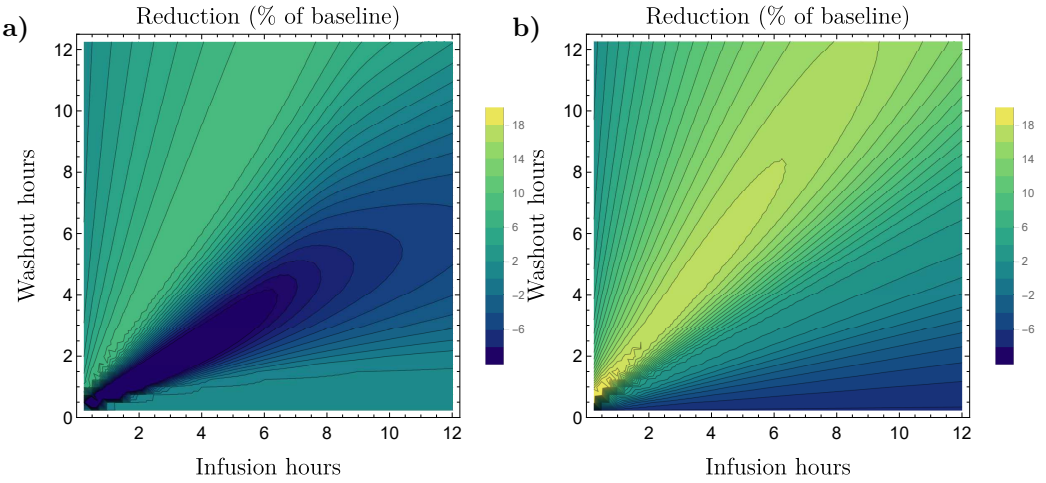

Figure 5.14: Model predicted reduction in FFA exposure in a median obese rat at steady-state (i.e., after multiple dosing), illustrated as the percentage reduction relative to the FFA baseline. (a) represents the predicted reduction in this DRT study, and (b) the predicted reduction in an exposure-driven analysis by Andersson et al. (2017). The predictions are made for a range of infusion protocols with 0.25-12 h of NiAc exposure followed by 0-12 h washout period. The x-axis represents the infusion time and the y-axis represents the washout time. The model predicts an optimal infusion regimen of ∼2 h longer washout period than the infusion.

5.6.5 Predicted FFA lowering

The resulting model was used to predict 24 h FFA lowering (AUC_{24}) for a range of protocols at steady-state (i.e., after multiple dosing). Here, the lowering over a period T is given by

$$\text{AUC}_{\text{T}} = F_0 \cdot T - \int_0^T F(\tau)\,\text{d}\tau. \tag{5.35}$$

The protocol design consisted of a 1-12 h NiAc exposure period followed by a 0.25-12 h washout period. The FFA lowering is illustrated as a reduction in percentage, relative baseline levels, for a median obese ratin Fig. 5.14. Here, Fig. 5.14a represents the predicted

reduction of the DRT model and Fig. 5.14b the predicted reduction of the exposure-driven model by Andersson et al. (2017). The DRT model predicted an optimal dosing strategy of ∼2 h longer washout period than the exposure period (Fig. 5.14a). The maximal reduction in percentage of the baseline was about 10%. The results were consistent when thes FFA reductions were predicted for outliers with high/low potencies ($ID_{50\mathrm{NF}}$), baseline responses (F_0), and/or moderator turnover rates (k_{tolF}). The exposure-drivne model predicted an optimal strategy of ∼1.25 h longer washout period than the exposure period (Fig. 5.14b). The maximal reduction in percentage of the baseline was about 18%.

5.6.6 Comparison to exposure-driven analysis

The estimates of the system parameters were compared to that of an exposure-driven analysis by Andersson et al. (2017) (the results of the study are presented in Appendix D). The comparison is given in Table 5.6.

	Lean Sprague Dawley rats		Obese Zucker rats	
Parameter	DRT study	Andersson et al. (2017)	DRT study	Andersson et al. (2017)
k_{outI} (min^{-1})	0.382(16)	0.110(14)	0.266(45)	0.180(17)
k_{tolI} (min^{-1})	0.0149(30)	0.0108(28)	0.00265(6.0)	0.00208(48)
k_{outRI} (min^{-1})	0.684(16)	1.08(17)	0.000417(54)	0.00102(27)
k_{NI} (min^{-1})	-	-	0.00229(170)	0.000403(35)
k_{outF} (min^{-1})	9.68(0.82)	7.13(140)	4.64(150)	2.88(120)
k_{tolF} (min^{-1})	0.0318(1000)	0.0202(67)	0.00950(4.3)	0.0118(24)
k_{outRF} (min^{-1})	0.143(300)	0.0161(29)	0.000150(58)	0.000275(38)
k_{NF} (min^{-1})	0.0000809(330)	0.000109(65)	0.000600(24)	0.000628(14)

Table 5.6: Pharmacodynamic parameter comparison between this dose-response-time analysis (DRT) and the exposure-driven pharmacodynamic analysis by Andersson et al. (2017) (results from this study are presented in Appendix D) for lean Sprague-Dawley and obese Zucker rats, respectively. The parameter estimates are given with corresponding relative standard errors (RSE%).

5.6.7 Goodness-of-fit plots

Goodness-of-fit plots were investigated to assess the distribution of the resiudals and any eventual systematic misspecifications. The plots showing these are given in Fig. 5.15 and 5.16 for lean and obese rats, respectively.

5.6.8 Sensitivity analysis

A local sensitivity analysis was performed to examine which of the model parameters affect the FFA response the most. The local analysis was conducted at the maximum likelihood estimate $\hat{\boldsymbol{\theta}}_{\mathrm{ML}}$ on systems perturbed by 300 min (acute) and 7200 min (chronic) constant rate infusions of NiAc with the infusion rate of 0.17 µmol min^{-1} kg^{-1}. The sensitivity of, for

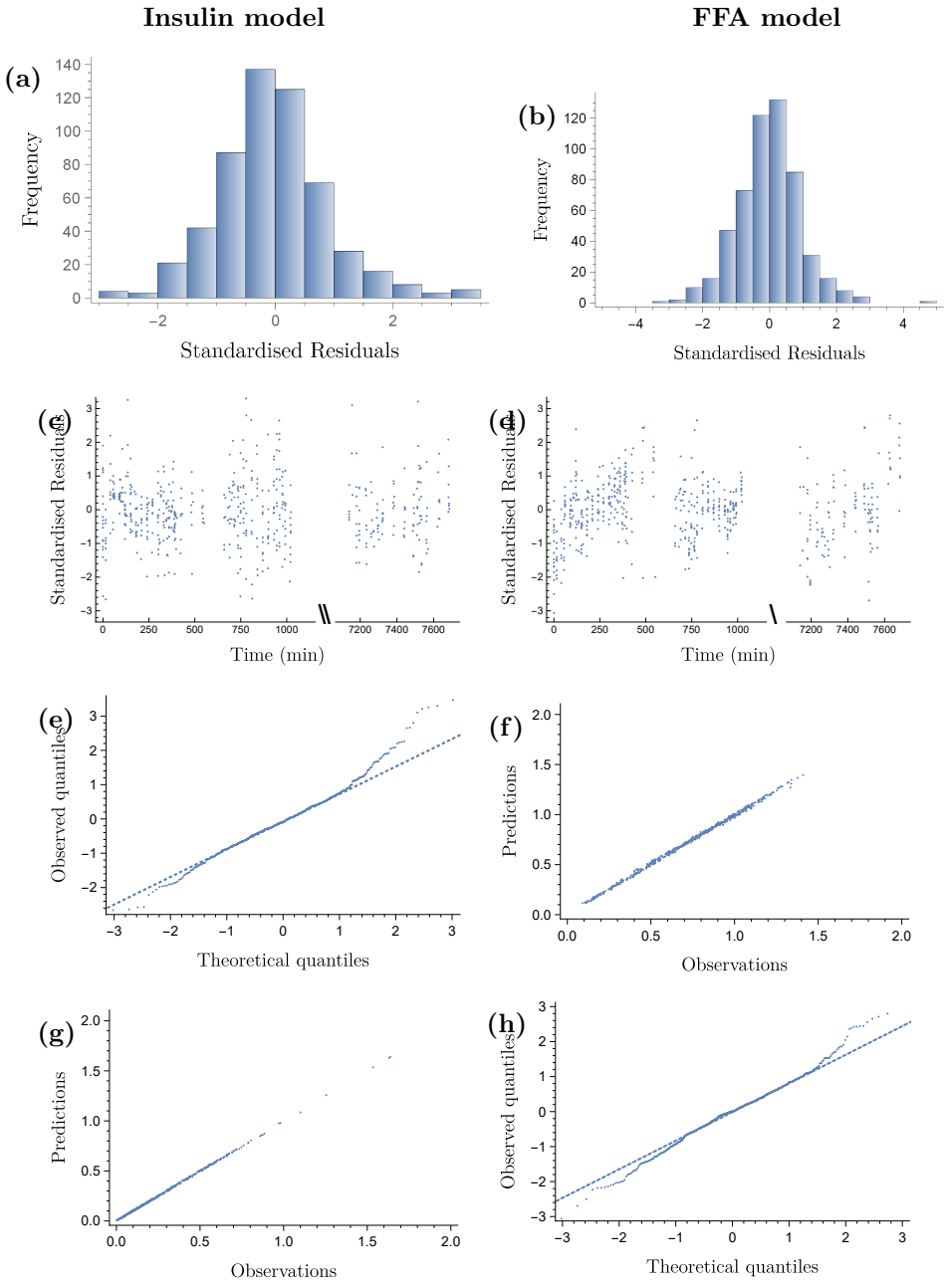

Figure 5.15: Goodness-of-fit plots for the insulin and FFA model for **lean Sprague-Dawley rats**. Histogram of the standardised residuals in (a) and (b), the standardised residuals over time in **??** and **??**, Q-Q plots of the observed residuals vs. the theoretical residuals in (e) and (f), scatter plots showing the relationships between the observed and predicted responses in (g) and (h). The left column represent the insulin model and the right the FFA model.

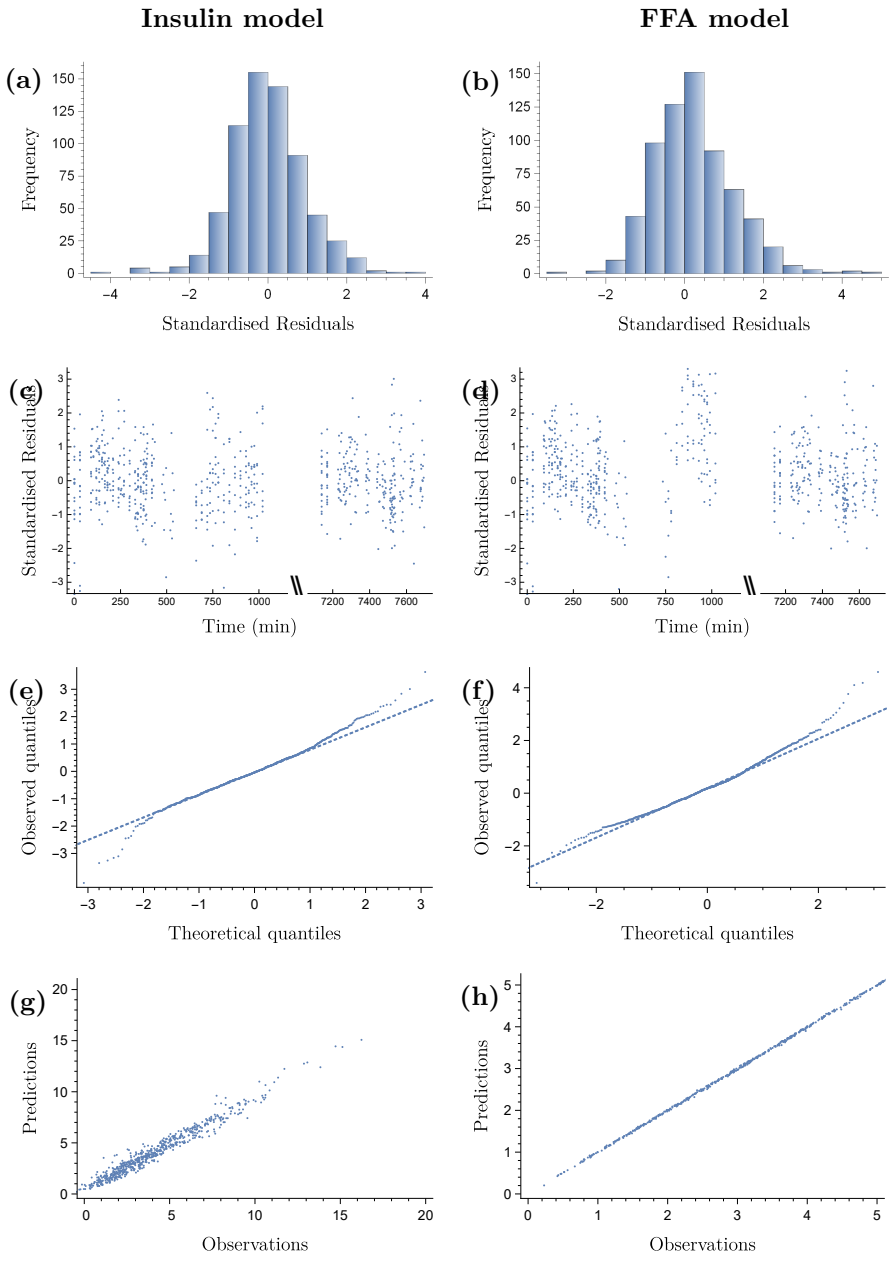

Figure 5.16: Goodness-of-fit plots for the insulin and FFA model for **obese Zucker rats**. Histogram of the standardised residuals in (a) and (b), the standardised residuals over time in (c) and (d), Q-Q plots of the observed residuals vs. the theoretical residuals in (e) and (f), scatter plots showing the relationships between the observed and predicted responses in (g) and (h). The left column represent the insulin model and the right the FFA model.

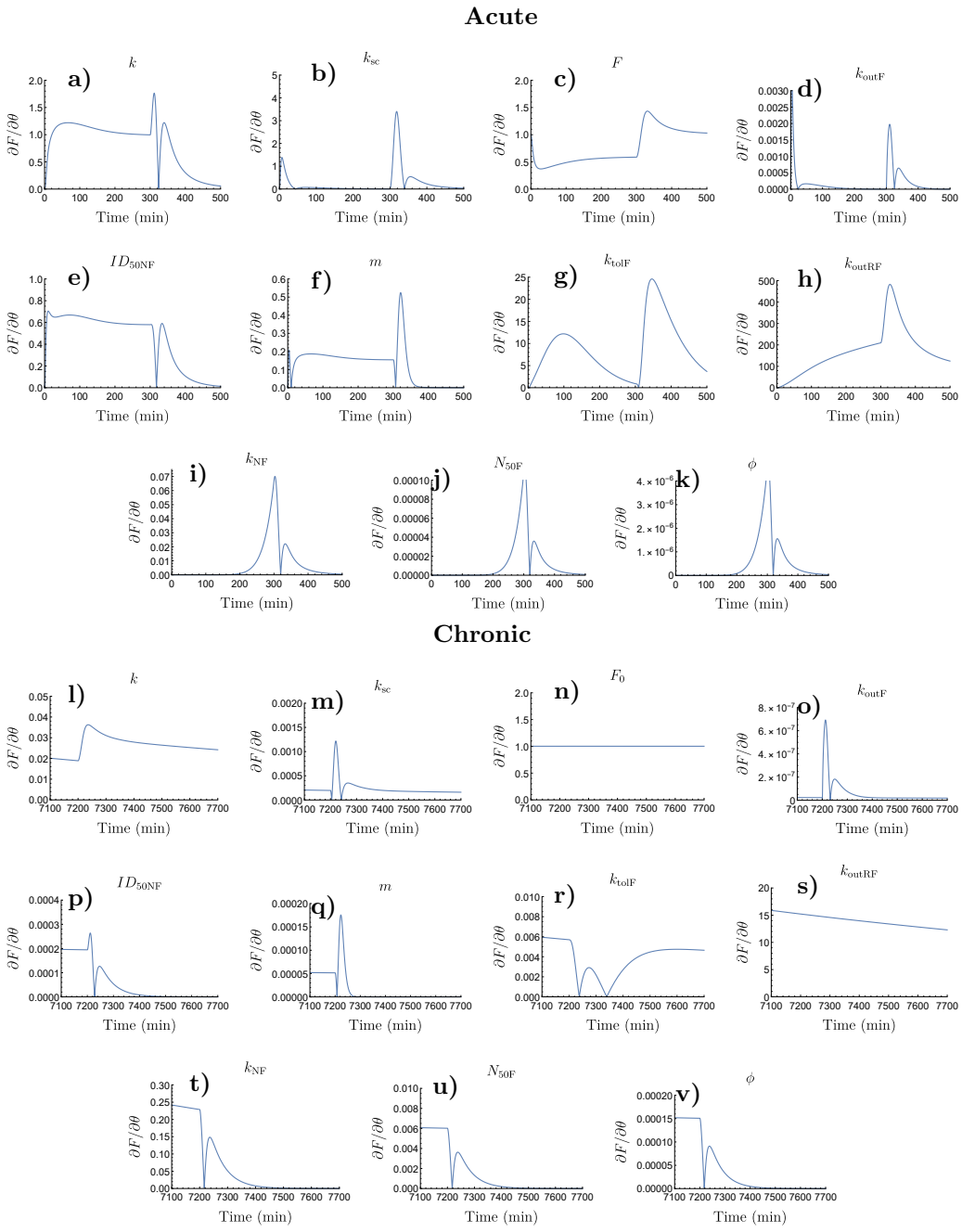

Figure 5.17: Local sensitivity analysis. The impact of each of the model parameters on the output is examined during 300 min (acute—upper plots) and 7200 min (chronic—lower plots) constant rate NiAc infusions at rates of 0.17 µmol min^{-1} kg^{-1}. The analysis was performed at the maximum likelihood estimate, obtained from the analysis of the obese rats.

example, the parameter F_0 is given by

$$\left.\frac{\partial F(t)}{\partial F_0}\right|_{\hat{\boldsymbol{\theta}}_{\mathrm{ML}}}. \tag{5.36}$$

The results of the analysis are seen in Fig. 5.17. The model output is more sensitive to changes in the parameters k, k_{sc}, F_0, k_{outF}, $ID_{50\mathrm{NF}}$, m, k_{tolF}, and k_{outRF} during acute treatments, while being more sensitive to changes in the parameters k_{NF}, $N_{50\mathrm{F}}$, and ϕ during the chronic treatments. In general, k_{tolF} and k_{outRF} have high sensitivity, while $N_{50\mathrm{F}}$ and ϕ have low sensitivity.

5.7 Discussion

In the present study, we applied a population modelling approach to a unique pre-clinical pharmacodynamic data set containing insulin and FFA-time courses obtained from acute and chronic provocations of NiAc in lean and obese rats. All information regarding the drug exposure was neglected to examine the utility of a dose-response-time (DRT) analysis. The aim was to identify a general model to be used in future predictions of optimal NiAc exposure profiles, to generate durable chronic dosing regimens.

5.7.1 Model evolution

Recent experimental data of long-term NiAc protocols have illustrated full systemic adaptation, with FFA concentration returning to its baseline value (Kroon et al., 2015). These findings challenge previous models (Ahlström et al., 2011b; Tapani et al., 2014) for long-term dosing predictions. Hence, new models are needed.
The PK/PD model applied in this study was derived based on previous models (Ahlström et al., 2011b; Andersson et al., 2015; Tapani et al., 2014). However, crucial mechanistic components were added to describe two different kinds of adaptation, one seen in lean rats and one in obese. In particular, insulin was included as an endogenous regulator of the turnover of FFA (Oh et al., 2011). To this end, a separate insulin model was developed to describe the insulin dynamics for all provocations of NiAc.

5.7.2 Model characteristics

A fundamental observation from the FFA-time course data is that both the lean and the obese rats acquire complete adaptation, with FFA levels returning towards baseline at equilibrium (Fig. 5.5). The post-infusion FFA rebound in lean rats implies a NiAc-sensitive system (Fig. 5.5b). However, the rebound was less pronounced than that for the 1-12 h experiments (cf. Fig. 5.5a). Consequently, the inhibiting effect of NiAc has been down-regulated during the long-term infusions. For obese rats, the rebound has completely vanished, which implies a NiAc-insensitive system (Fig. 5.5d). The observations above

suggest two separate feedback mechanisms that result in complete adaptation. An insulin-driven integral feedback control (Nocedal and Wright, 2006) was incorporated in the model to describe adaptation with drug effect (seen in lean rats). Control system techniques have previously been applied in glucose-insulin models in the form of PID (proportional-integral-derivative) controllers (Watson et al., 2011). The set-point of the insulin-driven integral controller is the insulin baseline and, hence, its action reflects the deviations from baseline insulin concentrations. The traditional $I_{\max}$-equation was modified with a dynamic efficacy function to capture the phenomenon of NiAc resistance. The insulin-driven integral controller represents the antilipolytic effect of insulin (Arner et al., 1981) about the insulin baseline; as the insulin level increases, the antilipolysis will be more pronounced and, consequently, the release of FFA will be lowered (and vice versa). Hence, the antilipolytic effects of insulin at baseline concentrations are included in the turnover rate of FFA, k_{in}, and the integral controller will provide any increase/decrease in antilipolysis in the form of an inhibitory/stimulatory effect. The dynamic efficacy could represent the down-regulation of the PDE3B gene expression (Heemskerk et al., 2014).
The impacts of the dynamic efficacy and the integral controller (Fig. 5.13) demonstrate that both adaptive actions push FFA concentrations back towards baseline (at equilibrium) despite ongoing NiAc exposure. The impact of the insulin-driven controller is lower for the obese rather than the lean rats in spite of 10-fold higher insulin concentrations in the obese rats (Fig. 5.13). This lack of impact of the insulin-driven controller reflects the insulin resistance of the obese rats (Heemskerk et al., 2014).

5.7.3 Model evaluation

Some estimated median responses for the insulin and FFA models were under- or over-predicted (cf. Fig. 5.7k or Fig. 5.7d). This is most likely due to the low number of individuals per trial (5-10), implying that every 4-9th population median will be estimated below or above the trends seen in the individual data (Grimmett and Stirzaker, 2002). Furthermore, some predicted 90 % population spans also under- or over-predicted the response for the insulin and FFA model (cf. Fig. 5.7k or Fig. 5.7d). This is most likely due to correlations of the between-subject parameter variabilities—which were not captured since diagonal covariance matrices were used in the FFA model (Bonate, 2011). When sampling from the resulting distributions to generate the VPCs, non-feasible parameter combinations may occur which render a skewed population (Bonate, 2011).

5.7.3.1 Lean rats

The VPCs in Fig. 5.7 and the individual fits in Fig. 5.8 demonstrate the flexibility of the insulin and FFA models in that response-time courses were captured in both acute and chronic settings. However, while the parameter estimates for the insulin model were precise in general, many of the estimates for the FFA model had extreme variability—indicating practical non-identifiability (Table 5.3). Consequently, the validity of the results of the FFA

model should be seriously questioned. As is Andersson et al. (2017) demonstrated that an exposure-driven FFA model could be identified for the same data set (see Table D.2 in Appendix D), the results of this study indicate that lack of exposure data have rendered parts of the PD model practically non-identifiable.

5.7.3.2 Obese rats

The VPCs in Fig. 5.10 and the individual fits in Fig. 5.11 demonstrate the flexibility of the insulin and FFA models in that response-time courses were captured in both acute and chronic settings. In contrast to the model for the lean rats, the parameters of the obese FFA model were generally practically identifiable (Table 5.3). However, the fractional turnover rate of FFA is functions on a significantly narrower time-scale than the feedback and adaptive mechanisms (Table 5.2). This resulted in a low precision of k_{outF} (RSE% of 150). To achieve higher precision a denser sampling of the FFA time-course is needed. Moreover, the parameter related to efficacy loss of NiAc on insulin, k_{NI}, $N_{50\mathrm{I}}$ and γ, had generally low precision (RSE% of 170, 27, 180, respectively). Precision in these estimates would probably increase if intermediate data, covering the time-span between the acute and chronic experiments, are added—thereby covering more of the time-course where efficacy is lost.

The insulin and FFA models have relatively low ε-shrinkages, indicating that the models were not overfitted (Table 5.5). Moreover, the standardised residuals appeared to be normally distributed, albeit with slightly heavier tails and slightly skewed distributions in comparison to the standard normal distribution for the insulin and FFA models, respectively (Fig.5.16a and Fig. 5.16b). Looking at the standardised residuals over time, there is no apparent bias in the insulin model (Fig. 5.16c). For the FFA model, the standardised residuals tend to have a slight positive trend between 750-1000 min (Fig. 5.16d). However, the bias is not overwhelmingly large.

The turnover processes in the insulin and FFA models operate over entirely different time scales (Table 5.2). In the FFA model, turnover of FFA is more than 100 times faster than for the moderator feedback and integral controller. Since the turnover of FFA acted on a very narrow time-scale, the precision of the estimate was low. Denser sampling of the FFA response-time course would have been decrease the uncertainty of k_{outF}. Furthermore, turnover of the NiAc action compartment had a half-life of more than 100 h for the lean rats, thus spanning the entire duration of the experiment. The corresponding half-life in the obese rats was 18 h.

The uncertainty in the estimate of the turnover of the integral gain parameter was high, even though the model output is sensitive to perturbations in k_{outRF} (Fig. 5.17). This suggests that the data are insufficient to identify the insulin-driven integral controller in the obese rats. A possible reason for this is that the obese rats experience severe insulin resistance.

The insulin and FFA models predicted similar biophase kinetics with elimination half-lives of 3.2 and 2.5 min^{-1} and absorption half-lives of 4.5 and 5.3 min^{-1} for the insulin and FFA

model, respectively.
Due to the nature of the FFA dynamics, with tolerance development and rebound post-infusions, constructing an optimal dosing protocol is complicated. By selecting an inappropriate dosing regimen, the NiAc provocation can yield an increased FFA exposure in comparison to controls (Fig. 5.14). There is an optimal strategy of having 2 h longer washout periods than infusion periods in rats; this is illustrated in Fig. 5.14 with the purple optimal lowering area. These strategies were consistent in that they were tested on both the median individual and on 90% quantiles (i.e., individuals that had the 5% and 95% quantiles of the parameters that varied in the population, $IC_{50\mathrm{NF}}$, F_0, and k_{tolF}). The predicted optimal designs were compared to those of the exposure-driven analysis by Andersson et al. (2017) (seen in Fig. 5.14b. The two model predictions are similar, but the DRT analysis predicts a somewhat narrower window of optimal designs as well as a slightly lower maxinal reduction. In general, there is high consistency between the parameter estimates derived from this DRT study and the exposure-driven PD study by Andersson et al. (2017) (see Table 5.6 and Appendix D for the results of the exposure-driven analysis), with differences mostly within one standard deviation.

We believe that the performance of the DRT models for the obese rats are better than those for the lean rats due to slightly more data (61 obese rats vs. 54 lean rats) being available in the obese case, and that the obese rats have developed more drug and insulin resistances during the experiments, thereby providing a wider range of response behaviours and richer data.

Chapter 6

Conclusions

This thesis has served as an introduction to dose-response-time (DRT) data analysis and as a demonstration of the utility of DRT modelling. The primary aim, stated in the Introduction, was to answer the following questions:

- When and how do we use DRT data analysis?
- What are the limitations of DRT data analysis?

This aim was obtained by conducting an extensive review of the published research, by providing a detailed tutorial on how to develop a DRT model, and by introducing two comprehensive DRT modelling case studies where the technique was applied. The following paragraphs will summarise the essence of this thesis and provide concluding remarks on the studies conducted. The first paragraph will examine the first of the main questions, while the last paragraph will summarise the limitations of the technique. In the intermediate paragraphs, the two case studies are discussed and conclusions are drawn from their respective results.

Dose-response-time (DRT) data analysis is a quantitative pharmacological modelling technique applied in pharmacodynamic studies where no exposure data are available. This includes situations when the drug exposure precedes the effect (for example pulmonary drug administration), when the drug is locally administered (for example ophthalmics), in clinical trials where invasiveness is undesired (for example in paediatrics or oncology), when measuring the exposure is complicated (for example small molecules or quick turnover), when

there are extreme differences between the initial and terminal disposition phases (such as with oligonucleotides), and so forth. In DRT modelling, we assume that the response data contain information about the drug kinetics, whereby a biophase model can be identified and act as the driver of the pharmacological response. The biophase function generally has a simple structure with few parameters. The choice of biophase depends on the route of administration, and its performance is assessed by evaluating the fit of the DRT model to response data. Given that the drug is administered directly into the biophase, the biophase function is typically described with a single-compartment model with first-order elimination. On the other hand, given indirect administration (such as oral administration when the biophase represent the plasma), the biophase is typically described with a single-compartment model with first-order absorption and first-order elimination.
This work has demonstrated that nonlinear biophase absorption or elimination can be identified, and utilised given that simpler first-order processes are insufficient in describing the biophase dynamics. Nonetheless, the lacking information about the drug kinetics heavily constrains the complexity of the biophase function, as involved biophase functions will suffer from structural or practical non-identifiability. Beyond the biophase dynamics, the pharmacodynamics of a DRT model are addressed in a similar fashion as in the standard pharmacokinetic-pharmacodynamic modelling framework; that is, by examine the characteristic behaviours observed in the response-time data. Examples include time-delays, saturations, nonlinear dose-response relations, feedback mechanisms, tolerance, and so forth.

The first DRT case study was a meta-analysis conducted on an extensive pre-clinical biomarker data set of the nicotinic acid-induced (NiAc) reduction of free fatty acids (FFA). The study was performed using the nonlinear mixed-effects modelling framework (NLME). The main objective was to demonstrate the utility of DRT data analysis on complex pharmacodynamic systems. To this end, FFA response-time course data were collected from experiments conducted on lean (normal) Sprague-Dawley and obese (diseased) Zucker rats. The experiments on the lean rats were comprehensive, covering various routes, rates, and modes of NiAc administration, while the experiments on the obese rats were limited in that only a single route and mode of NiAc administration was applied. In total, 95 lean rats were analysed and 19 obese rats. The FFA response-time data displayed indirect dose-response behaviour, rebound post infusion, and a gradual build-up of tolerance—all of which were captured by a turnover model with a moderator, and integral, feedback control. The corresponding biophase functions were developed sequentially; starting with data obtained from experiments with intravenous (IV) drug administration, the biophase elimination rate was assessed. Here, two candidate models were suggested; one single-compartment biophase with first-order elimination, and one single-compartment model with nonlinear Michaelis-Menten (MM) elimination. By applying the Akaike Information Criterion (AIC), the first-order elimination model was considered to be the best fit. Following the assessment of the biophase elimination, data obtained from experiments with oral drug administration were analysed to determine the biophase absorption rate. Again, two candidate models were suggested,

one with first-order absorption and one with MM absorption. The AIC suggested that the MM absorption model was the best fit. All model structures were proven to be structurally locally identifiable using the Exact Arithmetic Rank (EAR) approach, implemented in MATHEMATICA.

The DRT model was successfully fitted to all FFA-time courses in the lean rats, with high precision in the parameter estimates (all with relative standard errors (RSE) $\leq 25\%$), low ε-shrinkage (9.5% and 7.7% when fitting to the infusion and oral data, respectively, suggesting that the model was neither under- nor overfitted), and visual predictive checks that captured the median population behaviour, as well as the between-subject variations. Furthermore, the model was successfully fitted to all FFA-time courses in obese rats, yet with substantially lower precision in the estimates (when compared to those of the lean rats) with some of the parameters having RSE between 30-50%. Moreover, the adaptation rate had an RSE of 250%, indicating practical non-identifiability. These findings suggest the importance of having a rich pharmacological data set when conducting DRT modelling.

The results were compared to those of an exposure-driven analysis. In general, the precision of the parameter estimates of the DRT model was lower than that of the exposure-driven analysis. This is expected as less data generally imply lower precision. Finally, while the results of the study demonstrate the utility of DRT modelling in cases where exposure data are sparse or lacking, the technique is not meant to replace the traditional pharmacokinetic-pharmacodynamic framework when knowledge of the exposure is attainable.

The second study extended the DRT model applied in the previous analysis to develop a more general NiAc-FFA model, able to describe both acute and chronic response behaviours. The model aimed at quantitatively determine the impact of disease on the system, and to be applied in future predictions of optimal dosing design. To this end, a comprehensive meta-analysis on a pre-clinical biomarker data set of FFA and insulin response-time courses was conducted. The study was performed using the NLME framework. The data were obtained from experiments on lean (normal) Sprague-Dawley (a total of 54 individuals) and obese (diseased) Zucker rats (a total of 61 individuals) treated with intravenous or subcutaneous NiAc infusions during 5, 12, and 120 h, using different modes of administration (step-down protocols, intermittent drug flush-outs). The insulin and FFA data were analysed sequentially; starting with the development of an insulin turnover model, followed by the FFA turnover model. In this way, the insulin could be fixed, and act as an input signal into the FFA model. Both the insulin and FFA response-time data displayed indirect response behaviour, rebound post infusion, and two completely separate adaptive mechanisms present during chronic treatments; one observed in the lean rats and one in the obese rats. For the lean rats, the insulin and FFA level returned to their baselines during chronic treatments, with rebounds occurring when the infusions were terminated. The adaptations seen in the FFA is believed to be governed by insulin control. A similar mechanism was assumed for the insulin (i.e., a feedback insulin controller). The rebounds indicate that the lean rats were not resistant to the drug. For the obese rats, the insulin and FFA level returned to their baselines

during chronic treatment, but no rebounds occurred when the infusions were terminated. This is an indication of drug tolerance. These two different adaptive mechanisms of tolerance with, and without, resistance to NiAc were captured using an insulin-driven regulator and a dynamic efficacy. The insulin-driven regulator was designed to down-regulate the release of insulin and FFA if the insulin drops below its baseline levels, and increase the release of insulin and FFA if the insulin level reaches above its baseline. For the FFA dynamics, this model component serves to capture the physiological duality of insulin—where insulin has both an antilipolytic effect, which inhibits the release of FFA, and a slower re-esterification of FFA to triglycerides. The dynamic efficacy was governed by the amount in a hypothetical NiAc action compartment. During NiAc infusions, the amount in the action compartment increases until it reaches the steady-state biophase amount. As the amount of the action compartment increases, the effect of the drug gets down-regulated according to a nonlinear Hill relation. The insulin-driven regulator and the dynamic efficacy were incorporated into biophase-driven turnover models. The biophase was modelled either as a single-compartment model with zero-order input and first-order output (for IV administration—this model was adapted from DRT study I) or with a first-order input and first-order output (for subcutaneous administration). The full DRT models were proven to be locally structurally identifiable using the EAR approach, again implemented in MATHEMATICA. The VPCs generated from the insulin and FFA models followed the general trends seen in all populations. However, the parameter estimates of the insulin and FFA models for the lean rats displayed issues associated with practical non-identifiability as many of the parameters had extreme variability (for example, the integral gain parameter k_{outRF} and the turnover rate of the NiAc action compartment k_{NF} had RSE of $\sim 300\%$). Since the exposure-driven analysis generated a practically identifiable model, we conclude that the lack of exposure data have rendered parts of the DRT model practically non-identifiable. In contrast to the model for the lean rats, the parameters of the insulin and FFA models for the obese rats were generally practically identifiable. However, the part of the insulin model that describes the dynamic efficacy had low precision (RSE% of 170, 28, and 180 for the turnover of the NiAc action compartment k_{NI}, the potency of the NiAc action compartment $N_{50\text{F}}$, and the Hill coefficient γ). This is believed to be a consequence of the lack of data describing the dynamics between the 12 and 120 h treatments, where the tolerance for the drug is developed. Furthermore, the turnover of FFA acted on more narrow time-scale than the other turnover processes. As a consequence, the estimate for k_{outF} had low precision (150%). Denser sampling at certain stages of the experiments (for example, at the initial FFA drop) would increase the precision of the turnover rate. The ε-shrinkage for the insulin and FFA models for obese rats were relatively low, indicating that the models were not overfitted. Finally, there was generally high consistency between the parameter estimates of the DRT study and those of an exposure-driven analysis for the obese rats—indicating that the lack of exposure data did not radically alter the results.

DRT modelling poses structural and practical identifiability challenges. Since less data are available than in the standard pharmacokinetic-pharmacodynamic modelling framework,

the bias and variability of the model is expected to increase. This was shown when comparing the results of the two DRT meta analyses with those of exposure-driven analyses, and by the fact that one of the DRT submodels were practically non-identifiable (the FFA model for lean rats in DRT study II). Given these limitations of the technique, it is important to have rich pharmacodynamic data available, preferably with drug administered via different routes and using various rates and modes.

6.1 Future work

Dose-response-time (DRT) data analysis is a relatively unknown modelling technique (Table 1.1 comprises the majority of the published studies). We believe that the field has great potential in future pharmacological studies where drug exposure data are sparse or lacking. However, more extensive studies are needed to comprehend the full utility of the technique. The following discussion will encompass three aspects of possible extensions to this work; covering limitations in, and alternative approaches to, the studies conducted in this thesis, development of the DRT modelling methodology, and an exploration of the different areas where the framework could be applied.

Extensions of the presented studies

In neither of the presented case studies did we utilise the potential impact of the known covariates of the data sets; for example, the individual weights of the rats were known—a covariate that potentially could affect the individual pharmacology. It would be interesting to examine the relationships between the empirical Bayes estimates (EBEs) and the weight of the rats. Another possible alteration of the models would be to make obesity a covariate and estimate lean and obese rats simultaneously.

Moreover, plasma glucose concentration-time data were collected from the experiments in the second case study. Glucose is known to be a significant player in the analysed metabolic network—having a close connection to both insulin and FFA. However, these data were omitted in the current studies to reduce the complexity of the models. Furthermore, the primary aim of the PD modelling in the second study was to focus on how insulin affects FFA and not vice versa. To this end, the insulin was assumed to be unaffected by the FFA levels (for simplicity), while FFA was affected by insulin. A logical continuation of this project would be to integrate FFA dynamics in the insulin model, and thereby to approach a more mechanistic insulin model. However, this would require the insulin and FFA models to be fitted simultaneously, which is bound to be computationally heavy.

A potential model extension would be to include the effect of fasting and feeding on the FFA dynamics. A study by Kroon et al. (2016) suggests that NiAc administration timed with feeding profoundly improves the lipolytic effect of the drug.

The covariance matrices were assumed to be diagonal, to simplify the estimations (i.e., by reducing the number of parameters). From the estimated EBEs, one could investigate if

there are any potentially relevant correlations between the random effects. These could then be added to the covariance matrices in a subsequent estimation, where the initial guesses of the off-diagonal elements are estimated from the empirical distributions of the EBEs. By using non-diagonal covariance matrices, we could obtain a better understanding of the population variations, which may be of use when, for example, designing future experimental trials.
Finally, when optimising the NiAc protocol to predict the maximal AUC_{24} reduction (in DRT study II), a range of protocols was explored, rather than stating a proper optimisation problem with an objective function and certain constraints on the infusion protocol. A nonlinear programming approach could be applied in future studies.

Developing the DRT framework

In a study by Janzén et al. (2016), the parameter identifiability of fundamental pharmacodynamic models was investigated. A similar study for DRT models, incorporating both practical and structural identifiability on a variety of paired biophase functions and pharmacodynamic models, would be valuable. In such study, one could investigate how the practical identifiability of the DRT models changes about the extension of the pharmacodynamic data analysed. Furthermore, it would be of importance to examine if the design of experimental trials should change when conducting DRT modelling, rather than with traditional PK-PD modelling.

Examine DRT modelling in new areas

Over the recent years, a variety of clinical oncology studies has utilised the DRT modelling framework (Buil-Bruna et al., 2014; Frances et al., 2011; Parra-Guillen et al., 2013; Paule et al., 2012; Ramon-Lopez et al., 2009; Wilbaux and He, 2014). We envisage that the modelling framework will continue to play a fundamental role in future clinical oncology studies, as well as other clinical areas where it is desirable to avoid any unnecessary invasive procedure. One such area is paediatrics, where Tod (2008) has stressed the potential of the technique in a study from 2008.
Biologics have during the recent years rose up as one of the most significant advancements in modern medicine, due to their promise and potential (Zhao et al., 2012). Some biologics are administered during in small doses, with extended periods between each dose. Here, DRT modelling can play a paramount role in early development, such that a suitable dosing strategy can be decided without developing complex physiologically-based PK models (Lange and Schmidli, 2015).
To promote the technique and to provide these suggestive areas of future application to a wider audience, an extensive review of the field (which is currently lacking) would be of highly valuable. We aim to use this thesis as a blueprint of a future DRT modelling review article.

Bibliography

Aarons, L., Karlsson, M. O., Mentré, F., Rombout, F., Steimer, J.-L., van Peer, A., 2001. Role of modelling and simulation in Phase I drug development. Eur. J. Pharm. Sci. 13 (2), 115–122.

Abou Hammoud, H., Simon, N., Urien, S., Riou, B., Lechat, P., Aubrun, F., 2009. Intravenous morphine titration in immediate postoperative pain management: population kinetic-pharmacodynamic and logistic regression analysis. Pain. 144 (1-2), 139–46.

Agoram, B. M., Milligan, P. A., van der Graaf, P. H., 2008. A non-parametric method to analyse time-course of effect in the absence of pharmacokinetic data: Application to inhaled bronchodilators. Eur. J .Pharm. Sci. 34 (4-5), 250–256.

Ahlström, C., 2011. Modelling of tolerance and rebound in normal and diseased rats. Dissertation, University of Gothenburg.

Ahlström, C., Kroon, T., Peletier, L. A., Gabrielsson, J., 2013a. Feedback modeling of non-esterified fatty acids in obese Zucker rats after nicotinic acid infusions. J. Pharmacokinet. Pharmacodyn. 40 (6), 623–38.

Ahlström, C., Peletier, L. A., Gabrielsson, J., 2011a. Quantitative analysis of rate and extent of tolerance of biomarkers: application to nicotinic acid-induced changes in non-esterified fatty acids in rats. Eur. J. Pharm. Sci. 44 (3), 250–64.

Ahlström, C., Peletier, L. A., Gabrielsson, J., 2013b. Challenges of a mechanistic feedback model describing nicotinic acid-induced changes in non-esterified fatty acids in rats. J. Pharmacokinet. Pharmacodyn. 40 (4), 497–512.

Ahlström, C., Peletier, L. A., Jansson-Löfmark, R., Gabrielsson, J., 2011b. Feedback modeling of non-esterified fatty acids in rats after nicotinic acid infusions. J. Pharmacokinet. Pharmacodyn. 38 (1), 1–24.

Ahn, J. E., Jeon, S., Lee, J., Han, S., Yim, D.-S., 2014. Modeling of the Parathyroid Hormone Response after Calcium Intake in Healthy Subjects. Korean J. Physol Pharmacol 18 (3), 217.

Allerheiligen, S. R. B., 2014. Impact of modeling and simulation: myth or fact? Clin. Pharmacol. Ther. 96 (4), 413–5.

Almquist, J., Leander, J., Jirstrand, M., 2015. Using sensitivity equations for computing gradients of the FOCE and FOCEI approximations to the population likelihood. J. Pharmacokinet. Pharmacodyn. 42 (3), 191–209.

Altschul, R., Hoffer, A., 1960. The Effect of Nicotinic Acid on Hypercholesterolæmia. Can. Med. Assoc. J. 82 (15), 783–785.

Andersson, R., Jirstrand, M., Peletier, L., Chappell, M. J., Evans, N. D., Gabrielsson, J., 2015. Dose-response-time modelling: Second-generation turnover model with integral feedback control. Eur. J. Pharm. Sci. 81, 189–200.

Andersson, R., Kroon, T., Almquist, J., Jirstrand, M., Oakes, N. D., Evans, N. D., Chappel, M. J., Gabrielsson, J., 2017. Modeling of free fatty acid dynamics: insulin and nicotinic acid resistance under acute and chronic treatments. J. Pharmacokinet. Pharmacodyn. 44 (3), 203–222.

Andrews, L. C., 1997. Special Functions of Mathematics for Engineers. SPIE Publications, Washington.

Ang, J., Bagh, S., Ingalls, B. P., McMillen, D. R., 2010. Considerations for using integral feedback control to construct a perfectly adapting synthetic gene network. J. Theor. Biol. 266 (4), 723–38.

Anguelova, M., Karlsson, J., Jirstrand, M., 2012. Minimal output sets for identifiability. Math. Biosci. 239 (1), 139–53.

Arner, P., Bolinder, J., Engfeldt, P., Östman, J., 1981. The Antilipolytic Effect of Insulin in Human Adipose Tissue in Obesity, Diabetes Mellitus, Hyperinsulinemia, and Starvation. Metabolism 30 (8), 753–760.

Aronson, J. K., 2005. Biomarkers and surrogate endpoints. Br. J. Clin. Pharmacol. 59 (5), 491–4.

Audren, F., Tod, M., Massin, P., Benosman, R., Haouchine, B., Erginay, A., Caulin, C., Gaudric, A., Bergmann, J.-F., 2004. Pharmacokinetic–Pharmacodynamic Modeling of the Effect of Triamcinolone Acetonide on Central Macular Thickness in Patients with Diabetic Macular Edema. IOVS 45 (10), 3435–3441.

Barkai, N., Leibler, S., 1997. Robustness in simple biochemical networks. Nature 387, 913–917.

Barrett, J. S., Hirankarn, S., Holford, N., Hammer, G. B., Drover, D. R., Cohane, C. A., Anderson, B., Dombrowski, E., Reece, T., Zajicek, A., Schulman, S. R., 2015. A hemodynamic model to guide blood pressure control during deliberate hypotension with sodium nitroprusside in children. Front. Pharmacol. 6 (July), 1–10.

Bates, D. G., Cosetino, C., 2011. Feedback Control in System Biology. CRC Press (Taylor & Francis).

Bellman, R., Åström, K. J., 1970. On Structural Identifiability. Math. Biosci. 7, 329–339.

Bellu, G., Saccomani, M. P., Audoly, S., D'Angiò, L., 2007. DAISY: A new software tool to test global identifiability of biological and physiological systems. Comput. Meth. Prog. Bio. 88 (1), 52–61.

Benet, L. Z., Zia-Amirhosseini, P., 1995. Basic Principles of Pharmacokinetics. Toxicol. Pathol. 23 (2), 115–123.

Bergstrand, M., Hooker, A. C., Wallin, J. E., Karlsson, M. O., 2011. Prediction-Corrected Visual Predictive Checks for Diagnosing Nonlinear Mixed-Effects Models. AAPS J. 13 (2), 143–151.

Bogdańska, M. U., Bodnar, M., Belmonte-Beitia, J., Murek, M., Schucht, P., Beck, J., Pérez-García, V. M., 2017. A mathematical model of low grade gliomas treated with temozolomide and its therapeutical implications. Math. Biosci. 288, 1–13.

Bonate, P. L., 2011. Pharmacokinetic-Pharmacodynamic Modeling and Simulation. Springer, New York.

Bragg, P., Fisher, D. M., Shi, J., Donati, F., Meistelman, C., Lau, M., Sheiner, L. B., 1994. Comparison of twitch depression of the adductor pollicis and the respiratory muscles. Pharmacodynamic modeling without plasma concentrations. Anesthesiology 80 (2), 310–319.

Breimer, D. D., Danhof, M., 1997. Relevance of the Application of Pharmacokinetic-Pharmacodynamic Modelling Concepts in Drug Development. The 'Wooden Shoe' Paradigm. Clin. Pharmacokinet. 32 (4), 259–267.

Buil-Bruna, N., Moreno-Jiménez, M., Martín-Algarra, S., Ribba, B., Trocóniz, I. F., 2014. A Population Pharmacodynamic Model for Lactate Dehydrogenase and Neuron Specific Enolase to Predict Tumor Progression in Small Cell Lung Cancer Patients. AAPS Pharmsci. 16 (3), 609–619.

Burman, C. F., Wiklund, S. J., 2011. Modelling and simulation in the pharmaceutical industry-some reflections. Pharm. Stat. 10 (6), 508–516.

Callies, S., André, V., Patel, B., Waters, D., Francis, P., Burgess, M., Lahn, M., 2011. Integrated analysis of preclinical data to support the design of the first in man study of

LY2181308, a second generation antisense oligonucleotide. Br. J. Clin. Pharmacol. 71 (3), 416–28.

Carlson, L. A., 2005. Nicotinic acid: the broad-spectrum lipid drug. A 50th anniversary review. J. Intern. Med. 258 (2), 94–114.

Carlson, L. A., Orö, L., 1962. The Effect of Nicotinic Acid on the Plasma Free Fatty Acids. Acta. Med. Scand. 172, 641–645.

Cavanaugh, J. E., Neath, A., 2011. Akaike's Information Criterion: Background, Derivation, Properties, and Refinements. In: International Encyclopedia of Statistical Sciences. Springer, pp. 26–29.

Chen, L., Yan, W., Li, S. Y. T., Cheng, Q., Boucher, B. J., 2015. Molecular and Cellular Endocrinology Niacin-induced hyperglycemia is partially mediated via niacin receptor GPR109a in pancreatic islets. Mol. Cell. Endocrinol. 404, 56–66.

Clemson, B., Tang, Y., Pyne, J., Unal, R., 1995. Efficient methods for sensitivity analysis. Syst. Dynam. Rev. 11 (1), 31–49.

Cosentino, C., Bates, D., 2011. Feedback Control in Systems Biology. Taylor & Francis Group, Boca Raton.

Davidian, Marie, G. D., 2003. Nonlinear models for repeated measurement data: An overview and update. J. Agric. Biol. Environ. Stat. 8 (4), 387–419.

Davison, A., Hinkley, D., 1997. Bootstrap Methods and their Application. Cambridge University Press, New York.

Dayneka, N. L., Garg, V., Jusko, W. J., 1993. Comparison of four basic models of indirect pharmacodynamic responses. J. Pharmacokinet. Biopharm. 21 (4), 457–78.

Delyon, B., Lavielle, M., Moulines, E., 1999. Convergence of a stochastic approximation version of the EM algorithm. Ann. Stat. 27 (1), 94–128.

Dempster, A., Laird, N., Rubin, D. B., 1977. Maximum likelihood from incomplete data via the EM algorithm. J. R. Stat. Soc. Series B. Stat. Methodol. 39 (1), 1–38.

Eckel, R. H., Grundy, S. M., Zimmet, P. Z., 2005. The metabolic syndrome. Lancet 365 (9468), 1415–1428.

El-Samad, H., Goff, J. P., Khammash, M., 2002. Calcium homeostasis and parturient hypocalcemia: an integral feedback perspective. J .Theor. Biol. 214 (1), 17–29.

Evans, N., Moyse, H., Lowe, D., Briggs, D., Higgins, R., Mitchell, D., Zehnder, D., Chappell, M., 2013. Structural identifiability of surface binding reactions involving heterogeneous analyte: Application to surface plasmon resonance experiments. Automatica 49 (1), 48–57.

Fabbrini, E., Mohammed, B. S., Korenblat, K. M., Magkos, F., McCrea, J., Patterson, B. W., Klein, S., 2010. Effect of fenofibrate and niacin on intrahepatic triglyceride content, very low-density lipoprotein kinetics, and insulin action in obese subjects with nonalcoholic fatty liver disease. J. Clin. Endocrinol. Metab. 95 (6), 2727–35.

Fisher, D. M., Szenohradszky, J., Wright, P. M. C., 1997. Pharmacodynamic modeling of vecuronium-induced twitch depression. Rapid plasma-effect site equilibration explains faster onset at resistant laryngeal muscles than at the adductor pollicis. Anesthesiology 86 (3), 558–566.

Fisher, D. M., Wright, P. M. C., 1997. Are plasma concentration values necessary for pharmacodynamic modeling of muscle relaxants? Anesthesiology 86 (3), 567–575.

Folland, G. B., 1999. Real Analysis, 2nd Edition. John Wiley & Sons, Inc., New York.

Forsman, K., 1991. Constructive commutative algebra in nonlinear control theory. Ph.D. thesis, Linköping University.

Frances, N., Claret, L., Bruno, R., Iliadis, A., 2011. Tumor growth modeling from clinical trials reveals synergistic anticancer effect of the capecitabine and docetaxel combination in metastatic breast cancer. Cancer Chemoth. Pharmacol. 68, 1413–1419.

Frayn, K., Shadid, S., Hamlani, R., Humphreys, S., Clark, M., Fielding, B., Boland, O., Coppsack, S., 1994. Regulation of fatty acid movement in human adipose tissue in the postabsorptive-to-postprandial transition. Am. J. Physiol. Endocrinol. Metab. 266, 308–317.

Freedman, D., Pisani, R., Purves, R., 2007. Statistics, 4th Edition. WW Norton Co.

Gabrielsson, J., Jusko, W., Alari, L., 2000. Modeling of dose–response–time data: four examples of estimating the turnover parameters and generating kinetic functions from response profiles. Biopharm. Drug Dispos. 21 (2), 41–52.

Gabrielsson, J., Peletier, L. A., 2007. A nonlinear feedback model capturing different patterns of tolerance and rebound. Eur. J. Pharm. Sci. 32 (2), 85–104.

Gabrielsson, J., Peletier, L. A., 2014. Dose-response-time data analysis involving nonlinear dynamics, feedback and delay. Eur. J. Pharm. Sci. 59, 36–48.

Gabrielsson, J., Weiner, D., 2010. Pharmacokinetic & Pharmacodynamic Data Analysis: Concepts and Applications, 4th Edition. Swedish Pharmaceutical Press, Stockholm.

Gennemark, P., Nordlander, B., Hohmann, S., Wedelin, D., 2006. A simple mathematical model of adaptation to high osmolarity in yeast. In Silico Biol. 6 (3), 193–214.

Gesztelyi, R., Zsuga, J., Kemeny-Beke, A., Varga, B., Juhasz, B., Tosaki, A., 2012. The Hill equation and the origin of quantitative pharmacology. Arch. Hist. Exact Sci. 66, 427–438.

Gibaldi, M., Levy, G., 1972. Dose-Dependent Decline of Pharmacological Effects of Drugs with Linear Pharmacokinetic Characteristics. J. Pharm. Sci. (4), 567–569.

Gibaldi, M., Perrier, D., 1982. Pharmacokinetics, 2nd Edition. Marcel Dekker Inc, New York.

Gieschke, R., Pillai, G., Goggin, T., Jacqmin, P., Snoeck, E., Girard, P., Steimer, J.-L., 2001. Population PD and Clinical Trial Simulation: Investigating Oral Dosing Regimens for a new Bisphosphonate Drug for Treatment of Osteoporosis. In: 10th Population Approach Group Conference, Basel, Switzerland.

Glad, T., Ljung, L., 2000. Control Theory: Multivariable and Nonlinear Methods. Taylor & Francis Ltd, London.

Godfrey, K., 1983. Compartmental Models and Their Application. Academic Press, Orlando, Florida.

Goggin, T., Jacqmin, P., Gieschke, R., Pillai, G., Snoeck, E., Girard, P., Steimer, J.-L., 2001. Population PD(-PK) modeling and clinical trial simulation, characterizing schedule dependence of hematotoxicity and other Phase II trial design features for a new oral anticancer drug. In: 10th Population Approach Group Conference, Basel, Switzerland.

Greenland, S., 1996. Basic Methods for Sensitivity Analysis of Biases. Int. J. Epedemiol. 25 (6), 1107–1116.

Grimmett, G., Stirzaker, D., 2002. Probability and Random Process, 3rd Edition. Oxford University Press.

Gruwez, B., Dauphin, A., Tod, M., 2005. A Mathematical Model for Paroxetine Antidepressant Effect Time Course and Its Interaction with Pindolol. J. Pharmacokinet. Pharmacodyn. 32 (December), 663–683.

Gruwez, B., Poirier, M.-F., Dauphin, A., Olié, J.-P., Tod, M., 2007. A kinetic-pharmacodynamic model for clinical trial simulation of antidepressant action: application to clomipramine-lithium interaction. Contemp. Clin. Trials. 28 (3), 276–87.

Hamberg, A.-k., Wadelius, M., Friberg, L. E., Biss, T. T., Kamali, F., Jonsson, E. N., 2013. Characterizing variability in warfarin dose requirements in children using modelling and simulation. Br. J. Clin. Pharmacol. 78 (1), 158–169.

Hamberg, A.-K., Wadelius, M., Lindh, J. D., Dahl, M. L., Padrini, R., Deloukas, P., Rane, A., Jonsson, E. N., 2010. A pharmacometric model describing the relationship between warfarin dose and INR response with respect to variations in CYP2C9, VKORC1, and age. Clin. Pharmacol. Ther. 87 (6), 727–34.

He, F., Fromion, V., Westerhoff, H. V., 2013. (Im) Perfect robustness and adaptation of metabolic networks subject to metabolic and gene-expression regulation: marrying control engineering with metabolic control. BMC Syst. Biol. 7 (131).

Heath, M. T., 2002. Scientific Computing: an introductory survey. McGraw-Hill, Boston.

Heemskerk, H., de Winter, C., van Kuik, P., Heuvelmans, N., Sabatelli, P., Rimessi, P., Braghetta, P., van Ommen, G.-J. B., de Kimpe, S., Ferlini, A., Aartsma-Rus, A., van Deutekom, J. C. T., 2010. Preclinical PK and PD studies on 2'-O-methyl-phosphorothioate RNA antisense oligonucleotides in the mdx mouse model. Mol. Ther. 18 (6), 1210–7.

Heemskerk, M. M., van den Berg, S. A. A., Pronk, A. C. M., van Klinken, J.-B., Boon, M. R., Havekes, L. M., Rensen, P. C. N., van Dijk, K. W., van Harmelen, V., 2014. Long-term niacin treatment induces insulin resistance and adrenergic responsiveness in adipocytes by adaptive downregulation of phosphodiesterase 3B. Am. J. Physiol. Endocrinol. Metab. 306 (7), E808–13.

Holford, N. H. G., Sheiner, L. B., 1982. Kinetics of pharmacologic response. Pharmacol. Ther. 16 (2), 143–166.

Isaksson, C., Gabrielsson, J., Wallenius, K., Peletier, L. A., Toreson, H., 2009. Turnover modeling of non-esterified fatty acids in rats after multiple intravenous infusions of nicotinic acid. Dose-Response 7 (3), 247–69.

Iwaki, M., Ogiso, T., Hayashi, H., Tanino, T., Benet, L. Z., 1996. Acute Dose-Dependent Disposition Studies of Nicotinic Acid in Rats. Drug Metab. Dispos. 24 (7), 773–779.

Jacobs, T., Straetemans, R., Molenberghs, G., Bouwknecht, J. A., Bijnens, L., 2010. A Latent Pharmacokinetic Time Profile to Model Dose-response Survival Data. J. Biopharm. Stat. 20 (4), 759–767.

Jacqmin, P., Gieschke, R., Jordan, P., Steimer, J.-L., Goggin, T., Pillai, G., 2001. Modelling Drug Induced Changes in Biomarkers Without Using Drug Concentrations: Introducing the K-PD model. In: 10th Population Approach Group Conference, Basel, Switzerland.

Jacqmin, P., Snoeck, E., van Schaick, E. A., Gieschke, R., Pillai, P., Steimer, J.-L., Girard, P., 2007. Modelling response time profiles in the absence of drug concentrations: definition and performance evaluation of the K-PD model. J. Pharmacokinet. Pharmacodyn. 34 (1), 57–85.

Janzén, D. L. I., 2016. Structural Identifiability in Mixed-Effects Models: Methods & Insights. In: UK Quantitative Systems Pharmacology Network. Surrey.

Janzén, D. L. I., Bergenholm, L., Jirstrand, M., Parkinson, J., Yates, J., Evans, N. D., Chappell, M. J., 2016. Parameter Identifiability of Fundamental Pharmacodynamic Models. Front. Physiol. 7 (December), 1–12.

Karlsson, J., Anguelova, M., Jirstrand, M., 2012. An Efficient Method for Structural Identifiability Analysis of Large Dynamic Systems. 16th IFAC Symposium on System Identification (SYSID 2012) 16 (1), 941–946.

Kendall, D. M., Fitz-patrick, D., Ganda, O. P., Rosenson, R. S., Buse, J. B., 2002. Efficacy, Safety, and Tolerability of Once-Daily Niacin for the Treatment of Dyslipidemia Associated With Type 2 Diabetes. Arch. Intern. Med. 162 (14), 1568–1576.

Kim, S., Gaweda, A. E., Wu, D., Li, L., Rai, S. N., Michael, E., 2015. Simplified Warfarin Dose-response Pharmacodynamic Models. Biomed. Eng. 27 (1), 1–15.

Klebaner, F. C., 2005. Introduction to Stochastic Calculus with Applications, 2nd Edition. Imperial College Press, London.

Krauss, R. M., 2004. Lipids and Lipoproteins in Patients With Type 2 Diabetes. Diabetes Care 27 (6), 1496–1504.

Kroon, T., 2016. Optimizing Nicotinic Acid Delivery for Durable Antilipolysis and Improved Metabolic Control. Doctoral thesis, Swedish University of Agricultural Sciences.

Kroon, T., Baccega, T., Olsén, A., Gabrielsson, J., Oakes, N. D., 2016. Nicotinic acid timed to feeding reverses tissue lipid accumulation and improves glucose control in obese Zucker rats. J. Lipid Res., 1–35.

Kroon, T., Kjellstedt, A., Thalén, P., Gabrielsson, J., Oakes, N. D., 2015. Dosing profile profoundly influences nicotinic acid's ability to improve metabolic control in rats. J. Lipid Res. 56 (9), 1679–1690.

Krzyzanski, W., Jose, J., Harrold, P.-r. J., 2015. Pharmacodynamic model for chemoradiotherapy-induced thrombocytopenia in mice. J. Pharmacokinet. Pharmacodyn. 42 (6), 709–720.

Lalonde, R., Gaudreault, J., 1999. Mixed-effects modeling of the pharmacodynamic response to the calcimimetic agent R–568. Clin. Pharmacol. Ther. 65 (1), 40–49.

Lalonde, R. L., Kowalski, K. G., Hutmacher, M. M., Ewy, W., Nichols, D. J., Milligan, P. A., Corrigan, B. W., Lockwood, P. A., Marshall, S. A., Benincosa, L. J., Tensfeldt, T. G., Parivar, K., Amantea, M., Glue, P., Koide, H., Miller, R., 2007. Model-based Drug Development. Clin. Pharmacol. Ther. 82 (1), 21–32.

Lange, M. R., Schmidli, H., 2014. Optimal design of clinical trials with biologics using dose-time-response models. Stat. Med. 33 (October 2013), 5249–5264.

Lange, M. R., Schmidli, H., 2015. Analysis of clinical trials with biologics using dose – time-response models. Stat. Med. 34 (October 2013), 3017–3028.

Laporte-Simitidis, S., Girard, P., Mismetti, P., Chabaud, S., Decousus, H., Boissel, J.-P., 2000. Inter-study variability in population pharmacokinetic meta-analysis: When and how to estimate it? J .Pharm. Sci. 89 (2), 155–167.

Leander, J., Almquist, J., Ahlström, C., Gabrielsson, J., Jirstrand, M., 2015. Mixed Effects Modeling Using Stochastic Differential Equations : Illustrated by Pharmacokinetic Data of Nicotinic Acid in Obese Zucker Rats. AAPS J. 17 (3), 586–596.

Leander, J., Lundh, T., Jirstrand, M., 2014. Mathematical Biosciences Stochastic differential equations as a tool to regularize the parameter estimation problem for continuous time dynamical systems given discrete time measurements. Math. Biosci. 251, 54–62.

Lees, P., Cunningham, F. M., Elliott, J., 2004. Principles of pharmacodynamics and their applications in veterinary pharmacology. J. vet. Pharmacol. Therap. 27 (6), 397–414.

Lefèvre, G., Duval, M., Gauron, S., Brookman, L. J., Rolan, P. E., Morris, T. M., Piraino, a. J., Morgan, J. M., Palmisano, M., Close, P., 1997. Effect of renal impairment on the pharmacokinetics and pharmacodynamics of desirudin. Clin. Pharmacol. Ther. 62 (1), 50–59.

Leil, T. A., Bertz, R., 2014. Quantitative systems pharmacology can reduce attrition and improve productivity in pharmaceutical research and development. Front. Pharmacol. 5 (NOV), 1–6.

Levenberg, K., 1944. A Method for the Solution of Certain Non-Linear Problems in Least Squares. Q Appl. Math. 2, 164–168.

Levy, G., 1964a. Relationship Between Elimination Rate of Drugs and Rate of Decline of Their Pharmacologic Effects. J .Pharm. Sci. 53 (3), 342–343.

Levy, G., 1964b. Relationship between rate of elimination of tubocurarine and rate of decline of its pharmacological activity. Brit. J. Anaesth. 36, 694–695.

Levy, G., 1966. Kinetics of pharmacologic effects. Clin. Pharmacol. Ther. 7 (3), 362–372.

Li, H.-M., Zhang, M., Xu, S.-T., Li, D.-Z., Zhu, L.-Y., Peng, S.-W., Chen, G.-Q., Martin, P. M., Ganapathy, V., Wei, C.-J., 2011. Nicotinic Acid Inhibits Glucose-Stimulated Insulin Secretion Via the G Protein Y Coupled Receptor PUMA-G in Murine Islet A Cells. Pancreas 40 (4), 615–621.

Lindskog, P., 1996. Methods, Algorithms and Tools for System Identification Based on Prior Knowledge. Dissertation, Linköping University.

Luu, K., Zhang, E., Prasanna, G., 2009. Pharmacokinetic-pharmacodynamic and response sensitization modeling of the intraocular pressure-lowering effect of the EP4 Agonist 5-{3-[(2S)-2-{(3R)-3-hydroxy-4-[3-(trifluoromethyl)phenyl]butyl}-5-oxopyrrolidin-1-yl]propyl}thiophene-2-carboxylate. J. Pharmacol. Exp. Ther. 331 (2), 627–635.

Manolis, E., Rohou, S., Hemmings, R., Salmonson, T., Karlsson, M., Milligan, P. A., 2013. The Role of Modeling and Simulation in Development and Registration of Medicinal Products: Output From the EFPIA/EMA Modeling and Simulation Workshop. CPT Pharmacometrics Syst. Pharmacol. 2 (2), e31.

Marquardt, D. W., 1963. An algorithm for least-squares estimation of nonlinear parameters. J. Soc. Indust. Appl. Math 11 (2), 431–441.

Marshall, S., Burghaus, R., Cosson, V., Cheung, S., Chenel, M., DellaPasqua, O., Frey, N., Hamrén, B., Harnisch, L., Ivanow, F., Kerbusch, T., Lippert, J., Milligan, P., Rohou, S., Staab, A., Steimer, J., Tornøe, C., Visser, S., 2016. Good Practices in Model-Informed Drug Discovery and Development: Practice, Application, and Documentation. CPT Pharmacometrics Syst. Pharmacol. 5 (3), 93–122.

Mazzocco, P., Barthélémy, C., Kaloshi, G., Lavielle, M., Ricard, D., Idbaih, A., Psimaras, D., Renard, M.-A., Alentorn, A., Honnorat, J., Delattre, J.-Y., Ducray, F., Ribba, B., 2015. Prediction of Response to Temozolomide in Low-Grade Glioma Patients Based on Tumor Size Dynamics and Genetic Characteristics. CPT: Pharmacometrics Syst Pharmacol 4 (12), 728–737.

Mehrotra, S., Sharma, M. R., Gray, E., Wu, K., Barry, W. T., Hudis, C., Winer, E. P., Lyss, A. P., Toppmeyer, D. L., Moreno-Aspitia, A., Lad, T. E., Valasco, M., Overmoyer, B., Rugo, H., Ratain, M. J., Gobburu, J. V., 2017. Kinetic-Pharmacodynamic Model of Chemotherapy-Induced Peripheral Neuropathy in Patients with Metastatic Breast Cancer Treated with Paclitaxel, Nab-Paclitaxel, or Ixabepilone: CALGB 40502 (Alliance). AAPS J. 19 (5).

Mikaelian, I., Dunn, M. E., Mould, D. R., Hirkaler, G., Geng, W., Nicklaus, R., Singer, T., Reddy, M., 2013. Differential analysis of transient increases of serum cTnI in response to handling in rats. Pharma. Red. Per. 1 (2), 1–12.

Montgomery, S. A., Åsberg, M., 1979. A New Depression Scale Designed to be Sensitive to Change. Brit. J. Psychiat. 134, 382–389.

Morita, S., Shimajiri, Y., Sakagashira, S., Furuta, M., Sanke, T., 2012. Effect of exposure to non-esterified fatty acid on progressive deterioration of insulin secretion in patients with Type 2 diabetes: a long-term follow-up study. Diabet. Med. 29 (8), 980–985.

Morrow, T., Felcone, L. H., 2004. Defining the difference: What Makes Biologics Unique. Biotechnol. Healthc. 1 (4), 24–29.

Mould, D. R., Upton, R. N., 2012. Basic Concepts in Population Modeling, Simulation, and Model-Based Drug Development. CPT Pharmacometrics Syst. Pharmacol. 1 (9).

Mould, D. R., Upton, R. N., 2013. Basic concepts in population modeling, simulation, and model-based drug development-part 2: introduction to pharmacokinetic modeling methods. CPT Pharmacometrics Syst. Pharmacol. 2 (4), e38.

Musuamba, F. T., Teutonico, D., Maas, H. J., Facius, A., Yang, S., Danhof, M., Della Pasqua, O., 2015. Prediction of Disease Progression, Treatment Response and Dropout in Chronic Obstructive Pulmonary Disease (COPD). Pharm. Res. 32, 617–627.

Muzzey, D., Gómez-Uribe, C., Mettetal, J. T., van Oudenaarden, A., 2009. A systems-level analysis of perfect adaptation in yeast osmoregulation. Cell 138 (1), 160–171.

Myers, R. H., 2000. Classical and Modern Regression with Applications, 2nd Edition. Duxbury Press.

Nielsen, J. C., Hutmacher, M. M., Cleton, A., Martin, S. W., Ribbing, J., 2012. Longitudinal FEV1 dose – response model for inhaled PF-00610355 and salmeterol in patients with chronic obstructive pulmonary disease. J. Pharmacokinet. Pharmacodyn. 39, 619–634.

Nocedal, J., Wright, S., 2006. Numerical Optimization. Springer, New York.

Offermanns, S., 2006. The nicotinic acid receptor GPR109A (HM74A or PUMA-G) as a new therapeutic target. Trends Pharmacol. Sci. 27 (7), 384–90.

Oh, Y., Oh, K., Choi, Y., 2011. Continuous 24-h nicotinic acid infusion in rats causes FFA rebound and insulin resistance by altering gene expression and basal lipolysis in adipose tissue. Am. J. Physiol. Endocrinol. Metab. 300 (2), 1012–1021.

Parra-Guillen, Z. P., Berraondo, P., Ribba, B., Trocóniz, I. F., 2013. Modeling Tumor Response after Combined Administration of Different Immune-Stimulatory Agents. J. Pharmacol. Exp. Ther. 346, 432–442.

Paule, I., Tod, M., He, E., You, B., Freyer, G., Girard, P., Lyon, D., 2012. Dose adaptation of capecitabine based on individual prediction of limiting toxicity grade: evaluation by clinical trial simulation. Cancer Chemoter. Pharmacol. 69, 447–455.

Perez-Ruixo, J. J., Green, B., Doshi, S., Mould, D. R., 2012. Romiplostim Dose Response in Patients With Immune Thrombocytopenia. J. Clin. Pharmacol. 52, 1540–1551.

Persson, A., Böiers, L.-C., 2005. Analys i flera variabler, 3rd Edition. Studentlitteratur.

Pillai, G., Gieschke, R., 2004. A semimechanistic and mechanistic population PK–PD model for biomarker response to ibandronate, a new bisphosphonate for the treatment of osteoporosis. Brit. J. Clin. Pharmacol. 58 (6), 618–31.

Pillai, G., Gieschke, R., Goggin, T., Steimer, J.-L., 2001. A Population Pharmacokinetic-Pharmacodynamic Model for Ibandronate in Japanese Post-Menopausal Osteoporotic Women. In: 10th Population Approach Group Conference, Basel, Switzerland.

Pinheiro, J. C., Bates, D. M., Lindstrom, M. J., 1995. Model Building for Nonlinear Mixed- Effects Models. Tech. Rep. July, Department of Statistics, University of Wisconsin, Madison.

Plan, E. L., Maloney, A., Mentré, F., Karlsson, M. O., Bertrand, J., 2012. Performance Comparison of Various Maximum Likelihood Nonlinear Mixed-Effects Estimation Methods for Dose–Response Models. AAPS J. 14 (3), 420–432.

Pohjanpalo, H., 1978. System dentifiability based on the power series expansion of the solution. Math. Biosci. 41, 21–33.

Port, R. E., Ding, R. W., Fies, T., Schärer, K., 1998. Predicting the time course of haemoglobin in children treated with erythropoietin for renal anaemia. Br. J. Clin. Pharmacol. 46 (5), 461–466.

Post, T. M., Freijer, J. I., Ploeger, B. A., 2008. Extensions to the Visual Predictive Check to facilitate model performance evaluation. J. Pharmacokinet. Pharmacodyn. 35, 185–202.

Poynten, A. M., Gan, S. K., Kriketos, A. D., O'Sullivan, A., Kelly, J. J., Ellis, B. A., Crisholm, D. J., Campbell, L. V., 2003. Nicotinic acid-induced insulin resistance is related to increased circulating fatty acids and fat oxidation but not muscle lipid content. Metabolism 52 (6), 699–704.

Ramakrishnan, S., Rajaraman, S., Laxminarayan, S., Wesensten, N. J., Kamimori, G. H., Balkin, T. J., Reifman, J., 2013. A biomathematical model of the restoring effects of caffeine on cognitive performance during sleep deprivation. J. Theor. Biol. 319, 23–33.

Ramon-Lopez, A., Nalda-Molina, R., Valenzuela, B., Perez-Ruixo, J. J., 2009. Semi-Mechanistic Model for Neutropenia after High Dose of Chemotherapy in Breast Cancer Patients. Pharm. Res. 26 (8), 1952–1962.

Raue, A., Karlsson, J., Saccomani, M. P., Jirstrand, M., Timmer, J., 2014. Comparison of approaches for parameter identifiability analysis of biological systems. Bioinformatics 30 (10), 1440–8.

Raue, A., Kreutz, C., Maiwald, T., Bachmann, J., Schilling, M., Klingmüller, U., Timmer, J., 2009. Structural and practical identifiability analysis of partially observed dynamical models by exploiting the profile likelihood. Bioinformatics 25 (15), 1923–1929.

Rice, J. A., 1988. Mathematical Statistics and Data Analysis, 3rd Edition. Brooks/Cole Pub. Co.

Robert, C., Casella, G., 2004. Monte Carlo Statistical Methods. Springer, New York.

Rowland, M., Peck, C., Tucker, G., 2011. Physiologically-based pharmacokinetics in drug development and regulatory science. Annu. Rev. Pharmacol. Toxicol. 6 (1), 1–12.

Rowland, M., Tozer, T. N., 2011. Clinical Pharmacokinetics and Pharmacodynamics, 4th Edition. Lippincott Williams and Wilkins.

Sadur, C., Eckel, R., 1982. Insulin stimulation of adipose tissue lipoprotein lipase. Use of the euglycemic clamp technique. J. Clin. Invest. 69 (May), 1119–1125.

Salem, J.-E., El-Aissaoui, M., Alazard, M., Hulot, J.-S., Aissaoui, N., Le-Heuzey, J.-Y., Funck-Brentano, C., Faisy, C., Urien, S., 2016. Modeling of Amiodarone Effect on Heart

Rate Control in Critically Ill Patients with Atrial Tachyarrhythmias. Clin. Pharmacokinet. 55, 991–1002.

Saltelli, A., 2002. Sensitivity Analysis for Importance Assessment. Risk Anal. 22 (3), 579–590.

Saltelli, A., Ratto, M., Andres, T., Campolongo, F., Cariboni, J., Gatelli, D., Saisana, M., Tarantola, S., 2008. Global Sensitivity Analysis: The Primer. John Wiley & Sons.

Savic, R. M., Karlsson, M. O., 2009. Importance of shrinkage in empirical bayes estimates for diagnostics: problems and solutions. AAPS J. 11 (3), 558–69.

Schoenwald, R. D., Smolen, V. F., 1971. Drug-Absorption Analysis from Pharmacological Data II: Transcorneal Biophasic Availability of Tropicamide. J .Pharm. Sci. 60 (7), 1039–1045.

Schulte, B., Volz-Zang, C., Mutschier, E., Horne, C., Palm, D., Wellstein, A., Pitschner, H. F., 1991. AF-DX 116, a cardioselective muscarinic antagonist in humans: Pharmacodynamic and pharmacokinetic properties. Clin. Pharmacol. Ther. 50 (4), 372–378.

Schwildren, H., Schüttler, J., Stoeckel, H., 1987. Closed-loop Feedback Control of Methohexital Anesthesia by Quantitative EEF Analysis in Humans. Anesthesiology 67, 341–347.

Sedoglavic, A., 2002. A Probabilistic Algorithm to Test Local Algebraic Observability in Polynomial Time. J. Symbolic Computation 33 (5), 735–755.

Sheiner, L. B., Beal, S. L., 1980. Evaluation of methods for estimating population pharmacokinetics parameters. I. Michaelis-Menten model: routine clinical pharmacokinetic data. J. Pharmacokinet. Biopharm. 8 (6), 553–71.

Sheiner, L. B., Beal, S. L., 1981. Evaluation of methods for estimating population pharmacokinetic parameters. II. Biexponential model and experimental pharmacokinetic data. J. Pharmacokinet. Biopharm. 9 (5), 635–51.

Sheiner, L. B., Beal, S. L., 1983. Evaluation of methods for estimating population pharmacokinetic parameters. III. Monoexponential model: routine clinical pharmacokinetic data. J. Pharmacokinet. Biopharm. 11 (3), 303–19.

Sheiner, L. B., Rosenberg, B., Marathe, V. V., 1977. Estimation of population characteristics of pharmacokinetic parameters from routine clinical data. J. Pharmacokinet. Biopharm. 5 (5), 445–479.

Shoji, S., Suzuki, A., Conrado, D. J., Peterson, M. C., Hey-Hadavi, J., McCabe, D., Rojo, R., Tammara, B. K., 2017. Dissociated agonist of glucocorticoid receptor or prednisone for active rheumatoid arthritis: Effects on P1NP and osteocalcin pharmacodynamics. CPT Pharmacometrics Syst. Pharmacol. 6 (7), 439–448.

Smolen, V. F., 1971a. Determination of Time Course of In Viuo Pharmacological Effects from In Vitro Drug-Release Testing. J. Pharm. Sci. 60 (6), 878–882.

Smolen, V. F., 1971b. Quantitative determination of drug bioavailability and biokinetic behavior from pharmacological data for ophthalmic and oral administrations of a mydriatic drug. J. Pharm. Sci. 60 (3), 354–65.

Smolen, V. F., 1976a. Theoretical and Computational Basis for Drug Bioavailability Determinations Using Pharmacological Data . I . General Considerations and Procedures. J. Pharmacokinet. Biopharm. 4 (4), 337–353.

Smolen, V. F., 1976b. Theoretical and computational basis for drug bioavailability determinations using pharmacological data. II. Drug input in equilibrium to response relationships. J. Pharmacokinet. Biopharm. 4 (4), 355–75.

Smolen, V. F., 1976c. Theoretical and computational basis for drug bioavailability determinations using pharmacological data. II. Drug input in equilibrium to response relationships. J. Pharmacokinet. Biopharm. 4 (4), 355–75.

Smolen, V. F., 1978. Bioavialability and Pharmacokinetic Analysis of Drug Response Systems. Ann. Rev. Pharmacol. Toxicol. 18, 495–522.

Smolen, V. F., Murdock Jr., H. R., Williams, E. J., 1975. Bioavailability Analysis from Chlorpromazine in Humans from Pupilometric Data. J. Pharmacol. Exp. Ther. 195 (3), 404–415.

Smolen, V. F., Schoenwald, R. D., 1971. Drug-Absorption Analysis from Pharmacological Data I: Method and Confirmation Exemplified for the Mydriatic Drug Tropicamide. J. Pharm. Sci. 60 (1), 96–103.

Smolen, V. F., Weigand, W. A., 1973. Drug bioavailability and pharmacokinetic analysis from pharmacological data. J. Pharmacokinet. Biopharm. 1 (4), 329–336.

Sontag, E. D., 2003. Adaptation and regulation with signal detection implies internal model. Syst. Control Lett. 50 (2), 119–126.

Sostelly, A., Payen, L., Guitton, J., Pietro, A. D., Falson, P., Honorat, M., Boumendjel, A., Gèze, A., Freyer, G., Tod, M., 2014. Quantitative evaluation of the combination between cytotoxic drug and efflux transporter inhibitors based on a tumour growth inhibition model. Fundam. Clin. Pharmcol. 28 (2), 161–169.

Staab, A., Rook, E., Maliepaard, M., Aarons, L., Benson, C., 2013. Modeling and simulation in clinical pharmacology and dose finding. CPT Pharmacometrics Syst. Pharmacol. 2, 1–3.

Standing, J. F., Hammer, G. B., Sam, W. J., Drover, D. R., 2010. Pharmacokinetic-pharmacodynamic modeling of the hypotensive effect of remifentanil in infants undergoing cranioplasty. Paediatr. Anaesth. 20 (1), 7–18.

Stone, A. G. H., Howell, P. R., 2002. Use of the common gas outlet for the administration of supplemental oxygen during Caesarean section under regional anaesthesia. Anaesthesia 57, 690–709.

Strålfors, P., Björgell, P., Belfrage, P., 1984. Hormonal regulation of hormone-sensitive lipase in intact adipocytes: identification of phosphorylated sites and effects on the phosphorylation by lipolytic hormones. P. Natl. Acad. Sci. USA 81 (June), 3317–3321.

Tapani, S., Almquist, J., Leander, J., Ahlström, C., Peletier, L. A., Jirstrand, M., Gabrielsson, J., 2014. Joint feedback analysis modeling of nonesterified fatty acids in obese Zucker rats and normal Sprague-Dawley rats after different routes of administration of nicotinic acid. J. Pharm. Sci. 103 (8), 2571–84.

Taylor, J. R., 1996. An Introduction to Error Analysis - The Study of Uncertainties in Physical Measurements, 2nd Edition. University Science Books.

Tham, L.-S., Wang, L., Soo, R. A., Lee, S.-C., Lee, H.-S., Goh, B.-C., Holford, N. H. G., 2008. Cancer Therapy : Clinical A Pharmacodynamic Model for the Time Course of Tumor Shrinkage by Gemcitabine + Carboplatin in Non-Small Cell Lung Cancer Patients. Clin. Cancer Res. 14 (13), 4213–4218.

Thompson, W. C., Zhou, Y., Talukdar, S., Musante, C. J., 2016. PF-05231023, a long-acting FGF21 analogue, decreases body weight by reduction of food intake in non-human primates. J. Pharmacokinet. Pharmacodyn. 43 (4), 411–425.

Tod, M., 2008. Evaluation of drugs in pediatrics using K-PD models: perspectives. Fundam. Clin. Pharmcol. 22 (6), 589–94.

Tod, M., Farcy-Afif, M., Stocco, J., Boyer, N., Bouton, V., Sinègre, M., Marcellin, P., 2005. Pharmacokinetic / Pharmacodynamic and Time-to-Event Models of Ribavirin-Induced Anaemia in Chronic Hepatitis C. Clin. Pharmacokinet. 44 (4), 417–428.

Trefz, F., Lichtenberger, O., Blau, N., Muntau, A. C., Feillet, F., Bélanger-Quintana, A., van Spronsen, F., Munafo, A., 2015. Tetrahydrobiopterin (BH4) responsiveness in neonates with hyperphenylalaninemia: A semi-mechanistically-based, nonlinear mixed-effect modeling. Mol. Genet. Metab. 114 (4), 564–569.

Tunaru, S., Kero, J., Wufka, C., Blaukat, A., Pfeffer, K., Offermanns, S., 2003. PUMA-G and HM74 are receptors for nicotinic acid and mediate its anti-lipolytic effect. Nat. Med. 9 (3), 1–4.

Uehlinger, D., Gotch, F., Sheiner, L., 1992. A pharmacodynamic model of erythropoietin therapy for uremic anemia. Clin. Pharmacol. Ther. 51, 76–89.

Urquhart, J., Li, C., 1969a. Dynamic testing and modeling of adrenocortical secretory function. Ann. NY. Acad. Sci. 156 (2), 756–778.

Urquhart, J., Li, C. C., 1969b. Dynamic testing and modeling of adrenocortisol secretory function. Ann. NY. Acad. Sci. 156, 756–778.

van Schaick, E., Zheng, J., Ruixo, J. J. P., Gieschke, R., Jacqmin, P., 2015. A semi-mechanistic model of bone mineral density and bone turnover based on a circular model of bone remodeling. J. Pharmacokinet. Pharmacodyn. 42 (4), 315–332.

Veng-Pedersen, P., Modi, N. B., 1993. A system approach to pharmacodynamics. Input-effect control system analysis of central nervous system effect of alfentanil. J. Pharm. Sci. 82 (3), 266–72.

Verotta, D., Sheiner, L. B., 1991. Semiparametric analysis of non-steady-state pharmacodynamic data. J. Pharmacokinet. Biopharm. 19 (6), 691–712.

Vožch, S., Steimer, J.-L., 1985. Feedback Control Methods for Drug Dosage Optimisation. Clin. Pharmacokinet. 10 (6), 457–476.

Warwick, N., Graham, G., Torda, T., 1998. Pharmacokinetic analysis of the effect of vecuronium in surgical patients: pharmacokinetic and pharmacodynamic modeling without plasma concentrations. Anesthesiology 88 (4), 874–884.

Watson, E. M., Chappell, M. J., Ducrozet, F., Poucher, S. M., Yates, J. W. T., 2011. A new general glucose homeostatic model using a proportional-integral-derivative controller. Comput. Meth. Prog. Bio. 102 (2), 119–29.

Wilbaux, M., He, E., 2014. Prediction of tumour response induced by chemotherapy using modelling of CA-125 kinetics in recurrent ovarian cancer patients. Brit. J. Cancer 110, 1517–1524.

Wolfe, P., 1969. Convergence Conditions for Ascent Methods. SIAM Rev. 11 (2), 226–235.

Wolfe, P., 1971. Convergence Conditions for Ascent Methods. II: Some Corrections. SIAM Rev. 13 (2), 185–188.

Wright, D. F. B., Duffull, S. B., 2011. Development of a Bayesian Forecasting Method for Warfarin Dose Individualisation. Pharm. Res. 28, 1100–1111.

Wu, K., Looby, M., Pillai, G., Pinault, G., Drollman, A. F., Pascoe, S., 2011. Population pharmacodynamic model of the longitudinal FEV1 response to an inhaled long-acting anti-muscarinic in COPD patients. J. Pharmacokinet. Pharmacodyn. 38 (1), 105–19.

Yates, J. W. T., Evans, N. D., Chappell, M. J., 2009. Structural identifiability analysis via symmetries of differential equations. Automatica 45 (11), 2585–2591.

Yi, T. M., Huang, Y., Simon, M. I., Doyle, J., 2000. Robust perfect adaptation in bacterial chemotaxis through integral feedback control. P. Natl. Acad. Sci. USA 97 (9), 4649–53.

Zhang, L., Beal, S. L., Sheiner, L. B., 2003a. Simultaneous vs . Sequential Analysis for Population PK / PD Data I: Best-case Performance. J. Pharmacokinet. Pharmacodyn. 30 (6), 387–404.

Zhang, L., Beal, S. L., Sheiner, L. B., 2003b. Simultaneous vs. Sequential Analysis for Population PK/PD Data II: Robustness of Methods. J. Pharmacokinet. Pharmacodyn. 30 (6), 405–416.

Zhao, L., Ren, T.-h., Wang, D. D., 2012. Clinical pharmacology considerations in biologics development. Acta Pharmacologica Sinica 33 (11), 1339–1347.

Appendices

Chapter A

Mathematica code - Identifiability analysis of DRT I model

The following MATHEMATICA code was used for the EAR identifiability analysis of the DRT model used in the first study.

Load the `IdentifiabilityAnalysis` package.

```
In[7]:= Get["IdentifiabilityAnalysis`"];
```

Simplify the system by replacing k_{in} with $k_{\text{out}} \cdot R0$.

```
In[8]:= fixedParamRules={kin->kout*R0};
```

Define the system.

```
In[9]:= system = {Ab'[t] == u[t] - kb*Ab[t],
      B'[t] == n*B[t]*(u[t] - kb*Ab[t])/Ab[t],
      R'[t] == kin*(1+Ki*y[t])*(1 - Imax*B[t] /(ID50 + B[t]))*(z0/z[t]) -
               (M8[t]/R0)*kout*R[t],
      M1'[t] == ktol (R[t] - M1[t]),
      M2'[t] == ktol (M1[t] - M2[t]),
```

```
M3'[t] == ktol (M2[t] - M3[t]),
M4'[t] == ktol (M3[t] - M4[t]),
M5'[t] == ktol (M4[t] - M5[t]),
M6'[t] == ktol (M5[t] - M6[t]),
M7'[t] == ktol (M6[t] - M7[t]),
M8'[t] == ktol (M7[t] - M8[t]),
z'[t] == -p*ktol*(z[t]*R[t]/M1[t]-z[t]),
y'[t] == R0 - R[t],
Ab[0] == A0, B[0] == B0, R[0] == R0, M1[0] == R0, M2[0] == R0,
M3[0] == R0, M4[0] == R0, M5[0] == R0, M6[0] == R0, M7[0] == R0,
M8[0] == R0, z[0] == z0, y[0]==0};
```

Define the output.

```
In[10]:= output = {R[t]};
```

List of parameters, replace k_{in} in the system, and define list of state variables.

```
In[11]:= parameters = {kb, kout, R0, Imax, ID50, n, ktol, p, z0, A0, B0};
         system = system/.fixedParamRules;
         stateVariables = {Ab, B, R, M1, M2, M3, M4, M5, M6, M7, M8, z, y};
```

Run the identifiability analysis.

```
In[12]:= iad =  IdentifiabilityAnalysis[{system, output}, states,
                          parameters, t, input]

Out[12]= "IdentifiabilityAnalysisData[False, <>]"

In[13]:= iad["NonIdentifiableParameters"]

Out[13]= {B0, ID50}

In[14]:= iad["DegreesOfFreedom"]

Out[14]= 1
```

Since $B_0 = A_0^{\gamma} = 0$, where $A0$ and γ are identifiable, $B0$ is identifiable. Thus, ID_{50} is also identifiable due to the degrees of freedom.

Chapter B

Mathematica code - Parameter estimation of DRT I model

The following MATHEMATICA code was used for the parameter estimation of the DRT model used in the first study.

Define the system

Specify fixed parameter rules and random effects.

```
In[15]:= fixedParamRules = {kin -> R0*kout, Imax -> 1/(1 + Exp[-\[Theta]1])};
         randomEffects = {kb -> (kb*Exp[\[Eta]1]), Ki -> (Ki*Exp[\[Eta]2]),
         R0 -> (R0*Exp[\[Eta]3]), kout -> (kout*Exp[\[Eta]4]),
         ktol -> (ktol*Exp[\[Eta]5])};
```

Define system, initial conditions and measured variables.

```
In[16]:= system = {Ab'[t], R'[t], M1'[t], M2'[t], M3'[t], M4'[t], M5'[t],
         M6'[t], M7'[t], M8'[t], y'[t]} ==
          {bioInput - kb*Ab[t], (1 + Ki*y[t])*
             kin*(1 - Imax*Ab[t]^\[Gamma] /(ID50^\[Gamma] + Ab[t]^\[Gamma]))*
             (R0/M1[t])^p - kout*R[t]*(M8[t]/R0), ktol (R[t] - M1[t]),
           ktol (M1[t] - M2[t]), ktol (M2[t] - M3[t]),
           ktol (M3[t] - M4[t]), ktol (M4[t] - M5[t]),
```

```
  ktol (M5[t] - M6[t]),
  ktol (M6[t] - M7[t]),
  ktol (M7[t] - M8[t]),
  1 - R[t]/R0};
inititalConditions = {Ab[0], R[0], M1[0], M2[0], M3[0], M4[0], M5[0],
M6[0], M7[0], M8[0],
  y[0]} == {0, R0, R0, R0, R0, R0, R0, R0, R0, R0, 0};
output = {R[t]};
```

In[17]:=
```
oralSys = {Aa'[t], Ab'[t], R'[t], M1'[t], M2'[t], M3'[t], M4'[t],
M5'[t], M6'[t], M7'[t], M8'[t], y'[t]} ==
 {-aVmax*Aa[t]/(aKm + Aa[t]), bioInput - kb*Ab[t],
  (1 + Ki*y[t])*kin*
    (1 - Imax*Ab[t]^\[Gamma] /(ID50^\[Gamma] + Ab[t]^\[Gamma]))*
    (R0/M1[t])^p - kout*R[t]*(M8[t]/R0),
  ktol (R[t] - M1[t]), ktol (M1[t] - M2[t]), ktol (M2[t] - M3[t]),
  ktol (M3[t] - M4[t]), ktol (M4[t] - M5[t]), ktol (M5[t] - M6[t]),
  ktol (M6[t] - M7[t]), ktol (M7[t] - M8[t]),
  1 - R[t]/R0};
oralInitialConditions = {Aa[0], Ab[0], R[0], M1[0], M2[0], M3[0],
M4[0], M5[0], M6[0], M7[0], M8[0], y[0]} == {absInput, 0, R0,
R0, R0, R0, R0, R0, R0, R0, R0, 0};
```

Specify input.

In[18]:=
```
bioInputFunctions = {RATE*UnitStep[DOSE/RATE - t],
 RATE*UnitStep[30 - t] +
  Piecewise[{{RATE - Ceiling[(t - 30)/10]*RATE/19, t > 30 && t < 210}}] +
  Piecewise[{{RATE*UnitStep[210 + (DOSE - 20)/RATE - t], t > 210}}],
 Aa[t]*aVmax/(aKm + Aa[t])};
absInputFunctions = {RATE*DOSE};
```

Specify systems with correct inputs.

In[19]:=
```
infusionSystem = system /. Thread[bioInput -> bioInputFunctions[[1]]]
/. fixedParamRules;
stepSystem = system /. Thread[bioInput -> bioInputFunctions[[2]]]
/. fixedParamRules;
oralSystem = oralSys /. Thread[bioInput -> bioInputFunctions[[3]]]
/.
 fixedParamRules;
```

Define states.

```
In[20]:= stateVariables = {Aa[t], Ab[t], R[t], M1[t], M2[t], M3[t], M4[t],
         M5[t], M6[t], M7[t], M8[t], y[t]};
```

Define random variables.

```
In[21]:= randomParams = {\[Eta]1, \[Eta]2, \[Eta]3, \[Eta]4, \[Eta]5};
```

Set up models consisting of {sys}, {ic}, out.

```
In[22]:= modelInfusion = {{infusionSystem}, {initialCondition}, output}
         /. randomEffects;
         modelStep = {{stepSystem}, {initialConditions}, output}
         /. randomEffects;
         modelOral = {{oralSystem}, {oralInitialCondtions}
          /. Thread[absInput -> absInputFunctions], output} /. randomEffects;
         models = {modelInfusion, modelStep, modelOral};
```

Estimation of parameters

The following is the MATHEMATICA CODE used for the parameter estimation of the DRT of the first study.

Define Omega matrix (interindividual variation).

```
In[23]:= L = {{\[Omega]11, 0, 0, 0, 0}, {0, \[Omega]22, 0, 0, 0},
         {0, 0, \[Omega]33, 0, 0}, {0, 0, 0, \[Omega]44, 0},
         {0, 0, 0, 0, \[Omega]55}};
         \[CapitalOmega] = L.Transpose[L];
```

Define the S matrix for all models (measurment noise).

```
In[24]:= S1 = {{s1}};
         S2 = {{s2}};
         S3 = {{s3}};
         SList = {S1, S2, S3};
```

Construct a data list of data from all models.

```
In[25]:= infusionData = {Join[prepDataDose0Time0, prepDataDose1Time30,
         prepDataDose5Time30, prepDataDose20Time30, prepDataDose5Time300,
         prepDataDose10Time300, prepDataDose51Time300]};
         stepData = {Join[prepDataDose20, prepDataDose25]};
         oralData = {Join[prepDataOralDose24, prepDataOralDose81,
           prepDataOralDose812]};

         data = Join[infusionData, stepData, oralData];
```

Define covariates.

In[26]:=
```
listOfInputs = {DOSE, RATE};
```

Construct a parameter list with all the initial values - for the fixed effects, the random effects, and the measurement noises - and a list of all parameters.

In[27]:=
```
parameterStartValue = {{aVmax, 5}, {aKm, 30}, {\[Theta]1, 2},
{kb, 0.3}, {Ki, 0.001}, {ID50, 0.05}, {kout, 0.30}, {R0, 0.70},
{\[Gamma], 1}, {ktol, 0.03}, {p, 1}};
\[Omega]StartValue = {{\[Omega]11, 0.1}, {\[Omega]22, 0.1},
{\[Omega]33, 0.1}, {\[Omega]44, 0.1}, {\[Omega]55, 0.1}};
sStartValue = {{s1, 0.1}, {s2, 0.1}, {s3, 0.1}};
fullParameterList = Join[params, {s1, s2, s3}];
```

Call parameter estimation.

In[28]:=
```
{pExpValues, pValues, history} =
FitPopulationModel[data, models, listOfInputs,
 parameterStartValue, {SList,
  sStartValue}, {randomParams, \[CapitalOmega], \[Omega]StartValue}, t,
 fullParameterList];
```

Chapter C

Mathematica code - Identifiability analysis of DRT II insulin model

The following MATHEMATICA code was used for the EAR identifiability analysis of the DRT insulin model used in the second study.

Load the `IdentifiabilityAnalysis` package.

```
In[29]:= Get["IdentifiabilityAnalysis`"];
```

Simplify the system by replacing k_{in} with $k_{\text{out}} \cdot I_0$ and k_{inRI} with $k_{\text{outNI}} \cdot I_0$.

```
In[30]:= fixedParamRules={kin->kout*INS0,kinRI->koutRI*INS0};
```

Define the system.

```
In[31]:= system = {Ab'[t] == u[t] - kb*Ab[t],
      INS'[t] == kin*RI[t]*(1 -(1-X[t]/(X[t]+X50)) Imax*
              Y[t] /(Y50 + Y[t]))*(INS0/M1[t]) -
              (M2[t]/INS0)*kout*INS[t],
      M1'[t] == ktol (INS[t] - M1[t]),
      M2'[t] == ktol (M1[t] - M2[t]),
```

```
RI'[t] == kinRI-koutRI*INS[t],
NI'[t] == kNI*(Ab[t]-NI[t]),
X'[t] == m*X[t]*kNI*(Ab[t]-NI[t]),
Y'[t] == n*Y[t]*(u[t] - kb*Ab[t])/Ab[t],
Ab[0] == A0,  INS[0] == INS0, M1[0] == INS0, M2[0] == INS0,
RI[0] == 1, NI[0] == A0, X[0]==X0,Y[0]==0};
```

Here, $X(t) = N_{\mathrm{I}}^{m}(t)$[1] and $Y(t) = A_{\mathrm{b}}^{n}(t)$. These auxiliary state variables are introduced to transform the system to rational form. Define the output.

```
In[32]:= output = {INS[t]};
```

List of parameters, replace k_{in} and k_{inRI} in the system, and define list of state variables.

```
In[33]:= parameters = {kb, A0, X50, Imax, Y50, INS0, kout, ktol, koutRI,
         kNI, m, X0, n, Y0};
         system = system/.fixedParamRules;
         stateVariables = {Ab, INS, M1, M2, RI, NI, X, Y};
```

Run the identifiability analysis.

```
In[34]:= iad =  IdentifiabilityAnalysis[{system, output}, states,
                          parameters, t, input]

Out[34]= "IdentifiabilityAnalysisData[False, <>]"

In[35]:= iad["NonIdentifiableParameters"]

Out[35]= {X0, X50, Y0, Y50}

In[36]:= iad["DegreesOfFreedom"]

Out[36]= 2
```

But n and m are identifiable, and $X_{50} = ID_{50\mathrm{NI}}^{n}$ and $Y_{50} = N_{50I}^{m}$. Thus, X_{50} and Y_{50} can be found from the identities. Since the degress of freedom is 2, we conclude that the system is structurally locally identifiable.

[1] In the study, m was denoted γ.

Chapter D

Exposure-driven pharmacodynamic modelling - DRT II study

Using the pharmacokinetic model presented in Sec. 3.2 and the pharmacodynamic insulin model in Sec. 5.3 and FFA model in Sec. 5.4, a full, exposure-driven analysis was performed on the insulin- and FFA-response data used in DRT study II, as well as the corresponding exposure-time data (presented in Figs. D.1 and D.2) that were obtained during the experiments. This section will present the results from the exposure-driven study as a comparison to the DRT study conducted in this thesis.

NiAc exposure model

The base structure of the NiAc exposure model is presented in Sec. 3.2.

Between-subject and residual variability

The parameters that varied within the population were k_a, V_{max1}, and Synt, though Synt varied only in lean rats. These were assumed to be log-normally distributed in order to keep the parameter values positive. The five-day continuous infusion group of obese rats did not have exposure data. Consequently, these rats were assumed to behave like the estimated

median individual. The residual variability was assumed to be normally distributed, and modelled using a proportional error model.

Estimated parameters

Because of sparse sampling, all parameter values could not be estimated from the data. By applying an *a priori* sensitivity analysis Saltelli et al. (2008); Saltelli (2002), we identified the parameters that had the greatest influence on the output. These were then estimated from the data, while the remaining parameters were obtained from the literature Tapani et al. (2014). The population parameters estimated from the data were k_a, δ, and V_max1.

Insulin model

The insulin model used in the exposure-driven analysis was the same as the one presented in Sec. 5.3, with the exception that the drug-mechanism function was driven by the NiAc concentration in the plasma, rather than the biophase drug amount. Thus, the drug-mechanism function is given by

$$H_\mathrm{NI}(C_\mathrm{p}(t)) = 1 - E_\mathrm{NI}(N_\mathrm{I}(t)) \cdot \frac{C_\mathrm{p}^n(t)}{IC_\mathrm{50NI}^n + C_\mathrm{p}^n(t)}, \tag{D.1}$$

where IC_50NI is the potency of NiAc on insulin and n the Hill coefficient of the inhibitory function. Moreover, the term $E_\mathrm{NI}(N_\mathrm{I}(t))$ represents the drug efficacy, which is fixed for lean rats and dependent on the concentration in a hypothetical NiAc action compartment, $N_\mathrm{I}(t)$, for obese rats, according to

$$E_\mathrm{NI}(N_\mathrm{I}(t)) = \begin{cases} I_\mathrm{maxNI} & \text{lean} \\ I_\mathrm{maxNI}\left(1 - \frac{S_\mathrm{NI} \cdot N_\mathrm{I}^\gamma(t)}{N_\mathrm{50I}^\gamma + N_\mathrm{I}^\gamma(t)}\right) & \text{obese,} \end{cases} \tag{D.2}$$

where I_maxNI is the initial efficacy of NiAc on insulin, N_50I the potency of the NiAc action compartment, S_NI the long-term NiAc efficacy loss, and γ the corresponding Hill coefficient of the efficacy relation. The dynamics of N_I are in turn given by

$$\frac{\mathrm{d}N_\mathrm{I}(t)}{\mathrm{d}t} = k_\mathrm{NI} \cdot (C_\mathrm{p}(t) - N_\mathrm{I}(t)), \tag{D.3}$$

with $N_\mathrm{I}(0) = C_\mathrm{p}(0)$. Here k_NI is the turnover rate of the NiAc action concentration. Hence, the NiAc action compartment is driven by the NiAc concentration, rather than the biophase drug amount (which is the case in DRT study II).

Mechanistic FFA model

The FFA model used in the exposure-driven analysis was the same as the one presented in Sec. 5.4, with the exception that the drug-mechanism function was driven by the NiAc

plasma concentration, rather than the biophase drug amount. Thus, the drug-mechanism function is given by

$$H_{\mathrm{NF}}(C_{\mathrm{p}}(t)) = 1 - E_{\mathrm{NF}}(N_{\mathrm{F}}(t)) \cdot \frac{C_{\mathrm{p}}^{m}(t)}{IC_{50\mathrm{NF}}^{m} + C_{\mathrm{p}}^{m}(t)}, \tag{D.4}$$

where $IC_{50\mathrm{NF}}$ is the potency of NiAc as an inhibitor of FFA release and m is the Hill coefficient. As in DRT study II, the drug efficacy is dynamic and changes (down-regulates) during long-term infusions of NiAc. The efficacy is given by

$$E_{\mathrm{NF}}(N_{\mathrm{F}}(t)) = I_{\mathrm{maxNF}} \cdot \left(1 - \frac{S_{\mathrm{NF}} \cdot N_{\mathrm{F}}^{\phi}(t)}{N_{50\mathrm{F}}^{\phi} + N_{\mathrm{F}}^{\phi}(t)}\right), \tag{D.5}$$

where I_{maxNF} is the initial efficacy of NiAc on FFA, $N_{50\mathrm{F}}$ the potency of the NiAc action compartment, S_{NF} the long-term NiAc efficacy loss, ϕ the Hill coefficient, and $N_{\mathrm{F}}(t)$ the concentration in the NiAc action compartment. The dynamics of the NiAc action compartment are in turn described by

$$\frac{\mathrm{d}N_{\mathrm{F}}(t)}{\mathrm{d}t} = k_{\mathrm{NF}} \cdot (C_{\mathrm{p}}(t) - N_{\mathrm{F}}(t)), \tag{D.6}$$

with initial condition $N_{\mathrm{F}}(0) = C_{\mathrm{p}}(0)$. Here, the parameter k_{NF} is the turnover rate of the NiAc action state. Hence, as for the exposure-driven insulin model, the NiAc action compartment of the FFA model is driven by the NiAc concentration.

Results

The parameter estimation for the three sub-models (NiAc, insulin, and FFA) was performed sequentially. In this way, the PK were fixed in the insulin estimation and the PK and insulin were fixed in the FFA estimation. The estimates and between-subject variabilities (expressed in CV%), both with corresponding relative standard errors (RSE%), for normal Sprague-Dawley rats and obese Zucker rats are given in Table D.2. Weighted summaries Laporte-Simitidis et al. (2000) are presented for the parameters that varied between studies. The resulting models were qualitatively evaluated using visual predictive check (VPC) plots Bergstrand et al. (2011); illustrating the data, the model predicted median individual, and 90% Monte Carlo prediction intervals generated from the models Bergstrand et al. (2011); Post et al. (2008). The VPCs are shown in Fig. D.1 for lean Sprague-Dawley rats and in Fig. D.2 for obese Zucker rats. The VPCs are generated from the PK, insulin, and FFA models for all provocations of NiAc.

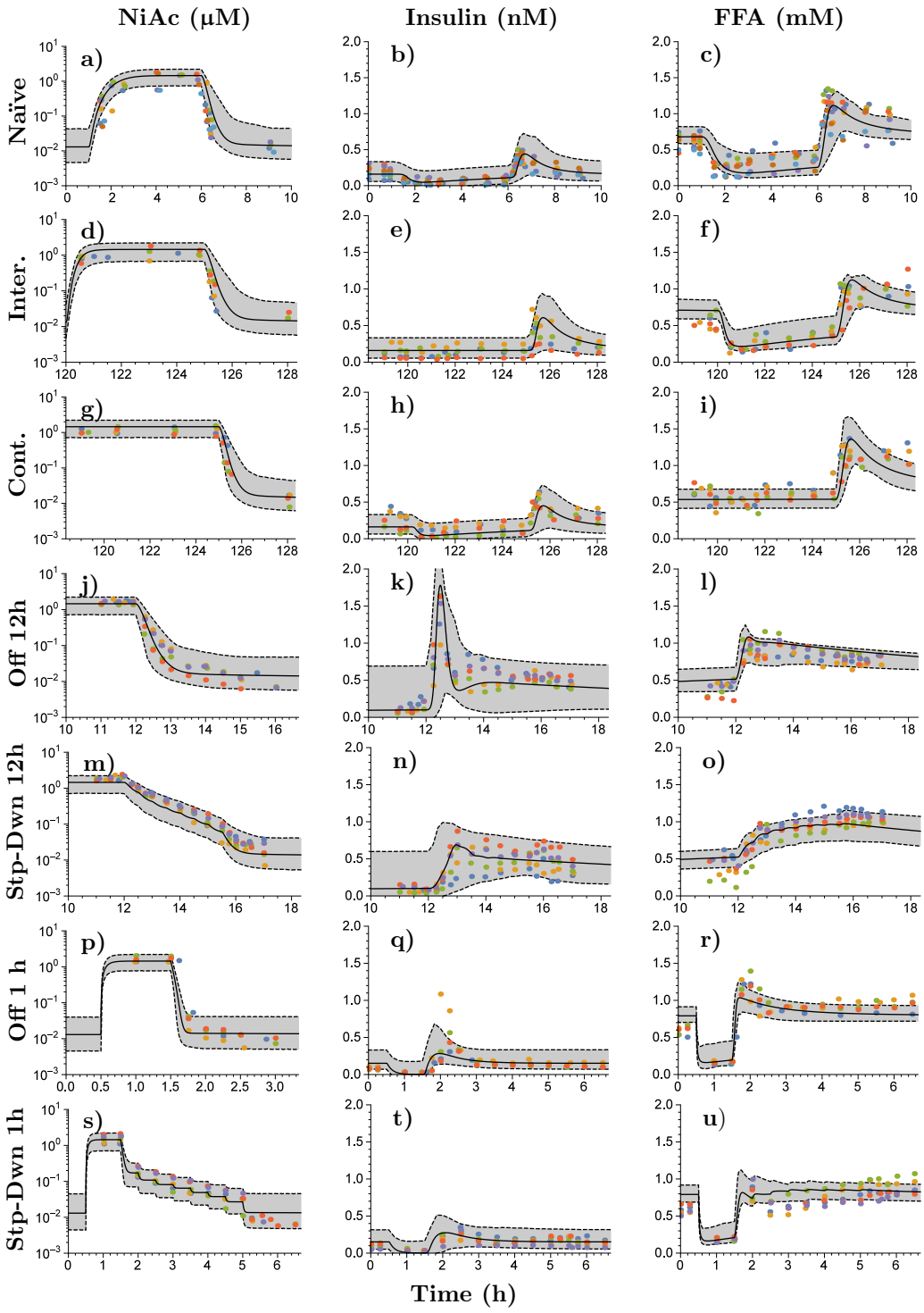

Figure D.1: Visual predictive checks for **lean Sprague-Dawley rats**. The first column shows the PK fits, the second column the insulin, and the third column the FFA. The rows represent the different protocols of NiAc (as described in the Experimental protocols section 3.3.1). The dots represent the data, with colours indicating separate individuals, the black lines the estimated median individual, and the grey areas the 90% population prediction intervals.

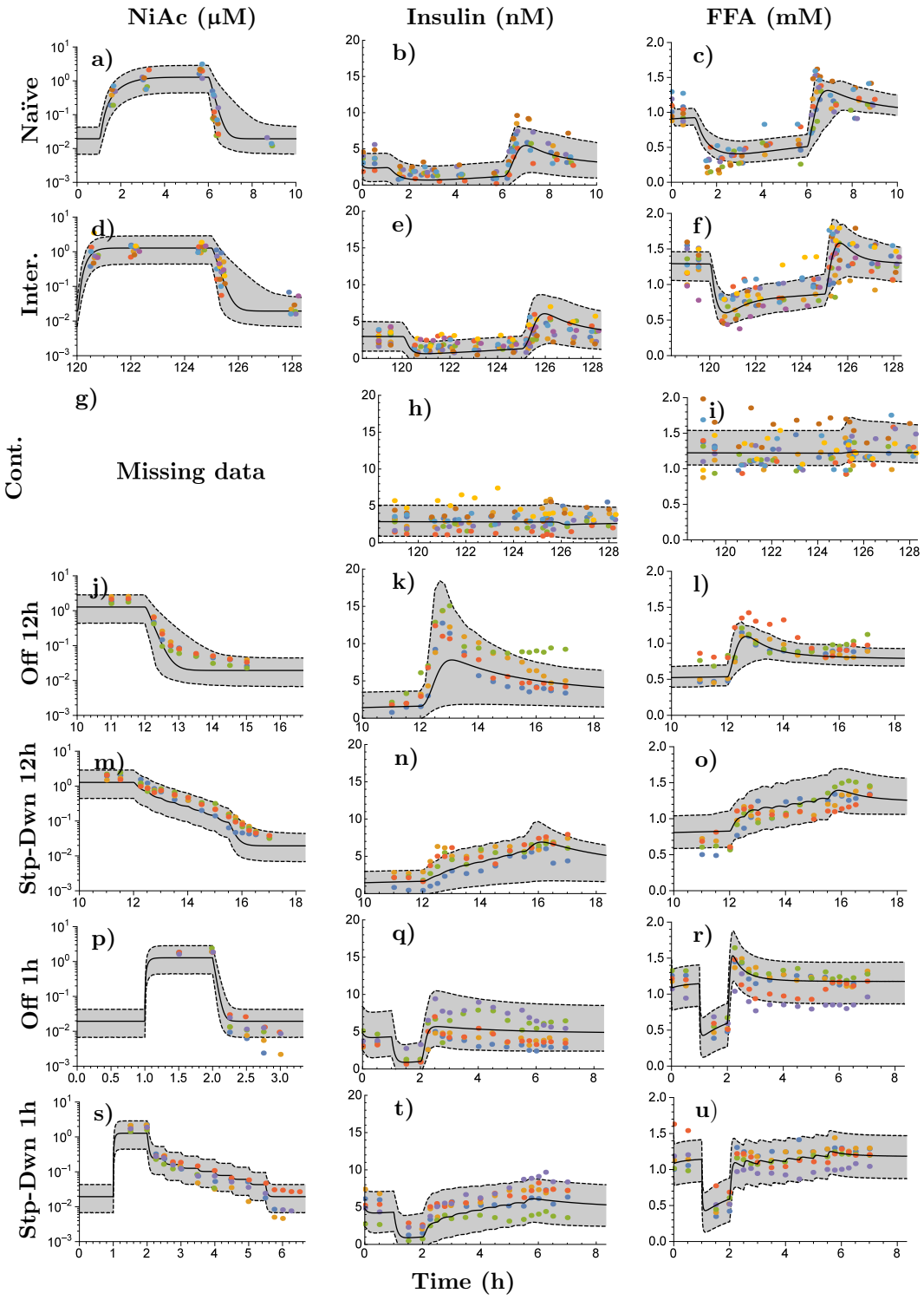

Figure D.2: Visual predictive checks for **obese Zucker rats**. The first column shows the PK fits, the second column the insulin, and the third column the FFA. The rows represent the different protocols of NiAc (as described in the Experimental protocols section 3.3.1). The dots represent the data, with colours indicating separate individuals, the black lines the estimated median individual, and the grey areas the 90% population prediction intervals. No exposure data were available from the **Cont.** protocol (Fig. (g)).

Pharmacokinetic model

The pharmacokinetic system reached a steady-state concentration of about 1 µM for all protocols, both in the lean and the obese rats (first column in Fig. 5.7 and first column in Fig. 5.10). The steady-state was attained faster with the intravenous rather than with the subcutaneous administration. When the infusions were terminated, the drug was cleared from the system within minutes and the NiAc concentration approached the endogenous level.

The absorption from the subcutaneous compartment had half-lives of 0.16 h and 0.13 h for the lean and the obese rats, respectively. At steady-state, the elimination of NiAc from the plasma compartment in the lean rats was approximately 3 times faster for the high affinity pathway than the low affinity one. Moreover, the drug elimination rate from the plasma at steady-state was $\sim$20 µmol kg^{-1} h^{-1} and $\sim$25 µmol kg^{-1} h^{-1} for the lean and the obese rats, respectively. The lumped diffusion coefficient was estimated to be 77 h$^{-1/2}$ and 62 h$^{-1/2}$ for the lean and the obese rats, respectively, implying that the NiAc dosing solution was diluted during the first $\sim$1.5 h.

Insulin model

	Half-lives (h)			
	Lean rats		Obese rats	
Turnover	Insulin	FFA	Insulin	FFA
Biomarker	0.105	0.00162	0.0643	0.00401
Moderator	1.07	0.570	5.53	0.979
Controller	0.176	0.719	11.3	42.0
NiAc action	-	106	28.7	18.4

Table D.1: Turnover half-lives (expressed in hours) in the insulin and FFA model for the lean and the obese rats of the biomarkers (insulin or FFA - corresponding rate constant k_{out}), the moderator (rate constant k_{tol}), the integral controller (rate constants k_{inR}l), and the NiAc action (rate constant k_{N}).

The median insulin baseline concentrations across groups were 0.233 nM and 3.51 nM for the lean and the obese rats, respectively. The estimates of the individual groups ranged between 0.151-0.264 nM for the lean rats and 2.69-4.82 nM for the obese rats. The median turnover half-lives of insulin, for the moderator, the integral controller, and the NiAc action level for the lean and the obese rats are given in Table D.1. For the lean rats, the efficacy of NiAc on insulin inhibition, I_{maxNI}, was estimated to be 0.793. The established NiAc exposure was about 1 µM which is approximately three times the NiAc potency related to inhibition of insulin ($IC_{50\text{NI}}$ =0.338 µM). This implies that the inhibitory function was saturated at steady-state. The estimated Hill coefficient n indicates a steep NiAc concentration-insulin response relationship at steady-state. Furthermore, for the obese rats, the efficacy was fixed to 1 and the corresponding potency was high since the $IC_{50\text{NI}}$ was low in comparison to

the NiAc steady-state exposure. However, since the estimated Hill coefficient was $0.84 < 1$, indicating a gentle NiAc-concentration insulin-response relationship at steady state, the NiAc concentrations never reached levels high enough to saturate the inhibitory function. The estimated N_{50I} of the NiAc action compartment was lower than the steady-state NiAc concentration (0.897¡1) and the Hill coefficient of the dynamic efficacy was estimated to be 18.9 (suggesting an all or non-response). This implies that the efficacy was completely down-regulated at the end of the long-term experiments in the obese rats, implying no NiAc inhibition on insulin release.

FFA model

The median FFA baseline concentrations across groups were 0.707 mM and 1.14 mM with corresponding ranges of 0.652-0.801 mM in the lean and 0.789-1.22 mM the obese rats, respectively. The median turnover half-lives of the FFA, the moderator, the integral controller, and the NiAc action level are given in Table D.1.
The potency of the NiAc action compartment was low for the lean rats, since $N_{50\mathrm{F}} >> N(t)$ at equilibrium (120 h), and high for the obese rats, since $N_{50\mathrm{F}} < N(t)$ at equilibrium (120 h). Consequently, the loss of efficacy was low in the lean rats and high in the obese ones. Furthermore, the estimate of Hill coefficient $\phi = 8.37$ for the obese rats suggests an all-or-none efficacy loss in the obese rats.

Model predictions

The resulting model was used to predict 24 h FFA lowering (AUC_{24}) for a range of protocols at steady-state (i.e., after multiple dosing). The protocol design consisted of a 0.25-12 h NiAc exposure period followed by a 0-12 h washout period. The NiAc infusions were designed to generate concentrations around the therapeutically relevant level ($\sim$1 µM) that was used in the experiments Ahlström (2011). The predicted AUC_{24} and proportional reduction, in comparison to baseline levels, on a median obese rat are given in Fig. D.3. The model predicted an optimal dosing strategy of $\sim$2 h longer washout period than the exposure period and the maximal AUC reduction is 5.60 mM h. These results were consistent when AUC_{24} was predicted for outliers with high/low potencies ($IC_{50\mathrm{NF}}$), baseline responses (F_0), and/or moderator turnover rates (k_{tolF}).
Furthermore, the NiAc-concentration FFA-response relationship at steady-state, for the obese rats, is illustrated in Fig. D.4, with the corresponding NiAc-, insulin-, and moderator actions. The largest reductions in FFA exposure occurs within a 'window of opportunity', with NiAc concentrations between the $IC_{50\mathrm{NF}}$ and the $N_{50\mathrm{F}}$. The predicted AUC_{24} at steady-state, for the optimal NiAc exposure of 0.500 µM, was 7.40 mM h.

Parameter	Definition	Normal Sprague-Dawley rats		Obese Zucker rats	
		Estimate (RSE%)	BSV[a] (RSE%)	Estimate (RSE%)	BSV[a] (RSE%)
		Pharmacokinetic model parameters			
k_a (h^{-1})	First order absorption rate	4.27(13)	80.1(51)	5.54(16)	80.2(47)
δ ($h^{1/2}$)	Lumped diffusion coeff. catheter	77.4(15)	-	62.4(17)	-
V_{max1} ($\mu mol\,kg^{-1}\,h^{-1}$)	Max. elimination - pathway 1	2.64(12)	93.5(51)	164(5.1)	22.4(13)
K_{m1} (μM)	Michaelis constant - pathway 1	0.235(29.2)	-	18.9(21.5)	-
V_{max2} ($\mu mol\,kg^{-1}\,h^{-1}$)	Max. elimination - pathway 2	425(39.6)	-	-	-
K_{m2} (μM)	Michaelis constant - pathway 2	74.5(43.4)	-	-	-
V_p ($L\,kg^{-1}$)	Volume of distribution - plasma	0.393(5.29)	-	0.323(12.4)	-
V_t ($L\,kg^{-1}$)	Volume of distribution - tissue	0.172(35.2)	-	-	-
Cl_d ($L\,kg^{-1}\,h^{-1}$)	Inter-compartmental distribution	0.0511(27.8)	-	-	-
Synt ($\mu mol\,kg^{-1}\,h^{-1}$)	Endogenous NiAc synthesis	0.213(23.3)	66.7(57)	0.168(10.1)	95(110)
σ_{propN}	Residual proportional error	0.313(5.1)	-	0.483(5.3)	-

[a]Between-subject variability expressed in CV%, calculated as $100 \times \sqrt{\omega^2}$.

		Insulin model parameters			
I_0 (nM)	Baseline insulin conc.	0.188(9.7)	49.3(5.5)	3.26(12)	10.3(21)
k_{outI} (h^{-1})	Fractional turnover rate insulin	6.58(14)	-	10.8(17)	-
I_{maxNI}	Efficacy - NiAc on insulin	0.793(11)	-	1[a]	-
$IC_{50\mathrm{NI}}$ (µM)	Potency - NiAc on insulin	0.338(15)	111(67)	0.175(27)	190(160)
n	Hill coefficient - NiAc on insulin	3.54(6.6)	-	0.840(6.0)	-
k_{tolI} (h^{-1})	Turnover rate moderator	0.646(28)	93.9(20)	0.125(48)	310(9.4)
k_{outRI} ($\mathrm{nM}^{-1}\,\mathrm{h}^{-1}$)	Integral gain parameter	3.94(17)	-	0.0612(27)	-
k_{NI} (h^{-1})	Turnover rate NiAc action comp.	-	-	0.0242(35)	-
$N_{50\mathrm{I}}$ (µM)	Potency NiAc action compartment	-	-	0.897(4.9)	-
γ	Hill coefficient	-	-	18.9(44)	-
S_{NI}	Long-term NiAc effect loss	-	-	1[a]	-
σ_{addI}(nM)	Residual additive error	0.0699(3.3)	-	0.748(3.0)	-

[a]Fixed in the estimations.

		Free fatty acid model parameters			
F_0 (mM)	Baseline FFA conc.	0.707(5.0)	17.8(26)	1.14(3.1)	0.874(25)
k_{outF} (h^{-1})	Fractional turnover rate FFA	428(140)	-	173(120)	-
I_{maxNF}	Efficacy - NiAc on FFA	1^a	-	1^a	-
$IC_{50\text{NF}}$ (µM)	Potency - NiAc on FFA	0.436(12)	41.8(28)	0.456(14)	41.8(26)
m	Hill coefficient - NiAc on FFA	1.24(11)	-	0.731(9.0)	-
k_{tolF} (h^{-1})	Turnover rate moderator	1.21(67)	58.4(9.6)	0.708(24)	34.2(15)
k_{outRF} ($\text{nM}^{-1}\,\text{h}^{-1}$)	Integral gain parameter	0.965(29)	-	0.0165(38)	-
k_{NF} (h^{-1})	Turnover rate NiAc action comp.	0.00654(65)	-	0.0377(14)	-
$N_{50\text{F}}$ (µM)	Potency NiAc action compartment	3.05(160)	-	0.854(4.5)	-
ϕ	Hill coefficient	1^a	-	8.83(33)	-
S_{NF}	Long-term NiAc effect loss	0.807(190)	-	1^a	-
σ_{addF}(mM)	Residual additive error	0.130(3.5)	-	0.135(3.0)	-

Table D.2: Estimates of parameter median values and between-subject variabilities with corresponding relative standard errors (RSE%) for normal Sprague-Dawley rats and obese Zucker rats. Estimates highlighted in blue were taken from the literature (Tapani et al. Tapani et al. (2014)) while the remaining parameters were estimated in this study.

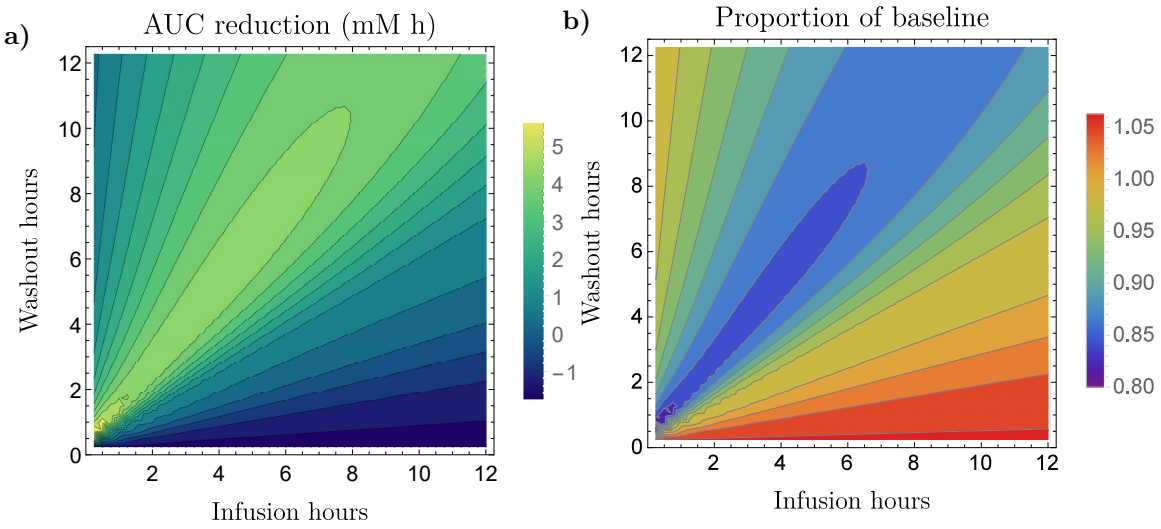

Figure D.3: Model predicted reduction in FFA exposure in a median obese rat at steady-state (i.e., after multiple dosing). (a) illustrates the predicted average reduction in 24 h FFA area under the curve and (b) illustrates the proportional reduction, in comparison to the baseline level. The predictions are made for a range of infusion protocols with 0.25-12 h of NiAc exposure followed by 0-12 h washout period. The x-axis represents the infusion time and the y-axis represents the washout time. The model predicts an optimal infusion regimen of ∼2 h longer washout period than the infusion. The maximal AUC reduction is 5.60 mM h.

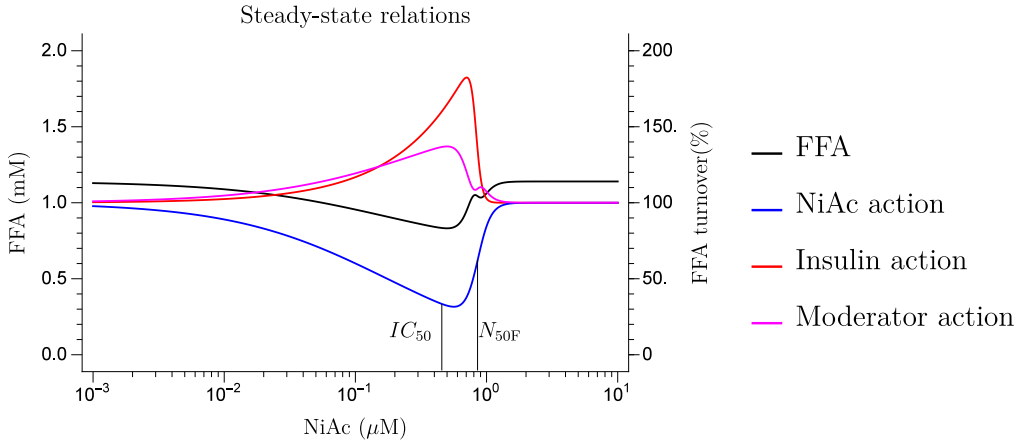

Figure D.4: Predicted steady-state concentration-response (left-hand y-axis) and concentration-action (right-hand y-axis) relationships for obese rats. The black line represents the FFA response, the blue line the inhibitory action of NiAc on FFA turnover, the red line the insulin action on FFA turnover, and the purple line the moderator action on the FFA turnover. The IC_{50F} and the N_{50F} concentrations are given by the black vertical lines.